An investigation into the use of 3D microscopy for the study of radiation-induced chromosome aberrations and nuclear architecture

Delphine Julie THENET

This thesis is being submitted in partial fulfilment of the requirements of Kingston University for the award of Doctor of Philosophy.

December 2012

DECLARATION

I declare that the work reported in this thesis is entirely my own and has been carried out at Kingston University, UK

This Thesis has not been submitted, in whole or in part, for any other degree at this or any other university.

Delphine Julie THENET December 2012

ACKNOWLEDGMENTS

Many thanks go to my Director of studies, Dr David Wertheim for his endless enthusiasm, patience and encouragements. Also many thanks for his help with the computer analysis and for sourcing a higher quality caffeine supply on campus.

I would like to thank my main supervisor, Dr John Peacock for his support, patience and input throughout the highs and lows of this adventure. I never thought your retirement would be that metaphorical kick in the backside to spur me into getting to completion.

I would like to also thank my co-supervisor, Dr Lucy Jones for her support, help with understanding cytogenetic related matters, data crunching and for her continued help with my "Frenglish"; 8 years on, it is still giving me grief.

I would like to thank Dr Tam Thring for being my rock when the future looked bleak and flicking the fuse box back on when the light at the end of the tunnel had gone out. They say a cup of tea solves all troubles. Many cups with you solved mine.

Many thanks go to Dr Theresa Hague for being a true friend and for lending me extra brain function during our brainstorming sessions. I have not looked at Thai cuisine and red wine the same since.

I would like to thank the technicians at the School of Life Sciences at Kingston University (Gurm, Jayne and Michael) for their help with lab logistics and advice on cell culture.

My thanks also go to my fellow Life Sciences research students at Kingston University for their help and continuous support. A special mention goes to Naomi Ikeda and Claire Ryall for keeping me sane outside of research hours each in their own way.

I would like to thank my boyfriend Jon for being understanding and supportive when I needed it most. There is a chance you'll get to see more of me now.
My wonderful friends outside of university Lam, Ebony, Gareth, Tania, Maxine, Petra, Rachel, Cécile, Els, Carine, Bruce, Morgane, Yann, Barbara and Michal for being there when I needed it and for knowing when not to ask about the PhD.

Finally, I would like to thank my family for their encouragements and support from the other side of the Channel. Thank you for giving me the space and time I needed to succeed in this venture.

ABSTRACT

Cellular exposure to ionising radiation (IR) generates chromosome aberrations (CA) that in turn lead to gene mutation and cell death. Although radiation-induced CA are known to result from the misrepair or lack of repair of DNA damage, the exact details of the conversion of such damage to CA remains unclear especially with regard to those CA that involve two or more chromosomes.

In interphase cells, chromosomes occupy discrete territories that under specific conditions appear conserved within any cell type. Territories appear to have both structural and functional importance and their position within the nucleus is apparently dynamic and changes during the cell cycle. The existence of territories suggests that in three dimensions, chromosomes differ in their spatial relationship.

The aims of this thesis were to develop methods for 3D analysis and visualisation of chromosome territories in human primary fibroblasts and bladder carcinoma (RT112) cell nuclei to enable chromosome characterisation.

The relationship between CA formation following irradiation and nuclear architecture was investigated using fluorescence *in situ* hybridization and confocal microscopy in the two cell lines. Analysis and visualisation methods were developed and applied in order to assess chromosome properties in relation to the nucleus.

Chromosome 1 and chromosome 2 territories were successfully imaged in non-irradiated and irradiated cell nuclei. 3D analysis and visualisation enabled the identification and quantification of complete and fragmented chromosomes territories.

The methods developed may thus help to elucidate the mechanisms of radiation induced chromosome aberrations and hence have application in cancer cell biology.

TABLE OF CONTENTS

LIST OF FIGURES

LIST OF TABLES

ABBREVIATIONS

2D	2 dimensional
3D	3 dimensional
1G	one green territory
2G	two green territories
3G	three green territories
4G	four green territories
1R	one red territory
2R	two red territories
3R	three red territories
4R	four red territories
1T	one territory
2T	two territories
3T	three territories
4T	four territories
ATM	Ataxia telangiectasia mutated
ATR	Ataxia telangiectasia and Rad3-related
CA	chromosome aberration
CAK	CDK activating kinase
Cdc	cluster of differentiation
CDK	cyclin-dependant kinase
ChK	Csk homologous kinase
CKI	cyclin-dependent kinases inhibitor
CLE	consequential late effect
CoG	centre of gravity
Csk	C-terminal Src kinase
CT	chromosome territory
CT-IC	chromosome territory-interchromatin domain
CV	coefficient of variation
Cy3	cyanine 3
DAPI	4',6-diamidino-2-phenylindole

ddH_2O	double distilled water
dfcs	dense fibrillar components
DMEM	Dulbecco's modified Eagles medium
DMSO	dimethylsulfoxide
DNA-PK	DNA dependent protein kinase
DNA-PKc	DNA dependent protein kinase C
DSB	double strand DNA break
EDTA	ethylenediaminotetraacetic acid
EM	electromagnetic
ESI	electron spectroscopic imaging
FBS	foetal bovine serum
Fcs	fibrillar centres
FDR	false discovery rate
FISH	fluorescence *in situ* hybridisation
FITC	fluorescein isothiocyanate
FLIM	fluorescence-lifetime imaging microscopy
FRET	fluorescence resonance energy transfer
G_0	gap 0
G_1	gap 1
G_2	gap 2
HCl	hydrochloric acid
HR	homologous recombination
HSA	human *Homo sapiens*
ICD	interchromatin domain
ICN	interchromosomal network
ISH	*in situ* hybridisation
IR	ionising radiation
LET	linear energy transfer
M	mitosis
M-FISH	multiple fluorescence *in situ* hybridisation
NHEJ	non-homologous end joining
NIR	non-Ionising radiations

PBS	phosphate buffered saline
PCC	premature chromosome condensation
PCR	polymerase chain reaction
PMT	photomultiplier tube
PR	perichromatin regions
RBE	relative biological efficiency
RNS	reactive nitrogen species
ROS	reactive oxygen species
RPMI	Roswell Park Memorial Institute
RT	radiotherapy
SD	standard deviation
SE	standard error of the mean
SSA	single strand annealing
SSB	single strand DNA break
SSC	saline-sodium citrate
UV	ultraviolet
WCP	whole chromosome paint

Chapter 1 General introduction and radiation biology

Living organisms are constantly exposed to radiation. Such radiation can come from varied sources such as, naturally occurring and man-made environmental material, gas emissions or cosmic rays bombarding the planet. The nature and dose of the radiation received will impact on the effects likely to be observed on exposed tissues, cells and organisms. Radiation is divided into two major types: Particle radiation and electromagnetic radiation (EM radiation). Within these two groups, radiation have also been distinguished as having ionising (IR) or non-ionising (NIR) properties. The ionising capability of a particular type of radiation is inferred by its ability to create ions via the removal of electrons upon contact with atoms and molecules present in the matter it travels through. This ability is directly linked to the energy of the radiation considered.

A summary of the different types of radiations as well as their ionising/non-ionising capacity is illustrated in Figure 1.1.

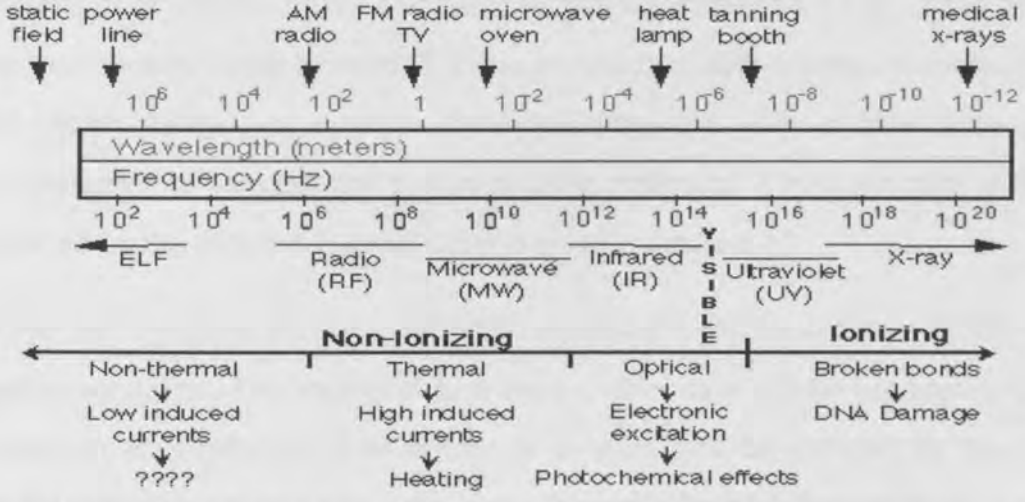

Figure 1.1: Illustration of the different characteristics of electromagnetic radiations as well as their ionising or non-ionising natures and summarised associated biological/chemical/physical effects taken from Moulder (1998).

1.1. General characteristics of radiations

1.1.1. Electromagnetic radiations

Electromagnetic radiation is the manifestation of the energy emitted and absorbed by charged particles. These particles behave like a wave. EM radiation is characterised by wavelength and energy. EM radiation includes radio waves, microwaves,

infrared waves, ultraviolet light (UV), γ-radiation as well as X-rays (Alpen, 1998a). Wavelength is inversely proportional to the energy. As a result, waves with short wavelengths are associated with higher energy.

At the short wavelength end of the spectrum radiation has sufficient energy to cause ionisation of atoms with which they interact hence they are termed "ionising radiation". This includes UV rays, γ- rays and X-rays (Cherry *et al.*, 2012).

Radiations between wavelengths of 10 and 0.01 nm are classified as X-rays. X-rays can result from natural sources or more commonly man-made sources as the result of a beam of electrons hitting target atoms. The resulting kinetic energy transfer generates a continuous beam of X-ray photons called Bremsstrahlung radiation (Cherry *et al.*, 2012). They can penetrate matter and are used at low doses in medical diagnosis. Penetrating ability is inferred by the X-ray energy where higher energies result in more penetrating X-rays. As a result, X-rays will be divided into soft X-rays and hard X-rays. Soft X-rays have a wavelength of 10 to 0.10 nm and energies ranging between 0.12 to 12 keV and hard X-rays wavelengths range between 0.10 nm and 0.01 nm with energies between 12 and 120 KeV (Alpen, 1998a). As a result, these radiations are likely to have more dangerous consequences on the cells and tissues of living organisms. A brief summary of the effects produced by the different EM radiations is given in Figure 1.1.

γ-Rays are naturally occurring radiation resulting from cosmic rays or the decay of radioactive atoms. The transition to a more stable state will be accompanied with the production of γ-radiation. The energy of a γ-ray will be dictated by the difference between the two energies the nucleus transitioned between following the decay.

1.1.2. Particle radiation

The second type of radiation is particle radiation. This form of radiation is due to electrons, protons, α-particles, neutrons and heavy charged ions (Alpen, 1998b). The main particles of interest here are the result of α and β decay.

α-Particles are the result of the decay of radioactive atoms. They consist of two protons and two neutrons bound together. α-Particles resemble a helium nucleus and are

positively charged. They travel at low speed due to their high mass and charge and have high ionising abilities. α-Particles have a short range of absorption and as a result become extremely dangerous if ingested.

β-Particles are electrons (β^- decay) or positrons (β^+ decay) emitted by the decay of radioactive elements. β-Particles travel much faster than α-particles and can have different energies depending on the element emitting the particle (Alpen, 1998b). β-Particles have lower ionizing abilities than α-particles but higher penetrative power for particles of same energies. For example, an α-particle can be stopped by a simple sheet of paper whereas a β-particle with the same energy requires a sheet of aluminium of the same thickness to be stopped.

1.1.3. Characterisation of IR

IR is usually characterised by their linear energy transfer (LET). LET describes the rate of energy transferred by a charged particle per unit on the distance of the track it follows while traversing matter (McNair, 1981). For example, high energy radiation will deposit very little energy due to few interactions with the cell ultrastructure and components (Goodhead, 1993). The different types of radiation are classified into three groups: low, medium and high LET radiations. Radiation such as X-rays and γ-rays are considered low-LET radiations. The intermediate to high LET is represented by neutrons as they produce protons or heavier particles. Finally, α-particles represent high-LET radiations due to their high mass, charge and low velocity making them highly ionizing. Up to 10^5 ionizations happen when an α-particle track traverses a nucleus (Goodhead, 1993).

Other terms such as the relative biological effectiveness (RBE) can be used to describe IR. RBE relates to the efficiency of radiations on a biological level according to the dose given and in comparison to the efficiency of X-rays, radiation with high LET being more efficient than radiation with low LET.

1.2. Biological effects of exposure to Ionizing radiations

In humans, exposure to IR can be of two types: involuntary and voluntary. Involuntary exposure to IR includes environmental, accidental, and occupational exposures. The dose received will vary with the conditions of exposure. For example, in accidental exposure like during the Chernobyl power plant catastrophe or during the aftermath of the nuclear bombing of Hiroshima and Nagasaki, high doses of radiations were received. On the other hand in the case of environmental exposure such as the exposure inhabitants close to a nuclear power plants or occupational exposure such as airline pilots or radiography personnel, the doses will be repeated but generally likely to be much smaller.

The non-lethal effects observed following exposure to IR are dose dependent and can be of three types: acute (early), consequential or late. The difference between the types of effects will differ in the timing of their manifestations. For example acute effects manifest early following accidental high exposure or up to a few weeks after radiotherapy exposure and usually happen in cells with a rapid proliferative rate such as cells of the skin surface or the digestive tract. In the case of consequential late effects (CLE), the healing of acute lesions is not complete and overlaps into the late period. CLE can result in fibrosis (deposition of collagen) in connective tissues (Rodemann & Bamberg, 1995) or atrophy of the vasculature (Dörr & Hendry, 2001). Such occurrence is most common in urinary system, skin, mucosa and intestinal system. Finally, the late effects can develop up to years after exposure and can have different degrees of severity as well as different speeds of progression.

The effects of IR on cells and tissues are also often observed in voluntary exposure such as radiotherapy (RT). Due to the ability of IR to cause cell death, IR makes an excellent candidate in the treatment of proliferative diseases such as some cancers. The IR effects on the cells within the cancerous tissues targeted should help to reduce the number of abnormal cells. However, due to the difficulty of specifically targeting the cancer cells exclusively, some normal tissue also may be irradiated in the process. The effects observed on the normal tissue in the treated area, define the side-effects of RT. The

different types of tissue responses and symptoms following RT have been reviewed by Stone *et al.* (2003).

The study of effect of IR on organisms is key in understanding the side-effects of RT. Progress in RT treatments lies in optimising disease eradication while reducing the side-effects in the surrounding normal tissues. This can only be achieved by understanding the mechanisms of action of IR in the cell as well as the mechanisms involved in the recovery from exposure to IR.

1.3. Cellular response to IR

Ionising radiation is so-called because of the ability to interact with matter and produce ions. In cells subjected to IR, it is possible that IR will have effects on every part of the cell. In other words the cell membrane, the cytoplasm and, the nucleus can potentially be subject to modification. The degree of permanence of these modifications will be dependent on the nature of the molecule or component affected. For example, the cell plasma membrane is mainly composed of a phospolipid bi-layer, glycolipids and, proteins and interactions with these molecules of a high turnover only result in transient damage.

Upon interaction with oxygen and nitrogen molecules, reactive oxygen species (ROS) and reactive nitrogen species (RNS) are created. The main effect on the cell will be the result of increased levels of ROS/RNS (Leach *et al.*, 2001). ROS occur naturally in cells at low levels and are dealt with by the cell anti-oxidant defence. Following IR, the increased levels of ROS and their interactions with the plasma membrane and the cytoplasm result in a perturbation of the metabolic balance of the cell and leads to oxidative stress. For example, polyunsaturated lipids are sensitive to oxygen radicals because of the double bonds between some of the carbon atoms. The production of ROS by IR leads to the formation of lipid peroxides. This results in modifications in the integrity and therefore the permeability of the plasma membrane (Chatterjee & Agarwal, 1988; Ianzini *et al.*, 1984).

The effects of oxidative stress can have two outcomes. The cell either increases the production of anti-oxidants to counteract the disruption in the balance or the cell dies by either necrosis or apoptosis. Necrosis is the result of metabolic collapse and damage to the cell elements such as the membrane permeability. This leads to swelling and leakage (Kerr *et al.*, 1972). Alternatively, cell death can occur in a more programmed manner through the process of apoptosis leading to the shrinkage of the cell and fragmentation of the nucleus before being cleared by phagocytosis (Kerr *et al.*, 1972).

The most important cellular effect of IR involves DNA damage. Possible damage undergone by DNA molecules plays an extremely important role in the outcome of the cell affected due to the major role of DNA in maintaining cell integrity. Compared to the membrane components the turnover of DNA is extremely low and as a result DNA lesions are likely to be more permanent. This increases the risk of lesions and defects being transmitted to the progeny of the cell. Radiation interaction with DNA can be direct or indirect (Hall & Giaccia, 2005). Direct interactions are the result of the contact of the DNA molecule directly with the radiation whereas indirect interactions happen via the creation of reactive molecules such as ROS.

DNA damage occurs as a result of one or more breakages of the phosphodiester bond in the DNA molecule. These breaks can occur on a single or on both strands of the DNA. IR mainly produces single-strand breaks (SSBs) in DNA. Exposure to IR generates 1000 single-strand breaks (SSBs) and approximately 40 double-strand breaks (DSBs) per diploid cell and per gray (Löbrich *et al.*, 1994; Mcgrath & Williams, 1966). The creation of DSBs by IR is believed to be random and also dependent on the dose received but DSBs are considered the most detrimental to the preservation of the integrity of the cell and its survival. Depending on the position of the cell within the cell cycle at the time of the damage, the resolution of DSBs can mean the processes happening have to be slowed down or even stopped until repair has taken place.

Three major checkpoints are in place throughout the cell cycle. The first one at the border between G_1 and the S-phase, the second one during the S-phase and finally the third one is at the border between G_2 and mitosis (G2/M). Upon creation of a DSB, the damage is detected, the cell cycle arrested and finally repair can take place before progression to

the next phase can happen. This prevents detrimental mutations from being passed on to the daughter cells. Tumorigenesis, genome instability and apoptosis are three examples of the possible outcome of a failure to repair DSBs.

REFERENCES

Alpen, E. L. (1998a). Electromagnetic Radiation: Its Nature and Properties. In *Radiation Biophysics* (2nd ed., pp. 11–26). San Diego: Elsevier.

Alpen, E. L. (1998b). Radioactivity. In *Radiation Biophysics* (2nd ed., pp. 27–49). San Diego: Elsevier.

Chatterjee, S. N., & Agarwal, S. (1988). Liposomes as membrane model for study of lipid peroxidation. *Free Radical Biology and Medicine*, **4**(1), 51–72.

Cherry, S. R., Sorenson, J. A., & Phelps, M. E. (2012). Basic Atomic and Nuclear Physics. In *Physics in Nuclear Medicine* (4th ed., pp. 7–18). Philidaelphia: Elsevier.

Dörr, W., & Hendry, J. H. (2001). Consequential late effects in normal tissues. *Radiotherapy and Oncology*, **61**(3), 223–231.

Goodhead, D. T. (1993). Biological Effects of High Energy Radiations. *Radiat Prot Dosimetry*, **48**(1), 111–114.

Hall, E. J., & Giaccia, A. J. (2005). *Radiobiology for the Radiologist* (p. 656). Lippincott Williams & Wilkins.

Ianzini, F., Guidoni, L., Indovina, P. L., Viti, V., Erriu, G., Onnis, S., & Randaccio, P. (1984). Gamma-irradiation effects on phosphatidylcholine multilayer liposomes: calorimetric, NMR, and spectrofluorimetric studies. *Radiation Research*, **98**(1), 154–66.

Kerr, J. F., Wyllie, A. H., & Currie, A. R. (1972). Apoptosis: a basic biological phenomenon with wide-ranging implications in tissue kinetics. *British Journal of Cancer*, **26**(4), 239–57.

Leach, J. K., Van Tuyle, G., Lin, P. S., Schmidt-Ullrich, R., & Mikkelsen, R. B. (2001). Ionizing radiation-induced, mitochondria-dependent generation of reactive oxygen/nitrogen. *Cancer Research*, **61**(10), 3894–901.

Löbrich, M., Ikpeme, S., & Kiefer, J. (1994). Measurement of DNA double-strand breaks in mammalian cells by pulsed-field gel electrophoresis: a new approach using rarely cutting restriction enzymes. *Radiation Research*, **138**(2), 186–92.

McGrath, R. A., & Williams, R. W. (1966). Reconstruction in vivo of Irradiated Escherichia coli Deoxyribonucleic Acid; the Rejoining of Broken Pieces. *Nature*, **212**(5061), 534–535.

McNair, A. (1981). ICRU Report 33 - Radiation Quantities and Units Pub: International Commission on Radiation Units and Measurements, Washington D.C. USA issued 15 April 1980, pp.25. *Journal of Labelled Compounds and Radiopharmaceuticals*, **18**(9), 1398–1398.

Moulder, J. E. (1998). Power-frequency fields and cancer. *Critical Reviews in Biomedical Engineering*, **26**(1-2), 1–116.

Rodemann, H. P., & Bamberg, M. (1995). Cellular basis of radiation-induced fibrosis. *Radiotherapy and Oncology,* **35**(2), 83–90.

Stone, H. B., Coleman, C. N., Anscher, M. S., & Mcbride, W. H. (2003). Reviews Effects of radiation on normal tissue : consequences and mechanisms. *The Lancet*, **4**, 529–536.

Chapter 2 Cell cycle, DNA damage, DNA damage repair and chromosome aberrations formation

2.1. The cell cycle, cell cycle checkpoints and DNA damage detection

Cell cycle progression in unperturbed normal cells is maintained by a well-defined series of molecular signals triggered by specific checkpoints through the cell cycle. These checkpoints ensure the preservation of the cell integrity throughout the different phases of the cycle as well as the orchestration of an appropriate response following DNA damage. Upon exposure to damaging agents such as ionizing radiations, the future of the cell will depend highly on its ability to preserve or restore its functional and structural integrity. The smooth progression of the cell cycle is ensured through the presence of checkpoints at the border between the different phases (G_1, S, G_2, and M). In order to deal with lesions generated following exposure to IR, this checkpoint system is complemented by damage detection and damage repair systems. The combination of these three systems is designed to ensure the maintenance of DNA integrity.

2.1.1. The cell cycle

All cells, regardless of their differentiation stage, proceed through the same steps during their life cycle. The cell cycle is divided into G_1, S, G_2, and mitosis with an extra step (G_0) for cells entering a quiescent state.

The mechanisms controlling cell cycle progression are now well characterised. The molecules involved are mainly cyclin-dependent kinases (CDKs) and cyclins, the activation and expression of which are interrelated. The CDKs belong to the serine/threonine protein kinase family and only exhibit their kinase activity when bound to cyclins. Each CDK acts at a specific moment in the cell cycle although their levels remain stable throughout the cell cycle unlike the cyclins (Evans *et al.*, 1983; Pines, 1991). The up or down regulation of cyclins resulting in the activation or inactivation of CDKs will dictate the progression of the cell cycle. Three CDKs are active during G_1 (CDK4, CDK6 and CDK2), one CDK is active during S phase (CDK2) and CDK1 is active during both G_2 and M (Figure 2.1). The fifth and remaining CDK, CDK7, is involved in the complex called CDK activating kinase, or CAK, when bound to cyclin H (Fisher & Morgan, 1994). The cyclins are divided into 5 types: cyclin A, cyclin B, cyclin D, cyclin E and cyclin H. Type D cyclins are key at the beginning of the cell cycle since their binding to CDK4 and CDK6 is necessary for the cell to

enter G_1 (Sherr, 1994). At the border between G_1 and S, the complex cyclin E/CDK2, is responsible for the regulation of the passage from one to the other (Ohtsubo *et al.*, 1995). Once the passage into S-phase has happened, the complex involved is now cyclin A/CDK2 (Girard *et al.*, 1991; Walker & Maller, 1991). Finally, CDK1 will then bind to cyclin A in G_2 in order to promote the passage into M and to cyclin B during the regulation of mitosis (Fisher, 1997; Arellano & Moreno, 1997).

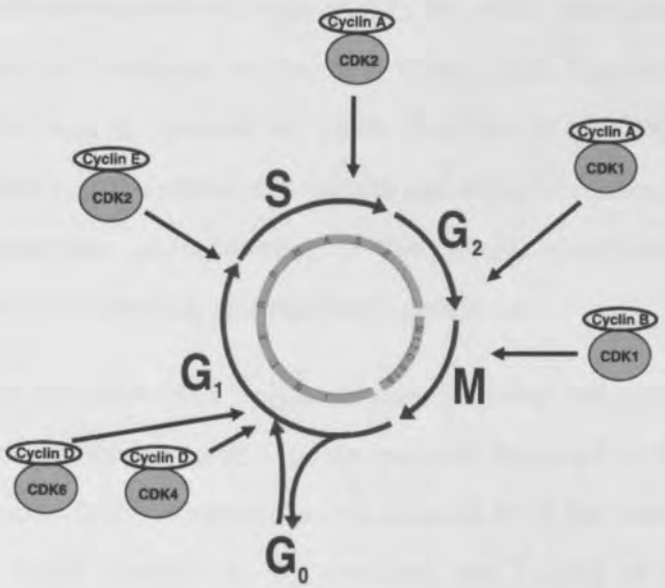

Figure 2.1: The different stages of the cell cycle and the regulatory complexes involved (Vermeulen *et al.*, 2003)

The activation of CDKs does not only occur by cyclin binding. Further activation is achieved by phosphorylation of threonine and tyrosine residues that are highly conserved. These phosphorylations enhance the binding of cyclins by inducing conformational changes in the CDK molecules (Jeffrey *et al.*, 1995; Paulovich & Hartwell, 1995).

Alternatively, the CDK's activity can be inhibited by inhibitors (CKI) which will bind to either the CDK or the CDK-cyclin complexes. These molecules act when DNA damage is detected and the cell cycle needs to be arrested at the next checkpoint. These are discussed more extensively in the next section.

2.1.2. DNA Damage detection and cell cycle checkpoints

2.1.2.1. DNA damage detection

The surveillance of genome integrity and the detection of DNA DSB through the cell cycle start with a series of molecules that bind to the unprotected ends of the DNA. Such molecules initiate the signalling cascades that will resolve any problem threatening the cell and the DNA integrity. The molecules involved are the MRN complex, PI(3)K (Phosphatidylinositol-3-OH kinase)-like kinases (or in this instance the DNA-PKCs), the ataxiatelangiecta mutated (ATM), the AMT- and Rad3-related (ATR) proteins and, the Ku proteins (reviewed by Burma & Chen, 2004; Kobayashi *et al.*, 2004; Koundrioukoff *et al.*, 2004; Kurz & Lees-Miller, 2004; Shechter *et al.*, 2004; Stracker *et al.*, 2004). Upon DNA damage, these molecules initiate signalling cascades that result in the stalling of cell cycle progression and activation of the cellular checkpoints allowing DNA repair or in some cases in triggering p53 mediated apoptosis.

ATM and DNA-PKCs appear to play a central role in the cell cycle stall thanks to its ability to phosphorylate and activate proteins involved in the DNA repair systems following IR-induced DSBs. However, in the case of ATM this cannot happen without the presence of the MRN complex. In G_1, similarly, the binding of the Ku proteins are essential to the activation of the DNA-PKCs. Moreover, DNA-PKCs are also activated in the presence of DSBs associated with errors during replication. Finally the ATR is mostly activated when error also happen during DNA replication.

2.1.2.2. Cell cycle checkpoints

The first of these checkpoints happens at the border between G_1 and S (G1/S), before DNA replication is initiated. At this point the ATM (ataxia-telangiectasia mutated) protein plays a major role. The expression of the ATM gene generates a 13-kbp transcript (Savitsky *et al.*, 1995) which will be later translated into a 350-kDa protein (Brown *et al.*, 1997; Watters *et al.*, 1997). The ATM protein possesses a kinase activity (phosphatidylinositol 3-kinase domain) which increases following irradiation (Banin, 1998; Canman, 1998) suggesting it plays a central role in the response to damage. The involvement of ATM in cell cycle checkpoints appears to occur through a p53 mediated

pathway (Khanna *et al.*, 1998a). ATM activates p53 by phosphorylating the serine-15 residue (Banin, 1998; Canman, 1998; Khanna *et al.*, 1998b). p53 activation then stimulates the transcription of the CKI protein genes p21 as well as Mdm2 and Bax (Agarwal *et al.*, 1998). p21 then binds to cyclin E/Cdk 2, cyclin D1/Cdk 4 or cyclin A/Cdk 2. This inhibits the S-cyclins binding to Cdks, blocking the cycle before it enters the replication phase (Harper *et al.*, 1995). Mdm2 plays its regulatory role using a negative feedback loop binding on p53 and as a result inhibiting its transcriptional activity as well as contributing to its degradation (Oren, 1999). In the event of severe damage to the cell, apoptosis is induced by p53 via the activation of genes involved in the oxidative stress pathways (Gottlieb & Oren, 1998; Owen-Schaub *et al.*, 1995; Polyak *et al.*, 1997). The S-phase checkpoint mechanisms are poorly understood but are believed to involve ATM-mediated phosphorylation of p95/nbs1 (Lim *et al.*, 2000).

The third checkpoint occurs at the end of the G_2 phase to ensure the DNA has been appropriately replicated (G2/M) and allows the cycle to undergo mitosis. Less is known about this third checkpoint. However, the arrest at this checkpoint is believed to be achieved through maintaining CDK1 in its inhibited form. M-cyclins such as CDK1 are responsible for mediating events during mitosis (Jin *et al.*, 1996). M-cyclins synthesis increases during the G_2 phase and their increase leads to the initiation of mitosis. M-Cdks complexes mediate the progression of the cell though mitosis unless damage is detected. When damage is detected, ATM activates the protein kinases Chk1 and Chk2 which in turn will phosphorylate Cdc25 leading to inhibition of its activity and increase of its protein binding activity. This in turn, results in its sequestration outside the nucleus preventing the activation of CDK1-cyclin B and delaying the entry into mitosis.

The different checkpoints present throughout the cell cycle represent an efficient DNA damage detection system as well as an important mechanism in initiating repair.

2.1.3. DNA DSB repair

2.1.3.1. DNA repair systems

Several different repair mechanisms can take place once damage is detected. Firstly, the damaged DNA can be repaired using single strand annealing (SSA). SSA occurs

when the DSB is located between two repeated sequences oriented in the same direction. The DNA between the break and the repeated sequence is cleaved on both strands creating two single stranded regions. The complementary sequences then anneal to each other allowing the removal of the single-stranded DNA before the synthesis of the missing sequence (Szostak *et al.*, 1983).

Alternatively, the DNA can be repaired using non-homologous end joining (NHEJ) or homologous recombination (HR). The two processes will differ in the degree of complementarity between the damaged sequence and the sequence used to perform the repair. HR requires homology whereas NHEJ does not.

The principle of HR is based on the use of the homologous undamaged chromosome or chromatid to repair the damaged area. In this case, the undamaged DNA from the sister chromatid is used as a template for the synthesis of the missing DNA sequence. One of the damaged strands invades the undamaged chromosome at the region of homology and the synthesis is initiated. Meanwhile the same process takes place between the two remaining strands (Szostak *et al.*, 1983). In NHEJ, the two pieces of the break are rejoined after degradation of some nucleotides, concluding by creating two blunt ends (Weterings & Van Gent, 2004).

The activation of one repair process over another will depend on different factors such as the stage of the cell cycle, the "dose" administered, the type of radiation, and the morphology of the break (blunt end or overhanging sequence). Even though homologous recombination is believed to be the main process involved in DNA repair accounting for 30-40% of the repair (Johnson & Jasin, 2000; Liang *et al.*, 1998) the predominant repair mechanism will differ depending on the advancement of the cell cycle. NHEJ appears to occur during all the phases of the cell cycle and is predominant during G_0/G_1 (Rothkamm *et al.*, 2001) and homologous recombination seems to be low in G_1 before becoming more predominant in S and G_2 (Rothkamm *et al.*, 2003). This is likely to be due to the necessity of the two homologous chromosomes to be in close proximity for homologous recombination to occur.

2.1.3.2. DNA repair complexes

As described above, diverse mechanisms are involved in repair of DNA double strand breaks (DSBs) and this can involve non-homologous end joining (NHEJ), homologous recombination (HR) or single strand annealing (SSA). The mechanisms of these three processes are fundamentally different; and they are operated by specific protein complexes.

The NHEJ process is characterised by the activity of a DNA dependent protein kinase (DNA-PK) along with the complex formed by the DNA ligase IV/Xrcc4. The DNA-PK is constituted by a heterodimer Ku of an 80 kDa and a 70 kDa subunit (ku70 and ku80) with DNA binding activities and a catalytic site (DNA-PKc) with substrate enzymatic properties (Hammarsten & Chu, 1998; Yaneva *et al.*, 1997). The activation of the DNA-PKc following the binding of Ku to the DNA triggers the intervention of the DNA ligase IV/Xrcc4 complex. The action of the ligase terminates the process of repair (Tsukamoto & Ikeda, 1998).

The second example of a repair process is homologous recombination. The proteins involved were first identified in *Saccharomyces cerevisiae* and belong to the RAD52 epistasis group (this includes RAD50-55, RAD57, RAD59, MRE11 and XRS2) (Petes *et al.*, 1991). Homologs to these proteins have also been identified in human (Kanaar & Hoeijmakers, 1997; Petrini *et al.*, 1997). The integrity of these proteins is essential to ensure efficient DSB repair. Mutations in RAD51 for example result in a diminution of embryo survival in mice (Tsuzuki *et al.*, 1996). A deficiency in RAD54 leads to chromosome instability and a reduced ability to repair DSBs (Essers *et al.*, 1997). RAD51 and RAD52 have shown similar binding properties to the DNA dependent protein kinase (DNA-PK) involved in the process of NHEJ (Haber, 1999). The competition between the two molecules might result in the initiation of one process over the other (Khanna & Jackson, 2001).

RAD51 has been observed interacting and co-localising *in situ* with p53, Brca1 and Brca2 (Haber, 1999). Brca1 and Brca2 participate in homologous recombination by modifying the chromatin structure. Mutations in brca2 result in predisposition to early onset of breast cancer (Tavtigian *et al.*, 1996; Wooster *et al.*, 1995).

The degree of fidelity of those complexes when dealing with DSB has to be extremely high since a mutation in the coding region of a protein can render it non-functional. Both HR and NHEJ have a different level of fidelity when repairing DSBs. They both display advantages and disadvantages. The lower fidelity of NHEJ is made up by the more direct approach to DNA end-joining. However, this inaccuracy is not always deleterious and is for example, exploited during V(D)J recombination leading the creation of varied antibodies which leads to increased antibodies and T-cell receptors diversity (Petrini *et al.*, 1997). In the case of HR, the high fidelity is counteracted by the need for a homologous sequence to be in the vicinity for successful repair to occur. Both processes can prove to be detrimental in the event of high numbers of DSBs where HR would be too complicated to ensure repair in a timely manner before the induction of apoptosis while the NHEJ pathway would rejoin a high number of non-homologous ends increasing the number of potential mis-repairs. The errors in DNA repair are visible at the chromosome level. They manifest in the form of DNA material exchange and are called chromosome aberrations (CA).

2.2. Chromosome aberration formation

Chromosome aberrations (CA) were discovered by Nowell & Hungerford in 1960 using cytogenetics. CA can be defined as the exchange of genetic material between chromosomes. Different types of CA occur depending on the nature of the DNA exchange or modification occurring to the chromosome. The exchange can either be balanced (reciprocal) or unbalanced (nonreciprocal). In the case of balanced exchange, no DNA material is lost whereas in unbalanced exchange material is lost in the process. Simple CA can be of different types: translocations, deletions, inversions, and formation of isochromosomes. Translocations involve the transfer of a fragment of the chromosome to another chromosome. Deletions involve the loss of DNA material. The formation of isochromosomes involves the breakage of the chromosome at the centromere region and the missing arm is replaced by the exact copy of the remaining arm. Finally, inversions involve a change in orientation of a fragment of the chromosome. Chromosome exchanges can be either simple (involving 2 chromosomes or less and 2 exchanges) or

complex (requiring 3 or more break-points distributed among 2 or more chromosomes) (Brown & Kovacs, 1993; Savage & Simpson, 1994).

2.2.1. The chromosome aberration formation theories

The nature of chromosome exchanges was for many years considered to be random. Different theories have been formulated concerning the mechanism of formation of CA. Serebrowsky (1929) proposed the contact-first hypothesis where the exchange is the result of a contact between the chromosomes at the time of irradiation. This hypothesis was challenged by Stadler (1931) who proposed the breakage-first hypothesis where the 2 candidates for exchange come in contact after damage.

This hypothesis was illustrated by Sax in (1940) on *Trandescantia*. Sax also observed that the number of exchanges increases in a quadratic manner (i.e. proportional to the square of the dose as opposed to being linear). The observations of Lea & Catcheside (1942) and Lea (1963) allowed the formulation of the breakage and reunion theory (also known as the 2-hits model) which requires the chromatid to be broken before being rejoined. Upon breakage of the backbone of the chromatid, two free open ends were generated. These open ends could have 3 fates: a legitimate rejoining, an illegitimate rejoining with another break close in space and time or no rejoining. This was also referred at the "spaghetti in a bowl" configuration. The dose–response curves with this theory are expected to be linear and this was the case with high LET radiations. However, exposure to low LET radiations showed curvilinear dose-response curves. In this breakage and reunion the majority of exchanges were expected to arise from two random breaks but advances in fluorescence *in situ* hybridisation (FISH) showed otherwise and the random factor was eliminated to be replaced by the element of proximity (Reviewed by Sachs *et al.*, 1997).

This theory was challenged by Revell (1955) who suggested the exchange theory after observing the presence of chemically induced chromatid-type aberrations. The exchange theory is based on the failure of an exchange process involving an unstable lesion rather than broken ends like in the breakage and rejoining theory. The unstable lesion would have a limited lifetime and have two possible fates: if left to decay no break would happen but if it entered in contact with a similar lesion, a link would be formed with a

possible exchange at a later time. This theory was dismissed with the advances of FISH (Lucas & Sachs, 1993).

The most recent theory is called the "molecular theory" and was formulated by Chadwick & Leenhouts (1981). This theory suggests that CAs arise as the result of the homologous repair of a single DSB. The repair of the DSB by homologous recombination repair leads to the creation of a second DSB at a local point of homology and would lead to the exchange. The work of Thacker *et al.* (1986) with ultrasoft X-rays (which are less likely to produce 2 breaks with a single track) showed that they produced simple and complex exchanges more efficiently than with hard X-rays. So a unique break could be sufficient to generate a CA.

2.2.2. The formation of chromosome aberration

The main difference between these theories lies in the number of DSB initially generated. In the breakage and reunion theory and in the Revell theory, 2 DSBs are necessary whereas in the molecular theory only 1 DSB is needed. The advances of FISH lead to the dismissal of the exchange theory (Lucas & Sachs, 1993).

However, the characteristics of each of the remaining theories can find similarities with DNA repair processes happening in the nucleus. The Breakage and Reunion theory bears resemblance to NHEJ and the Molecular theory is very similar to HR.

Since the repair systems are recruited at the sites of damage, it is possible that the particular repair process happening at a given site of damage will influence the outcome of the rejoining and therefore the creations of CA. There is evidence that the proximity of two DSB appears also to increase the probability of the formation of exchanges between different chromosomes following DNA damage (Brenner, 1987; Hlatky *et al.*, 2002; Sachs *et al.*, 1997; Savage, 2000). As a result, in the case of two breaks being close together and repaired by NHEJ, due to the NHEJ being a direct non homology based system, it might be possible that the resulting rejoining will lead to the creation of exchanges.

Initially the formation of CA was assumed to be random and that the genome did not have "hot-spots" of genome fragility (Ohno, 1970). This was documented by Mertens &

Johansson (1988) who did not find preferential "hot-spots" in cells from patients with mesenchymal tumours. The randomness of CA formations and absence of "hot-spots" was argued by Pevzner & Tesler (2003) and later by Sankoff & Trinh (2004). Moreover, these arguments were documented by studies showing the presence of preferential sites of recombination in mammalian genomes (Bailey *et al.*, 2004; Everts-van der Wind *et al.*, 2004; Hinsch & Hannenhalli, 2006; Kikuta *et al.*, 2007; Kolomietz *et al.*, 2002; Mehan *et al.*, 2007; Ruiz-Herrera *et al.*, 2006; Webber & Ponting, 2005; Yue & Haaf, 2006; Zhao *et al.*, 2004).

The proximity factor and the presence of "hot-spots" for recombination are in contradiction with the degree of randomness assumed in the breakage-and-reunion theory.

It seems that for two chromosomes to be preferentially involved in the formation of CAs, they must be in close proximity. As a result, for the same chromosomes always to be involved in the same type of CA, the factor of proximity at a random moment must be replaced by an actual preferential positioning within the cell nucleus. Factors such as nuclear architecture and chromosome positioning could then appear to be potentially involved in the preferential formation of CA between two chromosomes.

The exact relationship between chromosome aberration formation and nuclear architecture remains unclear. However, identification of chromosome properties possibly responsible in deciding their positioning within the cell nucleus could be the key to explaining the formation of CA.

REFERENCES

Agarwal, M. L., Taylor, W. R., Chernov, M. V, Chernova, O. B. & Stark, G. R. (1998). The p53 network. *The Journal of Biological Chemistry,* **273**(1), 1–4.

Arellano, M. & Moreno, S. (1997). Regulation of CDK/cyclin complexes during the cell cycle. *The International Journal of Biochemistry & Cell Biology,* 29(4), 559–73.

Bailey, J. A, Baertsch, R., Kent, W. J., Haussler, D. & Eichler, E. E. (2004). Hotspots of mammalian chromosomal evolution. *Genome Biology,* **5**(4), R23.

Banin, S. (1998). Enhanced Phosphorylation of p53 by ATM in Response to DNA Damage. *Science,* **281**(5383), 1674–1677.

Brenner, D. J. (1987). Concerning the Nature of the Initial Damage Required for the Production of Radiation-induced Exchange Aberrations. *International Journal of Radiation Biology,* **52**(5), 805–809.

Brown, J. M. & Kovacs, M. S. (1993). Visualization of nonreciprocal chromosome exchanges in irradiated human fibroblasts by fluorescence in situ hybridization. *Radiation Research,* **136**(1), 71–6.

Brown, K. D., Ziv, Y., Sadanandan, S. N., Chessa, L., Collins, F. S., Shiloh, Y. & Tagle, D. A (1997). The ataxia-telangiectasia gene product, a constitutively expressed nuclear protein that is not up-regulated following genome damage. *Proc. Nat. Acad. Sci. USA,* **94**(5), 1840–5.

Burma, S. & Chen, D. J. (2004). Role of DNA-PK in the cellular response to DNA double-strand breaks. *DNA Repair,* **3**(8–9), 909–18.

Canman, C. E. (1998). Activation of the ATM Kinase by Ionizing Radiation and Phosphorylation of p53. *Science,* **281**(5383), 1677–1679.

Chadwick, K. H. & Leenhouts, H. P. (1981). *Molecular theory of radiation biology*. Springer, 377.

Essers, J., Hendriks, R. W., Swagemakers, S. M., Troelstra, C., De Wit, J., Bootsma, D., Hoeijmakers, J. H. & Kanaar, R. (1997). Disruption of mouse RAD54 reduces ionizing radiation resistance and homologous recombination. *Cell,* **89**(2), 195–204.

Evans, T., Rosenthal, E. T., Youngblom, J., Distel, D. & Hunt, T. (1983). Cyclin: a protein specified by maternal mRNA in sea urchin eggs that is destroyed at each cleavage division. *Cell,* **33**(2), 389–96.

Everts-van der Wind, A., Kata, S. R., Band, M. R., Rebeiz, M., Larkin, D. M., Everts, R. E., Green, C. A., Liu, L., Natarajan, S., Goldammer, T., Lee, J. H., McKay, S., Womack, J. E. & Lewin, H. A. (2004). A 1463 gene cattle-human comparative map with anchor points defined by human genome sequence coordinates. *Genome Research,* **14**(7), 1424–37.

Fisher, R. P. (1997). CDKs and cyclins in transition(s). *Current Opinion In Genetics & Development,* **7**(1), 32–8.

Fisher, R. P. & Morgan, D. O. (1994). A novel cyclin associates with MO15/CDK7 to form the CDK-activating kinase. *Cell,* **78**(4), 713–24.

Girard, F., Strausfeld, U., Fernandez, A. & Lamb, N. J. C. (1991). Cyclin A is required for the onset of DNA replication in mammalian fibroblasts. *Cell,* **67**(6), 1169–1179.

Gottlieb, T. M. & Oren, M. (1998). P53 and Apoptosis. *Seminars in Cancer Biology,* **8**(5), 359–368.

Haber, J. E. (1999). DNA repair. Gatekeepers of recombination. *Nature,* **398**(6729), 665, 667.

Hammarsten, O. & Chu, G. (1998). 'DNA-dependent protein kinase: DNA binding and activation in the absence of Ku.'. *Proc. Nat. Acad. Sci. USA* 95 (2), 525–30.

Harper, J. W., Elledge, S. J., Keyomarsi, K., Dynlacht, B., Tsai, L., Zhang, P., Dobrowolski, S., Bai, C., Connell-crowley, L., Swindell, E., Fox, M. P. & Wei, N. (1995). Inhibition of Cyclin-dependent Kinases by p21. *Molecular Biology of the Cell,* **6**, 387–400.

Hinsch, H. & Hannenhalli, S. (2006). Recurring genomic breaks in independent lineages support genomic fragility. *BMC Evolutionary Biology,* **6**(1), 90.

Hlatky, L., Sachs, R. K., Vazquez, M. & Cornforth, M. N. (2002). Radiation-induced chromosome aberrations: insights gained from biophysical modeling. *BioEssays,* **24**(8), 714–23.

Jeffrey, P. D., Russo, A. A., Polyak, K, Gibbs, E., Hurwitz, J., Massagué, J. & Pavletich, N. P. (1995). Mechanism of CDK activation revealed by the structure of a cyclinA-CDK2 complex. *Nature,* **376**(6538), 313–20.

Jin, P., Gu, Y. & Morgan, D. O. (1996). Role of inhibitory CDC2 phosphorylation in radiation-induced G2 arrest in human cells. *The Journal of Cell Biology,* **134**(4), 963–70.

Johnson, R. D. & Jasin, M. (2000). Sister chromatid gene conversion is a prominent double-strand break repair pathway in mammalian cells. *EMBO,* **19**(13), 3398–407.

Kanaar, R. & Hoeijmakers, J. H. (1997). Recombination and joining: different means to the same ends. *Genes and Function,* **1**(3), 165–74.

Khanna, K. K. & Jackson, S. P. (2001) DNA double-strand breaks: signaling, repair and the cancer connection. *Nature Genetics,* **27**(3), 247–54.

Khanna, K. K., Gatti, R., Concannon, P., Weemaes, C., Hoekstra, M. F., Lavin, M. & d' Andrea., A. (1998a). Cellular responses to DNA damage and human chromosome instability syndromes. in *DNA damage and repair* ed. by Nickloff, J. A. & Hoekstra, M. F. Totowa (NJ): Humana Press, p. 395–442.

Khanna, K. K., Keating, K. E., Kozlov, S., Scott, S., Gatei, M., Hobson, K., Taya, Y., Gabrielli, B., Chan, D., Lees-Miller, S. P. & Lavin, M.F. (1998b). ATM associates with and phosphorylates p53: mapping the region of interaction. *Nature Genetics,* **20**(4), 398–400.

Kikuta, H., Laplante, M., Navratilova, P., Komisarczuk, A. Z., Engström, P. G., Fredman, D., Akalin, A., Caccamo, M., Sealy, I., Howe, K., Ghislain, J., Pezeron, G., Mourrain, P., Ellingsen, S., Oates, A. C., Thisse, C., Thisse, B., Foucher, I., Adolf, B., Geling, A., Lenhard, B. & Becker, T. S. (2007). Genomic regulatory blocks encompass multiple neighboring genes and maintain conserved synteny in vertebrates. *Genome Research,* **17**(5), 545–55.

Kobayashi, J., Antoccia, A., Tauchi, H., Matsuura, S. & Komatsu, K. (2004). NBS1 and its functional role in the DNA damage response. *DNA Repair,* **3**(8–9), 855–61.

Kolomietz, E., Meyn, M. S., Pandita, A. & Squire, J. A. (2002). The role of Alu repeat clusters as mediators of recurrent chromosomal aberrations in tumors. *Genes, Chromosomes & Cancer,* **35**(2), 97–112.

Koundrioukoff, S., Polo, S. & Almouzni, G. (2004). Interplay between chromatin and cell cycle checkpoints in the context of ATR/ATM-dependent checkpoints. *DNA Repair,* **3**(8–9), 969–78.

Kurz, E. U. & Lees-Miller, S. P (2004). DNA damage-induced activation of ATM and ATM-dependent signaling pathways. *DNA Repair,* **3**(8–9), 889–900.

Lea, D. E. (1963). Actions of Radiations on Living Cells. *American Journal of Human Genetics,* **15**(1), 121.

Lea, D. E. & Catcheside, D. G. (1942). The mechanism of the induction by radiation of chromosome aberrations in Tradescantia. *Journal of Genetics,* **44**(2–3), 216–245.

Liang, F., Han, M., Romanienko, P. J. & Jasin, M. (1998). Homology-directed repair is a major double-strand break repair pathway in mammalian cells. *Proc. Nat. Acad. Sci. USA,* **95**(9), 5172–5177.

Lim, D., Kim, S., Xu, B. & Maser, R. S. (2000). ATM phosphorylates p95/nbs1 in an S-phase checkpoint pathway. *Nature,* **404**, 613–618.

Lucas, J. N. & Sachs, R. K (1993) Using three-color chromosome painting to test chromosome aberration models. *Proc. Nat. Acad. Sci. USA,* **90**(4), 1484–7.

Mehan, M. R., Almonte, M., Slaten, E., Freimer, N. B., Rao, P. N. & Ophoff, R. A. (2007). Analysis of segmental duplications reveals a distinct pattern of continuation-of-synteny between human and mouse genomes. *Human Genetics,* **121**(1), 93–100.

Mertens, F. & Johansson, B. (1988). Distribution of structural chromosome aberrations in skin fibroblasts from patients with benign mesenchymal tumors. *Hereditas,* **109**(1), 125–9.

Nowell, P. C. & Hungerford, D. A. (1960). A minute chromosome in human chronic granulocytic leukemia. *Science,* **132**, 1497.

Ohno, S. (1970) *Evolution by gene duplication*. Berlin: Springer, 160.

Ohtsubo, M., Theodoras, A. M., Schumacher, J., Roberts, J. M. & Pagano, M. (1995). Human cyclin E, a nuclear protein essential for the G1-to-S phase transition. *Molecular and Cellular Biology,* **15**(5), 2612–24.

Oren, M. (1999). Regulation of the p53 tumor suppressor protein. *The Journal of biological Chemistry,* **274**(51), 36031–4.

Owen-Schaub, L. B., Zhang, W., Cusack, J. C., Angelo, L. S., Santee, S. M., Fujiwara, T., Roth, J. A, Deisseroth, A. B., Zhang, W. W. & Kruzel, E. (1995). Wild-type human p53 and a temperature-sensitive mutant induce Fas/APO-1 expression. *Molecular and cellular Biology,* **15**(6), 3032–40.

Paulovich, A. G. & Hartwell, L. H. (1995). A checkpoint regulates the rate of progression through S phase in S. cerevisiae in response to DNA damage. *Cell,* **82**(5), 841–7.

Petes, T. D., Malone, R. E. & Symington, L. S. (1991). Recombination in yeast. in *The Molecular and Cellular Biology of the Yeast Saccharomyces: Genome Dynamics, Protein Synthesis and Energetics* ed. by Broach, J. R.,Pringle, J. R. & Jones, E. W. Cold Spring Harbor, NY.: Cold Spring Harbor Laboratory Press, 407–521

Petrini, J. H., Bressan, D. A. & Yao, M. S. (1997). The RAD52 epistasis group in mammalian double strand break repair. *Seminars in immunology,* **9**(3), 181–8

Pevzner, P. & Tesler, G. (2003). Human and mouse genomic sequences reveal extensive breakpoint reuse in mammalian evolution. *Proc. Nat. Acad. Sci. USA,* **100**(13), 7672–7.

Pines, J. (1991). Cyclins: wheels within wheels. *Cell growth & differentiation,* **2**(6), 305–10.

Polyak, K., Xia, Y. & Zweier, J. L. (1997). A model for p53-induced apoptosis. *Nature,* **389**, 300–306.

Revell, S. H. (1955). A new hypothesis for "chromatid" changes. in *Proc. Radiobiology Symposium, 1954, Liège* ed. by Bacq, Z. M. & Alexander, P. London: Butterworth, 243–253.

Rothkamm, K., Krüger, I., Thompson, L. H., Kru, I. & Lo, M. (2003). Pathways of DNA Double-Strand Break Repair during the Mammalian Cell Cycle Pathways of DNA Double-Strand Break Repair during the Mammalian Cell Cycle. *Mol. Cell Biol.*, **23**(16) 5706–5715.

Rothkamm, K., Kühne, M., Jeggo, P. A., Ku, M. & Lo, M. (2001). Radiation-induced Genomic Rearrangements Formed by Nonhomologous End-Joining of DNA Double-Strand Breaks. *Cancer Research,* **10**, 3886–3893.

Ruiz-Herrera, A., Castresana, J. & Robinson, T. J. (2006). Is mammalian chromosomal evolution driven by regions of genome fragility? *Genome biology,* **7** (12), R115.

Sachs, R. K., Chen, A. M., & Brenner, D. J. (1997). Review: Proximity effects in the production of chromosome aberrations by ionizing radiation. *International Journal of Radiation Biology,* **71**(1), 1–19.

Sankoff, D. & Trinh, P. (2004). Chromosomal Breakpoint Re-use in the Inference of Genome Sequence Rearrangement. in *Proceedings of the Eighth Annual International*

Conference on Computational Molecular Biology (RECOMB). ed. by Bourne, P. & Gusfield, D. New york: ACM press, 30–35.

Savage, J. R. & Simpson, P.J. (1994) FISH "painting" patterns resulting from complex exchanges. *Mutation Research,* **312**(1), 51–60.

Savage, J. R. (2000). CANCER: Enhanced: Proximity Matters. *Science,* **290**(5489), 62–63.

Savitsky, K., Bar-Shira, A., Gilad, S., Rotman, G., Ziv, Y., Vanagaite, L., Tagle, D. A., Smith, S., Uziel, T., Sfez, S., Ashkenazi, M., Pecker, I., Frydman, M., Harnik, R., Patanjali, S.R., Simmons, A., Clines, G. A., Sartiel, A., Gatti, R. A., Chessa, L., Sanal, O., Lavin, M. F., Jaspers, N. G., Taylor, A. M., Arlett, C. F., Miki, T., Weissman, S. M., Lovett, M., Collins, F. S. & Shiloh, Y. (1995). A single ataxia telangiectasia gene with a product similar to PI-3 kinase. *Science,* **268**(5218), 1749–53.

Sax, K. (1940). An Analysis of X-Ray Induced Chromosomal Aberrations in *Tradescantia*. *Genetics,* **25**(1), 41–68.

Sax, K. (1939). The Time Factor in X-Ray Production of Chromosome Aberrations. *Proc. Nat. Acad. Sci. USA,* **25**(5), 225–33.

Serebrovsky, A. A. S. (1929). A General Scheme for the Origin of Mutations. *The American Naturalist,* **63**(687), 374–378.

Shechter, D., Costanzo, V. & Gautier, J. (2004). Regulation of DNA replication by ATR: signaling in response to DNA intermediates. *DNA Repair,* **3**(8–9), 901–8.

Sherr, C. J. (1994). G1 phase progression: cycling on cue. *Cell,* **79**(4), 551–5.

Stadler, L. (1931). *The experimental modification of heredity in crop plants.* [S.l.]: Scientific agriculture. 557-572.

Stracker, T. H., Theunissen, J.-W. F., Morales, M. & Petrini, J. H. J. (2004). The Mre11 complex and the metabolism of chromosome breaks: the importance of communicating and holding things together. *DNA repair,* **3**(8–9), 845–54.

Szostak, J. W., Orr-Weaver, T. L., Rothstein, R. J. & Stahl, F. W. (1983). The double-strand-break repair model for recombination. *Cell,* **33**(1), 25–35.

Tavtigian, S. V, Simard, J., Rommens, J., Couch, F., Shattuck-Eidens, D., Neuhausen, S., Merajver, S., Thorlacius, S., Offit, K., Stoppa-Lyonnet, D., Belanger, C., Bell, R., Berry, S., Bogden, R., Chen, Q., Davis, T., Dumont, M., Frye, C., Hattier, T., Jammulapati, S., Janecki, T., Jiang, P., Kehrer, R., Leblanc, J. F., Mitchell, J. T., McArthur-Morrison, J., Nguyen, K., Peng, Y., Samson, C., Schroeder, M., Snyder, S.C., Steele, L., Stringfellow, M., Stroup, C., Swedlund, B., Swense, J., Teng, D., Thomas, A., Tran, T., Tranchant, M., Weaver-Feldhaus, J., Wong, A.K., Shizuya, H., Eyfjord, J. E., Cannon-Albright, L., Labrie, F., Skolnick, M. H., Weber, B., Kamb, A. & Goldgar, D. E. (1996). The complete BRCA2 gene and mutations in chromosome 13q-linked kindreds. *Nature genetics,* **12**(3), 333–7.

Thacker, J., Wilkinson, R. E. & Goodhead, D. T. (1986). The induction of chromosome exchange aberrations by carbon ultrasoft X-rays in V79 hamster cells. *International Journal of Radiation Biology,* **49**(4), 645–56.

Tsukamoto, Y. & Ikeda, H. (1998). Double-strand break repair mediated by DNA end-joining. *Genes to Cells,* **3**(3), 135–44.

Tsuzuki, T., Fujii, Y., Sakumi, K., Tominaga, Y., Nakao, K., Sekiguchi, M., Matsushiro, A, Yoshimura, Y. & Morita, T. (1996). Targeted disruption of the Rad51 gene leads to lethality in embryonic mice. *Proc. Nat. Acad. Sci. USA,* **93**(13), 6236–40.

Vermeulen, K., Van Bockstaele, D. R. & Berneman, Z. N. (2003). The cell cycle: a review of regulation, deregulation and therapeutic targets in cancer. *Cell Proliferation,* **36**(3), 131–49.

Walker, D. H. & Maller, J. L. (1991). Role for cyclin A in the dependence of mitosis on completion of DNA replication. *Nature,* **354**(6351), 314–7.

Watters, D., Khanna, K. K., Beamish, H., Birrell, G., Spring, K., Kedar, P., Gatei, M., Stenzel, D., Hobson, K., Kozlov, S., Zhang, N., Farrell, a, Ramsay, J., Gatti, R. & Lavin, M.

(1997). Cellular localisation of the ataxia-telangiectasia (ATM) gene product and discrimination between mutated and normal forms. *Oncogene,* **14**(16), 1911–21.

Webber, C. & Ponting, C. P. (2005). Hotspots of mutation and breakage in dog and human chromosomes. *Genome Research,* **15**(12), 1787–97.

Weterings, E. & Van Gent, D. C. (2004). The mechanism of non-homologous end-joining: a synopsis of synapsis. *DNA Repair,* **3**(11), 1425–35.

Wooster, R., Bignell, G., Lancaster, J., Swift, S., Seal, S., Mangion, J., Collins, N., Gregory, S., Gumbs, C. & Micklem, G. (1995). Identification of the breast cancer susceptibility gene BRCA2. *Nature,* **378**(6559), 789–92.

Yaneva, M., Kowalewski, T. & Lieber, M. R. (1997). Interaction of DNA-dependent protein kinase with DNA and with Ku : biochemical and atomic-force microscopy studies. *EMBO,* **16**(16), 5098–5112.

Yue, Y. & Haaf, T. (2006). 7E olfactory receptor gene clusters and evolutionary chromosome rearrangements. *Cytogenetic and Genome Research,* **112**(1–2), 6–10.

Zhao, S., Shetty, J., Hou, L., Delcher, A., Zhu, B., Osoegawa, K., De Jong, P., Nierman, W. C., Strausberg, R. L. & Fraser, C. M. (2004). Human, mouse, and rat genome large-scale rearrangements: stability versus speciation. *Genome Research,* **14**(10A), 1851–60.

Chapter 3 Nuclear organisation and chromosome positioning

The dynamics of nuclear organisation have been the subject of many studies over the years (Reviewed by Schneider & Grosschedl, 2007). Different theories attempting to explain the arrangement of the different structures in the nucleus have been suggested. The considerations that govern chromosomes spatial arrangements in the interphase nucleus are yet to be completely understood but published evidence suggests different possibilities as to the criteria of organisation. The cell nucleus is a highly dynamic structure and organisation is not entirely regimented by the chromosomes but is also influenced by the structures involved in other nuclear events such as transcription factories.

Interest in chromosome organisation during interphase started when Rabl (1885), after working on *Salamandra maculata* anaphase-telophase chromosomes, formulated a theory suggesting that chromosomes order and neighbourhood are maintained through interphase.

Rabl observed chromosomes were orientated and positioned with centromeres at one pole of the nucleus and telomeres radiating towards the periphery. Sutton (1903) also discussed the preservation of individual chromosome characteristics through heredity and Mendelian processes in germ cells.

Later, Boveri (1909) also documented this theory working on *Ascaris megalocephala* showing the telomeres located at the nuclear envelope. Boveri also noted that chromosomes maintained positions during anaphase-telophase and suggested chromosomes were transformed into territories during interphase. The technical limitations at the time only allowed work on metaphase based techniques to visualise chromosomes. As a result, the Rabl-Boveri theory was mainly speculative and built on indirect conclusions.

It was not until many years later when advances in the technology available allowed Cremer *et al.* (1982) to document this theory using premature chromosome condensation (PCC), immuno-fluorescence experiments and micro-irradiation on Chinese hamster fibroblasts. Cremer *et al.* (1982) demonstrated that the relative positioning and the telophase orientation of chromosomes are conserved in the following interphase. It is with the advances in *in situ* hybridisation (ISH) in the early 1980's (Langer *et al.*, 1981) and

particularly of fluorescence ISH using DNA libraries (Lichter *et al.*, 1988) that interphase chromosomes could be more easily observed and the presence of chromosome territories (CTs) confirmed. However, at that time, very little was known about what actually dictates chromosome positioning. This led to attempts at characterising how the chromosomes are organised not only within the nucleus but also in relation to other structures and processes happening throughout the cell cycle.

3.1. The visualisation of chromosomes and DNA movement during interphase

The advances made in understanding nuclear architecture helped considerably with uncovering the relationship between chromosome positioning and chromosome aberration formation. However the approaches are slightly different when considering the parameters to investigate. In early studies, limitations of the techniques used (metaphase spreads) only allowed the visualisation of DNA exchanges on mitotic chromosomes.

The development of techniques such as premature chromosome condensation (PCC) assisted advances in the observations of translocations in interphase cells. This technique is based on the fusion of interphase cells with mitotic cells. The presence of mitotic chromosomes forces the interphase cell to undergo mitosis. This allows visualising the DNA exchanges at a more precise time during interphase without having to wait until the next mitosis to witness DNA exchanges. Despite the step forward achieved using this technique, account of technical considerations is important in relation to the limitations in the study of interphase nuclei. In fact, the introduction of the premature condensation is the key artefact that could lead to DNA exchanges inherent to the technique rather than the experimental conditions. The physical modifications induced by the fusion of the two cells could modify the nuclear organisation quite considerably resulting in an excess of aberrations.

The improvement of *in situ* hybridisation, especially with the development of different types of probes, has considerably helped with reducing artefacts introduced by the practical aspects of the protocol. The development of whole chromosome paints has

helped with studying the chromosome arrangement and aberration formation as well as the use of smaller probes such as telomeric probes and centromeric probes has enabled the possibility of dual painting to observe where each part of the chromosome is situated within the CT. The combination of FISH and microscopy facilitated the visualisation of aberrations without fundamentally disrupting the 3D arrangement of the chromosomes. Other advances in FISH such as the development of techniques like multiple-FISH (M-FISH) have allowed the visualisation of all the chromosomes at any given time.

Despite enabling the study of nuclear architecture, M-FISH presents some problems mainly linked to its cost and the technicality of the sample analysis. Due to the limited number of fluorochromes available in the visible spectrum of emission, the technique relies on the difference in staining intensity and requires computer software to analyse and visualise the results. The choice of the protocol adopted will vary with the aim of the experiment. M-FISH is mainly used to map the entire nucleus and maybe, for example, attempt to characterise differences in nuclear organisation between cell lines.

FISH has mainly been used to study nuclear positioning where the general approach will be similar in every case but the parameters investigated vary slightly and this influences the choice of probes. This comes from the different theories formulated as to whether the positioning is linked to the gene content or the size of the chromosome. The choice of the paint and the chromosome to target will be defined by whether the size or gene content is to be investigated. The use of a whole chromosome paint (WCP) and either a telomeric probe of a centromeric probe allows the visualisation of dynamics within the CTs. It seems that despite the possibilities of protocol optimisation, the dual painting of a given chromosome can be difficult with phenomena such as loss or absence of signal occurring. The use of two WCP targeting two different chromosomes seems to be a good approach to adopt when attempting to study chromosome positioning and aberration formation. Once again the choice of probe depending on their mode of synthesis is important to limit the presence of background staining which renders the sample processing more difficult. Probes are synthesised by PCR amplification of chromosomes using multiple primer sets targeting specific regions. In some cases the primers target Alu repeat regions leading to the presence of high quantity of repeat sequences present in chromosomes other than the one targeted. This often leads to an increase of background

staining making the sample analysis more difficult. Ideally the choice of probe should be done taking this factor into consideration.

The outcome of the analysis will depend highly on the processing and the mode of analysis of the samples. For example, the definition of the parameters one will want to compare. When trying to compare different samples and their nuclear organisation as well as the chromosome volumes/degree of condensation, the distance to the centre of the cell and the roundness factors have mainly been used (Goetze *et al.*, 2007). One of the limitations of 3D analysis comes from the shape of the object considered. Dealing with circles or regular shapes would considerably ease sample analysis. However, cells are very rarely (if ever) round and very often nuclei are of ellipsoidal shape. Moreover, it becomes more complicated with considering mapping the chromosome positioning, as the shapes considered are even more irregular. It is then necessary to introduce modifications to the data that will allow analysis without distorting the information. The use of fibroblasts for example can enable analysis using a 2-dimensional approach thanks to the flattening of the nuclei allowing analysis without considering the thickness of the cell (Sun *et al.*, 2000). However, in cases where comparisons between normal cells and a cell line are attempted, it is not always possible to treat the analysis using a 2D approach. The 3D aspect of chromosome positioning studies make them more complicated due to the addition of a third coordinate into the equation when attempting to map the chromosomes. A technique allowing the measurement of the parameters chosen in a 3D conformation is then required. This would allow the investigation of the relationship between chromosome positioning and nuclear architecture.

3.2. The different models of nuclear organisation

The constant improvements in the observations of the cell nucleus coupled with functional studies and the evolution of molecular techniques and microscopy techniques has allowed the formulation of theories as to how the nuclear components are organised throughout the cell cycle. This led to several theories and models emerging to attempt at joining the different pieces of the puzzle that make the cell nucleus.

3.2.1. The CT-IC model

This first theory was formulated following the observation of chromosome territories (CTs) and led to the investigation of the relationship between transcriptional activity and positioning within the CT. The investigation was done using double labelling of the chromosome and transcription and splicing machinery as well as the transcription products (Zirbel *et al.*, 1993). The multiple labelling of the different structures investigated showed that the transcription structures and products were localised at the periphery of the CTs. This indicated the presence of another compartment which was named the interchromosome domain (ICD).

As a result of these observations, the chromosome territory-interchromatin domain (CT-IC) model where the active genes are located at the periphery of the CTs and the non-active genes were situated more towards the interior of the domain was formulated (Cremer *et al.*, 1993). This configuration would allow better access to the active genes by the transcription complexes. The link between transcriptional activity and positioning was later documented by Kurz *et al.* (1996) who showed that the genes studied were located preferentially at the periphery of CTs regardless of the variations in transcriptional activity.

Each individual gene studied, however, presented a characteristic positioning confirming the non-random chromosomal arrangement. Further evidence for the role of the ICD in transcription was observed by Volpi *et al.* (2000) and Chambeyron *et al.* (2005) who showed that newly activated genes loop out of the CTs to be transcribed. So despite the presence of evidence of the role of the ICD in facilitation transcription a generalisation as to the degree of arrangement of the chromosome regions cannot be made since the positioning within the CT is not consistent with the level of transcription.

Mahy *et al.* (2002) showed that a gene located inside the CT can also be transcribed. With the exception of the X chromosome silencing where silenced genes migrate towards the interior of the X chromosome territory (Chaumeil *et al.*, 2006). Genes have been found to be scattered within the CTs (Verschure *et al.*, 1999) which led to the modification of the CT-IC model to include these observations. Cremer & Cremer (2001) helped define the CTs sub-division hierarchy by suggesting the presence of 1Mbp domains itself organised in

100kb loops arranged in the shape of a rosette with each loop in contact with the ICD with the active genes at the periphery and inactive genes more towards the interior regions of the 100kb pair loops. Observations of giant loops outside their CTs led to the suggestion of the random walk/giant-loop model where 3Mbp loops migrate outside the territory. The use of 3D-FISH gave further evidence of this phenomenon occurring for the gene dense region of 11p15.5 by Mahy *et al.* (2002) and Albiez *et al.* (2006). Channels and pores have also been observed within chromosome territories suggesting a flow of molecules (Verschure *et al.*, 1999; Visser *et al.*, 2000). These structural features were further confirmed by the observation of areas in the nucleus with no DNA by Fakan in 2004 suggesting the presence of an interchromatin compartment. The combination of these observations led to the belief that chromosomes territories are made of a 3D network of chromatin regions with different degrees of compaction surrounded by perichromatin regions (PR) (Cremer *et al.*, 2006). However, the exact chromatin structure of the PR, with regards to the transcription machinery, is still unclear. Also, very little intermingling is considered in the CT-IC model which led to progression towards a different approach to the CTs arrangement.

3.2.2. The lattice model

The lattice model has been more clearly defined from the observation of 10 nm and 30 nm fibres (Dehghani *et al.*, 2005) using electron spectroscopic imaging (ESI). ESI has allowed the selective observation of decondensed and condensed chromatin regions.

The fibres of a given chromosome are still positioned in a specific nuclear area and may intermingle with fibres of another chromosome forming a network of fibres. As a result inter- and intra-chromosomal spaces form an almost continuous network of fibres. The evolution of this model originated from the observation of the hierarchy of structures within the CTs using both light and electron microscopy (Belmont & Bruce 1994). Immediately following mitosis, DNA decondensation takes place until S-phase in preparation of DNA replication (Belmont & Bruce, 1994). Chromonema fibres of 100-130-nm of diameter are dominant at early G_1 further decondensing into 60-80-nm fibres themselves built of 10 nm and 30 nm fibres at late G_1 (Belmont & Bruce, 1994). This

model contradicts the CT-IC model due to the absence of an observable and clear compartment between the CTs as the ICD is filled by arrangements of 10 nm and 30 nm fibres in the lattice model.

Important intermingling between territories occurs during interphase (Branco & Pombo, 2006). The level of intermingling between chromosomes varies with the level of transcription as well as the degree of chromatin compaction (Branco & Pombo, 2006). A relationship was established between a high gene density and decondensed chromatin, however no evidence for a relation between levels of decondensed chromatin and high gene expression was found (Gilbert *et al.*, 2004).

The data obtained by Branco & Pombo (2006) also suggests that the chromatin is condensed into structures of a higher order than 10 or 30 nm fibres confirming the observations of Belmont & Bruce (1994). The 3D network connecting the chromosomes and the different fibres would be coherent with the accessibility of the whole nucleus by macromolecules (Verschure *et al.*, 2003). Despite the better understanding of the phenomena involved in the organisation of territories neither of these models addresses long-range interactions. This led to the formulation of the third model, the interchromosomal network (ICN) model.

3.2.3. The ICN model

This model focuses more extensively on long distance interaction taking into consideration the parameters in the previously described lattice model. The evidence of interactions between distal loci belonging to either the same chromosome or more than one chromosome suggests the presence of yet another higher level of organisation.

The phenomenon of looping has been observed in the β-globin locus where the control region interacts with domains 50kb away (Tolhuis *et al.*, 2002). Other interactions between genes situated on different chromosomes, such as the X inactivation centres, have been characterised and identified (Bacher *et al.*, 2006; Xu *et al.*, 2006).

These pieces of evidence tend to corroborate findings in chromatin motion studies aimed at defining the characteristics regulating the movement of chromatin. It has been

observed that chromatin generally moves 0.4 µm by constrained diffusion (Abney *et al.*, 1997; Gasser, 2002) but can, in some cases, cover distances of 1.5 µm (Chubb *et al.*, 2002). The presence of long distance interactions is in accordance with phenomena observed during radiation studies where complex DNA exchanges are observed and that confirm an important level of intermingling.

Establishing the level of intermingling can help understand the potential to exchange DNA material during translocation following irradiation. Branco & Pombo (2006) failed to detect a difference in DNA concentration between the peripheral region and the interior regions on the CTs giving evidence of a network of fibres as stated in the lattice model. This would then mean that any chromosome with DNA looping out of the territory is likely to be intermingled with CTs in its vicinity; however this still fails to explain the "long distance" exchange seen in the radiation studies. Studies have also established evidence of a link between levels of transcription and the degrees of intermingling. As a result it has been suggested that transcription factories are key factors in stabilising interchromatin interactions meaning transcription is responsible for CT organisation within the nucleus and also explains the difference in organisation between different tissues (Tanabe *et al.*, 2002) and different species (Mora *et al.*, 2006).

3.3. Replication/transcription factories

The term factories when applied to DNA replication and transcription, describes the spatial coordination of the different steps needed for the generation of mature mRNAs happening at specific nuclear sites (Cook, 1999; Jackson *et al.*, 1993). Transcription factors and RNA polymerase II components are found in compartments called fibrillar centres (fcs) whereas newly synthesized transcripts are located on the surface of the fcs in dense fibrillar components (dfcs) (Jackson, 2005). The presence of 500-1000 RNA polymerase II active sites per haploid chromosome set has been observed *in vitro* in proliferating mammalian cells (Jackson *et al.*, 1998).

Most of the main steps of the mRNA maturation take place in the transcription centres. Transcription sites are located at the surface of chromosomal subdomains. Newly synthesized RNA is located in interchromatin space inside and around the territories

(Verschure *et al.*, 1999). In these structures the mRNA is spliced, poly-A tailed, capped, bound to proteins responsible for the transport to the cytoplasm and quality controls of the mRNA structure integrity (Hieronymus & Silver, 2004; Hirose & Manley, 1998; Iborra *et al.*, 2004; McCracken *et al.*, 1997; Shuman, 1997).

A whole range of proteins are involved in the dynamics of transcription factories. Each protein has a different function and belongs to complexes such as repair complexes, DNA surveillance or signalling complexes. Cross-talk between DNA repair, RNA synthesis and DNA replication ensures regulation of chromatin function and the cohesion between the different structures involved in these mechanisms. Any region of the DNA can be engaged into either replication or transcription at any given time (Pliss *et al.*, 2005).

3.4. Approaches investigating chromosome positioning within the nucleus

As the nucleus is a highly dynamic entity with different levels of organisation, it is logical to want to understand which parameters could be key in chromosome positioning. However, it is not exactly straight forward as it seems many parameters could be considered.

There are different types of chromatin movements based on their range. The most common are short range movements (~ 1 μm) and can be observed in different types of nuclei. These movements appear to be directly linked with the chromatin fibre dynamics involved in the different processes such as transcription or replication. They have the same order of size in all nuclei but have different implications linked to the size of the nucleus considered. In other words a 1 μm movement within a small nucleus will have a different impact compared with a 1 μm movement within a bigger nucleus.

Longer range movements have also been observed following photobleaching experiments (Walter *et al.*, 2003; Gerlich *et al.*, 2003). However, they appear to be less common and very dependent on the actin/myosin system. In fact the short range movements timings involved, appear to be in the order of seconds whereas longer range movement occurs over several minutes. Some long range movements such as for telomere and centromere

relocation are more likely to be chromatin reorganisation because they are taking place across several steps of the cell cycle.

Advances in chromosomes painting have allowed further characterisation of territories. The positioning was initially studied with the chromosomes own characteristics in mind where similar approaches were used to study different characteristics. On one hand, chromosomes were believed to position according to size where due to physical constraints, larger chromosomes were located towards the periphery and smaller chromosomes located towards the nuclear centre. On the other hand, chromosomes were believed to position according to their gene content (Croft *et al.*, 1999; Bridger *et al.*, 2000; Tanabe *et al.*, 2002). As a result, studies have looked at the influence of size on the CT positioning (Sun *et al.*, 2000; Cremer & Cremer 2001; Bolzer *et al.*, 2005) and found that smaller chromosomes were located more towards the nuclear interior and larger chromosomes towards the periphery. Similarly, chromosomes with lower gene density were found to locate at the periphery (Croft *et al.*, 1999; Boyle *et al.*, 2001).

This was also supported by Murmann *et al.* (2005) as well as Walter *et al.* (2003) when looking at the difference in positioning of chromosome 18 (HSA 18) and chromosome 19 (HSA 19) which have similar sizes but different genes content. Chromosome 18 (HSA 18) and chromosome 19 (HSA 19) have similar sizes but different gene density. As a result, HSA 18 and HSA 19 were used to attempt at establishing whether gene content could influence chromosome positioning. HSA 19 was found to be located more towards the nucleus centre whereas HSA 18 was found to be located more towards the periphery (Croft *et al.*, 1999). HSA 19 has been reported to occupy a larger volume than HSA 18 despite the order of their gene content being reversed with HSA 18 gene content being bigger than HSA 19 gene content (Croft *et al.*, 1999). However, HSA 18 was found to locate towards the centre positions within the nucleus during quiescence before returning to a peripheral position during the following G_1 (Bridger *et al.*, 2000).

Gene density might also dictate chromosome positioning as seen In lymphocytes where gene dense regions are located towards the centre of the nucleus and gene poor regions are located at the periphery (Boyle *et al.*, 2001).

It appears that gene content and size are not the only parameters that may influence chromosome positioning; replication timing could play a role in the positioning of chromosomes during interphase. During the different stages of interphase, chromosomes will be relocalised where needed in order to facilitate the access to the DNA by the transcription machinery. It appears that chromosomes arrange themselves in subchromosomal domains and subtly decondense (Berezney *et al.*, 1996; Berezney *et al.*, 1995; Visser *et al.*, 1998). An example illustrating this point is that early and mid-replicating chromatin was found throughout the territory in both Xi and Xa and also in chromosome 8 (Visser *et al.*, 1998).

Interestingly, early replicating chromatin was distributed differently between the two X chromosomes. Where it was found everywhere in Xa, the early replicating chromatin appeared to be located at the surface for Xi. Replication timing could be responsible for the location and time of replication of a gene of interest.

Chromosome positioning appears to be tissue specific and the difference seen in distances from the centre of the nucleus are not due to the changes in cell size between the different tissues (Parada *et al.*, 2004). For example Parada *et al.* (2004) found that chromosomes 5 and 6 are more often in close proximity than 12 and 15 in hepatocytes whereas in lymphocytes chromosomes 12 and 15 appear to be in closer proximity. This results in hepatocytes being prone to translocation between 5 and 6 and between chromosome 1 and 15 in lymphocytes. This has also been observed by Roix *et al.* (2003). This adds to the observations of Tanabe *et al.* (2002) that chromosome positioning is non-random and evolutionary conserved.

When considering the parameters that govern chromosome positioning, it appears as though size, gene content, cell type, species and replication timing are involved in dictating chromosome positioning during interphase (Croft *et al.*, 1999; Bridger *et al.*, 2000; Sun *et al.*, 2000; Boyle *et al.*, 2001 Cremer & Cremer 2001; Parada *et al.*, 2004).

These have been studied in unperturbed cells and nuclei. As described in Chapter 1 and 2, IR exposure results in significant perturbations in the cell cytoplasm and nucleus. It is not clear to what extent exposure to IR perturbs the dynamics of chromosome positioning in normal and cancerous cells.

AIMS

The aims of this study were:

- To develop methods for 3D analysis and visualisation of cell nuclei.

- Characterise nuclear properties of chromosome 1 and 2 in both normal primary human fibroblasts and abnormal bladder carcinoma (RT112) untreated cells.

- Characterise nuclear organisation of chromosome 1 and 2 in irradiated normal primary human fibroblasts and abnormal bladder carcinoma cells (RT112).

REFERENCES

Abney, J. R., Cutler, B., Fillbach, M. L., Axelrod, D. & Scalettar, B. A. (1997). Chromatin dynamics in interphase nuclei and its implications for nuclear structure. *J. Cell Biol,* **137**, 1459–1468.

Albiez, H., Cremer, M., Tiberi, C., Vecchio, L., Schermelleh, L., Dittrich, S., Küpper, K., Joffe, B., Thormeyer, T., Von Hase, J., Yang, S., Rohr, K., Leonhardt, H., Solovei, I., Cremer, C., Fakan, S. & Cremer, T. (2006). Chromatin domains and the interchromatin compartment form structurally defined and functionally interacting nuclear networks. *Chromosome Research* , **14**(7), 707–33.

Bacher, C. P., Guggiari, M., Brors, B., Augui, S., Clerc, P., Avner, P., Eils, R. & Heard, E. (2006). Transient colocalization of X-inactivation centres accompanies the initiation of X inactivation. *Nature Cell Biology*, **8**(3), 293–9.

Belmont, A. S. & Bruce, K. (1994). 'Visualization of G1 chromosomes: a folded, twisted, supercoiled chromonema model of interphase chromatid structure. *The Journal of Cell Biology*, **127** (2), 287–302.

Berezney, R., Mortillaro, M., Ma, H., Meng, C., Samarabandu, J., Wei, X., Somanathan, S., Liou, W. S., Pan, S. J. & Cheng, P.C. (1996). Connecting nuclear architecture and genomic function. *Journal of Cellular Biochemistry*, **62** (2), 223–6.

Berezney, R., Mortillaro, M. J., Ma, H., Wei, X. & Samarabandu, J. (1995). The nuclear matrix: a structural milieu for genomic function. *International Review of Cytology*, **162**A, 1–65.

Bolzer, A., Kreth, G., Solovei, I., Koehler, D., Saracoglu, K., Fauth, C., Müller, S., Eils, R., Cremer, C., Speicher, M. R. & Cremer, T. (2005). Three-dimensional maps of all chromosomes in human male fibroblast nuclei and prometaphase rosettes. *PLoS Biology*, **3**(5), e157.

Boveri, T. (1909). Die Blastomerenkerne von Ascaris megalocephala und die Theorie der Chromosomenindividualitat. *Arch Zellforschung*, **3**, 181–186.

Boyle, S., Gilchrist, S., Bridger, J. M., Mahy, N. L., Ellis, J. A. & Bickmore, W. A. (2001). The spatial organization of human chromosomes within the nuclei of normal and emerin-mutant cells. *Human Molecular Genetics*, **10**(3), 211–9.

Branco, M. R. & Pombo, A. (2006). Intermingling of chromosome territories in interphase suggests role in translocations and transcription-dependent associations. *PLoS biology*, **4**(5), e138.

Bridger, J. M., Boyle, S, Kill, I. R. & Bickmore, W. A. (2000). Re-modelling of nuclear architecture in quiescent and senescent human fibroblasts. *Current Biology,* **10**(3), 149–52.

Chambeyron, S., Da Silva, N. R., Lawson, K. A. & Bickmore, W. A. (2005) Nuclear re-organisation of the Hoxb complex during mouse embryonic development. *Development*, **132**(9), 2215–23.

Chaumeil, J., Le Baccon, P., Wutz, A. & Heard, E. (2006). A novel role for Xist RNA in the formation of a repressive nuclear compartment into which genes are recruited when silenced. *Genes & Development*, **20**(16), 2223–37.

Chubb, J.R., Boyle, S., Perry, P. & Bickmore, W. A. (2002). Chromatin Motion Is Constrained by Association with Nuclear Compartments in Human Cells. *Current Biology*, **12**(6), 439–445.

Cook, P. R. (1999). The Organization of Replication and Transcription. *Science*, **284**(5421), 1790–1795.

Cremer, T. & Cremer, C. (2001). Chromosome territories, nuclear architecture and gene regulation in mammalian cells. *Nature reviews. Genetics*, **2**(4), 292–301.

Cremer, T., Cremer, C., Baumann, H., Luedtke, E. K., Sperling, K., Teuber, V. & Zorn, C. (1982). Rabl's model of the interphase chromosome arrangement tested in Chinese

hamster cells by premature chromosome condensation and laser-UV-microbeam experiments. *Human Genetics*, **60**(1), 46–56.

Cremer, T., Kurz, A., Zirbel, R., Dietzel, S., Rinke, B., Schrock, E., Speicher, M. R., Mathieu, U., Jauch, A., Emmerich, P., Scherthan, H., Ried, T., Cremer, C. & Lichter, P. (1993). Role of Chromosome Territories in the Functional Compartmentalization of the Cell Nucleus. *Cold Spring Harb Symp Quant Biol*, **58**, 777–792.

Cremer, T., Cremer, M., Dietzel, S., Müller, S., Solovei, I. & Fakan, S. (2006). Chromosome territories--a functional nuclear landscape. *Current Opinion in Cell Biology*, **18**(3), 307–16.

Croft, J. A., Bridger, J. M., Boyle, S., Perry, P., Teague, P. & Bickmore, W. A. (1999). Differences in the localization and morphology of chromosomes in the human nucleus. *The Journal of Cell Biology*, **145**(6), 1119–31.

Dehghani, H., Dellaire, G. & Bazett-Jones, D.P. (2005). Organization of chromatin in the interphase mammalian cell. *Micron*, **36**(2), 95–108.

Fakan, S. (2004). The functional architecture of the nucleus as analysed by ultrastructural cytochemistry. *Histochemistry and Cell Biology*, **122**(2), 83–93.

Gasser, S. M. (2002). Visualizing chromatin dynamics in interphase nuclei. *Science* , **296**(5572), 1412–6.

Gerlich, D., Kalbfuss, B., Daigle, N., Eils, Roland & Ellenberg, J. (2003). Global Chromosome Positions Are Transmitted through Mitosis in Mammalian Cells. *Cell*, **112**, 751–764.

Gilbert, N., Boyle, S., Fiegler, H., Woodfine, K., Carter, N. P. & Bickmore, W. A. (2004). Chromatin architecture of the human genome: gene-rich domains are enriched in open chromatin fibers. *Cell*, **118**(5), 555–66.

Goetze, S., Mateos-Langerak, J., Gierman, H. J., De Leeuw, W., Giromus, O., Indemans, M. H. G., Koster, J., Ondrej, V., Versteeg, R. & Van Driel, R. (2007). The three-

dimensional structure of human interphase chromosomes is related to the transcriptome map. *Molecular and Cellular Biology*, **27**(12), 4475–87.

Hieronymus, H. & Silver, P. A. (2004). A systems view of mRNP biology. *Genes & Development*, **18**(23), 2845–60.

Hirose, Y. & Manley, J. L. (1998). RNA polymerase II is an essential mRNA polyadenylation factor. *Nature*, **395**(6697), 93–6.

Iborra, F. J., Escargueil, A. E., Kwek, K. Y., Akoulitchev, A. & Cook, P. R. (2004). Molecular cross-talk between the transcription, translation, and nonsense-mediated decay machineries. *Journal of Cell Science*, **117**(6), 899–906.

Jackson, D. A., Hassan, A. B., Errington, R. J. & Cook, P. R. (1993). Visualization of focal sites of transcription within human nuclei. *EMBO*, **12**(3), 1059–65.

Jackson, D. A. (2005). The amazing complexity of transcription factories. *Briefings in Functional Genomics & Proteomics*, **4**(2), 143–57.

Jackson, D. A., Iborra, F. J., Manders, E. M. & Cook, Peter R. (1998). Numbers and Organization of RNA Polymerases, Nascent Transcripts, and Transcription Units in HeLa Nuclei. *Molecular Biology of the Cell*, **9**(6), 1523–1536.

Kurz, A., Lampel, S., Nickolenko, J. E., Bradl, J., Benner, A., Zirbel, R. M, Cremer, T & Lichter, P. (1996). Active and inactive genes localize preferentially in the periphery of chromosome territories. *The Journal of Cell Biology*, **135**(5), 1195–205.

Langer, P. R., Waldrop, A. A. & Ward, D. C. (1981). Enzymatic Synthesis of Biotin-Labeled Polynucleotides: Novel Nucleic Acid Affinity Probes. *Proc. Nat. Acad. Sci. USA*, **78**(11), 6633–6637.

Lichter, P, Cremer, T, Borden, J., Manuelidis, L. & Ward, D. C. (1988). Delineation of individual human chromosomes in metaphase and interphase cells by in situ suppression hybridization using recombinant DNA libraries. *Human Genetics*, **80**(3), 224–34.

Mahy, N. L, Perry, P. E. & Bickmore, W. A. (2002). Gene density and transcription influence the localization of chromatin outside of chromosome territories detectable by FISH.'. *The Journal of Cell Biology*, **159**(5), 753–63.

McCracken, S., Fong, N., Yankulov, K., Ballantyne, S., Pan, G., Greenblatt, J., Patterson, S. D., Wickens, M. & Bentley, D. L. (1997). The C-terminal domain of RNA polymerase II couples mRNA processing to transcription. *Nature*, **385**(6614), 357–61.

Mora, L., Sánchez, I., Garcia, M. & Ponsà, M. (2006). Chromosome territory positioning of conserved homologous chromosomes in different primate species. *Chromosoma*, **115**(5), 367–75.

Murmann, A. E., Gao, J., Encinosa, M., Gautier, M., Peter, M. E., Eils, R., Lichter, P. & Rowley, J. D. (2005). Local gene density predicts the spatial position of genetic loci in the interphase nucleus.'. *Experimental Cell Research*, **311**(1), 14–26.

Parada, L. A., Mcqueen, P. G. & Misteli, T. (2004). Tissue-specific spatial organization of genomes. *Genome Biology*, ***5**: R44.*

Pliss, A., Koberna, K., Vecerová, J., Malínský, J., Masata, M., Fialová, M., Raska, I. & Berezney, Ronald (2005). Spatio-temporal dynamics at rDNA foci: global switching between DNA replication and transcription. *Journal of Cellular Biochemistry*, **94**(3), 554–65.

Rabl, C. (1885). Über Zelltheilung. in *Morphologisches Jahrbuch.* Gengenbaur, Carl, 214–330.

Roix, J. J., McQueen, P. G., Munson, P. J., Parada, L. A. & Misteli, T. (2003). Spatial proximity of translocation-prone gene loci in human lymphomas. *Nature Genetics*, **34**(3), 287–91.

Schneider, R. & Grosschedl, R. (2007). Dynamics and interplay of nuclear architecture, genome organization, and gene expression. *Genes & Development*, **21**(23), 3027–43.

Shuman, S. (1997). Origins of mRNA identity: capping enzymes bind to the phosphorylated C-terminal domain of RNA polymerase II. *Proc. Nat. Acad. Sci. USA*, **94**(24), 12758–60.

Sun, H. B., Shen, J. & Yokota, H. (2000). Size-Dependent Positioning of Human Chromosomes in Interphase Nuclei. *Biophysical Journal*, **79**(1), 184–190.

Sutton, W. S. (1903).'The Chromosomes in Heredity. *Biological Bulletin*, **4**(5), 231.

Tanabe, H., Habermann, F. A, Solovei, I., Cremer, M. & Cremer, T. (2002). Non-random radial arrangements of interphase chromosome territories: evolutionary considerations and functional implications. *Mutation Research*, **504**(1–2), 37–45.

Tolhuis, B., Palstra, R.-J., Splinter, E., Grosveld, F. & De Laat, W. (2002). Looping and Interaction between Hypersensitive Sites in the Active β-globin Locus. *Molecular Cell*, **10**(6), 1453–1465.

Verschure, P. J., Van Der Kraan, I, Manders, E. M. & Van Driel, R. (1999). Spatial relationship between transcription sites and chromosome territories. *The Journal of Cell Biology*, **147**(1), 13–24.

Verschure, P. J., Van der Kraan, I., Manders, E. M., Hoogstraten, D., Houtsmuller, A. B. & Van Driel, R. (2003). Condensed chromatin domains in the mammalian nucleus are accessible to large macromolecules. *EMBO Reports*, **4**(9), 861–6.

Visser, A. E., Eils, R, Jauch, A., Little, G., Bakker, P. J., Cremer, T. & Aten, J. A. (1998). Spatial distributions of early and late replicating chromatin in interphase chromosome territories. *Experimental Cell Research*, **243**(2), 398–407.

Visser, A. E., Jaunin, F., Fakan, S & Aten, J. A. (2000). High resolution analysis of interphase chromosome domains. *Journal of Cell Science*, **113**, 2585–93.

Volpi, E. V., Chevret, E., Jones, T., Vatcheva, R., Williamson, J., Beck, S., Campbell, R. D., Goldsworthy, M., Powis, S. H., Ragoussis, J., Trowsdale, J. & Sheer, D. (2000). Large-scale chromatin organization of the major histocompatibility complex and other

regions of human chromosome 6 and its response to interferon in interphase nuclei. *Journal of Cell Science*, **113**(9), 1565–1576.

Walter, J., Schermelleh, L., Cremer, M., Tashiro, S. & Cremer, Thomas (2003). Chromosome order in HeLa cells changes during mitosis and early G1, but is stably maintained during subsequent interphase stages. *The Journal of Cell Biology*, **160**(5), 685–97.

Xu, N., Tsai, C.-L. & Lee, J. T. (2006). Transient homologous chromosome pairing marks the onset of X inactivation. *Science*, **311**(5764), 1149–52.

Zirbel, R. M., Mathieu, U. R., Kurz, A., Cremer, T. & Lichter, P. (1993). Evidence for a nuclear compartment of transcription and splicing located at chromosome domain boundaries. *Chromosome Research*, **1**(2), 93–106.

Chapter 4 Material and methods

4.1. Cell lines

The primary fibroblast cell lines had been established at the Institute of Cancer Research from anonymous normal breast tissue of women aged 25 to 35. The tissue were cut into $0.5mm^3$ pieces and incubated in cell culture flasks with a small amount of Dulbecco's modified Eagles medium (DMEM) allowing the cells to grow out of the tissue and form a monolayer at the bottom of the cell culture flask.

The human bladder carcinoma cells (RT112) were kindly provided by Professor J. Masters (Institute of Urology, University College London). All the work undertaken in this project was done on a single clone (RT112/C2) previously isolated by serial dilution.

4.2. Methods

4.2.1. Cell culture

4.2.1.1. Fibroblasts

The fibroblasts were cultured in Dulbecco's modified Eagles medium (DMEM) supplemented with 10% (v/v) Foetal bovine serum (FBS), penicillin-streptomycin (40 U penicillin, 40 μg streptomycin per 100 ml), 1% (v/v) non-essential amino-acids and 2 mM L-glutamine. The cells were grown at 37°C in non-vented flasks in a 5% (v/v) CO_2 in air environment. The cell stock solution was maintained between 10^5 and 10^6 cells/ml.

4.2.1.2. RT112

The RT112 cells were cultured in Roswell Park Memorial Institute medium (RPMI) 1640 supplemented with 15% (v/v) Foetal bovine serum, and penicillin-streptomycin (40 U penicillin, 40 μg streptomycin per 100 ml). The cells were grown at 37°C in filter capped flasks in a 5% (v/v) CO_2 environment. The cell stock was also maintained around 10^5 cells/ml.

4.2.2. Single cell preparation

4.2.2.1. Fibroblasts

The medium in the flask was emptied into a diluted bleach solution for disposal. The flasks were then rinsed with 3 ml of Trypsin- Ethylenediaminotetraacetic acid (EDTA) (0.05 % w/v) avoid any interference from the proteins present in the FBS from the culture medium on the action of the trypsin and the monolayer was dispersed with an extra 1 ml of trypsin-EDTA. Once the trypsin- EDTA had been added, the cells were incubated at 37°C for between 1 and 3 minutes in order to allow all of them to detach. Trypsin is used in this procedure due to its protease activity specifically breaking the bonds between arginine and lysine at the carboxyl group. The trypsin solution is supplemented with EDTA (0.05% w/v) acting as a chelating agent and dissociating links such as tight junctions (Doyle & Griffiths, 2000). The detachment process was monitored using an inverted microscope. Towards the end of the incubation period, the flasks were gently knocked in order to help with generating the single cell suspension. The cell suspension was then gently aspirated, deposited into a disposable conical based centrifuge tube and the volume made up to 10 ml with culture medium in order to dilute the trypsin. The tubes were then centrifuged at 201x g for 5 minutes. The supernatant was then discarded and the pellet re-suspended with the chosen amount of media depending on the experiment following directly after this procedure.

4.2.2.2. RT112

The medium in the flask was emptied into a diluted bleach solution for disposal. The flasks were then rinsed with 5 ml of Trypsin-EDTA (0.05% w/v) to prevent inactivation of the trypsin by the proteins present in the FBS found in the culture medium and the monolayer was dispersed with an extra 1 ml of trypsin-EDTA. Once the trypsin had been added, the flasks were incubated at 37°C for 20 minutes in order to allow all the cells to detach. The rest of the procedure was exactly as the one described for the fibroblasts.

4.2.3. Cell count for both cell lines

Cells were washed and the monolayer subjected to trypsin treatment as described above and then re-suspended in 1 ml of DMEM medium. After mixing, the sample was added onto both counting chambers of an Improved Neubauer haemocytometer with the coverslip already in place. The number of viable cells was counted in 0.1 µl under a light microscope at 10x magnification and the cell concentration calculated to allow dilutions for further experiments such as growth curves and clonogenic assays.

4.2.4. Growth curve for both cell lines

The cells were plated at 1 x 10^5 cells per 25 cm^2 culture flasks. Every day one flask would be counted at the same time of the day in order to allow homogeneity and regularity in the cell counts.

The monolayer disruption process was performed in a similar way to the one described above. Firstly, the flask was emptied and rinsed with 5 ml of trypsin. The monolayer was then subjected to a trypsin treatment using 5 ml of trypsin-EDTA (0.05%) for up to 3 minutes with detachment monitored regularly with an inverted microscope. The single cell suspension was then transferred into a conical centrifuge tube and the flask rinsed with an extra 5 ml of DMEM in order to allow the collection of the highest number of cells possible. The tubes were centrifuged for 3 minutes at 201x g. The supernatant was discarded and the pellet re-suspended in 2 ml of medium.

The cells were counted for 15 days and the cell count values were plotted against time to determine the doubling time and growth rate constant.

4.2.5. Cell preservation for both cell lines

The cells were prepared for cryo-preservation using freshly made medium supplemented with 20% (v/v) Foetal bovine serum (FBS) and 10% (v/v) dimethylsulfoxide (DMSO) kept cold over ice. The freezing process was done in two steps. The cells were aliquoted into 1.5 ml labelled cryovials and placed in a cryo 1°C freezing container filled

with Isopropanol. The first step involved cooling down the vials to -80°C for 24 to 48 hours. The use of isopropanol with a cooling rate of 1°C/minute allowed a slow but steady cooling. Used in conjunction with the cryoprotective abilities of DMSO, it allows the freezing of cells limiting the formation of ice crystals and reducing damage to the samples. After 24 to 48 hours in the -80°C freezer, the samples were transferred into a liquid nitrogen freezer to be stored until future use.

One week later, a vial was removed and quickly defrosted in a 37°C waterbath. The content was emptied into 9 ml of culture media in a 25 cm^2 non-vented capped flask. The cells were then checked for attachment at the end of that day and the following day. The cryopreservation was deemed successful if the cells covered more than 50% of the flask. This procedure was also used to defrost the remaining vials when needed.

4.2.6. Cell irradiation

The flasks containing fibroblasts and RT112 cells in confluence were trypsinised, counted, aliquoted into tubes maintained on ice to be transported to the St Luke's Cancer Centre, Guildford, Surrey.

Cells were irradiated on ice using a Pantak 250 kV X-ray machine at St Luke's Cancer Centre, Guildford, Surrey. Irradiations were performed at 250 kV and a dose rate of 1 gray/minute. For the study of nuclear architecture following irradiation, the cells received the equivalent of 8 gy.

Once the irradiation was done the cells were transported on ice back to the Kingston University laboratory. The use of ice was done in order to maintain the cells in a similar state throughout the irradiation. At the laboratory, the cells were resuspended in media and seeded into the glass chambers on the slides in petri dishes. The petri dishes were then incubated at 37°C and fixed at 30 min, 1 h, 2 h, 4 h and 24 h from the start of the incubation.

4.2.7. *In situ* hybridisation pre-treatments

4.2.7.1. Slide preparation

Slides were washed with anti-bacterial soap, rinsed, thoroughly dried and stored in 100 % ethanol in order to ensure sterile conditions. Glass rings were prepared following the same procedure and kept in the 100 % ethanol too. The slides and rings were then dried in a Laminar flow hood on a sterile surface. Two rings were stuck to the slides using nail varnish in order to designate growing areas. The nail varnish was allowed to dry for at least 5 minutes before the slides were put in empty petri dishes to facilitate incubation at 37°C.

A cell suspension (0.5 ml) at 10^3 cells/ml was seeded into each chamber. The cells were then allowed to attach to the slides for times ranging between 20 minutes and 24 hours before proceeding to fixation.

4.2.7.2. Slide fixation

The slides were fixed in freshly prepared fixative solution made at a ratio of 3:1 (v/v) of methanol and acetic acid. The fixation time was a minimum of 30 minutes with times extending to overnight (18 hours) fixation. The slides were dried and rinsed with non-sterile PBS prior to subjecting them to Fluorescence *in situ* hybridisation (FISH).

Alternatively, the slides were fixed in 4% paraformaldehyde for 10 minutes before being subjected to pre-treatments.

During the experiment investigating changes occurring in cell nuclei organisation following irradiation, the slides were fixed 30 minutes, 1 hour, 2 hours, 4 hours, 24 hours, and 48 hours following plating on the slides.

4.2.7.3. Slides pre-treatment

The initial pre-treatment used was the one specified by the probe supplier. In the case of Star*FISH© probes, the dried slides were pre-treated by an initial dehydration using 100% ethanol for 5 minutes at room temperature. The slides were then dipped in

pepsin solution (1 % stock solution diluted by 1/1000 in 10 mM HCl) for up to 5 minutes and washed in 2x saline-sodium citrate (SSC) solution (20x SSC stock solution was made of 3 M sodium chloride and 300 mM sodium citrate with pH adjusted to 7 with HCl) for 1 minute. This dual step was repeated twice. After a distilled water rinse, the slides were serially dehydrated for 2 minutes in respectively 70% (v/v) ethanol, 70%, 90%, 90%, and finally 5 minutes in 100% ethanol. The slides were then aged for 60 minutes at 65°C. This step allows a better attachment of the material to the slide and helps with increasing the chromosome structure resistance to subsequent DNA denaturation.

A number of additional pre-treatments described in the literature as well as different aging times were also investigated in order to increase the success rate of the *in situ* hybridisation. The additional solutions needed for these procedures are described in Table 4.1.

Solution type	Concentration	Diluent	Reference
Paraformaldehyde	4%	PBS	Visser *et al.* 1998
RNAse	100ug/ml	2XSSC	Scheuermann *et al.* 2004
Triton-X	0.50%	PBS	Visser *et al.* 1998
Saponin	0.50%	PBS	Visser *et al.* 1998
Glycerol	20%	PBS	Visser *et al.* 1998
HCl	0.1M	ddH2O	Cremer *et al* .2001

Table 4.1: List of the different pre-treatment solutions used and their concentrations.

Slides were subjected to pre-treatments as described in Cremer *et al.* (2001) and Visser *et al.* (1998) in order to obtain some hybridisation. Briefly, the slides were fixed in 4% paraformaldehyde for 10 minutes before being incubated in 0.5% (v/v) Triton-X100 solution for 20 minutes, 20% glycerol for 30 minutes, frozen in liquid nitrogen and thawed before finally be subjected to pepsin permeabilisation for 5 minutes.

An alternative and slightly less aggressive pre-treatment was also tested in order to prevent the loss of samples. This treatment, as described in Vershure *et al.* (1999) involved rinsing the slides with PBS prior to a fixation with 4% paraformaldehyde, Triton-

X100 treatment for 10 minutes followed by saponin treatment for 10 minutes with a final PBS wash prior to *in situ* hybridisation.

Finally, slides aging times and temperature was also investigated in order to establish their implication in the outcome of the hybridisation. During the aging stage in the Star*FISH© protocol, slides were subjected to temperatures of 45°C or 65°C for either 30 or 60 minutes.

In the case of Poseidon™ probes the pre-treatment used was the one recommended by the supplier. In brief, it consisted of incubating the freshly fixed samples in 2x SSC/0.5% igepal (pH 7.0) at 37°C for 15 minutes followed by serial dehydration in 70%, 85% and 100% ethanol for 1 minute each time. Finally, the slides were air dried at room temperature prior to codenaturation- hybridisation. An additional step involving a pepsin treatment was also performed prior to the serial dehydration.

Finally, the pre-treatment chosen to be implemented routinely during the remainder of the project involved incubation for 5 minutes in PBS at 37°C followed by 10 minutes in pepsin solution at 37°C and 15 minutes in 2x SSC/0.5% igepal (pH 7.0) at 37°C. The slides were then serially dehydrated and underwent *in situ* hybridisation.

4.2.8. Fluorescence *in situ* hybridisation (FISH)

4.2.8.1. FISH using Star*FISH© probes

The initial protocol used was the one provided by the supplier. Following pre-treatment, the denaturation was performed by incubating the slides in denaturation solution (70% formamide in 2x SSC) at 65°C for 1½ - 2 minutes. The slides were then quenched in ice cold ethanol (70%) for 4 minutes and subjected a serial dilution consisting of 2 minutes in respectively 70% (v/v) ethanol, 70%, 90%, 90%, and finally 5 minutes in 100% ethanol. The slides were then dried at room temperature before hybridisation. Once dried, 15 µl of the ready-to-use probes were applied to the slides, covered with a 22 x 22 mm coverslip and any remaining air bubbles removed by applying gentle pressure on the coverslip. The hybridisation areas were then sealed using rubber solution and incubated overnight in a pre-warmed humidified chamber at 37°C.

To proceed to the stringency washes, 2 coplin jars with stringency washes (50% Formamide in 1x SSC), 3 coplin jars with 1x SSC and 1 coplin jar with detergent wash solution (Detergent DT in 4x SSC) were heated in a water bath to 45°C. The rubber solution was removed from the slides and the slides then placed in 1x SSC solution to allow the coverslip to gently slide off without damaging the preparation. The slides were then placed successively in each of the Stringency wash solutions for 5 minutes, followed by 5 minutes in each on the 2 remaining 1x SSC solutions. Finally, the slides were incubated for 4 minutes in the detergent wash solution.

4.2.8.2. FISH using Poseidon™ probes

The initial protocol used was the one provided by the Poseidon™ probes supplier. The probes were supplied concentrated 5x and were diluted according to manufacturer guidelines where 2 µl of the probe was added to 8 µl of the hybridisation buffer supplied with the probes. In the event of combining several probes, 2 µl of each probe was combined with hybridisation buffer to make up to a final volume of 10 µl.

The co-denaturation was done by application of the 10 µl of the probe preparation to the sample. The hybridization zone was then covered with a 22 x 22 mm coverslip and sealed with rubber solution. The slides were then denatured for between 5 and 10 minutes at 75°C and hybridised overnight at 37°C using a Thermobrite™ half automated hybridization machine

Following the removal of the rubber solution, the post-hybridisation treatment was done by washing the slides with 2x SSC/0.1% igepal for 2 minutes at room temperature to ease the coverslips off. The slides were then washed with 0.4x SSC/0.3% igepal at 72°C for 2 minutes directly followed by 1 minute with 2x SSC/0.1% igepal at room temperature. The samples were then serially dehydrated in 70%, 85% and 100% ethanol for 1 minute each time. The slides were then dried at air temperature and counterstained.

4.2.8.3. Counterstaining and mounting

Following the post-hybridisation washes, the counterstaining was done using the MD solution (DAPI concentration of 1 µg/ml) supplied by Cambio Ltd. The solution was diluted at different concentrations in order to establish the optimum concentration needed for the project. The dilutions tested were 1/2, 1/3, 1/5, 1/6 and 1/8. The dilution was performed using the mounting medium with antifade Vectashield.

Alternatively, samples were also mounted with 15 µl of Counterstain DAPI/Antifade (1 µg/ml) 10x concentrate supplied by Kreatech (Amsterdam, The Netherlands). The same concentrations were investigated and the dilutions were performed using the counterstain diluents supplied by Kreatech.

Finally the coverslips were sealed using transparent nail varnish.

4.2.9. Confocal microscopy

The slides were visualised using a Leica TCS SP2 AOBS laser scanning confocal microscope equipped with a beam splitter and using a 63x immersion objective for the acquisition of the final image stacks. The numerical aperture of the confocal microscope objective lens used was 1.4 and the pinhole size was 1 airy for the entirety of the study.

Cy3, FITC, and PlatinumBright 495 were excited using a 488 nm argon laser. PlatiniumBright 550 was excited using a 543 nm Helium-Neon laser. DAPI was excited using a 355 nm UV laser.

The fluorochromes photon emissions were detected using photomultipliers that convert the signal received (photons) into electrons. The electrons are then multiplied and a read-out of the signal (picture) generated. The width of the emission wavelength ranges detection was set according to the fluorochromes used. Fluorescein isothiocyanate (FITC) emission detection was set between 500 nm and 540 nm and Cy3 emission detection was set between 550 nm and 600 nm. For the Kreatech probes the PlatinumBright 495 (green) and PlatinumBright 550 (red) emission spectra were 525 ±30 nm and 580 ±30 nm respectively so the width of the detection band were kept between 500 nm and 600 nm

for both fluorochromes. DAPI emission detection range was set between 420 nm and 520 nm.

Due to an overlap between the DAPI and FITC emission spectra, artefacts were observed between DAPI and FITC signals. As a result, two separate stacks were generated for each sample. The first image stack included the signal of the two fluorochromes and the second image stack, included the DAPI counterstain signal.

During the scanning process a line average of 4 was applied in order to reduce the background noise artefact and hence to obtain clearer images. In this study the DAPI (405 nm excitation), PlatinumBright 495 (488 nm excitation, green) and PlatinumBright 550 (543 nm excitation, red) the corresponding lateral resolutions were 116 nm, 139 nm and 155 nm respectively. The images were acquired in a 1024 x1024 pixels format. The influence of the number of slices per stack was investigated in order to decide an adequate alternative to the optimum value given by the software. As the optimum values were of the order of 100, it was decided to compare the data obtained when 20- and 50-slice stacks were generated. It was decided that 50-slices stacks were to be generated instead of the suggested 100 slice stack due to consideration of fluorochrome consumption and fading.

4.2.10. Digital image processing and analysis

The raw data was processed to allow volume measurements and 3-dimensional visualisation and analysis. This part of the methodology is divided into two major steps: the processing and the analysis. During the processing step, the image stacks were converted into labelled binary images using software developed with MATLAB (The MathWorks Inc, Natick, MA, USA). This allowed the visualisation and calculations performed in the following parts of the analysis.

The software written in MATLAB was specifically developed for this project and hence was adapted in order to find the best procedure to generate accurate sets of data. Initially, it was designed to process the stacks quickly by automating the procedure to allow high volumes of data to be processed. The parameters of brightness and contrast

were set using a picture with a good level of signal within the stack and then applied to the whole stack.

The code was then adapted to allow for more user control of image brightness. Variations in intensity between the images of the same stack introduced artefacts and interfered in removing non-specific binding background captured during laser scanning confocal microscopy. As a result brightness and contrast could be adjusted for every picture in the stack.

The same fundamental basis of the process is used. In brief, the script is run and the image stack to process is chosen. The first step is the application of a 5 x 5 median filter to remove 'salt and pepper' type noise characterised by the presence of black pixels randomly present in bright areas and white pixels in black areas. The next step involves removing groups of pixels with sizes below a selected value. In this study, groups of pixels below 50 for the stacks corresponding to the painted chromosomes and below 100 for the stacks with the nuclei were removed. This allowed further reduction of artefacts due to background staining. Following the small pixel area removal, the brightness and contrast were adjusted such as to be as close as possible to the raw image (Figure 4.1) while eliminating background artefacts.

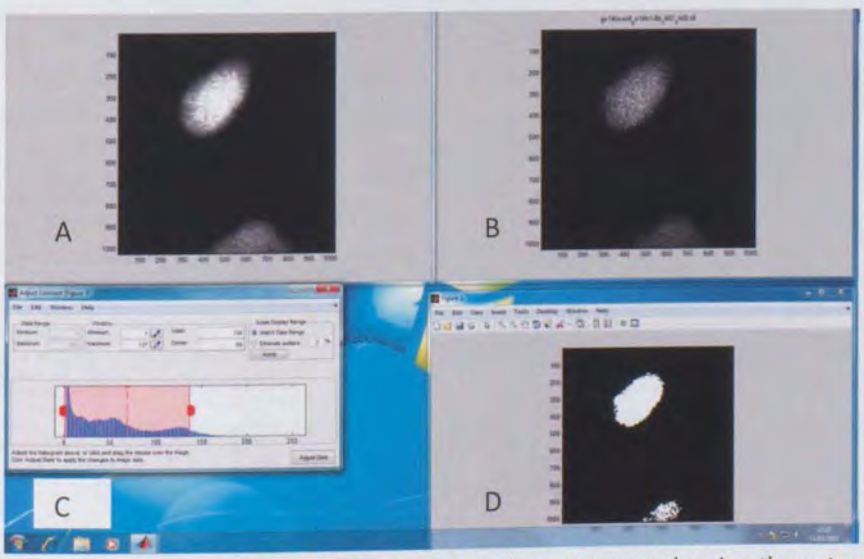

Figure 4.1: Example screenshot of the MATLAB picture interface. A: Image showing the outcome of contrast and brightness adjustment. B: grey scale representation of the original picture after application of the median filter. C: Brightness and contrast interface adjustment interface. D: Final binary black and white image.

After adjustment of the brightness and contrast, the software then converted the grayscale image to a binary black and white picture; the bright areas in the binary image were labelled thus allowing features such as area to be calculated. Summation of the area values allowed calculation of the volume occupied by the nucleus and the territories considered. An Excel (Microsoft Corporation, USA) spreadsheet with all the parameters of the labelling, calculations for the stack as a whole and also each individual image was also created for each stack processed.

Further analysis and measurements were performed using Amira (VSG, Visualization Sciences Group). Amira is a platform allowing the visualisation and manipulation as well as analysis of 3-dimensional objects and hence can generate sets of analysis measurements on the data.

Firstly, the black and white binary pictures of each of the 3 considered fluorochromes were loaded into the current network. Then the data were visualised by applying isosurfaces to the labelled regions; the data were assigned a colour of green, red and blue corresponding to the fluorochrome. At this point, it was possible to examine the data to assess the spatial arrangement of the chromosome territories within the nucleus (Figure 4.2).

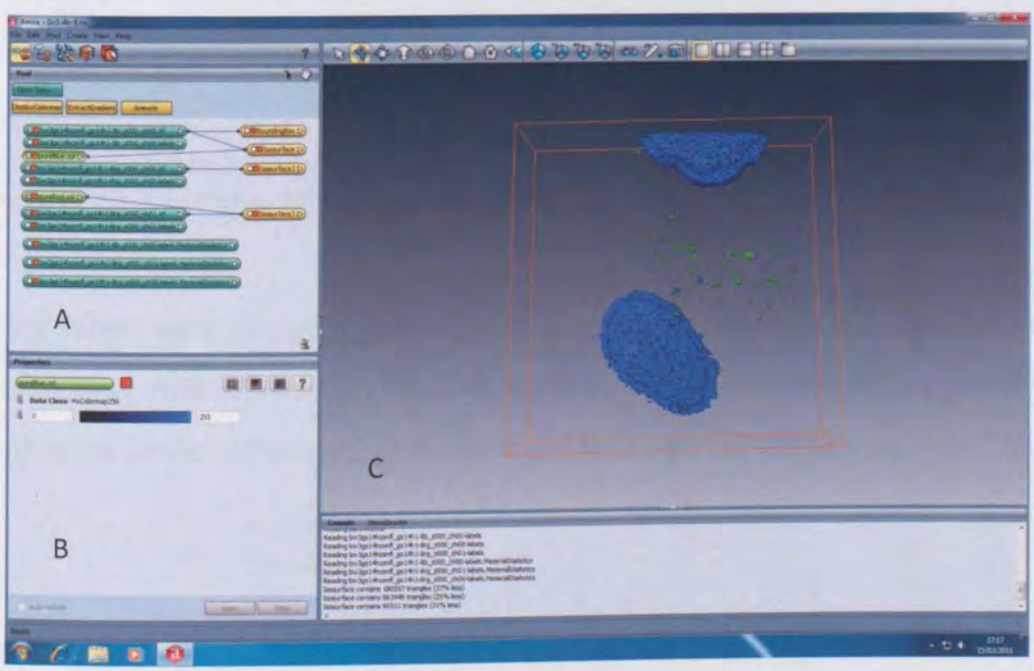

Figure 4.2: Representation of the user interface in Amira. A: Network window. The series of commands applied to the data are visualised using a graphic representation. B: The indvidual command properties are input and set. C: Visualisation window. The sample can be rotated and distance measurements to be performed drawn directly on the visualisation.

The samples were then labelled in order to allow volumes and material statistics to be generated. Each object to be considered was assigned a colour and labelled. The labelling was performed for the entire 3D visualisation. This enabled the selection of data belonging to the same object (territory or cell nucleus) across the 3D image stack (Figure 4.3).

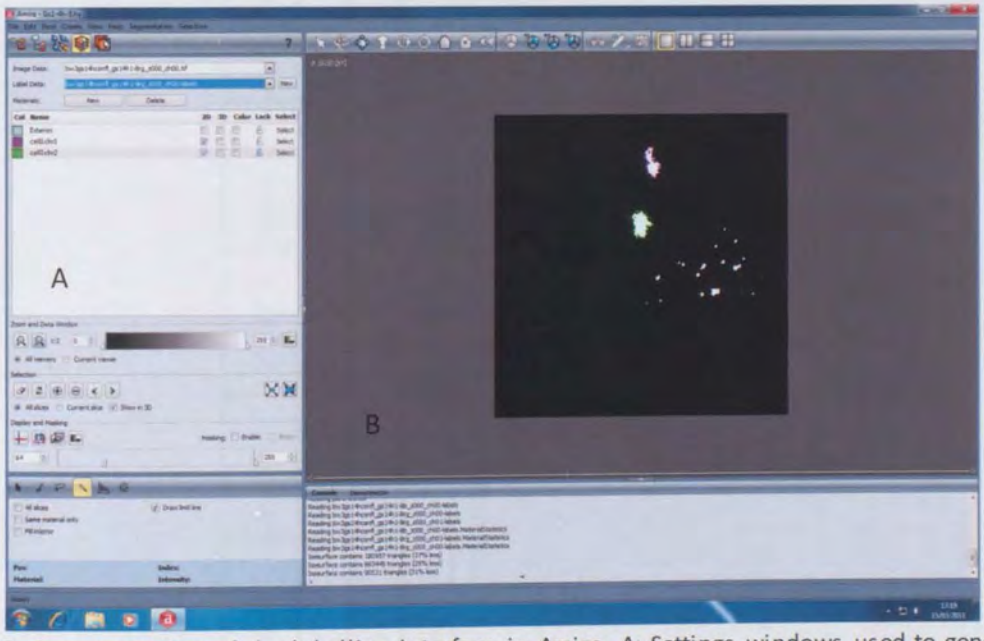

Figure 4.3: Representation of the labelling interface in Amira. A: Settings windows used to generate the different materials labels. B: Visualisation window allowing the material selection with possibility to move from one frame to the other within the stack of images.

Once the labels were assigned, the software was able to calculate the volume values of each individual material defined. The data generated was output to an Excel document in order to allow easier compilation of the different data sets (Table 4.2).

Nr	Material	Count	Volume	CenterX	CenterY	CenterZ	Mean	Deviation	Variance	Min	Max	Cumulative Sum
1	Exterior	52248672	51111.31	29.75704	29.8	7.092515	0.18	6.773	45.87	0	255	9405165
2	cell1chr1	74435	72.81468	31.941	10.2	3.510833	255	0	0	255	255	18980925
3	cell1chr2	105692	103.3913	29.68656	21.4785	3.406753	255	0	0	255	255	26951460

Table 4.2: Example of data generated following the material statistics calculations using Amira software.

Finally, 3D measurements were performed from the data generated following the labelling of the different materials (nucleus and chromosome territories). Due to the irregular shapes of the objects considered (CTs) and the non-spherical nature of the nuclei, the analysis was done by mapping the centre point of each of the volumes considered. The materials centre values obtained for each dimentions (x, y, z), as shown in Table 4.2, allowed the mapping of each object within the area (picture field) to be considered. As a result, it was then possible to draw and visualise the distances between the different chromosome territories within the cell nuclei (Figure 4.4).

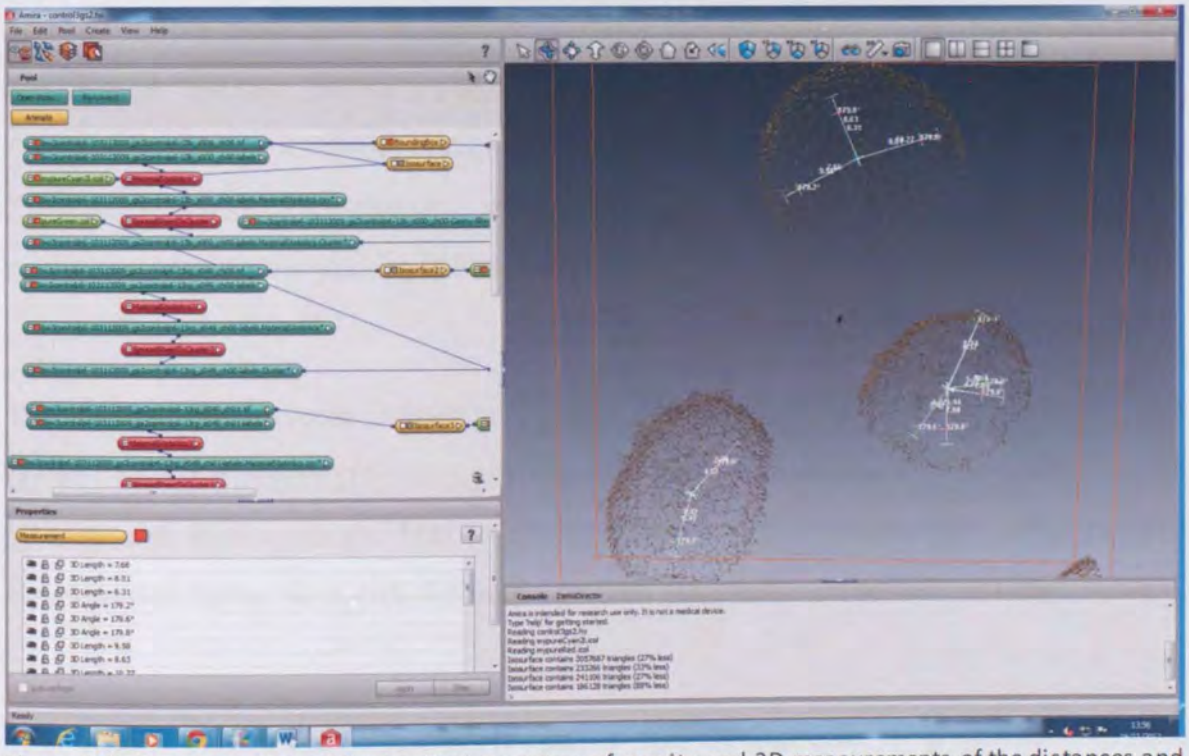

Figure 4.4: Representation of the territories centres of gravity and 3D measurements of the distances and the radii in human non-irradiated fibroblasts. The nuclear surfaces are visualised in gold to allow visualisation of the territories centres of gravity and subsequent measurements.

The measurements were performed using the measurement tool in the Amira software. The centre points were computed and the distance between the cell centre and the different objects as well as the radii (distance between the cell centre and the nuclear surface through the object centre) were drawn. This allowed the calculation of the object position with respect to the nucleus surface. This was performed in order to eliminate possible variations introduced by the range of nuclei sizes. The values were then expressed as a percentage of the total radius.

4.3. Materials

The cell culture media RPMI 1640, Trypsin-EDTA (0.05%), Foetal bovine serum (FBS), Penicillin streptomycin solution, Phosphate buffered saline tablets and solution, glass ring cells, concentrated bleach, slides, 22 x 22 mm coverslips, 22 x 40 mm coverslips, circular coverslips, glacial acetic acid, methanol, absolute ethanol, fluorescence microscopy immersion oil, cell culture flasks (25 cm^2, 75 cm^2), single use pipettes, disposable conical centrifuge tubes were purchased from Fisher-scientific (Loughborough, UK).

The cell culture media DMEM, hydrogen chloride solution (36.45 M), MEM non- essential amino-acids solution (100x), L-glutamine solution (200 mM), Giemsa staining solution, Formamide, Sodium chloride, sodium citrate, sodium hydroxide, dextran, igepal, Triton-X100, sodium phosphate dibasic, sodium phosphate monobasic, DMSO, and Pepsin were purchased from Sigma- Aldrich (Gillingham, UK).

The Whole chromosome Poseidon™ paints for chromosome 1 (PlatinumBright 495 (green) and PlatinumBright 550 (red) labelled) and chromosome 2 (PlatinumBright 495 (green) and PlatinumBright 550 (red)), DAPI counterstain, Counterstain diluents, and Hybridization buffer were ordered from Kreatech (Amsterdam, The Netherlands).

The Whole chromosome Star*FISH© paints for chromosome 1 (FITC-labelled) and chromosome 2 (Cy3- labelled), DT Detergent Tween 20, and MD Mountant with DAPI were purchased from Cambio Ltd (Dry Drayton, UK).

Rubber solution, used to seal coverslips during hybridisation, was purchased from Halfords plc (Kingston-Upon-Thames, UK).

Clear nail varnish used to seal coverslips upon completion of staining procedure was purchased from Boots UK Limited (Kingston-Upon-Thames, UK).

The mounting medium with antifade Vectashield was purchased from Vector Labs (Peterborough, UK).

REFERENCES

Cremer, T., & Cremer, C. (2001). Chromosome territories, nuclear architecture and gene regulation in mammalian cells. *Nature Reviews. Genetics*, ***2***(4), 292–301.

Doyle, A., & Griffiths, J. B. (2000). *Cell and Tissue Culture for Medical Research* (p. 38). Wiley-Blackwell .

Scheuermann, M. O., Tajbakhsh, J., Kurz, A., Saracoglu, K., Eils, R., & Lichter, P. (2004). Topology of genes and nontranscribed sequences in human interphase nuclei. *Experimental Cell Research*, ***301***(2), 266–79.

Verschure, P. J., Van Der Kraan, I., Manders, E. M., & Van Driel, R. (1999). Spatial relationship between transcription sites and chromosome territories. *The Journal of Cell Biology*, ***147***(1), 13–24.

Visser, A. E., Eils, R., Jauch, A., Little, G., Bakker, P. J., Cremer, T., & Aten, J. A. (1998). Spatial distributions of early and late replicating chromatin in interphase chromosome territories. *Experimental Cell Research*, ***243***(2), 398–407.

Chapter 5 Fluorescence *in situ* hybridisation and methodology optimisation

5.1. Introduction

This project relied highly on the successful production of good quality 3D images in order to achieve the planned measurements. Considerable time was spent on the development of a technique using FISH (fluorescence *in situ* hybridisation), confocal microscopy and image analysis that could allow processing in an optimal timeframe. The use of a more automated process could lead to better repeatability than if relying on manual assessment.

The quality of the 3D visualisations achieved for this study is dependent on the quality of the initial 2D images obtained using confocal microscopy. This chapter describes the processes involved in optimisation of the protocol that will later be used in the study of non-irradiated and irradiated fibroblasts and RT112 cell nuclei. The different steps in the protocol can have an important impact on the outcome of the preparation. The optimisation of the protocol and the sample preparation allowed the possible routine implementation of the technique in later cytogenetic studies. The protocol was divided into three main steps in order to consider the variables to be optimised: FISH, image acquisition (confocal microscopy) and, image processing and analysis.

5.2. Material and methods

5.2.1. Choice of the cell lines

Two cell lines were used in the study. Normal human fibroblasts were used as a control group. The second cell line used was human bladder carcinoma cells (RT112). This cell line was chosen because the cells possess an average of 46 chromosomes which unlike other aberrant cell lines is similar to the number of chromosomes encountered in normal cells. The similarity with the normal cell nucleus in terms of chromosome numbers allows a better identification of possible preserved similarities as well as the difference between normal and cancer cells. RT112 cells have also been characterised using FISH with possessing several deletions, isochromosomes and translocations (Strefford *et al.*, 2002; Wang *et al.*, 1995). The cell nuclei are likely to present some instability which will contribute in assessing the effect on the number of chromosome aberrations following being subjected to ionizing irradiation.

5.2.2. Slide preparation, hybridisation and confocal microscopy

The slides were prepared according to the protocol described in Chapter 4 Section 4.2.7. Briefly, the cells were seeded in the form of a single cell suspension into temporarily attached glass chambers. The cells were them allowed to attach to the slide before undergoing fixation, pre-treatment and FISH. The different steps involved in the preparation of slides for FISH as well as several parameters of the FISH itself were scrutinised during the protocol optimisation in order to ensure successful *in situ* hybridisation. Briefly, the parameters investigated were the fixation, pre-treatment, the probes as well as the denaturation/hybridisation step, the post-hybridisation washes and the counterstaining during the *in situ* hybridisation. The fixation, pre-treatment and FISH protocols are described more extensively in Chapter 4 Section 4.2.7.

Following successful hybridisation, the samples were observed using confocal microscopy as described in Chapter 4 Section 4.2.9. Some of the parameters of the confocal microscopy such as: the laser intensity, excitation wavelength, emission wavelength, scanning mode, scan average, photomultiplier settings, digital zoom, resolution and slice number were also investigated during the optimisation process. Phenomena such as photobleaching were identified and addressed in order to obtain the highest quality images possible using this method.

5.2.3. Image processing and analysis

The image stacks obtained using confocal microscopy were subjected to image processing and image analysis. The data stacks were processed using MATLAB (The MathWorks Inc, Natick, MA, USA) and the measurement performed using Amira (VSG, Visualization Sciences Group, USA) as described in Chapter 4 Section 4.2.10.

The images were converted into binary images in order to allow further processing. Parameters such as brightness and contrast were investigated when the values were applied to the whole stack or to individual images. This allowed the reduction of potential artefacts still present despite the optimisation of the FISH protocol.

The measurements in Amira were performed using the in-built tools of the software. Parameters such as volumes and relative distances were established for the relevant parts of the study as described in Chapter 4 Section 4.2.10.

5.3. Results of the protocol optimisation

5.3.1. Protocol optimisation at the 2D level: FISH optimisation

The protocol was divided into three main steps in order to consider the variables to be optimised: FISH, image acquisition (confocal microscopy) and image processing and analysis.

The FISH technique is itself based on three main steps: pre-treatment; denaturation/hybridisation; post-hybridisation washes. The table below summarises the different steps and parameters that have been investigated in this study in order to obtain good quality 2D images.

Protocol step	Purpose	Methods/variables tested	Mechanism	Advantages/disadvantages
Fixation	To fix physical structure of cells	4% formalin	Cross-linking agent	May influence cellular structure and access of probe to target
		3:1 Methanol/acetic acid Carnoy's fluid	Coagulative fixative	
Pre-treatment	To improve access of probe to target sequence	pepsin treatment	Degrades membrane proteins to permeabilise cells	May alter cellular structures
		Saponin	Surfactant-like: induces pores in the membrane bilayer	
		Triton-X	Disrupts the phopholipid bilayer by lowering surface tension	
		Temperature aging	Disrupts the membranes using heat	
		Freeze/thaw cycles	Disrupts the membranes using changes in temperature	
		Acid treatment	Disrupts the membranes	
Denaturation	To ensure separation of both parent and probe double-stranded DNA to allow probe access	Temperature	Higher temp increases rate of denaturation	Complicated control of temperature required at all times
		Time	Longer times enable maximum denaturation	
		Separate or combined denaturation of probe and target	Alter the efficiency of subsequent hybridization	
Hybridization	To allow preferential binding of probe to target sequence.	Hybridisation time	Longer times enable maximum hybridisation	Excess probe or longer time may lead to non-specific binding
		Probe quantities	Increased probe concentration, increased probe binding	
Post-hybridisation treatment	To optimize signal/noise ratio	Use increasing wash times	Decrease non-specific binding and background	May reduce specific signal strength
		Number of washes		
Counterstaining	To visualise the nucleus	DAPI countertain concentration	Binds to the DNA	Helps visualise the entire nucleus
				Very bright signal in high concentrations

Table 5.1: Summary table of the different parameters investigated during FISH protocol optimisation.

5.3.1.1. Choice of probes

The outcome of FISH is reliant on successful hybridisation of the fluorescent probes used. Probes can be synthesised chemically or by using PCR. In the latter, the sequence of the genome to be stained is amplified using a specific set of primers. To ensure the best homology between probe and target, ideally the preparation has to be performed on homologous if not the same DNA as the samples to be studied. During the initial amplification, the target region is amplified using a mix of primers targeting shorter sequences but overall spanning the entire region of interest with overlapping sequences. After the first amplification, the amplicons are then used as a template for the next PCR cycle. Probes can be synthesised for targets ranging from a few hundred base pairs up to an entire chromosome, whole chromosome paints (WCP). Once the DNA has been amplified, the PCR products need to be labelled with the fluorochrome of choice. This is performed using nick-translation where nucleotides are replaced with labelled analogues. Probes can be made routinely and usually are tailored case by case. In the case of whole chromosome paints (used in this project) the fabrication of probes requires the ability to generate amplicons from whole chromosomes sorted using flow cytometry. This adds to the already intricate and lengthy process. Where possible, the availability of commercial probes helps resolving the difficulties probe fabrication can generate. In the case of WCP, suppliers provide probes with a number of possible fluorochomes allowing the staining of more than one chromosome simultaneously.

The purchase of commercially available probes presents some advantages. For example, the purchase of a significant amount of product from the same batch can ensure the homogeneity of the reactions and probe quality during the length of the project. This option can also represent a cost effective solution for laboratories that do not possess the material set-up to produce FISH paints routinely. The use of commercially available probes can also present some disadvantages in relation to precise information about how the probes are synthesised. The presence of repetitive sequences in the genome can lead to the presence of increased levels of background hybridisation. The two available options to solve this are the use of Cot1 DNA blocking agent or the use of repeat free probes. In this study, WCP from two suppliers were used in order to find the best probe combination: initially Star*FISH© probes supplied by Cambio Ltd. (Cambridge, UK) and

later Repeat-Free™ (RF) Poseidon™ FISH probes from Kreatech Diagnostics (Amsterdam, The Netherlands).

5.3.1.2. Fixation

The protocol is initiated by the fixation of the sample preparations. The samples are fixed to ensure the preservation of the cell structures. Solutions of 4% formalin or 3:1 methanol/acetic acid (Carnoy's fluid) have been used to fix samples (Bolzer *et al.*, 2005; Croft *et al.*, 1999; Eils *et al.*, 1996; Scheuermann et *al.*, 2004; Tanabe *et al.*, 2002; Visser *et al.*, 1998). The preference of one method over the other is mainly linked to the procedures used to permeabilise the cell membranes following the fixation. The two fixative agents differ in their mode of action due to their difference in nature. Formalin is a cross-linking agent and will fix the structures by linking them together.

On the other hand, Carnoy's fluid is a coagulative fixative. Its chemical properties will lead to the coagulation of proteins and as a result the immobilisation of the cell and nuclear structures of the sample preparations. The aim of the fixation is to preserve the integrity of the samples. As a result, the method of choice needs to ensure strong fixation with limited damage to the sample structures.

The influence of the fixation on the *in situ* hybridisation signal and on the cell structure was studied by Hepperger *et al.* (2007) on metaphase preparations and interphase nuclei. It appears, according to Hepperger *et al.*, that fixation using Carnoy's fluid is the most appropriate in order to obtain good quality *in situ* hybridisation signal; this fixation method was thus adopted in our study.

5.3.1.3. Pre-treatment optimisation

During the pre-treatment, the cells are prepared to facilitate the passage of the probe through the natural barriers present in the cell (the cellular membrane and the nuclear membrane). In the case of metaphase preparation, this is mainly done using physical disruption of the membrane (metaphase spreads) after hypotonic treatment. In the case of interphase preparations, since the aim was to study unperturbed nuclei, the cells were to stay intact. It was also necessary to ensure cellular components that could

be responsible for non-specific binding (RNA) were eliminated as much as possible. Different approaches can be used to ensure the membrane permeabilisation. These techniques rely on the use of chemicals/biological agents for their effect on the membrane components or physical and acid treatments (Bolzer *et al.*, 2005; Croft *et al.*, 1999; Eils *et al.*, 1996; Scheuermann *et al.*, 2004; Tanabe *et al.*, 2002; Visser *et al.*, 1998). The different agents tested in this study were surfactants or surfactant-like agents such as saponin and Triton-X as well as pepsin and acid treatment. Surfactants lower the surface tension of liquids leading to the disruption of the bilayer and formation of micelles. Depending of the characteristics of the surfactant used, the disruption process will vary slightly. For example, saponin is a glycoside that will foam and induce cell lysis for the former or act like a detergent and solubilise membrane proteins for the latter. Triton-X100, a non-ionic surfactant, has also been used as an alternative to disrupt the lipidic bilayer. On the other hand, pepsin degrades membrane proteins resulting in the creation of pores that will facilitate access to the DNA material. Alternatively, slides can be pre-treated using physical treatment where the samples are subjected to freeze/thaw cycles and alternatively dipped into liquid nitrogen and glycerol or subjected to heat for a given length of time.

The initial pre-treatment combination tested was the one supplied by the Star*FISH© probes manufacturer. It involved dehydration in 100% ethanol then a two-step membrane permeabilisation involving a pepsin treatment and a wash in 2x SSC repeated twice before the final dehydration prior to heat aging treatment. This combination did not successfully lead to obtaining a hybridisation signal. As a result, the slide aging treatment times and temperature were investigated to evaluate how they influence hybridisation outcome. The slides underwent the initial stages of the pre-treatment and were then subjected to aging times of 30 minutes and 60 minutes at temperatures of 45°C or 65°C (Table 5.2).

Temperature/ Aging Time	30min	40min	60min
45°C	No signal detected	No signal detected	No signal detected
65°C	No signal detected	No signal detected	No signal detected

Table 5.2: Summary of the different aging times and aging temperatures tested in order to increase the occurrence of hybridisation using Star*FISH© probes and protocol.

The modifications of the aging time and temperature in this protocol tested did not lead to successful hybridisation. The supplier's protocol was then adapted slightly after consultation of the literature in order to adapt the samples' pre-treatments and to investigate whether the presence of cytoplasm and other cellular components could be responsible for the absence of hybridisation (Bolzer *et al.*, 2005; Croft *et al.*, 1999; Eils *et al.*, 1996; Scheuermann *et al.*, 2004; Tanabe *et al.*, 2002; Visser *et al.*, 1998). Different combinations of pre-treatments were then tested as detailed in Table 5.3 below.

Treatment combination/Steps	Fixation	Step 1	Step 2	Step 3
1	Paraformaldehyde	Triton-x	liquid nitrogen and glycerol Freeze thaw cycles	HCl treatment
2	Methanol/acetic acid	HCl treatment	Triton-x	Saponin
3	Methanol/acetic acid	PBS wash	Pepsin solution	Triton-x
4	Paraformaldehyde	Triton-x	Saponin	liquid nitrogen and glycerol Freeze thaw cycles
5	Paraformaldehyde	Triton-x	liquid nitrogen and glycerol Freeze thaw cycles	Pepsin solution
6	Methanol/acetic acid	PBS wash	Digitonin treatment	Pepsin solution

Table 5.3: Combinations of pre-treatments tested in order to obtain hybridisation. NB: Despite the preference for Carnoy's fixation, the use of paraformaldehyde fixation was performed exclusively to comply with protocols described in the literature.

None of the pre-treatments listed above led to successful hybridisation. As the solutions prepared had been fresh and the guidelines provided had been carefully followed, other steps in the protocol were scrutinised in order to understand the absence of hybridisation.

5.3.1.4. Denaturation/hybridisation

The denaturation step involves denaturation of both the cell DNA and the probe DNA. This step denatures the sample's double stranded DNA to create single stranded DNA to which the probes can hybridise during the hybridisation step. Time and temperature are two factors that will most influence the outcome of this part of the procedure. According to DNA thermodynamics, the temperature for denaturation is dependent on the G-C content of the DNA considered. As a result the denaturation temperatures can vary between 65°C and 75°C and the denaturation time between 2 and 10 minutes depending on the protocol used. The success of the hybridisation will depend highly on the successful denaturation of the DNA which can tend to encourage longer denaturation times. However, longer denaturation times also means higher risks for the DNA to be degraded and the results affected. Hybridisation occurs at 37°C (physiological temperature) overnight as it is a slow process during which the denatured DNA comes back to its natural conformation while the probes are incorporated.

In this project, the use of commercially supplied probes led to the choice of denaturation/hybridisation times and temperatures according to the supplier recommendations. In the interest of homogeneity during the entire duration of the project, the probes used to target chromosome 1 were FITC-labelled (or equivalent fluorochrome) and the probes targeting chromosome 2 were Cy3-labelled (or equivalent fluorochrome).

In the case of the Star*FISH© paints supplied by Cambio Ltd (Cambridge, UK), the denaturation and hybridization are conducted in successive order with denaturation occurring at 65°C for 1.5 minutes to 2 minutes and overnight hybridisation at 37°C. Evidence of hybridization could not be obtained when using separate denaturation and hybridisation steps with single pepsin pre-treatment according to the supplier's protocol. The initial absence of hybridisation was thought to be the result of insufficient pre-treatment preventing the probe accessing the target DNA; this led to the investigation of several combinations of pre-treatment steps (as described in 5.3.1.3.). Despite the investigation of alternative pre-treatments prior to denaturation/hybridisation no staining was obtained. As a result, an alternative protocol was researched and obtained from Toon Min (Min, 2003) from the Royal Marsden cancer centre in Sutton where routine

diagnostic techniques are carried out on a daily basis. The main difference in the protocol (which was adapted from the protocol supplied by Vysis Inc. (San Francisco, USA) for the use of their paints) was the co-denaturation and hybridisation of the probes. The combination of the two steps allows better access of the denatured DNA to the probes with reducing the risks of DNA re-naturation that could prevent the probes from hybridising to their targets. This technique was also automated and facilitated by the acquisition and the use of a hybridisation chamber. Hybridisation was finally obtained after simultaneous application of the two steps on the slides. However, the signal obtained was not sufficient to allow capture of useable 2D images with the fluorescence microscope system available at Kingston University. Moreover a disparity in signal quality between the two probes was observed with chromosome 1 paint showing a slightly better result than chromosome 2 paint.

In order to attempt increasing the hybridisation signal, different hybridisation solutions were tested. The difference between the solutions tested is due to the quantity of each probe. In other words, increasing quantities of probes were tried in order to obtain a strong enough signal to allow the capture of images of sufficient quality to allow the production of exploitable images. The composition of the different hybridisation solutions tested is described in Table 5.4.

	Mix #1 (µl)	Mix #2 (µl)	Mix #3 (µl)	Mix #4 (µl)
Chr1 WCP	1	2	3	4
Chr2 WCP	1	2	3	4
Hybridisation buffer	8	6	4	2
Total volume	10	10	10	10

Table 5.4: Composition of the different co-denaturation/hybridisation solutions tested.

The signal intensity obtained increased with increasing quantities of probes but also led to the increase of nuclear background straining when observing the preparations under the microscope. Visual analysis suggested that the signal to background ratio did not appear high enough to allow easy identification of the territories limits.

The diminution of the signal to background ratio with increasing quantities of probes could possibly be due to a phenomenon of saturation where increasing probe quantities do not improve the signal intensity but contribute to a more notable background staining.

Unfortunately, a combination of weak signal and limitations from the 2D fluorescence microscope set-up did not allow the capture of pictures of a good enough quality to allow a precise quantification of the variations in background staining.

Since the increase of paint quantities did not result in obtaining clearly better quality 2D images, the amount of paint in the hybridisation buffer was kept as a total of 2 µl which is in compliance with the supplier's recommendations.

One of the possible causes of background staining is the presence of RNA in the nucleus so the use of an RNAse pre-treatment could possibly help with reducing the amount of background staining. As a result an extra pre-treatment step using RNase was added to the protocol in order to attempt at reducing the background. The new set of slides was observed alongside the ones processed without the extra pre-treatment in order to evaluate the differences in background artefacts. The presence of background did not appear to be reduced which means that the background hybridisation obtained is not necessarily due to non-specific binding to the cytoplasmic RNA.

As a result, in order to attempt at improving the quality of the signal, DNA probes supplied by Kreatech diagnostics were used to replace the Star*FISH© probes. The Repeat-free™ Poseidon™ FISH Probes are produced to give a brighter signal with minimum background staining. Green labelled probes were used to paint chromosome 1 and red labelled probes were used to paint chromosome 2. The protocol followed initially was the one provided with the paints by Kreatech diagnostics as it also uses a co-denaturation/hybridisation step. The initial staining appeared to be successful albeit relatively weak. In order to increase the signal intensity, the optional (according to the supplier guidelines) pepsin pre-treatment to permeabilise the cells was performed. The red paint appeared to work very well and give good quality images (Figure 5.1).

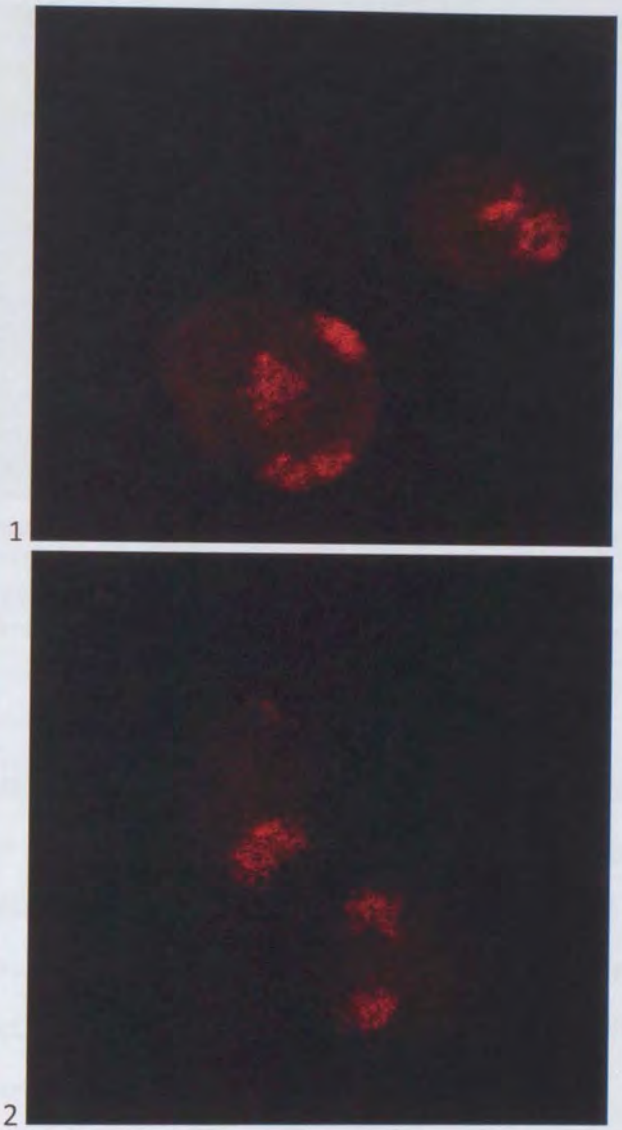

Figure 5.1: 1) Normal human fibroblast painted with Poseidon™ FISH whole chromosome paints for chromosome 2 and Platinum-red labelled. 2) Human bladder carcinoma cells (RT112) painted with Poseidon™ FISH whole chromosome paints for chromosome 2 and Platinum-red labelled. Both pictures observed with a x63 immersion objective and x4 digital zoom. Full height x full width of image equivalent to 59.5 µm x 59.5 µm

Despite the good outcome of the chromosome 2 painting, staining chromosome 1 proved to be more difficult and as a result, a combination of Star*FISH© paints (Chromosome 1 FITC-labelled) and Poseidon™ (chromosome 2 red-labelled) were used until different batches of Poseidon™ paints for chromosome 1 were tested (Figure 5.2). The use of 1 µl of Star*FISH© paint seemed to yield satisfying hybridisation with manageable background staining which was ideal for the use of total of 2 µl of combined paint.

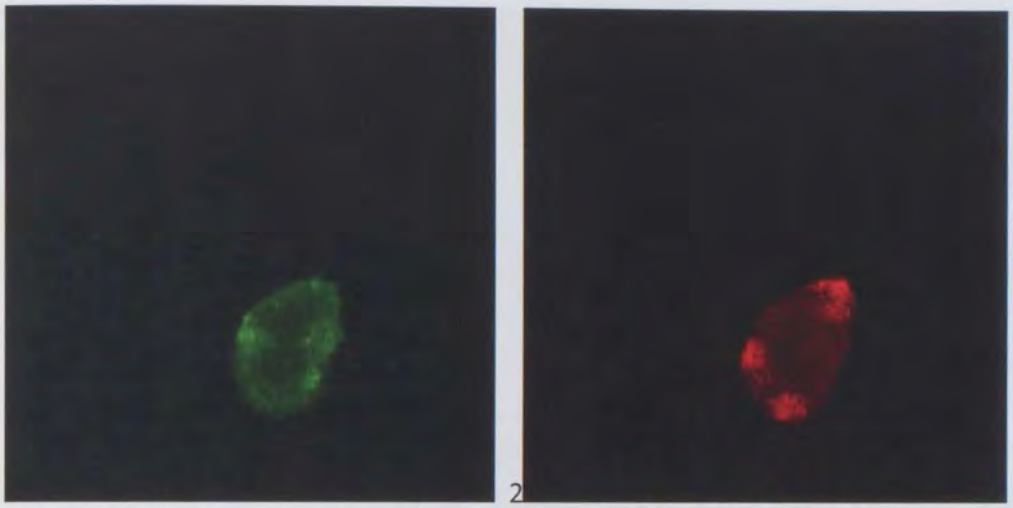

Figure 5.2: 1) Human bladder carcinoma cells (RT112) painted with Star*FISH© whole chromosome paints for chromosome 1 and FITC-labelled. 2) Human bladder carcinoma cells (RT112) painted with Poseidon™ FISH whole chromosome paints for chromosome 2 and Platinum-red labelled. Both pictures observed with a x63 immersion objective and a x4 digital zoom. Full height x full width of image equivalent to 59.5 µm x 59.5 µm

After consultation with the manufacturer, it appears that chromosome 1 paints with the platinium green label give less satisfactory results than the other chromosomes. The reason as to why this phenomenon happens was unknown to the manufacturer; there seems to be variability in the paint batches. This could be due to the principle behind the paint synthesis. In fact, the DNA fragments are synthesised by amplification of fragments from chromosomes sorted using flow cytometry. Despite using the same set of primers during the multiplex PCR, the exact nature and yield of each fragments amplified will vary. As a result, even though the whole chromosome is covered, each region of the chromosome, unlike with smaller probes, will be amplified to different degrees. After different batches had been tested, a successful combination of Poseidon™ paints was found and used for the remainder of the project (Figure 5.3).

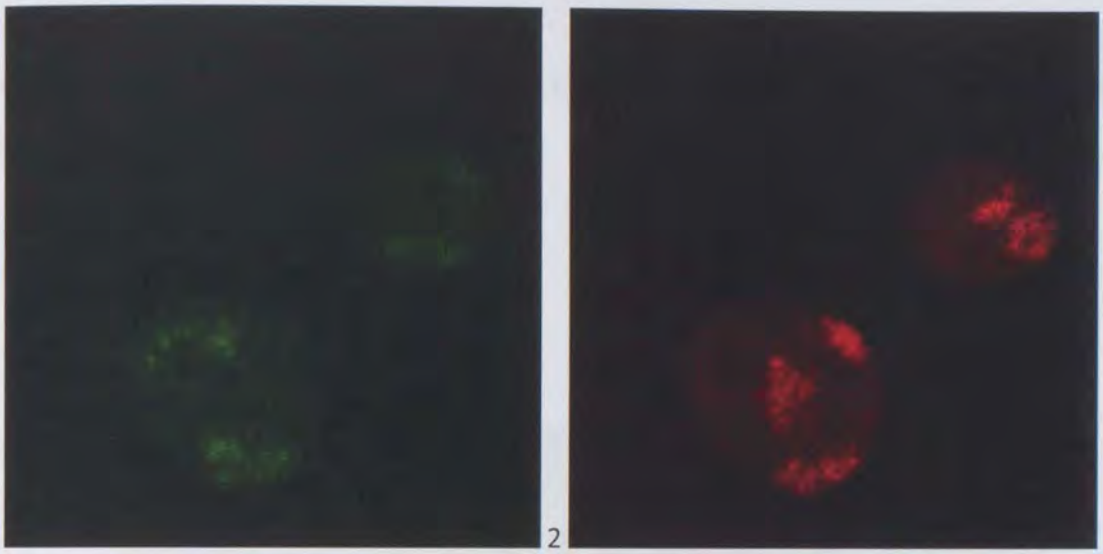

Figure 5.3: 1) Human bladder carcinoma cells (RT112) painted with Poseidon™ FISH whole chromosome paints for chromosome 1 and Platinum green-labelled. 2) Human bladder carcinoma cells (RT112) painted with Poseidon™ FISH whole chromosome paints for chromosome 2 and Platinum-red labelled. Both pictures observed using a x63 immersion objective with x4 digital zoom. Full height x full width of image equivalent to 59.5 µm x 59.5 µm

5.3.1.5. Post-hybridisation washes

The post-hybridisation washes aim to eliminate as much non-specific binding as possible. This step is based on the stringency of the washing solution and is controlled by the salt and surfactant concentrations as well as the temperature and the duration of the wash. This part of the procedure is composed of two individual washes with solutions containing different concentrations of salt and of surfactant. The first wash is conducted at a high temperature (between 60°C to 72°C) in a solution containing low salt concentrations and considerable quantity of surfactant (commonly igepal) whereas on the contrary the second wash is done at room temperature with high salt concentrations and low quantities on surfactant. Since, as mentioned before, the stringency of the probe hybridisation is closely linked to the optimum temperature chosen for the DNA sequence targeted, the two-step washing procedure uses this characteristic to attempt at removing the excess background staining. In other words, the initial wash, performed in this study at 72°C for 2 minutes, aimed at removing the non-specific binding as well as the partially bound probes. The affinity of the probe for the DNA it targets being the highest, the short wash results in the elimination of probe/DNA or probe/cellular components non-specific associations. The second wash, performed at room temperature for 1 minute in this study, aimed at removing the excess of unbound probe. Since the temperature of the

solution is not close to the hybridisation temperature, the signal is not affected by the second post-hybridisation wash and only the unbound probe is washed away thanks to the surfactants present in the solution. When initially using the Star*FISH© paints supplied by Cambio Ltd, the presence of background staining in the nuclei was considerable (Figure 5.4).

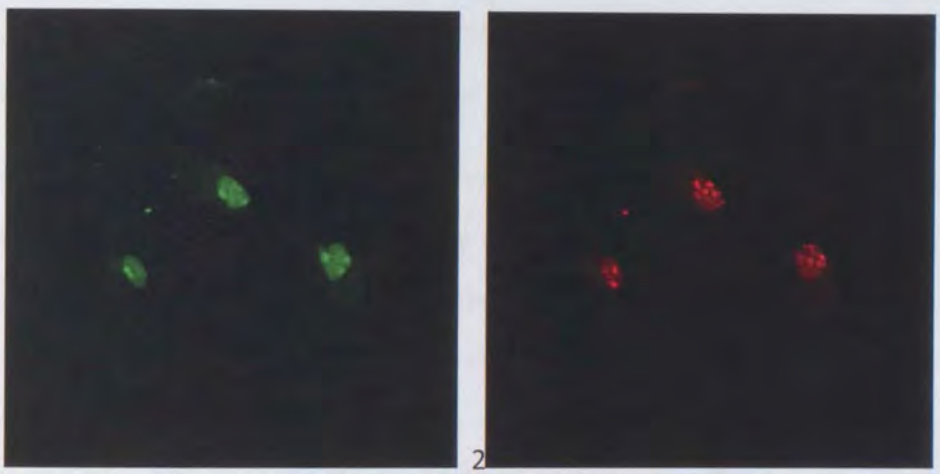

Figure 5.4: Human normal fibroblasts stained with Star*FISH© paints showing important background staining. 1) Chromosome 1 was painted with a FITC-labelled probe (green). 2) Chromosome 2 was painted with a Cy3-labelled probe (red). Both pictures observed using a x63 immersion objective. Full height x full width of image equivalent to 238 µm x 238 µm

It is important to attempt to remove excess background staining prior to 3D visualisation. The presence of excess background could prove to be detrimental in the attempt at creating faithful representations of the nuclear architecture and chromosome positioning of the cell lines studied. The fidelity and quality of 2D images will impact on the subsequent 3D visualisation quality by creating possible artefacts.

As a result, in order to attempt to reduce background staining and improve the staining quality, the length and also the number of washes could be adapted in order to remove as much non-specific binding as possible.

1st wash time	2 min	2min 30s	3min	3min 30s	4 min	4 min 30s
2nd wash time	1 min	1 min	1 min	1 min	1 min	1 min
2nd wash time	1min 30s	1min 30s	1min 30s	1min 30s	1min 30s	1min 30s
2nd wash time	2 min	2 min	2 min	2 min	2 min	2 min
2nd wash time	2min30s	2min30s	2min30s	2min30s	2min30s	2min30s

Table 5.5: description of the different wash times combinations tested.

Increasing the washing times of both low and high stringency washes did not clearly remove background staining and even at times reduced the hybridisation signal. The close proximity of the high stringency wash temperature to the hybridisation temperature might result in a loss of binding of the probe with extended washing times.

To address this, a slightly different approach was taken to attempt at removing the excess background staining. An extra washing step was added with the total washing time at 72°C still being 2 minutes but divided into steps of 1 minute. Splitting the washing time was done in the expectation that the first wash would remove most of the excess staining and the second wash, performed in a fresh solution, allowing the removal of yet more non-specific binding. This process did not seem to decrease the non-specific binding.

The difficulty in removing excess background staining could be due to a characteristic inherent in the process by which the probes are manufactured. It could be as a result of the presence of numerous repeats sequences in the DNA used in the manufacture of the probes. In other words, the use of *Alu*-repeat targeting primers in the probe synthesis leads to the synthesis of DNA probes targeting areas found in other chromosomes leading to the presence of non-specific binding alongside the expected specific binding.

This issue was resolved when the use of the Repeat-free™ Poseidon™ FISH Probes supplied by Kreatech diagnostics were used instead of the Star*FISH© probes. The Repeat-free™ Poseidon™ FISH Probes are produced to give a brighter signal with minimum background staining. Green labelled probes were used to paint chromosome 1 and red labelled probes were used to paint chromosome 2 and a successful combination was identified (as described in 5.3.1.4.). The quality of the probes and the post-hybridisation washes suggested by the supplier were sufficient to ensure the acquisition of good quality images with minimum background staining with confocal microscopy. The presence of any residual background staining could only be assessed during confocal

microscopy. As a result, adjustment of the microscopy imaging parameters allowed the removal of residual background signal.

5.3.1.6. DAPI counterstaining

Since the visualisation of the chromosomes studied is performed using fluorescent probes it is important that sufficient staining takes places for appropriate detection during microscopy. As mentioned previously in the 2D analysis results (Section 5.3.1.), the quality of the staining depends heavily on the quality of the probes but also on the absence of non-specific binding and background. Since it has been taken into consideration during the protocol optimisation, the only parameter left regarding staining is the counterstaining and mounting. Counterstaining is most commonly performed using 4',6-diamidino-2-phenylindole or DAPI. DAPI is an acid stain that binds to double stranded DNA and is blue-fluorescent. DAPI binds to AT clusters in the minor groove. The blue fluorescence is ideal to use as a counterstain as it is very different from the usual fluorochromes used in *in situ* hybridisation. DAPI is commonly used at a concentration of 1 µg/ml. However, it seems that using DAPI at this concentration leads to the signal being too strong. This could lead to the apparent volumes of nuclei being represented as bigger than their actual size.

To investigate the influence of DAPI counterstaining on the nuclear volumes, the stock solution used for mounting was tested at different dilutions: 1/2, 1/3, 1/4, 1/5 and 1/6. Image stacks were then taken in order to establish the optimum concentration of DAPI to be used in the study.

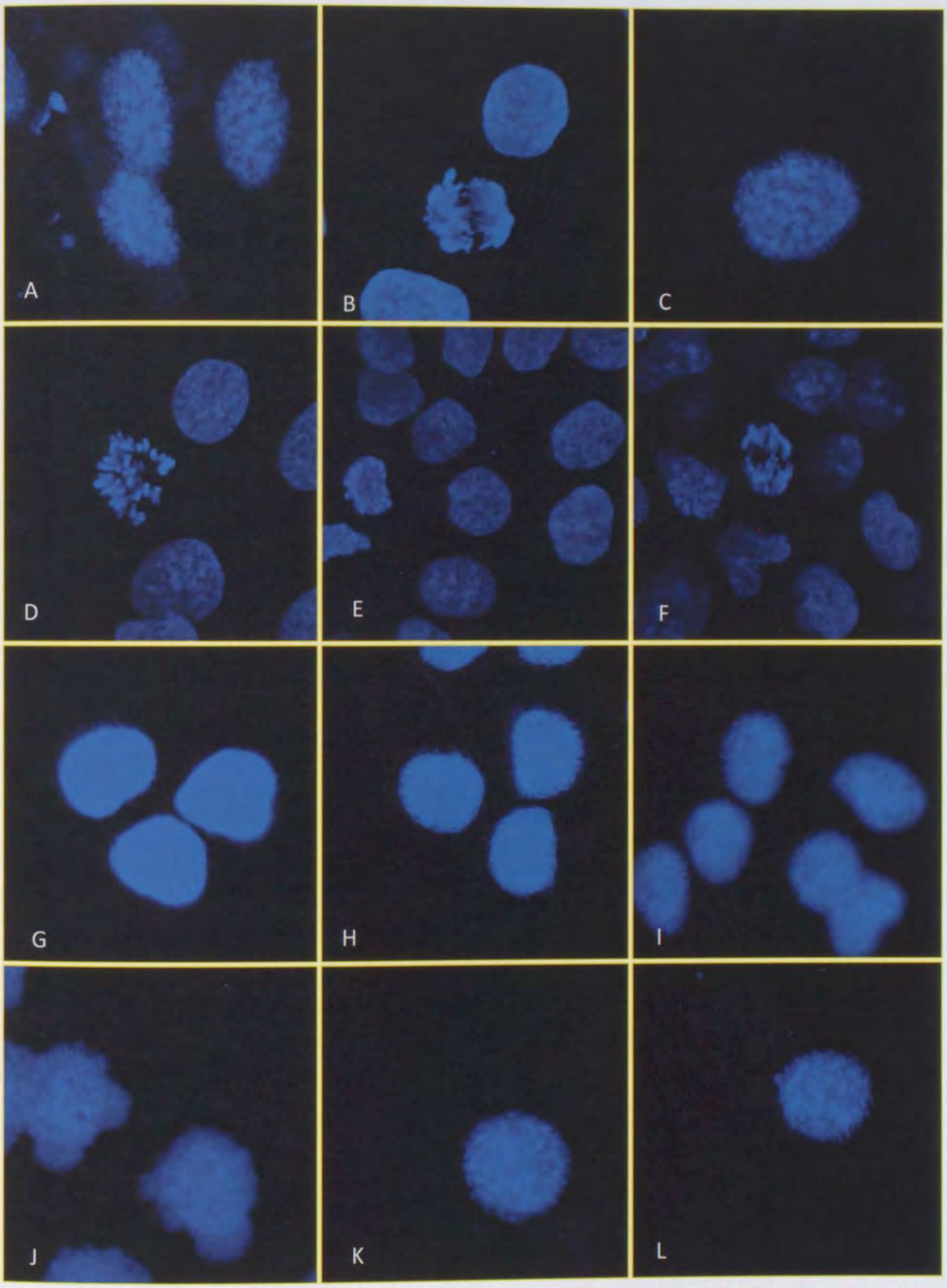

Figure 5.5: Illustration of the result of DAPI counterstaining using two different solutions at different concentrations on RT112 non-irradiated cells nuclei. (A)Nuclei stained with DAPI stock solution supplied by Cambio Ltd (B) Nuclei stained with DAPI solution supplied by Cambio Ltd diluted 1:2 (C) Nuclei stained with DAPI solution supplied by Cambio Ltd diluted 1:3 (D) Nuclei stained with DAPI solution supplied by Cambio Ltd diluted 1:4 (E) Nuclei stained with DAPI solution supplied by Cambio Ltd diluted 1:5 (F) Nuclei stained with DAPI solution supplied by Cambio Ltd diluted 1:6 (G) Nuclei stained with DAPI stock solution supplied by Kreatech (H) Nuclei stained with DAPI solution supplied Kreatech diluted 1:2 (I) Nuclei stained with DAPI solution supplied Kreatech diluted 1:3 (J) Nuclei stained with DAPI solution supplied Kreatech diluted 1:4 (K) Nuclei stained with DAPI solution supplied Kreatech diluted 1:5 (L) Nuclei stained with DAPI solution supplied Kreatech diluted 1:6. Full height x full width of each image is equivalent to 59.5 µm x 59.5 µm.

It appears that with higher concentrations of DAPI the intensity of the signal was very bright which could have led to an artefactual increase of the nuclear volumes which in turn would influence the results concerning the chromosome volumes and proportions within the nuclei considered.

Out of the different dilutions considered, a 1/3 dilution (0.33 µg/ml) of the Kreatech counterstain appears to be the most appropriate as the intensity seems to help avoid artefacts. As a result the slides were mounted with a concentration of DAPI of 0.33 µg/ml. There seemed to be no differences between the two different cell types, so as a result this concentration was used during the entire study.

5.3.2. Optimisation of the 2D imaging acquisition: Confocal microscopy

The acquisition of image stacks using confocal microscopy is required in order to generate 3D visualisations. Appropriate confocal acquisition settings are important in order to obtain good quality images. Adjustable parameters are listed in the summary Table 5.6 below.

Protocol step	Purpose	Methods/variables tested	Mechanism	Advantages/disadvantages
Laser intensity	To establish the optimum settings for image acquisition	Laser intensity	Variation in the flurorochome excitation intensity	Exhaustion of the fluorochome leading to fading
Excitation wavelength		Wavelength range	Optimum wavelength will produce the best signal	Possible wavelength ranges overlap
Emission wavelength				
Reading frequency	To reduce background staining and optimise signal	Number of readings averaged	Each line is scanned a number of time and the	Exhaust of the fluorochrome and fading
Scanning mode		Sequential versus simultaneous	Eliminate the bleeding through between fluorochromes	Eliminate wavelength overlaps
Photomultiplicateurs settings		PMT intensity	PMT gain influences the noise and the noise to signal ratio.	Risk of increasing noise and reduce signal quality
Resolution	To obtain the highest quality images	Resolutions and zoom values	Influences Images quality	Increases image quality
Digital zoom			Influences object definition	Enable the visualisation of smaller structures
Slice number	To define the best combination to avoid loss of signal and limit fading	Range of values: 20; 40; 50 slices	The variation in slice thickness allows smaller strutures visualisation	Fading drastically increases with number of slices

Table 5.6: Summary table of parameters that can be optimised during the confocal microscopy step.

5.3.2.1. Resolution

Image resolution is one of the first parameters to take into account when setting up the series of parallel 2D stack image acquisition. When moving from 2D images to the 3D visualisation, the ability to identify fine detail and differences between two samples for comparisons is key to the investigations. The image resolution is characterised by the microscope ability to show the fine details of the specimen and particularly the minimum distance between distinguishable objects. The resolution is dependent the numerical

aperture of the objective and the wavelength of excitation of the fluorochromes. In this study the DAPI (405 nm excitation), PlatinumBright 495 (488 nm excitation, green) and PlatinumBright 550 (543 nm excitation, red) the corresponding lateral resolutions were 116 nm, 139 nm and 155 nm respectively. The images were of size 1024x1024 pixels.

5.3.2.2. Laser intensity, excitation wavelength

The first group of parameters to set concern the laser intensity and the excitation wavelength appropriate for the type of fluorochromes. The detail of the wavelength ranges settings can be found in the material and methods section. This part of the setting-up process was decided according to the probe supplier guidelines and kept for the entire duration of the study. In the case of the laser, the level of intensity has a direct effect on the phenomenon of fading. Fading is the phenomenon by which fluorescent paint signal intensity decreases following excitation. This comes from the consumption of the paint during the laser scanning microscopy process. In other words, following excitation and after returning to its ground state with emission of light, the fluorochrome is consumed (Tsien *et al.*, 2006). The intensity of the laser was determined on the basis of signal quality at the beginning of the study and modified when necessary at a later stage.

Since, the speed of the consumption increases with the intensity of excitation, one of the solutions to attempt at preventing fading is to use an anti-fading solution when mounting the slides. Despite being effective in reducing fading, it is impossible to totally eliminate that phenomenon. As a result, the lasers were set at an appropriate level to obtain a good quality image and any loss of signal was compensated through the other modifiable parameters of the experimental setting such as the PMTs gain.

5.3.2.3. Scan average and scanning mode

The scanning parameters can also be adapted according to the experiment. In this study, in order to reduce the possible bleeding between the different fluorochromes, the scanning was done sequentially. In other words, each fluorochrome was excited successively and the emission signal collected as such. This reduced the artefact induced

when fluorochrome spectrums overlap but also eliminated the potential cumulative background signal present in the preparation.

Secondly in the eventuality of persistence of background noise signal, the scanning average can be increased so the images appear cleaner and the background noise appears removed. In other words, the number of scans for each line of the preparation is modified. The values obtained will then be averaged and the overall signal to noise ratio thus improved. This manipulation is based in the difference of intensity between real cell signal (strong intensity) and background staining (low intensity). The addition and averaging of the values for the pixel intensity for each line results in the apparent overall reduction of the noise present.

5.3.2.4. Photomultiplier intensity

As mentioned above, confocal images can be affected by laser intensity. They also can be affected by the photomultiplier tube (PMT) gain utilised during scanning. The Leica SP2 confocal microscope system (Leica Microsystems GmbH, Germany) contains 3 photomultiplier tubes for fluorescence. After excitation, each fluorescent dye will return to its ground state emitting photons at a specific wavelength. Each of the PMT is set to detect and to collect the light emitted by one of the fluorescent dye signals. If the laser intensity is high, the required gain is lower which improves signal to noise ratio of the images i.e. the images look cleaner. However increasing the laser power causes more bleaching of the fluorescent dye which is particularly important to consider with high resolution scanning of stacks with many images. By increasing the PMT gain, it is possible to increase the signal collected and visualised on the images. However, high PMT gain results in increased levels of noise i.e. a poorer signal to noise ratio. Hence there has to be some compromise involving the laser power and image intensifier gain used. Since there does not seem to be a clear empirical way to proceed, the setting of the PMT values will rely on the perception of the user doing the analysis.

During the setting up process for the PMTs, the detection range is also an important factor. In fact, it is essential for each PMT to cover the best emission range possible for the fluorochrome considered in order to eliminate scattering. The PMTs wavelength

ranges were set according to the manufacturer suggestions. The spectrums for the platinum red and platinum green dyes were close. This led to colour bleeding between the two signals. As a result, sequential scanning was required in order to increase the resolution of the pictures collected and to avoid artefacts from the bleeding through from one dye to the other. Moreover, it appeared that the emission spectrums of two of the three dyes used overlapped. The emission spectrum for DAPI is very broad meaning it overlaps the emission spectrum for platinum green. Despite being scanned sequentially, the DAPI signal showed bleeding through to the other signals. As a result, two image stacks were generated for each sample considered. The first stack would contain 2 channels: platinum green and red signals and the second stack would contain the DAPI signal. Both stacks were collected using the same settings without any modifications. This preserved the homogeneity in the pictures but also enabled their collation at a later stage of the processing in order to generate complete 3D visualisation of the nuclei considered.

5.3.3. Optimisation of the image acquisition at the 3D level: Confocal microscopy

The parameter to be taken into consideration when generating image stacks of the sample is the number of slices (and pictures as a result) collected during scanning. The objective lens numerical aperture and wavelength of the laser determines the optimal slice thickness. As a result, depending on the limits of the zone to be scanned set by the user, the system will calculate an optimum number of slices that should be generated. In some cases the suggested values were in the order of 100 slices. In view of the restrictions linked to the fading phenomenon occurring during the process, it was essential to establish whether fewer slices could be used without clearly altering the outcome of the scanning and therefore the quality of the data. In order to investigate the influence of the slice number, 2 image stacks were generated for the same nucleus as well as chromosome 2. The reason for this choice was mainly due to the fact that DAPI staining is not subject to intensive fading allowing the scanning to be done without great impact on the quality of the data and in the case of chromosome 2 it was due to the fact that the signal obtained was generally of better quality and intensity compared to the one obtained for chromosome 1. Two values of 20 and 50 (approximately half of the

suggested value) were chosen to be tested alongside the optimised value suggested by the apparatus. In view of the degree of fading during scanning, the slice volumes were assessed using 20 and 50 slices.

Slice number	20	50
volume territory 1	17.69939	21.14358
volume territory 2	14.42395	19.44758
volume territory 3	41.54224	54.00744

Table 5.7: influence of the number of slices in the stack acquisition on the volume values (μm^3) obtained.

The difference between 20 slices and 50 slices appears to result in a clear loss of resolution affecting the volume values. As a result, it was decided that between 40 and 50 slices would be acquired. In the case of samples where the hybridisation appeared less successful 40 slices would be acquired.

5.3.4. Optimisation at the 3D level: Image processing and analysis

The main aim of this optimisation step was to attempt at designing MATLAB code that would allow processing the data in an approach as automated as possible and to use Amira to perform the volume calculations and distance measurements. The different parameters considered in this part are summarised in Table 5.8.

Protocol step	Purpose	Methods/variables tested	Mechanism	Advantages/disadvantages
Matlab - Conversion to binary images				
Brightness and contr	To reduce artefacts and background	The Brightness and contrast input format	Adapting the brightness and contrast reduces artefacts	Artefacts can possibly be reduced but not removed at times
Amira -combined slices - 3D image				
Identify objects	To allow characterisation of territories	The software used	The creation of labelled objects allows the calculations	Helps reducing the processing time
Identify CG of chromosomes and nuclei			The CG of the items are materialised	Allows measurements
Amira- Analysis				
Calculate volume	To characterise territories within the nucleus	The Volume calculation method	Volumes calculated using MATLAB and Amira	Using Amira offers a quicker option
Measure interchromosome distances		The measurement method	Distances calculated using MATLAB and Amira	Measurements and calculations quicker using Amira
Measure distances of chromosome relative to centre		The Relative distances measurement method	3D measurements are drawn of the visualisations	Distances only measureable using Amira

Table 5.8: Summary of the different steps and parameters considered during the protocol optimisation of the image processing and analysis.

The initial consideration concerns the preparation of the raw data and its conversion into black and white images to then allow the analysis using Amira. The initial procedure was to set contrast and brightness using the middle of the stack picture and applying both brightness and contrast identically to all images. This allowed a process without alterations of parameters during a given stack. However, it appeared that as a result some of the signal was lost in the process. This meant that due to the variation in the signal intensity inherent to the hybridisation protocol, the brightness and contrast had to be adjusted for each image in a given stack in order to obtain the best possible representation of the nuclei studied.

The measurements in Amira were performed by tracing a line between two points using the inbuilt 3D tool. The measurements in this study were performed by calculation of the centre of gravity of the entities considered. For example, the distance of a territory from the centre was established by measuring the distance between the centre of gravity of the nucleus and the centre of gravity of the territory in question. The radius was established by measuring the length of the line between centre of gravity of the nucleus and the surface and going through the centre of gravity (CoG) of the territory considered. The distance of the CoG of the Chromosome territories from the nucleus CoG was expressed as a percentage; this allows comparison of the values for cells with different nucleus sizes.

REFERENCES

Bolzer, A., Kreth, G., Solovei, I., Koehler, D., Saracoglu, Kaan, Fauth, C., Müller, S., Eils, Roland, Cremer, Christoph, Speicher, Michael R & Cremer, Thomas (2005). Three-dimensional maps of all chromosomes in human male fibroblast nuclei and prometaphase rosettes. *PLoS Biology*, **3**(5), e157.

Croft, J. A., Bridger, J. M., Boyle, S., Perry, P., Teague, P. & Bickmore, W. A. (1999). Differences in the localization and morphology of chromosomes in the human nucleus. *The Journal of Cell Biology*, **145**, 1119–1131.

Eils, R., Dietzel, S, Bertin, E., Schröck, E., Speicher, M R, Ried, T., Robert-Nicoud, M., Cremer, C. & Cremer, T. (1996). Three-dimensional reconstruction of painted human interphase chromosomes: active and inactive X chromosome territories have similar volumes but differ in shape and surface structure. *The Journal of Cell Biology*, **135**(6), 1427–1440.

Hepperger, C., Otten, S., Von Hase, J. & Dietzel, S. (2007). Preservation of large-scale chromatin structure in FISH experiments. *Chromosoma*, **116**(2), 117–33.

Min, T. (2003). FISH techniques. *Methods in Molecular Biology*, **220**, 193–212.

Scheuermann, M. O., Tajbakhsh, J., Kurz, A., Saracoglu, K, Eils, R & Lichter, P. (2004). Topology of genes and nontranscribed sequences in human interphase nuclei. *Experiemental Cell Research*, **301**, 266–279.

Strefford, J. C., Lillington, D. M., Steggall, M., Lane, T. M., Nouri, A. M. E., Young, B. D. & Oliver, R. T. D. (2002). Novel chromosome findings in bladder cancer cell lines detected with multiplex fluorescence in situ hybridization. *Cancer Genetics and Cytogenetics*, **135**(2), 139–46.

Tanabe, H., Habermann, F. A, Solovei, I., Cremer, M. & Cremer, T. (2002). Non-random radial arrangements of interphase chromosome territories: evolutionary considerations and functional implications. *Mutation Researchl*, **504**(1–2), 37–45.

Tsien, R. & Waggoner, A. (1995). Fluorophores for confocal microscopy: photophysics and photochemistry. in *Handbook of Biological Confocal Microscopy* ed. by Pawley, J. B., 338–352.

Visser, A. E., Eils, R, Jauch, A., Little, G., Bakker, P. J., Cremer, T. & Aten, J. A. (1998). Spatial distributions of early and late replicating chromatin in interphase chromosome territories. *Experimental Cell Research*, **243**(2), 398–407.

Wang, M., Perissel, B. & Malet, P. (1995). Cytogenetic characterization of a bladder carcinoma cell line by fluorescence *in situ* hybridization. *Public Health*, **174**, 170–174.

Chapter 6 Characterisation of chromosome territories in human primary fibroblasts and RT112 bladder carcinoma cells

6.1. Introduction

The first hours following irradiation are crucial in maintaining cell integrity and cell survival. Following the generation and detection of the double strand breaks, the repair is initiated and the bulk of double strand breaks (DSBs) repair is completed within 60 minutes with the remaining breaks repaired between 24 and 48 hours (Cornforth & Bedford, 1983; Löbrich *et al.*, 1995; Nevaldine *et al.*, 1993). It is essential for the cell that repair is done fast and efficiently in order to allow the cell to pass the next cell cycle checkpoint and move on to the next cell cycle phase. During interphase, the territories occupied by the chromosomes change and chromosomes appear to be highly dynamic entities. Several aspects can be considered when attempting to characterise chromosome territories (CTs). Despite being dynamic, the positioning within the nucleus has been identified to be size (Bolzer *et al.*, 2005) or gene content dependent. A difference has been observed between different transcription timing and gene content which could influence positioning (Visser *et al.*, 1998; Croft *et al.*, 1999).

An exhaustive list of the exact parameters that govern chromosome positioning has yet to be determined. It is possible that effectively, due to the processes happening throughout the cell cycle, the gene content and replication times could be the main features governing chromosome positioning. However, territory size cannot be overlooked due to the physical constraints that arise when considering a cell nucleus. Positioning according to gene content would therefore result in a constant movement of an area of the genome in and out of the nuclear centre according to the levels of transcription occurring. Despite the evidence of intermingling happening between territories (Branco & Pombo, 2006), it appears that the main body of the chromosome stays within the territory, with levels of chromatin compaction varying throughout the cell cycle. Despite being documented by Branco & Pombo (2006) it is very difficult to establish the exact levels of intermingling occurring at a given time, as the levels of transcription appear to have an influence on intermingling.

The use of FISH only allows the visualisation of CTs at the time considered. It is therefore not currently possible to establish the exact nature of all the processes involving protein complexes occurring at the time of the fixation using only FISH. The visualisation of protein complexes would require the use of FISH in conjunction with immunochemistry

which adds complexity to the experiment and increases the risks of artefacts. Hence this study investigates parameters including nuclear volume, territory volume as well as the number of territories at different times following irradiation. In addition the relative distances of the CTs observed within the 3-dimensional configuration of the cell nucleus were measured hence building on the studies of Sun *et al.* (2000) and Bolzer *et al.* (2005); this also allowed the application of the approach to irradiated cells in order to characterise the cell lines studied and highlight possible differences.

6.2. Material and methods

6.2.1. Choice of the cell lines

This chapter concentrates on the characterisation of two cell lines: Normal human fibroblasts and human bladder carcinoma cells (RT112) before irradiation. Fibroblasts were chosen as the reference for normal nuclear settings. On the other hand, RT112 cells have also been characterised with possessing several deletions, isochromosomes and translocations (Strefford *et al.*, 2002; Wang *et al.*, 1995; Williams *et al.*, 2005). RT112 were chosen because the cells possess 46/47 chromosomes which unlike other aberrant cell lines is similar to the number of chromosomes encountered in normal cells (Williams *et al.*, 2005). The similarity with the normal cell nucleus in terms of chromosome numbers allows better identification of possible preserved similarities as well as the difference between normal and cancer cells. The cell nuclei are likely to present some instability which will contribute to assessing the impact on the number of chromosome aberrations following ionizing irradiations.

6.2.2. Slide preparation, hybridisation and confocal microscopy

The slides were prepared according to the protocol described in Chapter 4 (Section 4.2.7. to 4.2.9.). Briefly, the cells were seeded in the form of a single cell suspension into temporarily attached glass chambers. The cells were them allowed to attach to the slide before undergoing fixation, pre-treatment and FISH. The slides were subjected to the chosen FISH protocol following optimisation (as described in Chapter 5)

and the data collected using confocal microscopy as described in Chapter 5 before being processed and analysed using MATLAB and Amira.

6.2.3. Image processing and analysis

The image stacks obtained using confocal microscopy were subjected to image processing and image analysis. The data stacks were processed using MATLAB and the measurements of the different parameters of interest for the study were performed using Amira as described in Chapter 4 Section 4.2.10.

Briefly, the images were converted into binary images in order to allow further processing. Parameters such as brightness and contrast were adjusted in order to obtain suitable image clarity for this part of the study. This allowed the reduction of potential artefacts still present despite the optimisation of the FISH protocol.

The measurements in Amira were performed using the in-built tools of the software package. Parameters such as volumes and number of territories were established for every cell included in the study as described in Chapter 4 Section 4.2.10.

6.3. Results

6.3.1. Characterisation of cell nuclei

Nuclear staining with DAPI provides a high contrast means of measuring nuclear volume. There is little background staining (Figure 6.1) and therefore the nuclear volume can be clearly delineated enabling three-dimensional visualisation and appropriate subsequent volume calculations. The nuclear volume measurements provide a reference to enable the characterisation of the chromosome territories of interest.

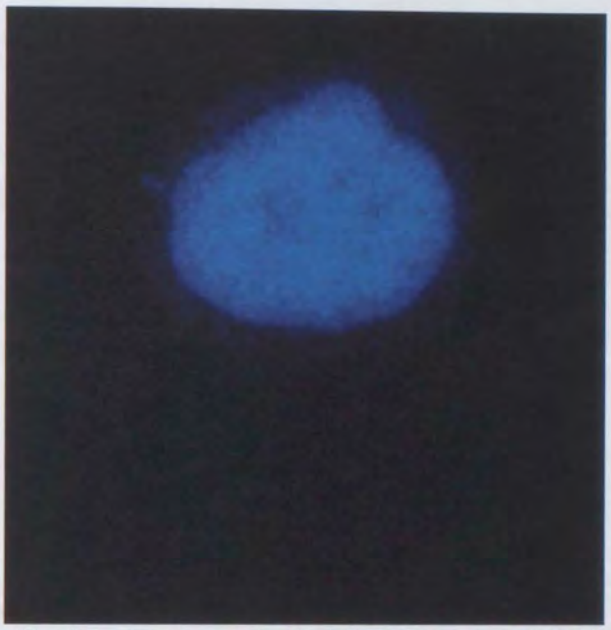

Figure 6.1: Normal human fibroblast nucleus stained with DAPI acquired using laser confocal microscopy. Image captured with a x63 immersion objective and digitally zoomed x4. Full height x full width of image equivalent to 58.5 µm x 58.5 µm.

Nuclear volumes were measured from 0 hours to 24 hours after irradiation for both normal fibroblasts and RT112 cells; the results are presented in Figure 6.2 as frequency distribution plots. The resulting descriptive statistics are presented in Tables 6.1 and 6.2.

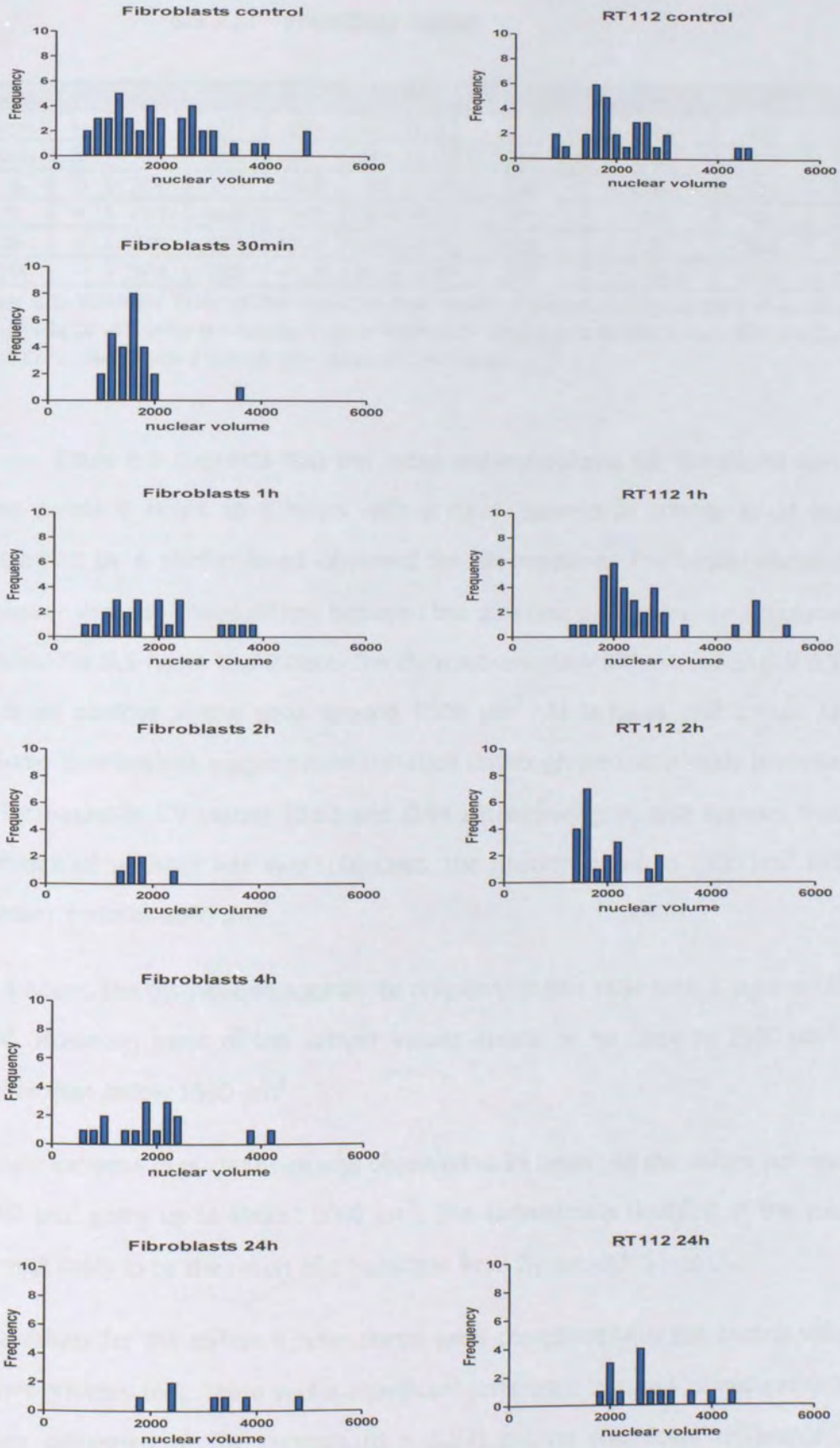

Figure 6.2: Column 1: Nuclear volume distributions for fibroblast controls, 30 min, 1 h, 2 h, 4 h and 24 h post-irradiation. Column 2: Nuclear volume distributions for the RT112 cell line controls, 1 h, 2 h and 24 h post-irradiation. Volumes are expressed in μm^3.

6.3.1.1. Fibroblast nuclei

Sample	N	Mean	Median	SD	SE	CV	25% percentile	75% percentile	75%-25%	Normal?	P
Control	41	2024	1811	1070	167.2	0.53	1125	2633	1508	Yes	P > 0.10
30min	26	1581	1552	504.3	98.9	0.32	1229	1749	520	No	0.0195
1h	23	1892	1574	901.91	188	0.48	1142	2388	1246	Yes	P > 0.10
2h	6	1711	1646	334.2	136.44	0.20	1491	1919	428	Yes	P > 0.10
4h	17	1964	1896	943.41	228.81	0.48	1268	2332	1064	Yes	0.0954
24h	7	3114	3189	956.42	361.49	0.31	2439	3765	1326	Yes	P > 0.10

Table 6.1: Summary table of the mean, median, standard deviation (SD),standard error of the mean (SE), range and CV values for the nuclear sizes of each of the time points for the human fibroblasts. Volume units μm^3. Consistency with a normal distribution is indicated.

Table 6.1 suggests that the mean nuclear volume for fibroblasts was similar for time points 0 hours to 4 hours with a clear increase in volume at 24 hours. This is confirmed by a similar trend observed for the medians. The actual distributions show however that the shape differs between the different time points as suggested by the CV values. For 0.5 hours and 2 hours the distributions show little variation (CV 0.32 and 0.20) with an obvious single peak around 1500 μm^3. At 0 hours and 1 hour however, the volume distributions suggest more variation (although the mean value is similar) reflected in increased in CV values (0.53 and 0.48 respectively); it also appears that there is a partition of volumes into two subgroups, the majority close to 1500 μm^3 with a smaller number close to 3000 μm^3.

At 4 hours, the distribution appears to only exhibit two cells with a volume close to 4000 μm^3. However, most of the sample values appear to be close to 1500 μm^3 and above rather than below 1500 μm^3

A clear increase in nuclear size was observed at 24 hours. All the values bar one are above 2000 μm^3 going up to almost 5000 μm^3. The approximate doubling of the volume values is most likely to be the result of a transition from G_1 through S into G_2.

The values for the different time points were compared with the control values using a Mann-Whitney test. There was a significant difference in terms of nuclear volumes at 24 hours compared to the controls ($p = 0.02$) but no significant difference was found between the controls and 30 minutes, 1 hour and, 2 hours and 4 hours ($p = 0.17$, $p = 0.61$, $p = 0.48$ and $p = 0.84$ respectively). The results were confirmed using a false discovery rate (FDR) method (Benjamini & Hochberg, 1995) with a maximum FDR of 10%.

6.3.1.2. RT112 nuclei

Sample	N	Mean	Median	SD	SE	CV	25% percentile	75% percentile	75%-25%	Normal?	P
Control	30	2100.72	1805.19	879.83	160.64	0.42	1584	2544	960	No	0.0392
1h	35	2611.68	2268.89	1042.41	176.20	0.40	1928	2860	932	No	0.0017
2h	20	1922.11	1660.29	544.57	121.77	0.28	1575	2258	683	No	0.009
24h	15	2757.52	2667.16	766.37	197.88	0.28	2024	3111	1087	Yes	P > 0.10

Table 6.2: Summary table of the mean, median, standard error of the mean, standard deviation, range and CV values for the nuclear sizes of each of the time points for the RT112 cell line. Volume units μm^3. Consistency with a normal distribution is indicated.

It appears the median values for the RT112 nuclear volumes are similar for the time points 0 hours and 2 hours and appear to be higher at 1 hour and 24 hours.

Unlike the median values, the distributions seem to become tighter with time which translates into decreasing interquartile range/median values after 0 hours (0.53, 0.41, 0.41 and 0.41 at 0, 1, 2, and 24 hours respectively). The majority of values are clustered around (1 h) or just below (0 h) 2000 μm^3. However, the presence of a small number of higher values at 1 hour could explain the difference in median value at 1 hour.

Despite having similar median values, the 0 hours and 2 hours samples appear to exhibit different distribution which is confirmed by the different interquartile range/median values (0.53 and 0.41 respectively). At 2 hours the distribution shows little variation around 1500 μm^3 whereas at 0 hours the values show more variation around 2000 μm^3. Similarly, the distributions at 1 hour and 24 hours have comparable median values with similar interquartile range/median values of 0.41. The values at 1 hour appear to be mostly around 2000 to 3000 μm^3 with a cluster of nuclei with higher volumes (close to 6000 μm^3) whereas most of the values at 24 hours are near 3000 μm^3.

The values for the different time points were compared with the control values using a Mann-Whitney test. There was a significant difference in terms of nuclear volumes at 1 hour and 24 hours compared to the controls ($p = 0.02$ and $p = 0.004$ respectively) but no significant difference was found between the controls 2 hours ($p = 0.43$). The results were confirmed using a false discovery rate (FDR) method (Benjamini & Hochberg, 1995) with a maximum FDR of 10%.

6.3.1.3. Comparison between fibroblasts and RT112 distributions

The distributions appear similar for both cell lines at 2 hours (interquartile range/median values of 0.26 for fibroblasts and 0.41 for RT112) with values clustered between 1500 and 2000 μm^3. The distributions also appear to be similar at 24 hours with interquartile range/median of 0.42 for fibroblasts and 0.41 for RT112 and the nuclei sizes varying from 2000 to 4000 μm^3.

The RT112 distribution at 1 hour seems to exhibit a similar pattern to the fibroblasts controls and also the fibroblast 1 hour (the first group of values near 2000 μm^3 and the second over 4000 μm^3).

The values for the fibroblast controls and RT112 controls were compared using a Mann-Whitney test. There was no significant difference in terms of nuclear volumes between the controls ($p = 0.58$).

6.3.2. Characterisation of the chromosome territories in non-irradiated cells

The characterisation of chromosome territories (CTs) should provide deeper insight into the consequences of radiation treatment on the organisation of the nucleus. In this study, the two chromosomes considered were chromosome 1 and 2. These two chromosomes are the largest encountered in the cell nucleus. This presents an advantage as after irradiation, it can help with being able to visualise fragments that could potentially be generated more easily. In this study, the individual volumes, the total chromosome volumes, the number of CTs, and their relative distances were examined for both cell lines and in 3-dimensions at different time points following irradiation. The individual volumes, the total volumes and their relation to the nuclear volume will help with visualising changes between the different time points and also possibly potential changes in chromatin condensation. The study of the CT numbers allows the investigation of DNA repair and chromosome aberration formation.

The relation between chromosome volume and nucleus volume was studied for both normal (fibroblasts) and abnormal (RT112) cells. The analysis was performed similarly for both cell lines. As each chromosome could exist as part of several fragments, the analyses were performed in four ways to compare with nucleus volume:

1. individual fragment volume
2. ratio of individual fragment volume / nucleus volume
3. total of fragment volumes for each chromosome
4. ratio of total of fragment volumes for each chromosome / nucleus volume

The number of territories was studied in terms of number, volumes depending on the number of territories seen in the nucleus, ratio of each individual territory volume / the total chromosome volume.

Distances were studied in terms of actual distance from the centre of the nucleus as well as the percentage of the radius.

6.3.2.1. Characterisation of chromosome 1 and 2 in human fibroblasts non-irradiated

6.3.2.1.1. Individual and total chromosome volumes

The image processing allowed measurement of the volume occupied by the chromosome considered during interphase. Assessment was performed on the raw data using MATLAB and Amira to generate 3D visualisations of the cells studied. This was performed to characterise the nature of the positioning as well as defining basic parameters of individual chromosome within the nucleus.

The distributions for individual territories values, total chromosome volumes and their percentage occupied in the nucleus were assessed for chromosome 1 and 2 (Figure 6.3). The sample group contained 41 cells. The mean values, median, standard deviations, standard errors of the mean as well as CV values were computed (Table 6.3).

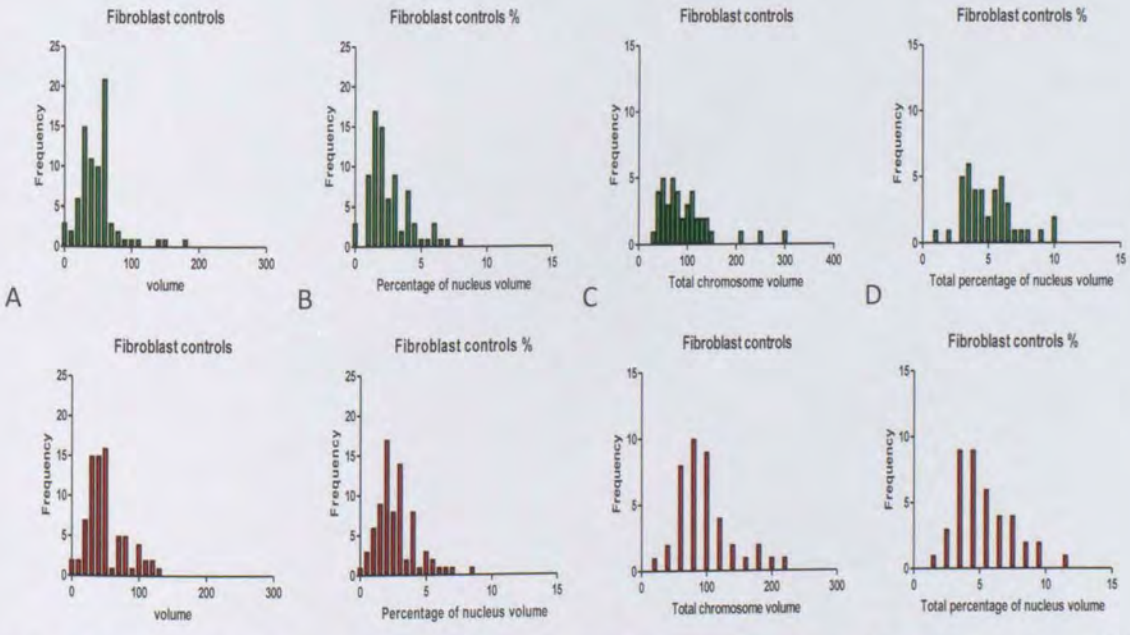

Figure 6.3: The volume measurements in fibroblasts for Chromosome 1 and 2 at 0 hours (controls) are presented as frequency histograms. The mean values together with standard error and CV are presented in Table 6.3. Horizontally, the four graphs show A: actual individual chromosome volumes, B: volumes expressed as a percentage of the nuclear volume C: total actual chromosome volume calculated as the sum of the volume of all fragments in each nucleus and D: the sum of all fragments expressed as a percentage of the nuclear volume. The y axes show the number observed for each volume category for chromosome 1 (green) and chromosome 2 (red). Volumes are expressed in μm^3.

The ratio of the median value for the individual volumes for chromosome 1 and 2 and their corresponding median values for the total chromosome volume appear to be

approximately 2 (see Table 6.3). This could indicate that the degree of compaction between the two members of the chromosome pairs for both chromosome 1 and 2 is similar and each one corresponds to approximately 50% of the total chromosome volume. This is also observed for the percentages of nucleus median values. When testing for normality using Kolmogorov-Smirnov normality test individual volume values and total volume values distributions for both chromosomes were not consistent with a normal distribution (P values given in Table 6.3).

Fibroblast control	N	Mean	Median	SD	SE	CV	25% percentile	75% percentile	75%-25%	Normal?	P
Chr1 volume	79	49.40	45.98	29.83	3.36	0.60	29.60	60.97	31.37	No	P<0.0001
Chr1 percentage	79	2.60	2.12	1.61	0.18	0.62	1.60	3.27	1.68	No	0.0002
Chr2 volume	78	50.83	44.10	28.92	3.27	0.57	32.63	67.6	34.95	No	0.0464
Chr2 percentage	78	2.75	2.32	1.54	0.17	0.56	1.74	3.47	1.73	No	P > 0.10
Chr1 total Volume	41	95.18	84.42	55.51	8.67	0.58	57.65	114.20	56.55	No	0.0464
Chr1 total percentage	41	5.01	4.52	2.07	0.32	0.41	3.46	6.10	2.64	Yes	P > 0.10
Chr2 total volume	41	96.71	88.76	42.70	6.67	0.44	68.6	114.8	46.20	No	0.0174
Chr2 total percentage	41	5.23	4.63	2.13	0.33	0.41	3.587	6.934	3.35	No	0.0309

Table 6.3: Summary table of descriptive statistics corresponding to the distributions presented in Figure 6.3 for chromosome 1 and 2 at 0 hours (controls) in fibroblasts. Volumes are expressed in μm^3.

The different values obtained for individual chromosome volumes and total chromosome volumes as well as their corresponding percentages were plotted against the corresponding nuclei volumes (Figure 6.4) in order to attempt to establish whether there is a relation between volumes and nucleus size.

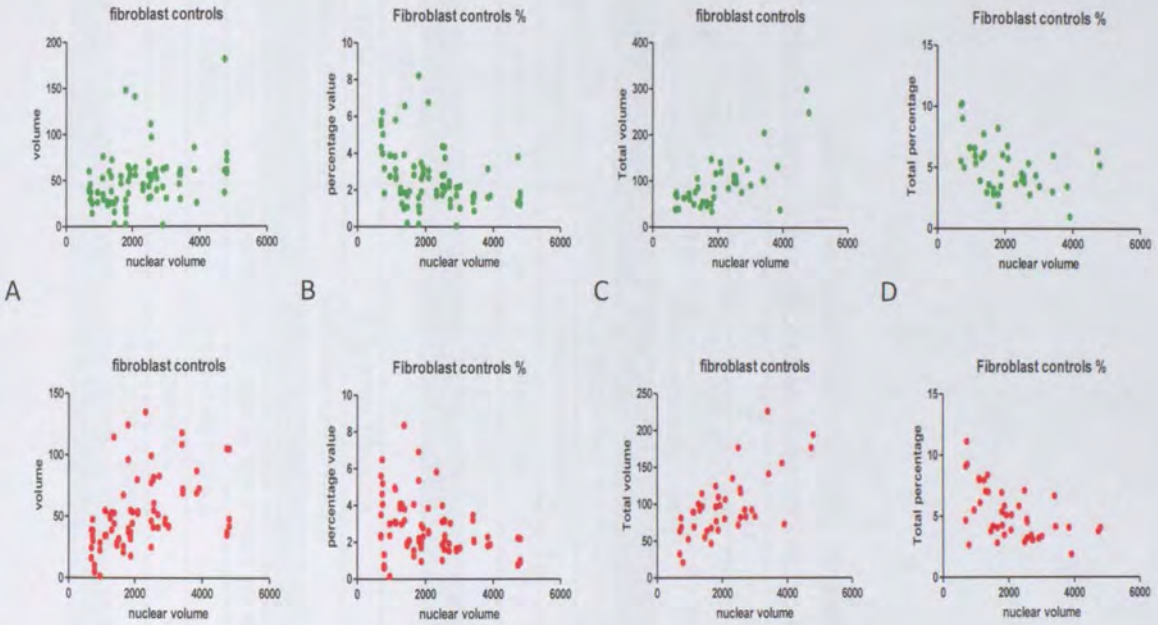

Figure 6.4: The volume measurements of each chromosome 1 and 2 at 0 hours (controls) are plotted against the corresponding nucleus size for fibroblasts. From left to right the four graphs show 1: actual individual chromosome volumes, 2: volumes expressed as a percentage of the nuclear volume 3: total actual chromosome volume calculated as the sum of the volume of all fragments in each nucleus and 4: the sum of all fragments expressed as a percentage of the nuclear volume. Vertically the graphs show the respective distributions for chromosome 1 (green) and chromosome 2 (red). Volumes are expressed in μm^3.

Visual inspection of the scatter plots in Figure 6.4 suggests a relation between individual chromosome volume and nucleus volume as well as total chromosome volume and nucleus volume for both chromosomes. Figure 6.4 suggests that individual volumes as well as total chromosome volumes increase with nucleus size for both chromosome 1 and chromosome 2. This relation appears to be clearer for the total chromosome values. There is a significant relation between the volumes of territories (both individual and sums) and nuclear volumes with a positive Spearman's correlation coefficient (nucleus compared with chromosome 1 total volume, $r = 0.6$, $p < 0.0001$). If more than 2 territories occur in individual cells, the individual territories are likely to have smaller volumes and the relation between individual chromosome volumes and nucleus size is thus likely to be less evident.

Chr 1 Individual values	fibroblast controls	fibroblasts controls %	Chr 1 Total volumes	fibroblast controls	fibroblasts controls %
Number of XY Pairs	79	79	Number of XY Pairs	41	41
Spearman r	0.4147	-0.454	Spearman r	0.6026	-0.4272
P value (two-tailed)	0.0001	P<0.0001	P value (two-tailed)	P<0.0001	0.0053
Is the correlation significant? (alpha=0.05)	Yes	Yes	Is the correlation significant? (alpha=0.05)	Yes	Yes
Linear regression					
Linear regression slope	0.009110 ± 0.002725	-0.0005523 ± 0.0001444	Linear regression slope	0.03759 ± 0.005866	-0.0007944 ± 0.0002871
Intercept when X=0	28.90 ± 6.895	3.842 ± 0.3653	Intercept when X=0	17.02 ± 13.65	6.661 ± 0.6682
r^2	0.1268	0.1597	r^2	0.5129	0.1641
Chr 2 Individual values	fibroblast controls	fibroblasts controls %	Chr 2 Total volumes	fibroblast controls	fibroblasts controls %
Number of XY Pairs	78	78	Number of XY Pairs	41	41
Spearman r	0.5617	-0.3852	Spearman r	0.5969	-0.5596
P value (two-tailed)	P<0.0001	0.0005	P value (two-tailed)	P<0.0001	0.0001
Is the correlation significant? (alpha=0.05)	Yes	Yes	Is the correlation significant? (alpha=0.05)	Yes	Yes
Linear regression					
Linear regression slope	0.01150 ± 0.002563	-0.0005004 ± 0.0001423	Linear regression slope	0.02764 ± 0.004713	-0.001064 ± 0.0002743
Intercept when X=0	26.74 ± 6.117	3.797 ± 0.3396	Intercept when X=0	39.24 ± 10.97	7.441 ± 0.6383
r^2	0.2095	0.14	r^2	0.4686	0.2782

Table 6.4: Summary of the results of the correlation analysis between chromosome territory volumes, total chromosome volumes, their respective ratios with nucleus volume for chromosome 1 and 2 in fibroblasts. Volumes are expressed in μm^3.

In the case of chromosome 1 the median value for the total chromosome volume was 4.52 and in the case of chromosome 2, the median value was 4.63. These values appear to be consistent with the slopes obtained for the total chromosome volumes (Table 6.4).

6.3.2.1.2. Individual territory occurrence

The 41 nuclei examined presented between 1 and 4 territories for chromosome 1 (green label) and between 1 and 3 territories for chromosome 2 (red label).

The individual volumes for each territory were plotted against the total number of territories observed in the cell considered; this allows examination of whether individual volumes are related to the number of territories observed in the nucleus (Figure 6.5). A summary of the median values and the number of occurrences for each territory number is presented in Table 6.5.

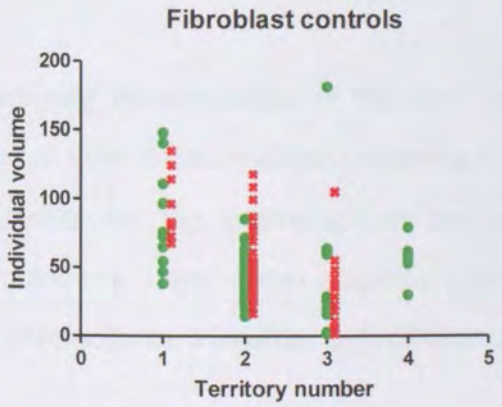

Figure 6.5: in this graph the individual volumes values for both chromosome 1 and 2 are plotted according to the territory number observed within their respective cells. The corresponding median values and scenario occurrences are summarised in Table 6.5. Chromosome 1 is illustrated in green and chromosome 2 in red. Volumes are expressed in μm^3.

In the cells where 1 or 2 territories (1T and 2T) occurred for chromosome 1 and 2, the median values (72 μm^3 and 83 μm^3) when a unique territory is observed appears to be approximately double the values observed when 2 territories (40 μm^3 and 43 μm^3) are present in the nucleus considered.

When 3 territories (3T) occur within the cell, the median obtained for 3 territories is lower than when 2 territories are present for chromosome 1 and chromosome 2 with a greater difference for chromosome 1 (Table 6.5).

Chr 1	Territory number	1 territory	2 territories	3 territories	4 territories
Control	occurrence	11	24	4	2
	Median	72.27	39.73	26.66	58.18
	25% Percentile	46.67	29.51	5.914	53.38
	75% Percentile	110.7	55.36	61.37	61.34
	75%-25% Percentile	64.03	25.85	55.456	7.96
Chr2	Territory number	1 territory	2 territories	3 territories	4 territories
control	occurrence	9	27	5	
	Median	82.52	42.84	34.7	
	25% Percentile	76.11	33.48	10.34	
	75% Percentile	119.1	54.04	47.73	
	75%-25% Percentile	42.99	20.56	37.39	

Table 6.5: Median values for the territory volumes for chromosome 1 and chromosome 2 in fibroblasts sorted according to the number found in the cell nucleus considered and occurrences for each scenario. The 25% percentile, 75% percentile and the difference between the two are also given. Volume medians are expressed in μm^3.

Examining the proportion of the total chromosome volume occupied by each territory in the cell considered enables assessing the chromosome territories distribution properties. The data for the control group are presented in Figure 6.6. The data obtained for chromosome 1 are shown graphically and have been aligned with the corresponding data for chromosome 2 in order to facilitate comparison.

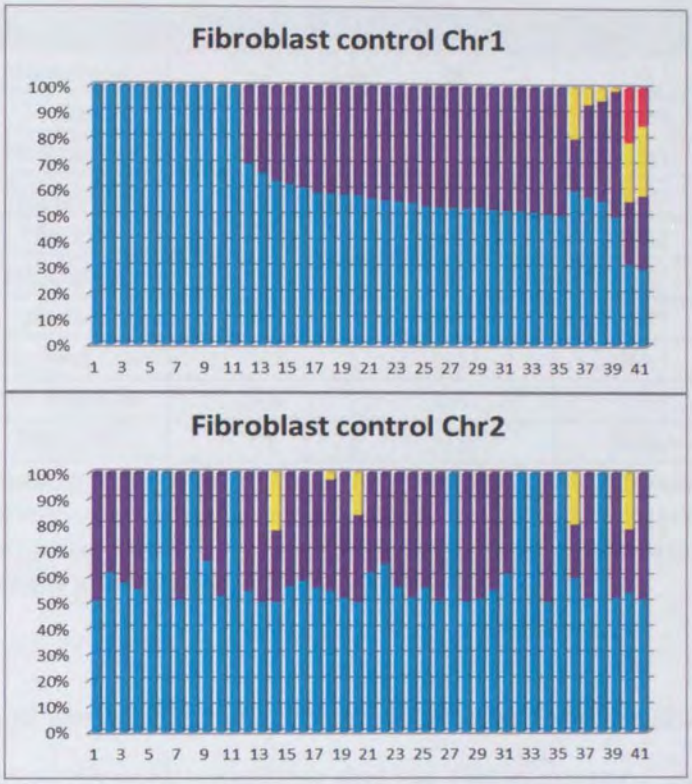

Figure 6.6: Graphic representation of the proportion of each individual territory volume compared to the corresponding total chromosome volume (100%) for both chromosome 1 (top) and 2 (bottom). Each bar corresponds to the territories observed in on cell nucleus for the chromosome considered. Each colour in the bar represents a fragment (territory) observed for the given chromosome. The data has been sorted using the number of territory observed for chromosome 1 with the corresponding chromosome 2 data aligned accordingly in the bottom graph. Territory 1, blue; territory 2, purple; territory 3, yellow; territory 4, pink.

Figure 6.6 illustrates there are two occurrences of 4 territories. After close examination it appears as though the nuclear size for one of those 2 occurrences (4801 μm^3) is twice the size of the other values (Figure 6.7). In the case of the second 4T for chromosome 1 occurrence, the nuclear volume (3428 μm^3) appears to be also close to twice but slightly lower than the median size value (Table 6.6) of nuclei presenting 2 territories. Moreover, the total chromosome volumes measured for the 4T occurrences for chromosome 1 are much higher than the average of the values measured (251 μm^3 and 205 μm^3) which is also an indication of the cells being in G_2. 3T and 2T were observed for the corresponding chromosome 2 (red).

Chr1	Territory Number	1 territory	2 territories	3 territories	4 territories
Nuclei data	Occurrence	11	24	4	2
	Median	1796	1844	2353	4115
	25% Percentile	1304	1121	1545	3429
	75% Percentile	2550	2543	4277	4802
	75%-25%	1246	1422	2732	1373
Chr2	Occurrence	9	27	5	
Nuclei data	Median	2077	1811	1877	
	25% Percentile	1728	1132	869.5	
	75% Percentile	2644	2569	4768	
	75%-25%	916	1437	3898.5	

Table 6.6: Median values for the nuclear volumes for chromosome 1 and chromosome 2 in fibroblasts sorted according to the number of territories found in the cell nucleus considered and occurrences for each scenario. The 25 % percentile, 75 % percentile and the difference between the two (interquartile range) are also given. Volume medians are expressed in μm^3.

In the case of the 4G/3R, the split appeared to be 25%/25%/25%/25% (Figure 6.6) and roughly 50%/25%/25% which confirms that the cell in question was tetraploid at the time of the fixation and that it is not the result of the generation of fragments or chromosome aberrations. In the case of the 4G/2R the splits appeared to be 25%/25%/25%/25% and 50%/50%. The presence of only 2T for chromosome 2 could be either due to both copies of each chromosome being too close to each other to be differentiable or that chromosome 2 had not yet been replicated. The corresponding nucleus being bigger than the median but smaller than the 4G/3R nucleus could suggest it is the latter.

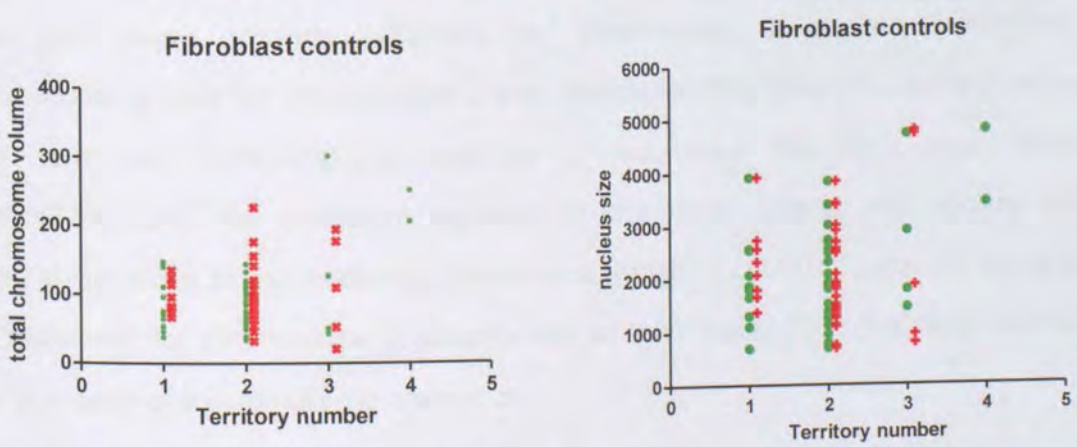

Figure 6.7: In this graph the nucleus volume values for both chromosome 1 (green) and 2 (red) in fibroblasts are plotted according to the number of territories observed. Volume are expressed in μm^3.

When 3T occurs for chromosome 1 (4 cells) the splits are 60%/20%/20%, 58%/36%/6%, 56%/39%/5%, 50%/49%/1%. The corresponding splits for chromosome 2 are 60%/20%/20%, 50%/50%, 100%, 50%/50%. So the resulting combinations are 3G/3R, 3G/2R(1), 3G/1R, 3G/2R(2). In the 3G/2R(1) and 3G/1R combinations, the corresponding total volumes were 43 μm^3/54 μm^3 and 50 μm^3/96 μm^3 respectively.

Since the total chromosome volumes are close to the median calculated before, the presence of an extra fragment for chromosome 1 could be the result of the generation of a non-repaired break, as the fragments represent 6% and 5% respectively which is a considerable proportion of the total chromosome volume and the split between fragments is not even. The 1 % fragment seen in the remaining 3G/2R(2) (total chromosome volumes of 126 μm^3 and 92 μm^3) could also be a fragment but may be an artefact introduced during the image processing as the examination of the picture stacks does not show the presence of a clear fragment.

Finally, the 3G/3R combination the total chromosome value for chromosome 1 was 301 μm^3 and the total chromosome volume for chromosome 2 was 176 μm^3. Both the splits are 60%/20%/20% and the nuclear volume was 4733 μm^3. All these parameters indicate that the cell is likely to be in G_2 and have 2 copies of each chromosome with the two copies of one of them not differentiable using this method.

When 2T occurred for chromosome 1 within the cell nuclei studied, the splits were very close to a 50%/50% split in most occasions and for both chromosomes considered. When the split edges towards 60%/40% for chromosome 1 on one occurrence the corresponding split for chromosome 2 was similar to 50%/25%/25%, on one occurrence the split was 50%/34%/16% and on 1 occurrence the split was similar to 55%/42.5%/2.5%. The corresponding total chromosome volumes and nuclear volumes were either close to the median or slightly smaller which could indicate that the presence of fragments for chromosome 2 (despite one of them being 25%/25%) was the result of the presence of a chromosome aberration.

When 1T was observed for chromosome 1, either 1T or 2T were observed for the corresponding chromosome 2. In the cases of 1G/2R, the split was 50%/50% or close for most occurrences except for 2 cells where the splits were 66%/34%, 62%/38%.

Corresponding total chromosome volumes were 120 μm^3 (4% of nuclear volume) and 89 μm^3 (8% of nuclear volume).

6.3.2.1.3. Territory distances and ratio of corresponding radii

Distances were measured from the centre of gravity of the nucleus to the centre of gravity of the territory considered using the in-built 3D tool in Amira (Figure 6.8). The radii from the centre of gravity of the nucleus and passing through the centre of gravity of the territory were also measured. The ratios of the radii were then calculated for analysis.

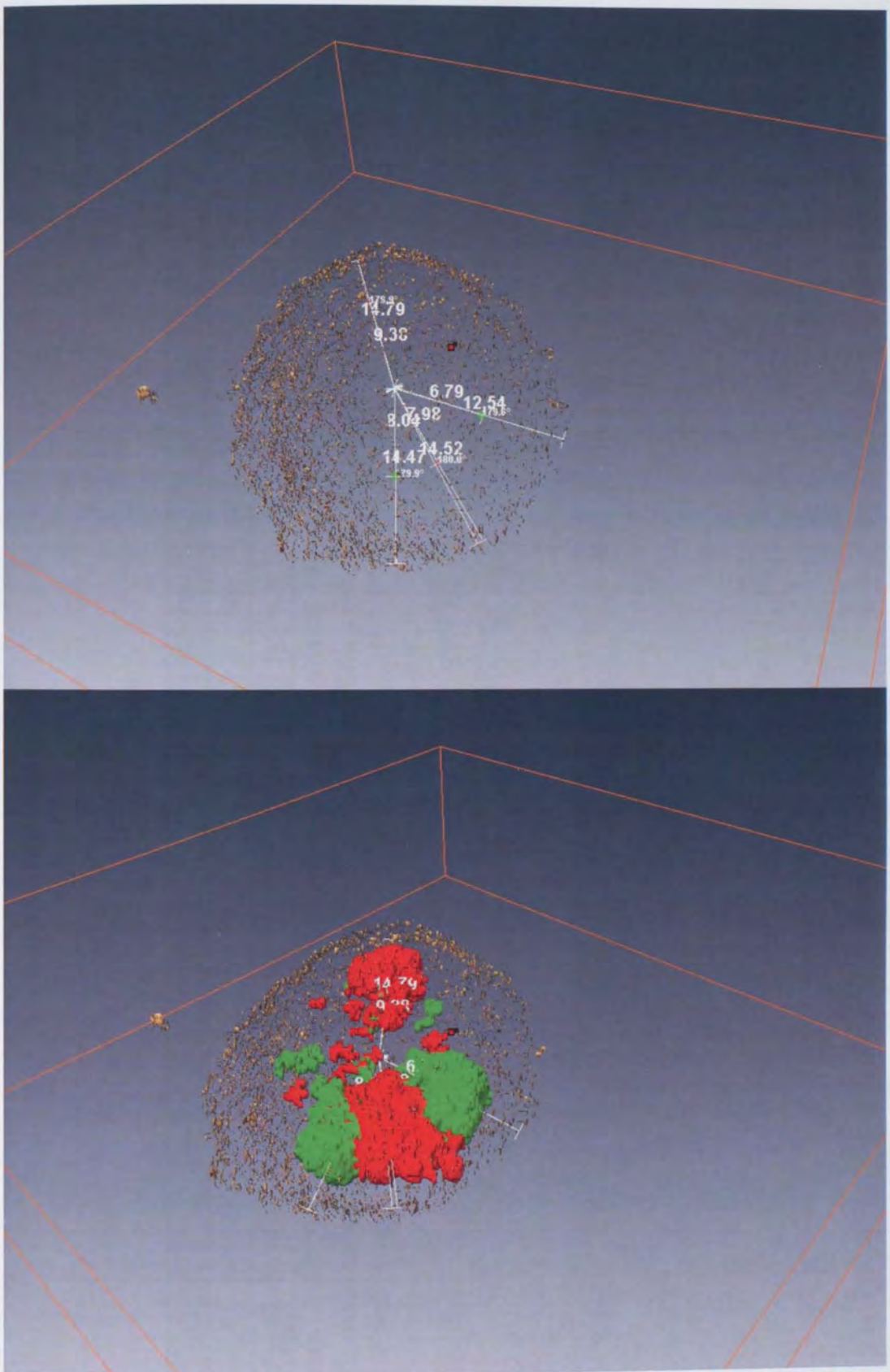

Figure 6.8: 3D visualisation example of chromosome territories for chromosome 1 (green) and chromosome 2 (red) within a non-irradiated fibroblast nucleus (gold). The upper figure shows of the measurements of distances between the nucleus centre of gravity and the territories' centres of gravity. The lower figure shows the same measurements with the visualisation of the whole territories. Measurements are expressed in µm.

Fibroblasts controls	N	Mean	SD	SE	CV	Normal?	P	Fibroblasts controls	N	Median	25% percentile	75% percentile	75%-25%	Normal?	P
Chr1 distances	79	6.889	2.325	0.262	0.34	Yes	P > 0.10	Chr1 Ratio of radius	79	65.96	54.15	74.3	20.15	No	0.02
Chr2 distances	78	6.448	1.979	0.224	0.31	Yes	P> 0.10	Chr2 Ratio of radius	78	64.58	55.23	74.81	19.58	No	0.01

Table 6.7: Table of descriptive statistics for the distances between the nucleus centre of gravity and the territory centre of gravity measured using Amira software for chromosome 1 and chromosome 2 in fibroblast controls. Distances are expressed in µm. Ratios of Radii are expressed in percentages.

It appears the distances for both chromosome 1 and chromosome 2 are consistent with a normal distribution ($p > 0.1$ for both distributions). The mean values obtained were 6.89 µm and 6.45 µm for chromosome 1 and 2 respectively. The ratios of radii data are not however consistent with a normal distribution ($p = 0.02$ for chromosome 1 and $p = 0.01$ for chromosome 2). The distance values and the radius ratios for both chromosomes were plotted with their corresponding nuclear volumes and also with the corresponding territory volumes values (Figure 6.9).

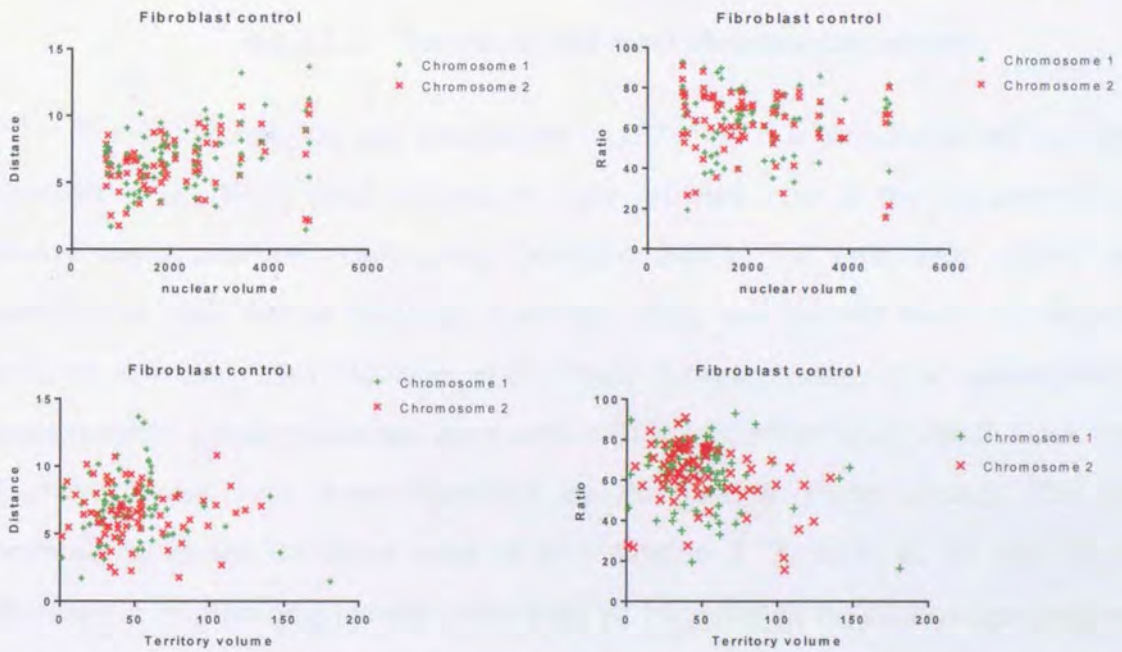

Figure 6.9: The distance from the centre of gravity of the nucleus to the centre of gravity of the territory are plotted against both corresponding nuclei volumes (top left) and the corresponding territory volumes (bottom left). Ratios of radii are also plotted against nuclei volumes (top right) and territory volumes (bottom right). The measurements are given in µm for the distances and in μm^3 for the volumes.

The graphs in Figure 6.9 suggest that chromosome 1 and 2 are located at similar distances from the centre of the nucleus. Chromosome 1 and 2 distance values were compared using an unpaired t-test. No significant difference was found between the two sets of distances ($p = 0.20$). It can be concluded that chromosome 1 and 2 territories appear to be located at similar distances from the centre of gravity of the nucleus. The ratios of radii were compared using a Mann-Whitney test and there was no significant difference

between the ratios of radii of chromosome 1 territories and chromosome 2 territories ($p = 0.94$).

6.3.2.2. Characterisation of chromosome 1 and 2 in non-irradiated bladder carcinoma cells (RT112)

The relation between chromosome volume and nucleus volume was studied similarly for tumour cell line (RT112); the analysis was performed similarly to fibroblasts.

6.3.2.2.1. Individual and total chromosome volumes

The RT112 cell line was established in 1977 and is a transitional cell carcinoma (Marshall *et al.*, 1977) which appears to have retained most of the characteristics of primary transitional cell carcinomas (Masters, 2000). The cells have mostly been identified as near diploid (Hastings & Franks, 1981) and present 46-47 chromosomes (Hastings & Franks, 1981; Williams *et al.*, 2005). However, presence of hypotriploid and hypertetraploid complements has been seen in RT112 (Strefford *et al.*, 2002). Extra copies of chromosomes have been identified by Hastings & Franks (1981). The extra chromosome copies identified were of chromosome 1, 3, 4, 5, 8, 19 and 21. The difference in chromosome number could have an influence on the nucleus rearrangement following irradiation as well as leading to the exhibition of significant differences in nuclear architecture. In order to allow the comparison between the two cell types studied, the same parameters used for the fibroblasts were measured for 30 RT112 cells at 0 hours, without irradiation treatment.

The corresponding data were plotted for distribution assessment (Figure 6.10) and the median and quartile values computed as summarised in Table 6.8.

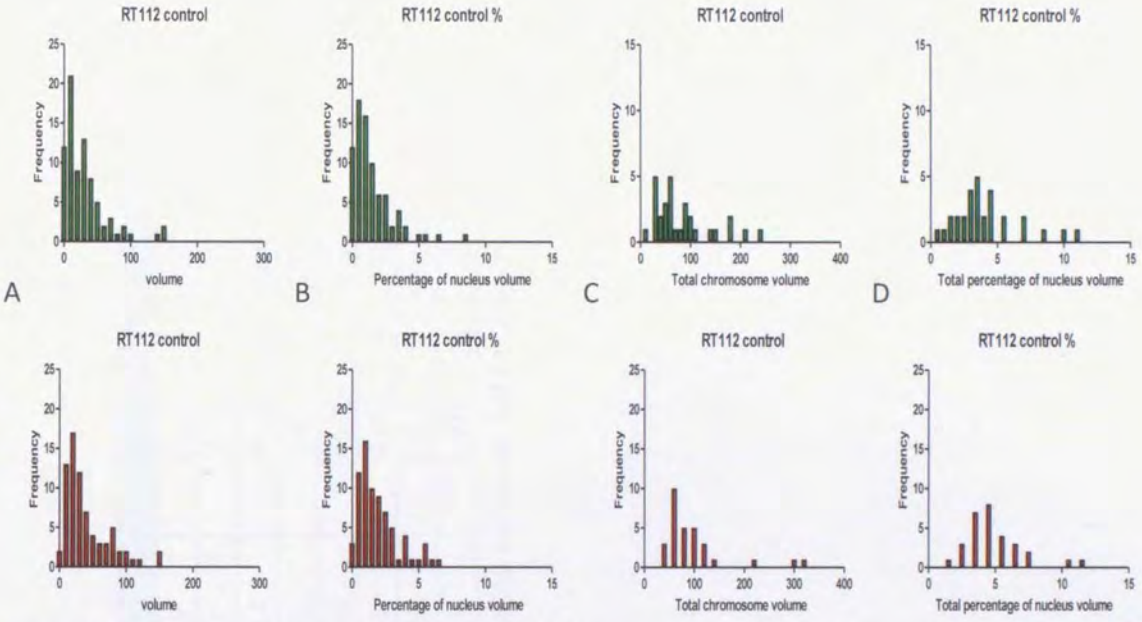

Figure 6.10: The volume measurements for RT112 Chromosome 1 and 2 at 0 hours (controls) are presented as frequency histograms. Also see Table 6.8 for descriptive statistics. Horizontally, the four graphs show A: actual individual chromosome volumes, B: volumes expressed as a percentage of the nuclear volume C: total actual chromosome volume calculated as the sum of the volume of all fragments in each nucleus and D: the sum of all fragments expressed as a percentage of the nuclear volume. Vertically the graphs show the respective distributions for chromosome 1 (green) and chromosome 2 (red). Volumes are expressed in μm^3.

The individual volumes and individual percentages distributions for chromosome 1 do not appear to be consistent with a normal distribution as confirmed by performing a Kolmogorov-Smirnov normality test (P values indicated in Table 6.8). The interquartile range for chromosome 1 being 32 μm^3 is an indication of the variability of the volumes. A similar result was obtained when testing the chromosome 2 with a similar interquartile range of 40 μm^3 (Table 6.8). The variability observed in the RT112 cell line could be due to the chromosome aberrations present in the cell line.

RT112 Controls	N	Mean	Median	SD	SE	CV	Min	Max	25% percentile	75% percentile	75%-25%	Normal?	P
Chr1 volume	80	31.56	23.55	32.73	3.66	1.04	2.02	152.40	8.39	40.16	31.77	No	P<0.0001
Chr1 percentage	80	1.53	1.00	1.54	0.17	1.00	0.06	8.46	0.51	2.19	1.67	No	P<0.0001
Chr2 volume	74	40.65	28.19	33.05	3.84	0.81	2.93	147.30	16.14	56.22	40.08	No	P<0.0001
Chr2 percentage	74	1.97	1.50	1.53	0.18	0.77	0.12	6.56	0.83	2.65	1.81	No	0.0002
Chr1 total volume	30	84.16	63.22	58.87	10.75	0.70	7.36	241.60	42.10	104.20	62.10	No	0.0054
Chr1 total percentage	30	4.09	3.50	2.45	0.45	0.60	0.67	10.76	2.54	4.85	2.31	No	0.0188
Chr2 total volume	30	100.26	81.11	68.84	12.57	0.69	46.79	323.2	55.49	108.9	53.41	Yes	P<0.0001
Chr2 total percentage	30	4.87	4.50	2.22	0.40	0.46	1.934	11.42	3.305	5.997	2.69	No	P > 0.10

Table 6.8: Summary table of descriptive statistics corresponding to the distributions presented in Figure 6.9 for chromosome 1 and 2 at 0 hours (controls) in RT112. Volumes are expressed in μm^3.

Chromosome deletions are common aberrations in cancer cells lines. In the case of RT112 the loss of a part of the proximal arm of chromosome 1 (1p) is common. This has been documented by Williams *et al.* (2005). This led to the generation of two clusters of values within the distributions. The first cluster of values is close to 25 μm^3 and the second one close to 75 μm^3. A similar pattern can be observed for chromosome 2. The percentage values distributions also appear to follow this pattern with a peak at 2% and another cluster of values around 5%.

The total chromosome distributions appear more consistent with a normal distribution. The sum of the individual values to give a total chromosome volume for each nucleus appears to be associated with less variability as indicated by the ratio of interquartile range to median.

The median values for the total chromosome volumes and total percentages appear to be approximately twice the individual volumes and percentage values.

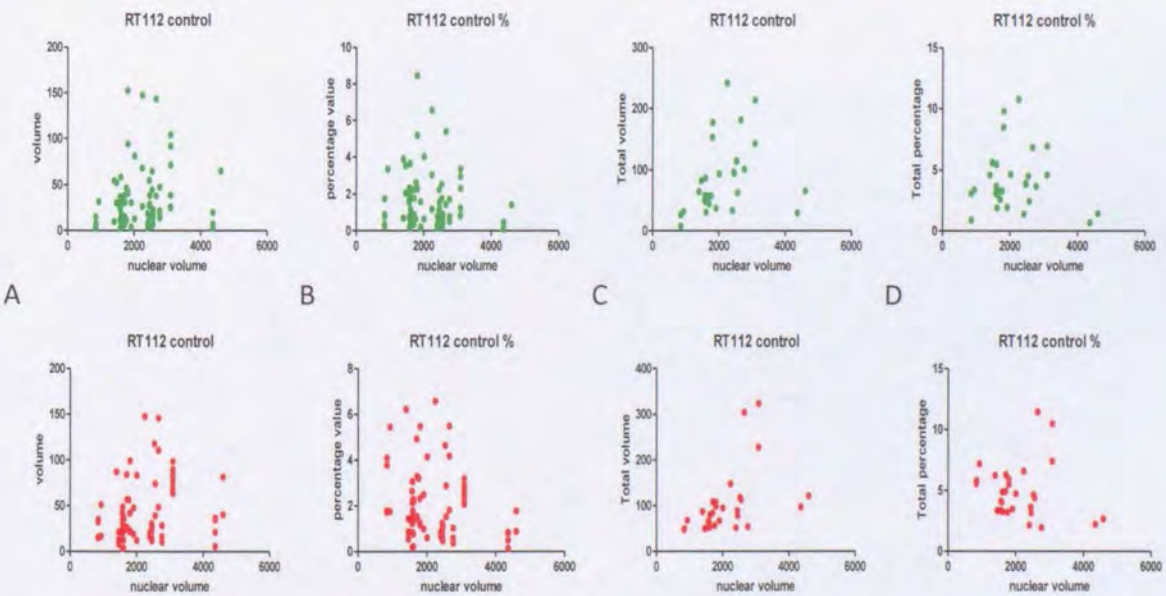

Figure 6.11: Volume measurements for RT112 chromosome 1 and 2 at 0 hours (controls) are plotted versus the corresponding nucleus size. Horizontally, the four graphs show A: actual individual chromosome volumes, B: volumes expressed as a percentage of the nuclear volume C: total actual chromosome volume calculated as the sum of the volume of all fragments in each nucleus and D: the sum of all fragments expressed as a percentage of the nuclear volume. Vertically the graphs show the respective distributions for chromosome 1 (green) and chromosome 2 (red). Volumes are expressed in μm^3.

As done for fibroblasts, the chromosome volume data for RT112 cells were plotted against their corresponding nuclear volume value (Figure 6.11 and Table 6.9). Descriptive

statistics were calculated and the relation between nuclear volume and individual volumes, total chromosome volumes and their ratios was investigated.

As seen with fibroblasts, there appears to be a significant relation with a positive Spearman's correlation coefficient between territory volumes (both individual volumes and sums) and the nuclear volumes for both chromosome 1 and 2. The values increase with larger nuclei. This relation appears clearer with total chromosome volumes. If more than 2 territories occur in individual cells, the individual territories are likely to have smaller volumes and the relation between individual chromosome volumes and nucleus size is thus likely to be less evident. The ratios on the other hand do not seem to be related to the nuclear volume (descriptive statistics are summarised in Table 6.9).

Chr 1 Individual values	RT112 control	RT112 control %	Chr 1 Total volumes	RT112 control	RT112 control %
Number of XY Pairs	80	80	Number of XY Pairs	30	30
Spearman r	0.252	-0.05494	Spearman r	0.5208	0.0812
P value (two-tailed)	0.0242	0.6284	P value (two-tailed)	0.0032	0.6697
Is the correlation significant? (alpha=0.05)	Yes	No	Is the correlation significant? (alpha=0.05)	Yes	No
Linear regression					
Linear regression slope	0.007262 ± 0.004607	-0.0001698 ± 0.0002187	Linear regression slope	0.01920 ± 0.01211	-0.0002203 ± 0.0005243
Intercept when X=0	16.10 ± 10.46	1.893 ± 0.4964	Intercept when X=0	43.82 ± 27.52	4.548 ± 1.191
r^2	0.03087	0.007671	r^2	0.08237	0.006268
Chr 2 Individual values	RT112 control	RT112 control %	Chr 2 Total volumes	RT112 control	RT112 control %
Number of XY Pairs	74	74	Number of XY Pairs	30	30
Spearman r	0.2997	-0.1385	Spearman r	0.6725	-0.164
P value (two-tailed)	0.0095	0.2392	P value (two-tailed)	P<0.0001	0.3866
Is the correlation significant? (alpha=0.05)	Yes	No	Is the correlation significant? (alpha=0.05)	Yes	No
Linear regression					
Linear regression slope	0.008319 ± 0.004205	-0.0003610 ± 0.0001948	Linear regression slope	0.03629 ± 0.01310	-0.0002622 ± 0.0004732
Intercept when X=0	22.29 ± 10.02	2.770 ± 0.4642	Intercept when X=0	24.03 ± 29.76	5.417 ± 1.075
r^2	0.05155	0.0455	r^2	0.2151	0.01084

Table 6.9: Summary of the results of the correlation analysis between chromosome territories volumes, total chromosome volumes, their respective ratios of nucleus volume and nuclear volumes for chromosome 1 and 2 in RT112. The slope of the linear regressions curves are also presented as well as the intercept values and r^2 values. Volumes are expressed in μm^3.

Finally, most of the nuclear volumes appear to be about 2000 μm^3 with only a few values at roughly 4000 μm^3 and the total chromosome volumes for those nuclei are within the same range as the ones for the smaller nuclei in the group sampled.

6.3.2.2.2. Individual territory occurrence

Between 1 and 4 territories were observed for both chromosome 1 and chromosome 2 in the 30 cells considered. Descriptive statistics observed for each occurrence for both chromosome 1 and 2 are summarised in Table 6.10.

The median values when 1T and 2T occurs for chromosome 1 were approximately 48 μm^3 and 33μm^3 respectively. In the case of chromosome 2, the median values for 1T and 2T were approximately 92 μm^3 and 34 μm^3 respectively. The factor of 2 between the two medians observed in fibroblasts for both chromosomes is only observed in chromosome 2 for RT112.

When 3T occurred, no decrease in median values for the volume was observed compared to 2T for both chromosomes (Table 6.10). This can be explained by the presence of larger total chromosome volumes present for both chromosome 1 and 2 for the cells presenting 3T (Figure 6.12). As a result, despite a higher number of territories observed, the median values for 2G and 3G (approximately 33 μm^3 and 27 μm^3 respectively) and the median values for 2R and 3R (approximately 34 μm^3 and 25 μm^3 respectively) are similar.

When 4T occurred for chromosome 1 the median value (approximately 11 μm^3) corresponded to half the volume measured for 2T at 33 μm^3. This is illustrated in Figure 6.12 by a cluster of points for chromosome 1 (green) being very close to the x-axis. The results are slightly different for chromosome 2 with a 4T median value of approximately 22 μm^3, close to the median when 2T occurred (approximately 34 μm^3) as 4 individual values are much higher than the rest of the values obtained for 4T.

Chr1	Territory number	1 territory	2 territories	3 territories	4 territories
Control	occurrence	4	8	12	6
	Median	48.21	33.49	27.64	11.48
	25% Percentile	13.36	11.82	13.81	3.414
	75% Percentile	130.6	50.68	52.15	18.5
	75%-25% Percentile	117.24	38.86	38.34	15.086
Chr2	Territory number	1 territory	2 territories	3 territories	4 territories
Control	occurrence	6	10	8	6
	Median	92.64	33.98	25.69	22.15
	25% Percentile	76.76	18.83	15.37	12.9
	75% Percentile	124.8	45.82	54.4	35.57
	75%-25% Percentile	48.04	26.99	39.03	22.67

Table 6.10: Median values for the territory volumes for chromosome 1 and chromosome 2 in RT112 sorted according to the number found in the cell nucleus considered and occurrences for each scenario. The 25% percentile, 75% percentile and the interquartile range are also given. Volumes are expressed in μm^3.

Only two nuclear volume values (4602 μm^3 and 4364 μm^3) seem to be clearly different from the rest of the group , the median volume for the nuclei being 2100 μm^3 (Figure 6.12). This indicates that in terms of nuclear volumes these two cells are the only ones that could be in G_2 (as described previously with fibroblasts).

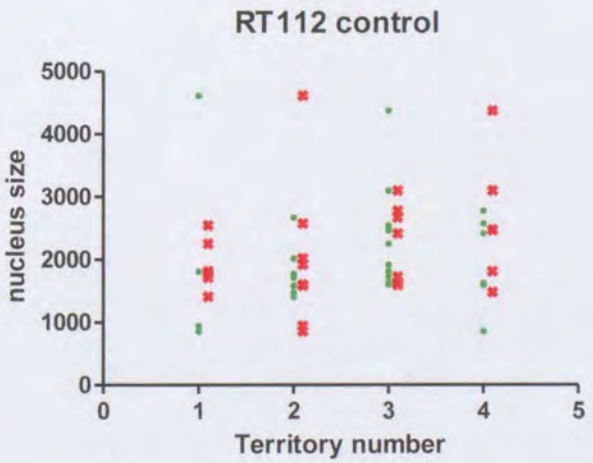

Figure 6.12: Corresponding nucleus volumes for both chromosome 1 and 2 are plotted according to the territory number observed within their respective cells. The corresponding median values and scenario occurrences are summarised in Table 6.10.

The corresponding total chromosome volumes for the two cells with larger nuclei were 65 μm^3 (1G)/121μm^3 (2R) and 29 μm^3 (3G)/91 μm^3 (4R). Despite the nuclear volumes indicating those two cells could have been in G_2, the total chromosome volumes only appear to partially suggest the progression into G_2. In fact, the total chromosome volumes observed appear to be similar to the median values for 1G and 4R (medians of 48

μm^3, 93 μm^3 for 1G and 4R respectively) but seem to double or a third for 2R and 3G respectively when comparing to the corresponding median values obtained (65 μm^3 and 95 μm^3 in Table 6.11).

Chr1	Territory Number	1 territory	2 territories	3 territories	4 territories
Sum	Occurrence	4	8	12	6
	Median	48.21	60.72	95.29	45.5
	25% Percentile	13.36	48.95	50.69	29.29
	75% Percentile	130.6	90.63	168	72.06
	75%-25%	117.24	41.68	117.31	42.77
Chr2	Occurrence	6	10	8	6
Sum	Median	92.64	65.33	71.49	92.59
	25% Percentile	76.76	51.67	52.38	70.25
	75% Percentile	124.8	99.07	197.6	161
	75%-25%	48.04	47.4	145.22	90.75

Table 6.11: Median values for the total volumes for chromosome 1 and chromosome 2 sorted according to the number found in the cell nucleus considered and occurrences for each scenario. The 25% percentile, 75% percentile and the difference between the two are also given. Volume medians are expressed in μm^3.

Interestingly, three of the total chromosome volumes for chromosome 2 (4T, 3T, and 3T) and their corresponding values for chromosome 1 (3T, 3T and 2T) are much higher than the rest of the values measured for cells with the same territories number (Figure 6.13). Similarly one of the total chromosome volumes for chromosome 1 (3T) and the corresponding value for chromosome 2 (1T) are higher than median measured for cells with the same number of territories. The corresponding nuclear volumes, despite some being towards the higher end of the samples values, are not much greater than the two values discussed above. So as a result, unlike with fibroblasts, the use of nuclear volumes combined with total chromosome volume and territory number might not allow an exact indication of the position in the cell cycle for RT112.

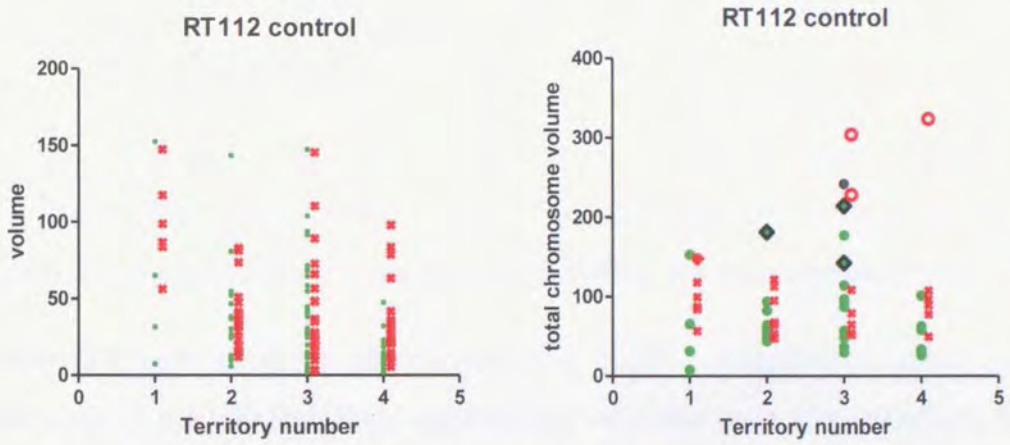

Figure 6.13: In this graph the nucleus volumes for both chromosome 1 and 2 in RT112 are plotted against the number of territories observed. The red circles/green lozenges and red star/grey circle represent the outliers data excluded from the analysis. Volumes are expressed in μm^3.

The outlier values obtained for total chromosome volumes were excluded from the rest of the analysis as way of simplification and clarity (red circles/green lozenges and red star/grey circle Figure 6.13).

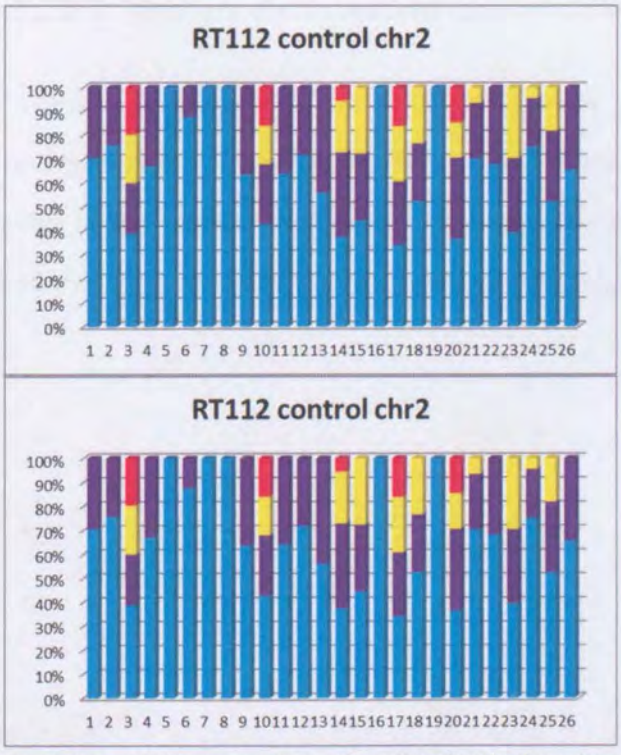

Figure 6.14: Graphic representation of the proportion of each individual territory volume compared to the corresponding total chromosome volume (100%) for both chromosome 1 (top) and 2 (bottom). Each bar corresponds to the territories observed in on cell nucleus for the chromosome considered. Each colour in the bar represents a fragment (territory) observed for the given chromosome. The data has been sorted using the number of territory observed for chromosome 1 with the corresponding chromosome 2 data aligned accordingly in the bottom graph. Territory 1, blue; territory 2, purple; territory 3, yellow; territory 4, pink.

Both 2G and 3G have been observed in this study (Figure 6.14).

When 2T are observed for chromosome 1, the corresponding splits observed were: 50%/50%, 60%/40%, 75%/25%, 80%/20% and on 3 occasions 85%/15% (excluding the one high total chromosome volume value). This illustrates the variation in the size of the deleted fragment within the cell population before any radiation treatment.

When 3T were observed for chromosome 1 the corresponding splits (following the exclusion of the two high total chromosome volumes) were 80%/10%/10%, 67%/30%/3%, 66%/25%/9%, on two occasions 57%/28%/15%; 54%/20%/26%; 57%/39%/4%, 53%/23%/24% and 40%/31%/29%.

When 4T were observed for chromosome 1 the corresponding splits were 62%/17%/11%/10%; 56%/24%/10%/10%; 47%/21%/18%/14%; 56%/25%/11%/8%; 37%/30%/23%/10%; 55%/21%/19%/5%.

6.3.2.2.3. Territory distances and ratio of corresponding radii

The distances were measured from the centre of gravity of the nucleus to the centre of gravity of the territory considered using the in-built 3D tool in Amira. The radii from the centre of gravity of the nucleus and passing through the centre of gravity of the territory were also measured. The ratios of the radii were then calculated for analysis.

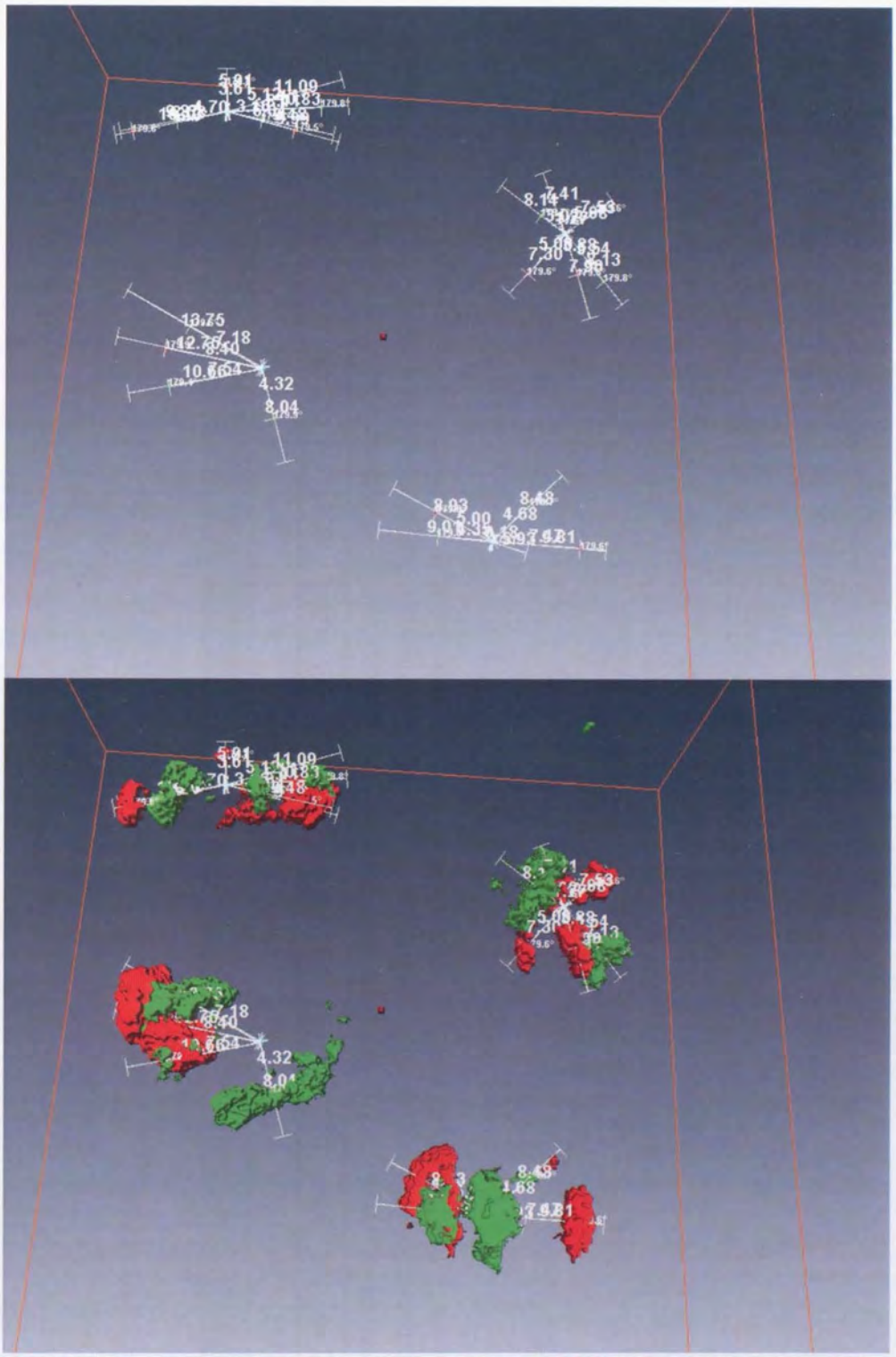

Figure 6.15: Example 3D visualisation of chromosome territories for chromosome 1 (green) and chromosome 2 (red) within non-irradiated RT112 nuclei. The upper figure shows measurements of distances between the nucleus centre of gravity and the territories' centres of gravity. The lower figure shows the same measurements with the visualisation of the whole territories. Measurements are expressed in µm.

RT112 Controls	N	Mean	SD	SE	CV	Normal?	P	RT112 Controls	N	Median	25% percentile	75% percentile	75%-25%	Normal?	P
Chr1 distance	80	5.812	1.895	0.212	0.33	yes	0.2	Chr1 Ratio of radius	80	67.2	50.59	74.41	23.82	No	0.001
Chr2 distance	74	5.795	2.23	0.259	0.38	yes	0.2	Chr2 Ratio of radius	74	66.07	51.33	76.04	24.71	No	0.001

Table 6.12: Summary descriptive statistics for the distances between the nucleus centre of gravity and the territory centre of gravity measured using Amira software for chromosome 1 and chromosome 2 in RT112 controls. Summary of the median and range for the ratios of the radius for chromosome 1 and 2 in RT112 controls. Distances are expressed in µm. Ratios of Radii are expressed in percentages.

It appears the distances for both chromosome 1 and chromosome 2 are consistent with a normal distribution (p = 0.20 for both distributions). The mean values obtained were 5.81 μm and 5.80 μm for chromosome 1 and 2 respectively. The ratios of radii data are not however consistent with a normal distribution (p = 0.02 for chromosome 1 and p = 0.01 for chromosome 2). The distance values and the radius ratios for both chromosomes were plotted with their corresponding nuclear volumes and also with the corresponding territory volumes values (Figure 6.16).

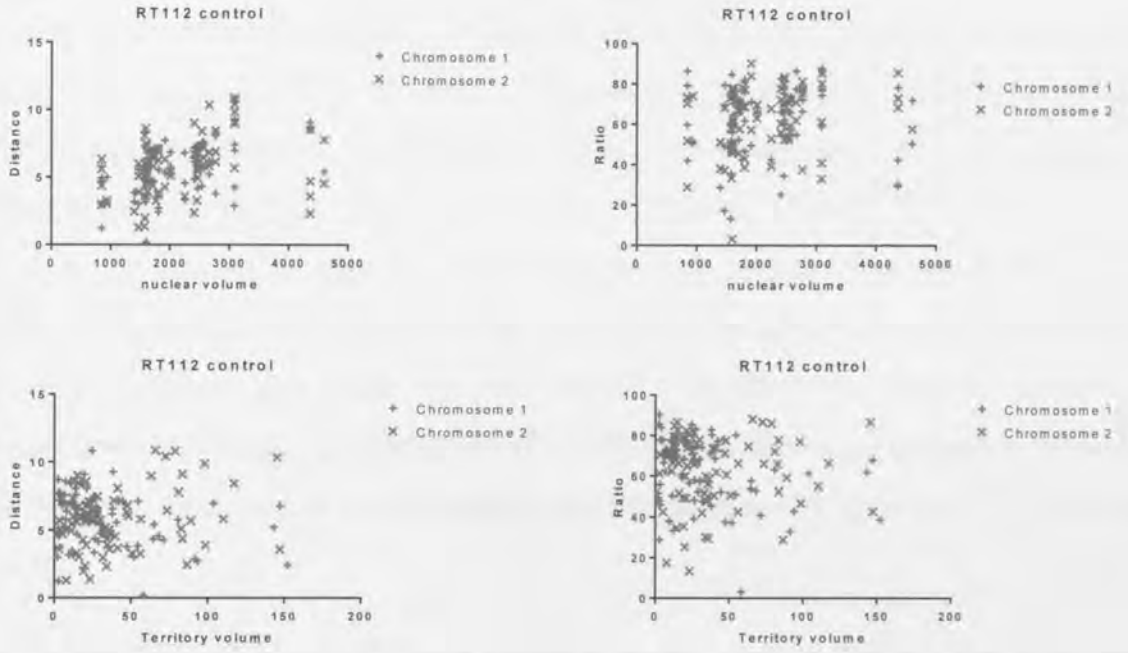

Figure 6.16: The distance from the centre of gravity of the nucleus to the centre of gravity of the territory are plotted against both corresponding nuclei volumes (top left) and the corresponding territory volumes (bottom left). Ratios of radii are also plotted against nuclei volumes (top right) and territory volumes (bottom right). The measurements are given in μm for the distances and in μm^3 for the volumes.

As with fibroblasts, it appears as though chromosome 1 and 2 are located at similar distances from the centre of the nucleus. Chromosome 1 and 2 distances values were compared using an unpaired t-test. No significant difference was found between the two sets of distances (p = 0.95). We can conclude that chromosome 1 and 2 territories appear to be located at similar distances from the centre of gravity of the nucleus. The ratios of radii were compared using a Mann-Whitney test and there was no significant difference between the ratios of radii of chromosome 1 territories and chromosome 2 territories (p = 0.74).

6.3.2.3. Chromosome territory positioning comparison between fibroblasts controls and RT112 controls

In view of the different sizes of RT112 and fibroblast nuclei, the ratios of the relative position of the chromosome territory centre of gravity (CoG) to the nucleus radius were compared. The cell nucleus radii (distance between the nucleus CoG and the nucleus surface through the territory CoG) of RT112 and fibroblast nuclei measured for chromosome 1 and 2 appear statistically significant ($p < 0.0001$ and $p = 0.0002$) when analysed using an unpaired t-test.

Both distributions of ratios radii for chromosome 1 were not consistent with a normal distribution ($p = 0.02$ for fibroblasts chromosome 1 and $p = 0.0007$ for RT112 chromosome 1). Likewise chromosome 2 ratios distributions were also not consistent with a normal distribution ($p = 0.0004$ for fibroblasts and $p = 0.0009$ for RT112). In order to assess a possible difference in relative positioning between fibroblasts and RT112 controls, the ratios were compared using a Mann-Whitney test. There was no significant difference between the ratios for chromosome 1 in fibroblasts and the ratios for chromosome 1 in RT112 ($p = 0.85$). Similarly there was no significant difference between the ratios for chromosome 2 in fibroblasts and the ratios for chromosome 2 in RT112 ($p = 0.70$).

So despite the significant difference between nucleus radii of the two cell types, the relative positioning (ratios of radii) of the two chromosome appear to be similar.

6.4. Discussion

6.4.1. Nucleus size analysis

The variation in distribution shape observed for fibroblasts is difficult to explain. The presence of a ratio of 2 between the two "sub-groups" in the controls (and 1 hour) could be explained by cells being distributed through the cell cycle. If this were the explanation however, one would expect similar distributions at all the time points, and this was not observed; this may be affected by the number of cells at each time point. In this study the cells used had been harvested after being held in confluent conditions for

at least one week, conditions that had been shown previously as well as in this study to result more than 90% of the cells being in G_1/G_0. As a result of the conditions used in these experiments, it is likely that cells did not start to exit G_1 and progress into S-phase for at least 8 hours after plating. In these experiments the 0 hour time point was immediately after plating. This slight shift towards higher size nuclei could be the initiation of the passage into the next step of the cell cycle following the completion of DNA repair resulting in an overall increase in nuclear volumes. A significant increase in nuclear sizes was observed at 24 hours. All the nuclear volumes bar one are above 2000 μm^3 going up to almost 5000 μm^3. The approximate doubling of the volumes values could be the result of a transition into G_2.

The doubling time for fibroblasts was approximately 24 hours. The increase in median value and volumes at 24 hours, as also seen with the fibroblasts, could be the result of a passage of the nuclei into G_2.

Similarly, the presence of the ratio of 2 between the 2 "sub-groups" at 1 hour could be the manifestation of the presence of cells at a different stage of the cell cycle. When in G_2, both DNA material and nuclear structures have been duplicated in preparation for mitosis. Two copies of each chromosome in a pair can be visualised.

Both cell lines, despite presenting a similar number of chromosomes, behave differently. Fibroblasts enter G_0 when grown to confluency. RT112 being a tumour cell line, do not possess a fully functional cell cycle arrest but carry on proliferating. However, since the growing conditions were very similar, the presence of this "sub-group" at the same time point for both cell lines is nonetheless interesting to observe.

Details of the effect of radiation on the cells are not easy to analyse when only considering the total nuclear volumes. The changes observed between the time points and the different cell lines considered could be the tip of the iceberg and the study of individual territories characteristics and numbers will help with understanding the nature of the cells considered (repaired or surviving and "mis-repaired") and maybe shed light on the effects happening at the chromosome level.

6.4.2. Fibroblasts territories characterisation

The ratio of the median value for the individual volumes divided by their corresponding median values for the total chromosome volume for chromosome 1 and 2 appears to be approximately one half; this could suggest that the degree of compaction between the two members of the chromosome pairs for both chromosome 1 and 2 is similar and each one corresponds to approximately 50% of the total chromosome volume. This is also observed for the percentages of nucleus median values. Some possible explanations can be considered in order to attempt to explain this difference.

The first aspect that could be considered when trying to understand the factors influencing the difference in correlation observed could be linked to the method itself. In other words, the variability introduced by the process may have influenced the value of the correlation found in the analysis. However, considering the data obtained, it is unlikely that significant degrees of error were introduced during the process. In the eventuality of an error being introduced, it appears that the error was introduced with homogeneity throughout the whole set.

The second aspect to consider that could possibly influence the correlation between the chromosome pair volume and the nuclear volume relates to the degree of intermingling the chromosome considered is involved with. It has been established that intermingling occurs between different chromosome territories (Branco & Pombo, 2006). Intermingling also appears to be linked to transcriptional activity (Goetze *et al.*, 2007) where materials from chromosomes with similar transcriptional patterns will migrate towards replication and transcription centres (Hozák *et al.*, 1993). The exact level of DNA involved in intermingling is not known. It is highly likely that the fraction of the chromosomes involved in the phenomenon at the time of the data acquisition was not accounted for in the final volumes values and was excluded at the same time as the excess background staining during image processing. The resolution level of the method used in this study is not high enough to allow accurate visualisation of DNA intermingling between chromosomes and determine the influence of the phenomenon

on the correlation values found between the chromosome pair volume and nuclear volume.

Finally, the chromatin compaction varies throughout the genome and the cell cycle. Depending on the level of gene expression the chromatin had been classified into two types: hetero- and euchromatin (Wolffe & Kurumizaka, 1998) where the latter is less condensed than the former due to higher transcriptional activity. Each chromosome will possess regions with each of the two types of chromatin. However, due to the link between transcriptional activity and chromatin compaction, it is possible that a range of chromatin in different states of compaction could in fact be present in the cell nucleus instead of only two (Huisinga *et al.*, 2006). The nucleus being a highly dynamic entity, chromatin transition through states with varying degrees of compaction depending on the fluctuating degrees of transcriptional activity cannot be excluded. Some variations in chromatin compaction have been measured using FLIM-FRET by Llères *et al.* (2009). The technique used was based on measuring the fluorescence signals in HeLa cells expressing GFP and mCherry on the histone H2B. The measurements were performed using live cells during interphase and mitosis and highlighted regions with different levels of compaction. It is however, due mainly to technical limitations, difficult to accurately assess and measure the compaction fluctuation of any and every region of the genome at any given time. Heterogeneity in chromatin compaction at the time of the data acquisition could play a role in the difference of correlation observed between the nuclear volume and the chromosome pair volume. Considering that the difference between the chromosome length and the volume in relation to the genome size and nuclear volume appears to be different for chromosome 1 and 2 it is possible that both chromosomes had different degrees of compaction at the time of data acquisition and/or that their physical length is not representative of the volume occupied by the territories within the nucleus. Moreover, Marella *et al.* (2009) showed a variation in the volumes occupied by chromosomes 19 and 18 during keratinocyte differentiation and also observed differences from the data obtained for human fibroblasts. So it is possible that the territory values obtained are influenced by several factors such as position in the cell cycle, stage of differentiation and cell type.

In this study and under the experimental conditions used, chromosome 1 pair appears to occupy about 4.5% of the nucleus and chromosome 2 pair occupies about 4.6% of the nuclear volume.

In the cells where 1 or 2 territories (1T and 2T) occurred for chromosome 1 and 2, the median values (72 μm^3 and 83 μm^3) when a unique territory is observed appears to be in the range of double the values observed when 2 territories (40 μm^3 and 43 μm^3) are present in the nucleus considered. This could mainly be due to the fact that, at the time of the images acquisition, the two territories were too close to be distinguished using FISH or were in fact in contact with each other. The very close proximity of the two chromosomes could be the result of the possible relationship between them or the orientation of the cell on the slide during the image acquisition. Since there is no absolute possibility to control the orientation of the cell when it lands and attaches to the slide, the occurrences of one unique territory could be due to the close proximity of the two territories combined with physical constraints resulting from the flattening of the cell nuclei post-attachment to the slide and prior to the fixation.

In the case of 2T, the split should theoretically be close to 50%/50%. Similarly, in the case of 4T the split should be 25%/25%/25%/25%. However for reasons explained before, sometimes 2 territories cannot be differentiated. As a result 4T can become 3T with a 50%/25%/25% even be 2T with a 75%/25% or a 50%/50% split and 2T can become 1T.

The presence of 4 territories (4T) of similar sizes on two occasions for chromosome 1 could be the indication of the presence of tetraploid cells whose DNA material has been copied. In this instance, the nuclear size would be approximately twice the size of a diploid cell as the DNA takes up much more space.

6.4.3. Chromosome positioning in non-irradiated fibroblasts

Chromosome 1 and 2 were found to locate within similar radial distances at 6.9 and 6.5 µm from the centre of gravity of the cell nucleus respectively. This also corresponds to 66 and 65% of the relative radius they are positioned on. These values

agree with the data found by Bolzer *et al.* (2005) in prometaphase rosettes. There was no significant difference in distances between chromosome 1 and 2 within the cell nuclei considered which is also in accordance Bolzer *et al.* (2005). Chromosome 1 and 2 being two large chromosomes, their positioning on the outer shell of the nucleus could corroborate the theory of positioning relative to size, where larger chromosomes are positioned towards the nuclear periphery.

There seems to be a relationship between the distances from the CoG of the nucleus to the CoG of the territory. It appears as though distances increase with larger nuclei. However, the ratios of relative positioning do not appear to increase with larger nuclei which can suggest that chromosome are positioned within a shell within the nucleus which has also been demonstrated by Sun *et al.* (2000) in 2D nuclei.

6.4.4. RT112 territories characterisation

The changes and volume of individual chromosomes in RT112 including translocations and marker chromosomes during interphase has not been previously documented. As a result it is difficult to establish the level of impact these aberrations have on the variations observed.

A 1p deletion has been characteristically observed in bladder tumour cell lines (Hastings & Franks, 1981; Williams *et al.*, 2005; Walker *et al.*, 1990). As a result, the number of territories observed in addition to the still complete chromosome, provided no extra chromosome aberration has spontaneously been generated, should logically be either 1 or 2 depending on whether the different fragments could be differentiated using the method. In the eventuality where fragments were too close to be differentiated the outcome should be identifiable by examining the total chromosome volumes. Chromosome 1 being metacentric, the largest possible deletion would roughly be half of the chromosome or approximately 25% of the total chromosome volume. As a result the possible outcomes for the territories split would be: 75%/25%, 50%/25%/25% in the eventualities where the break is closest to the centromere possible. If the deletion involved a fragment anywhere else on the p arm the outcome could be 75%+/25%- (the largest fragment cannot be differentiated from the still complete chromosome),

50%/25%+/25%- (all 3 fragments can be differentiated), 50%+/25%+ (the smallest fragment cannot be differentiated from the still complete chromosome).

The relation between territories volumes (both individual and sums) appears less clear for RT112 cells than for fibroblast cells. This could be the result of the presence of smaller fragments either involved in deletions or in translocations within chromosome 1 in RT112. A change in numbers for chromosome one in bladder carcinomas was initially identified by Hastings & Franks (1981) and was also detected by Hopman *et al.* (1991). This could explain the variability and the lack of relationship between individual chromosome volumes and nuclear size. The loss of 1p, as mentioned before, could be the explanation for smaller volumes being measured. This variability seems to disappear when considering total chromosome volumes for chromosome 2. The total volume values should be similar since the variability induced by possible fragments being present is eliminated.

No reference to aberration on chromosome 2 appears to have been characterised and reported in the literature for RT112. The analysis of fragments observed could be interesting to explore as would any abnormal fragmentation of chromosome 2.

When 1G is observed, the corresponding occurrences for chromosome 2 are 3 times 2R with splits of 70%/30%, 76%/24%, 67%/33% and 1 occurrence of 4R with a 40%/20%/20%/20% split.

Unlike fibroblasts the 50%/50% normal split is not often observed if observed at all. The common split appears to be 60%+/40%- in the case of 2R. The 4R split of 40%/20%/20%/20% does not entirely resemble the 25%/25%/25%/25% observed with cells in G_2. However, this might be the result of difference in degree of compaction.

When 2G was observed, 3 occurrences of 1R, 3 occurrences of 2R and 1 occurrence of 4R were observed for the corresponding chromosomes 2. The splits observed for 2R were 64%/36%, 64%/36%, 87.5%/12.5%. The split observed for 4R was 42.5%/25.5%/16%/16%.

Once again the splits appear to vary from the usual 50%/50%, 75%/25% or 4x 25% observed previously for chromosome 2 in fibroblasts.

When 3G was observed, 2 occurrences of 1R, 2 occurrences of 2R (with splits of 56%/44% and 72%/28%), 2 occurrences of 3R (with splits of 52%/24%/24% and 44%/28%/28%) and 3 occurrences of 4R (with splits of 36%/34%/15%/15%, 34%/27%/23%/16% and 37%/35%/22%/16%) were observed for the corresponding chromosomes 2.

Finally, when 4G was observed, 2 occurrences of 2R (with splits of 68%/32% and 66%/34%) and 4 occurrences of 3R (with splits of 70%/23%/7%, 39%/31%/30%, 75%/20%/5% and 52%/30%/18%) were observed for the corresponding chromosomes 2.

The presence of 50%/25%/25%-like split for both chromosomes in the 3G/3R where the splits are 54%/20%/26% and 52%/24%/24% respectively could indicate that this particular cell could have been in G_2. RT112 cells are deficient in some of the cell cycle arrest mechanism which explains their aberrant growth and in turn could lead to higher numbers of cells in G_2 in the sample tested.

The other splits with the presence of higher numbers of territories with much smaller fragments could be a manifestation of an overall genome instability resulting in the presence or generation of small fragments even before the radiation treatment.

The presence of a fragment of approximately 50% or more indicates that one of the chromosomes 1 is still whole and that the excess fragmentation occurred on the already fragmented chromosome possibly due to the instability created by the characteristic loss of 1p (Hastings & Franks, 1981; Williams *et al.,* 2005; Walker *et al.,* 1990). In the one case where all fragments are much smaller than 50 % of the total chromosome volume, it is possible that chromosome 1 suffered deletions due to instability introduced by the deletion already present.

6.4.5. Territory positioning in non-irradiated RT112

As seen with fibroblasts, no significant difference in positioning was observed between chromosome 1 and chromosome 2 in RT112. Both chromosomes were located at 5.8 µm from the nucleus CoG which corresponds to 67% of the corresponding relative radii. Despite the distances being slightly shorter than in fibroblasts, the ratio of relative

radii are the same which could be explained by the difference in shape of the two cell lines considered. The fibroblasts being ellipsoid and the RT112 being rounder, the radii are likely to be different. Moreover as seen in 6.3.1 and 6.3.2, the nuclear sizes are slightly different which influences the length of the radii.

The similarities in positioning indicate that chromosome positioning is conserved between the two cell lines for chromosome 1 and 2.

REFERENCES

Bolzer, A., Kreth, G., Solovei, I., Koehler, D., Saracoglu, K., Fauth, C., Müller, S., Eils, Roland, Cremer, C., Speicher, M. R. & Cremer, Thomas (2005). Three-dimensional maps of all chromosomes in human male fibroblast nuclei and prometaphase rosettes. *PLoS Biology*, **3**(5), e157.

Branco, M. R. & Pombo, A. (2006). Intermingling of chromosome territories in interphase suggests role in translocations and transcription-dependent associations. *PLoS Biology*, **4**(5), e138.

Cornforth, M. N. & Bedford, J. S. (1983) X-ray--induced breakage and rejoining of human interphase chromosomes. *Science*, **222**(4628), 1141–3.

Croft, J. A., Bridger, J. M., Boyle, S., Perry, P., Teague, P. & Bickmore, W. A. (1999). Differences in the localization and morphology of chromosomes in the human nucleus. *The Journal of Cell Biology*, **145**(6), 1119–31.

Goetze, S., Mateos-langerak, J. & Van Driel, R. (2007). Three-dimensional genome organization in interphase and its relation to genome function. *Seminars in Cell & Developmental Biology*, **18**(5), 707–14.

Hastings, R. J. & Franks, L. M. (1981). Chromosome pattern, growth in agar and tumorigenicity in nude mice of four human bladder carcinoma cell lines. *International Journal of Cancer*, **27**(1), 15–21.

Hopman, A. H., Moesker, O., Smeets, A. W., Pauwels, R. P., Vooijs, G. P. & Ramaekers, F. C. (1991). Numerical chromosome 1, 7, 9, and 11 aberrations in bladder cancer detected by *in situ* hybridization. *Cancer Research*, **51**(2), 644–51.

Hozák, P., Hassan, A. B., Jackson, D. A. & Cook, P. R. (1993). Visualization of replication factories attached to a nucleoskeleton. *Cell*, **73** (2), 361–373.

Huisinga, K. L., Brower-Toland, B. & Elgin, S. C. R. (2006). The contradictory definitions of heterochromatin: transcription and silencing. *Chromosoma*, **115**(2), 110–22.

Llères, D., James, J., Swift, S., Norman, D. G. & Lamond, A. I. (2009). Quantitative analysis of chromatin compaction in living cells using FLIM-FRET. *The Journal of Cell Biology*, **187**(4), 481–96.

Löbrich, M., Rydberg, B. & Cooper, P. K. (1995). Repair of x-ray-induced DNA double-strand breaks in specific Not I restriction fragments in human fibroblasts: joining of correct and incorrect ends. *Proc. Nat. Acad. Sci. USA*, **92**(26), 12050–4.

Marella, N. V, Seifert, B., Nagarajan, P., Sinha, S. & Berezney, R. (2009). Chromosomal rearrangements during human epidermal keratinocyte differentiation. *Journal of Cellular Physiology*, **221**(1), 139–46.

Marshall, C. J., Franks, L. M. & Carbonell, A. W. (1977). Markers of neoplastic transformation in epithelial cell lines derived from human carcinomas. *Journal of the National Cancer Institute*, **58**(6), 1743–51.

Masters, J. R. (2000). Human cancer cell lines: fact and fantasy. *Nature reviews. Molecular Cell Biology*, **1**(3), 233–6.

Nevaldine, B., Longo, J. A., King, G. A., Vilenchik, M., Sagerman, R. H. & Hahn, P. J. (1993). Induction and repair of DNA double-strand breaks. *Radiation Research*, **133**(3), 370–4.

Strefford, J. C., Lillington, D. M., Steggall, M., Lane, T. M., Nouri, A. M. E., Young, B. D.. & Oliver, R. T. D. (2002). Novel chromosome findings in bladder cancer cell lines detected with multiplex fluorescence in situ hybridization. *Cancer Genetics and Cytogenetics*, **135**(2), 139–46.

Sun, H. Bin, Shen, J. & Yokota, H. (2000). Size-Dependent Positioning of Human Chromosomes in Interphase Nuclei. *Biophysical Journal*, **79**(1), 184–190.

Visser, A. E., Eils, R, Jauch, A., Little, G., Bakker, P. J., Cremer, T & Aten, J. A. (1998). Spatial distributions of early and late replicating chromatin in interphase chromosome territories. *Experimental Cell Research*, **243**(2), 398–407.

Walker, M. C., Povey, S., Parrington, J. M., Riddle, P. N., Knuechel, R. & Masters, J. R. (1990). Development and characterization of cisplatin-resistant human testicular and bladder tumour cell lines. *European Journal of Cancer*, **26**(6), 742–7.

Wang, M., Perissel, B. & Malet, P. (1995). Cytogenetic Characterization of a Bladder Carcinoma Cell Line by Fluorescence In Situ Hybridization. *Public Health*, **174**, 170–174.

Williams, S. V, Adams, J., Coulter, J., Summersgill, B. M., Shipley, J. & Knowles, M. A (2005). Assessment by M-FISH of karyotypic complexity and cytogenetic evolution in bladder cancer in vitro. *Genes, Chromosomes & Cancer*, **43**(4), 315–28

Wolffe, A. P. & Kurumizaka, H. (1998). The nucleosome: a powerful regulator of transcription. *Progress in Nucleic Acid Research and Molecular Biology*, **61**, 379–422.

Chapter 7 Characterisation of the chromosome territories following irradiation in human fibroblasts and RT112 bladder carcinoma cells

7.1. Introduction

This chapter describes the investigation of human fibroblast nuclei and RT112 nuclei following irradiation. The aim was to identify possible changes in nuclear arrangement of chromosome 1 and 2 in the early stages post-irradiation. The analysis performed was very similar to the one performed in chapter 6. The different time point data sets were compared to the non-irradiated data.

7.2. Material and methods

7.2.1. Choice of the cell lines and irradiation

In this chapter two cell lines, normal human fibroblasts and human bladder carcinoma cells (RT112), were prepared and subjected to radiation as described in Chapter 4 Section 4.2.6.

Cells were irradiated on ice using a Pantak 250 kV X-ray machine at St Luke's Cancer Centre, Guildford, Surrey. Irradiations were performed at 250 kV and a dose rate of 1 gray/min.

For the study of nuclear architecture following irradiation, the cells received the equivalent of 8 gy.

7.2.2. Slide preparation, hybridisation and confocal microscopy

The slides were prepared according to the protocol described in chapter 4 (Section 4.2.7. to 4.2.9.). Briefly, the cells were seeded in the form of a single cell suspension into temporarily attached glass chambers. The cells were them allowed to attach to the slide before undergoing fixation, pre-treatment and FISH. The slides were subjected to the chosen FISH protocol following optimisation (as described in Chapter 5) and the data collected using confocal microscopy as described in Chapter 5 before being processed and analysed using MATLAB and Amira.

7.2.3. Image processing and analysis

The images stacks obtained using confocal microscopy were subjected to image processing and image analysis. The data stacks were processed using MATLAB and the measurements of the different parameters of interest for the study were performed using Amira as described in chapter 4 section 4.2.10.

Briefly, the images were converted into binary images in order to allow the processing. Parameters such as brightness and contrast were adjusted in order to obtain suitable data to allow this part of the study. This allowed the reduction of potential artefacts still present despite the optimisation of the FISH protocol.

The measurements in Amira were performed using the in-built tools of the program. Parameters such as volumes and number of territories were established for every item included in the study as described in chapter 4 section 4.2.10.

7.3. Results

7.3.1. Characterisation of chromosome 1 and 2 in human fibroblasts following irradiation

7.3.1.1. Characterisation of chromosome 1 in human fibroblasts following irradiation

The characterisation of the chromosome territories involves a number of parameters. The study revolves mainly on the characterisation of individual territory volumes (including the proportion of the nuclei they occupy), their number within the cell nuclei studied as well as the total volume occupied by the chromosome in question and the total proportion of the nuclei occupied. These parameters can give an indication as to whether the degree of overall compaction of the territory changes noticeably with time. The evaluation of the number of fragments will help with identifying the presence of stable aberrations following irradiation.

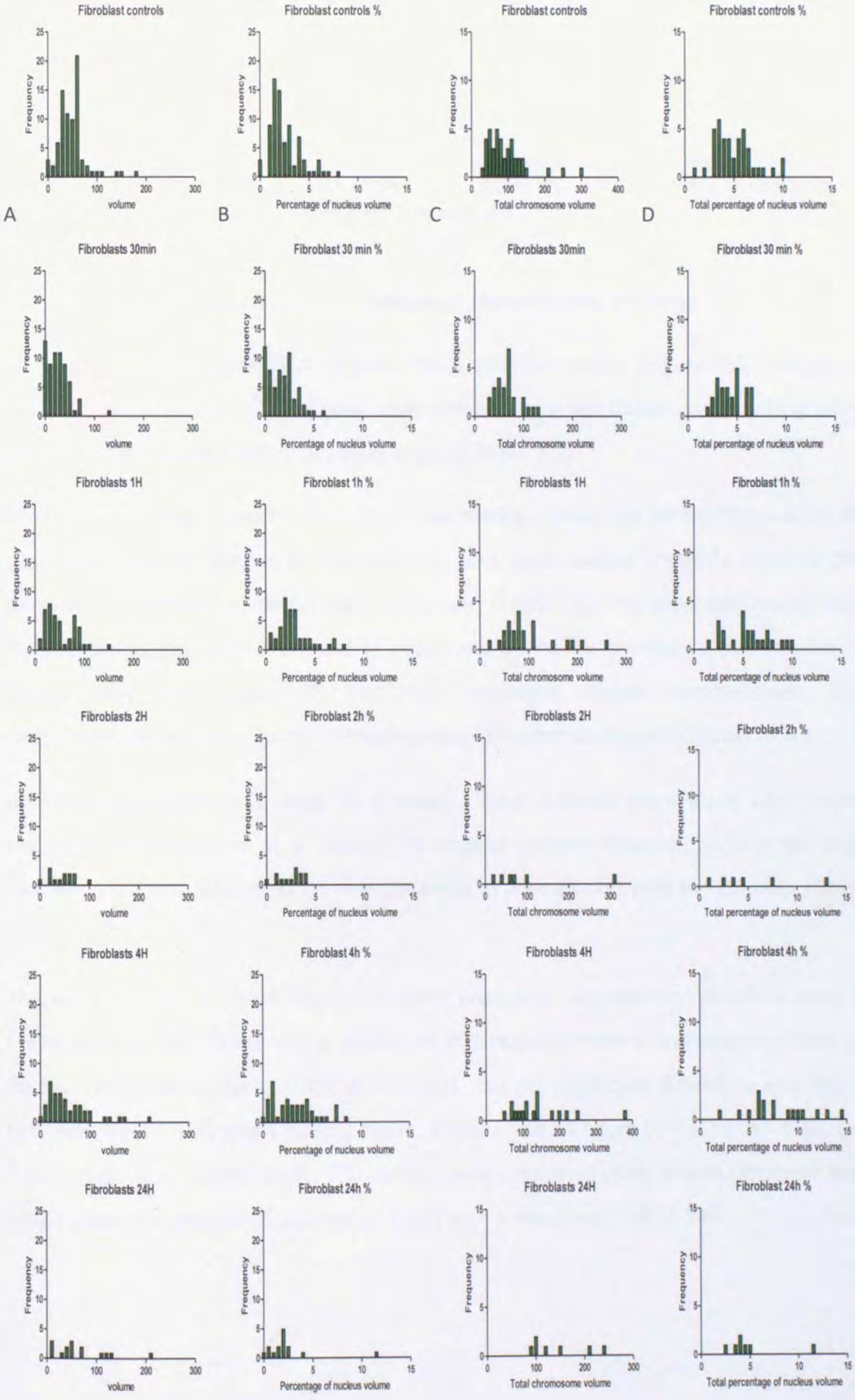
A
Fibroblast controls
Frequency
volume
B
Fibroblast controls %
Frequency
Percentage of nucleus volume
C
Fibroblast controls
Frequency
Total chromosome volume
D
Fibroblast controls %
Frequency
Total percentage of nucleus volume
Fibroblasts 30min
Frequency
volume
Fibroblast 30 min %
Frequency
Percentage of nucleus volume
Fibroblasts 30min
Frequency
Total chromosome volume
Fibroblast 30 min %
Frequency
Total percentage of nucleus volume
Fibroblasts 1H
Frequency
volume
Fibroblast 1h %
Frequency
Percentage of nucleus volume
Fibroblasts 1H
Frequency
Total chromosome volume
Fibroblast 1h %
Frequency
Total percentage of nucleus volume
Fibroblasts 2H
Frequency
volume
Fibroblast 2h %
Frequency
Percentage of nucleus volume
Fibroblasts 2H
Frequency
Total chromosome volume
Fibroblast 2h %
Frequency
Total percentage of nucleus volume
Fibroblasts 4H
Frequency
volume
Fibroblast 4h %
Frequency
Percentage of nucleus volume
Fibroblasts 4H
Frequency
Total chromosome volume
Fibroblast 4h %
Frequency
Total percentage of nucleus volume
Fibroblasts 24H
Frequency
volume
Fibroblast 24h %
Frequency
Percentage of nucleus volume
Fibroblasts 24H
Frequency
Total chromosome volume
Fibroblast 24h %
Frequency
Total percentage of nucleus volume

Figure 7.1: The volume measurements for Chromosome 1 at various times after irradiation at 8gy are presented as frequency histograms. The descriptive statistics are presented in Table 7.1. Horizontally, the four graphs show A: actual individual chromosome volumes, B: volumes expressed as a percentage of the nuclear volume, C: total actual chromosome volume calculated as the sum of the volume of all fragments in each nucleus and D: the sum of all fragments expressed as a percentage of the nuclear volume. Vertically the graphs show the respective distributions at given times after irradiation from control (from Figure 6.3) to 24h. Volumes are expressed in μm^3.

7.3.1.1.1. Individual chromosome volumes

Comparison of the data at given times after irradiation (Figure 7.1, Columns A and B) shows that data are not consistent with a normal distribution at every time point except at 2 hours and 4 hours (P values given in Table 7.1).

For 0 hours, 1 hour, 2 hours and 4 hours the median values are similar (from 42 to 46 μm^3), at 30 min the median for fragment size was much smaller (25 μm^3), whilst at 24h there was an increase in median value to 52 μm^3 (Table 7.1). The latter observation may be affected by the smaller number of observations and the occurrence of a number of exceptionally large fragments that may represent merged chromosomes. The relationship between fragment size and number is further analysed in Section 7.3.3.

A similar observation was made for 0 hours, 1 hour, 2 hours and 4 hours when those volumes were expressed as a ratio of the nuclear volume. However, at 24 h the ratio median value was similar to the one observed at 2 hours and with the controls (Table 7.1).

The values for the different time points were compared with the control values using a Mann-Whitney test. There was a significant difference in terms of individual volumes at 30 min compared to the controls ($p < 0.0001$) but no significant difference was found between the controls and 1 hour, 2 hours, 4 hours and 24 hours ($p = 0.71$, $p = 0.88$, $p = 0.82$ and $p = 0.42$ respectively). The results were confirmed using a false discovery rate (FDR) method (Benjamini & Hochberg, 1995) with a maximum FDR of 10%.

Chr1 volume	N	Mean	Median	SD	SE	CV	25% percentile	75% percentile	75%-25%	Normal?	P
Fibroblast Control	79	49.40	45.98	29.83	3.36	0.60	29.60	60.97	31.37	No	P<0.0001
Fibroblast 30 min	64	27.43	24.78	23.43	2.93	0.85	7.01	40.79	33.78	No	0.0096
Fibroblast 1h	44	52.39	42.60	31.35	4.73	0.60	30.20	80.97	50.77	No	0.0154
Fibroblast 2h	13	45.81	46.26	27.18	7.54	0.59	21.35	68.30	46.95	Yes	P > 0.10
Fibroblast 4h	42	58.67	45.22	47.55	7.34	0.81	22.58	80.75	58.17	No	0.007
Fibroblast 24h	15	66.98	51.68	54.74	14.13	0.82	34.49	111.10	76.61	Yes	0.0871
Chr1 percentage	N	Mean	Median	SD	SE	CV	25% percentile	75% percentile	75%-25%	Normal?	P
Fibroblast Control	79	2.60	2.12	1.61	0.18	0.62	1.60	3.27	1.68	No	0.0002
Fibroblast 30 min	64	1.77	1.68	1.37	0.17	0.78	0.39	2.59	2.20	No	0.0206
Fibroblast 1h	44	2.90	2.58	1.75	0.26	0.60	1.87	3.36	1.49	No	0.0048
Fibroblast 2h	13	2.49	2.77	1.24	0.34	0.50	1.32	3.36	2.05	Yes	P > 0.10
Fibroblast 4h	42	3.22	3.07	2.21	0.34	0.69	1.14	4.72	3.58	Yes	P > 0.10
Fibroblast 24h	15	2.33	1.89	2.66	0.69	1.15	0.92	2.35	1.44	No	0.0003

Table 7.1: Summary table of the mean, median, standard error of the mean, standard deviation, range and CV values for the corresponding distributions of individual territories volumes and individual ratios presented in Figure 7.1 for chromosome 1 in fibroblasts at the different time points considered. Volumes are expressed in μm^3.

When subjecting the ratio values to the same analysis, the comparison between controls and both 30 minutes and 4 hours showed a significant difference ($p = 0.003$ and $p < 0.0001$) whereas no significant difference between the control and 1 hour, 2 hours and, 24 hours was found ($p = 0.21$, $p = 0.83$ and $p = 0.20$ respectively). The results were confirmed using a false discovery rate (FDR) method (Benjamini & Hochberg, 1995) with a maximum FDR of 10%.

7.3.1.1.2. Total chromosome volumes

By calculating the sum of all chromosome fragments in each nucleus the influence of possible radiation-induced chromosome fragments is eliminated. However as a result of the summation the number of individual data points is obviously reduced (Figure 7.1, Column C and D).

At 0 hours, 1 hour the total volumes medians are very similar, 85 and, 84 μm^3 respectively; at 30 minutes and 2 hours the total volume was considerably less at 65 μm^3. At 4 hours and 24 hours the volumes were larger at 135 and 120 μm^3 respectively (Table 7.2).

When total volumes are expressed as a ratio of nuclear volume, the resulting median values for 0 hours, 30 minutes, 1 hour, 2 hours and, 24 hours appear to be within a similar order with 1 hours being slightly higher. The median for the ratios at 4 hours, like for the total volumes appears much higher however.

The total chromosome volume values for the different time points were compared with the control values using a Mann-Whitney test. There was a significant difference in terms of total chromosome volumes at 30 min, 4 hours and 24 hours compared to the controls ($p = 0.03$, $p = 0.008$ and $p = 0.02$ respectively) but no significant difference was found between the controls and 1 hour and 2 hours ($p = 0.81$ and $p = 0.39$ respectively). The results were confirmed using a false discovery rate (FDR) method (Benjamini & Hochberg, 1995) with a maximum FDR of 10%.

Chr1 total Volume	N	Mean	Median	SD	SE	CV	25% percentile	75% percentile	75%-25%	Normal?	P
Fibroblast Control	41	95.18	84.42	55.51	8.67	0.58	57.65	114.20	56.55	No	0.0464
Fibroblast 30 min	26	67.53	65.88	25.84	5.07	0.38	46.70	80.31	33.61	No	0.0397
Fibroblast 1h	23	100.22	83.94	59.65	12.44	0.60	59.85	114.50	54.65	No	0.0028
Fibroblast 2h	6	99.25	65.04	104.85	42.81	1.06	36.39	150.50	114.11	No	0.0334
Fibroblast 4h	17	144.96	134.60	82.29	19.96	0.57	88.39	190.50	102.11	No	0.0165
Fibroblast 24h	7	143.52	120.00	59.42	22.46	0.41	95.26	209.60	114.34	Yes	P > 0.10
Chr1 total percentage	N	Mean	Median	SD	SE	CV	25% percentile	75% percentile	75%-25%	Normal?	P
Fibroblast Control	41	5.01	4.52	2.07	0.32	0.41	3.46	6.10	2.64	Yes	P > 0.10
Fibroblast 30 min	26	4.35	4.42	1.34	0.26	0.31	3.22	5.22	2.01	Yes	P > 0.10
Fibroblast 1h	23	5.54	5.51	2.37	0.49	0.43	2.91	7.27	4.36	Yes	P > 0.10
Fibroblast 2h	6	5.39	3.96	4.40	1.80	0.82	2.31	8.85	6.54	Yes	P > 0.10
Fibroblast 4h	17	7.96	7.35	3.33	0.81	0.42	5.97	10.12	4.15	Yes	P > 0.10
Fibroblast 24h	7	4.98	3.99	2.90	1.10	0.58	3.65	5.04	1.39	No	0.0102

Table 7.2: Summary table of the mean, median, standard error of the mean, standard deviation, range and CV values for the corresponding distributions for total chromosome volumes and total ratios presented in Figure 7.1 for chromosome 1 in fibroblasts at the different time points considered. Volumes are expressed in μm^3.

When subjecting the total volume ratio values to the same analysis, only the comparison between controls and 4 hours showed a significant difference ($p = 0.0005$) and no significant difference between the control and 30 min, 1 hour, 2 hours and, 24 hours was found ($p = 0.22$, $p = 0.45$, $p = 0.63$ and $p = 0.67$ respectively). The results were confirmed using a false discovery rate (FDR) method (Benjamini & Hochberg, 1995) with a maximum FDR of 10%.

7.3.1.2. Characterisation of chromosome 2 in human fibroblasts following irradiation

7.3.1.2.1. Individual chromosome volumes

The distributions obtained for the individual territory volumes (Figure 7.2, Column A and B) at the different time points do appear to be consistent with a normal distribution at 1 hour and 2 hours (Table 7.3). The difference in sizes seen for chromosome 1 at 30 minutes are not observed for chromosome 2 (Table 7.3). The individual volumes medians appear to stay within the same range (44 μm^3 to 48 μm^3) until 4 hours when they increase to 59 μm^3 and at 24 hours to 62 μm^3 (Table 7.3).

On the other hand, when looking at the percentage of the nucleus occupied by the individual territories, the trend appears to be very similar to the actual territories except for 24 hours as the individual volume values appear to be bigger but median for the percentage of the nucleus occupied appears to be smaller than the other time points and similar to the control group.

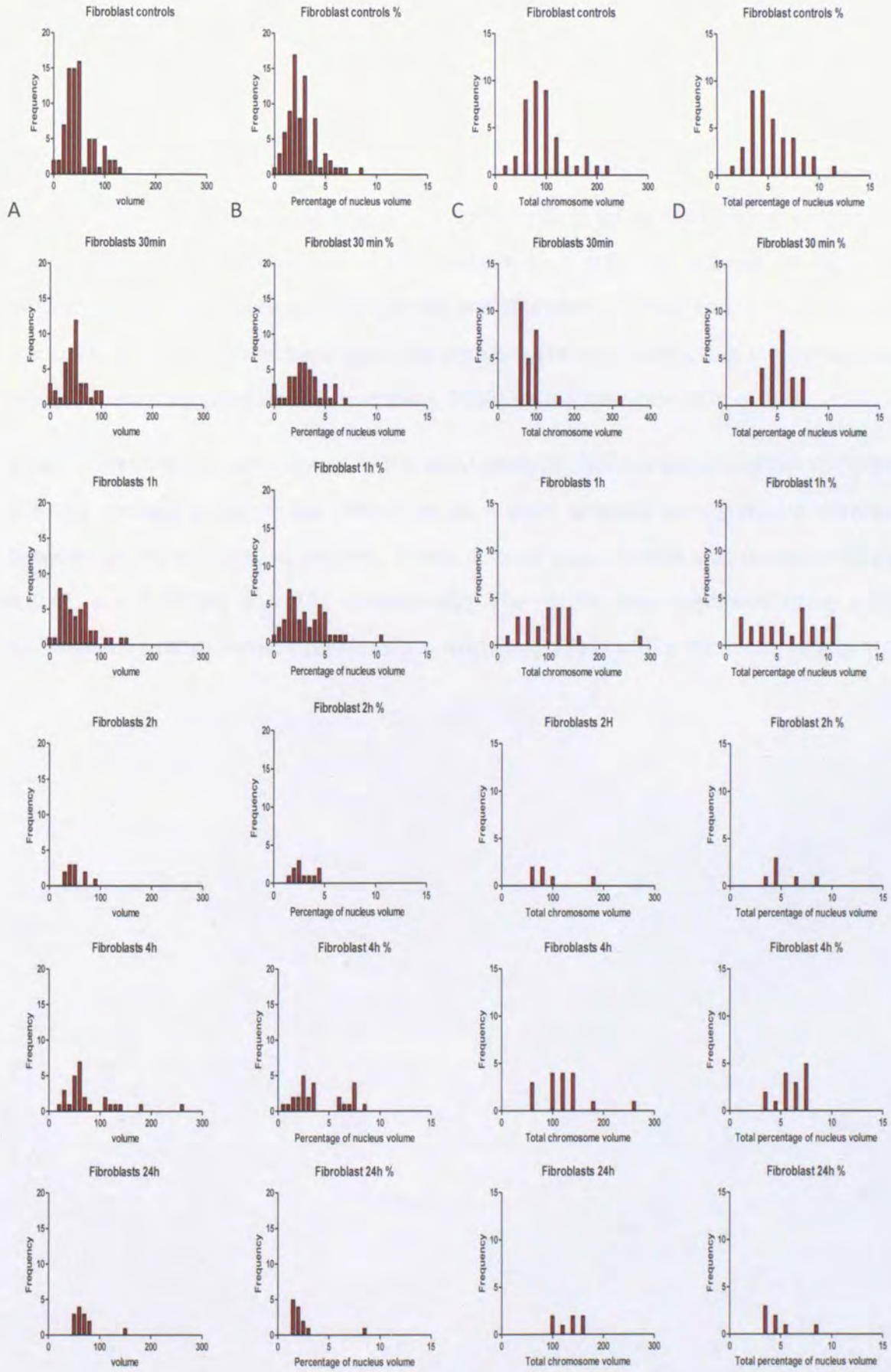

Figure 7.2: The volume measurements for Chromosome 2 after irradiation at 8 gray are presented as frequency histograms. Descriptive statistics are presented in Table 7.2. Horizontally, the four graphs show A: actual

individual chromosome volumes, B: volumes expressed as a percentage of the nuclear volume, C: total actual chromosome volume calculated as the sum of the volume of all fragments in each nucleus and D: the sum of all fragments expressed as a percentage of the nuclear volume. Vertically the graphs show the respective distributions at various times after irradiation from 0 (see Figure 6.3) to 24h. Volumes are expressed in μm^3.

The values for the different time points were compared with the control values using a Mann-Whitney test. There was a significant difference in terms of individual volumes at 4 hours and 24 hours compared to the controls ($p < 0.01$ for all) but no significant difference was found between the controls and 30 minutes, 1 hour and, 2 hours ($p = 0.87$, $p = 0.99$, $p = 0.60$ and respectively). The results were confirmed using a false discovery rate (FDR) method (Benjamini & Hochberg, 1995) with a maximum FDR of 10%.

When subjecting the ratio values to the same analysis, the comparison between controls 4 hours showed a significant difference ($p = 0.01$) whereas no significant difference between the control and 30 minutes, 1 hour, 2 hours and, 24 hours was found ($p = 0.11$, $p = 0.41$, $p = 0.43$ and $p = 0.19$ respectively). The results were confirmed using a false discovery rate (FDR) method (Benjamini & Hochberg, 1995) with a maximum FDR of 10%.

Chr2 volume	N	Mean	Median	SD	SE	CV	25% percentile	75% percentile	75%-25%	Normal?	P
Fibroblast Control	78	50.83	44.10	28.92	3.27	0.57	32.63	67.6	34.95	No	P<0.0001
Fibroblast 30 min	44	52.75	48.27	47.03	7.09	0.89	31.75	55.52	23.77	No	P<0.0001
Fibroblast 1h	45	52.36	48.00	32.79	4.89	0.63	27.43	67.82	40.39	Yes	P > 0.10
Fibroblast 2h	11	51.45	48.10	18.46	5.57	0.36	40.88	69.65	28.77	Yes	P > 0.10
Fibroblast 4h	27	77.13	59.17	52.25	10.05	0.68	48.44	110.00	61.56	No	0.0002
Fibroblast 24h	13	70.81	62.58	26.77	7.43	0.38	55.47	75.79	20.32	No	0.016
Chr2 percentage	N	Mean	Median	SD	SE	CV	25% percentile	75% percentile	75%-25%	Normal?	P
Fibroblast Control	78	2.75	2.32	1.54	0.17	0.56	1.74	3.47	1.73	No	0.0007
Fibroblast 30 min	44	3.35	2.97	2.48	0.37	0.74	2.11	4.09	1.98	No	0.0145
Fibroblast 1h	45	3.17	2.80	2.06	0.31	0.65	1.56	4.52	2.96	Yes	P > 0.10
Fibroblast 2h	11	2.94	2.69	1.07	0.32	0.36	1.85	3.92	2.07	Yes	P > 0.10
Fibroblast 4h	27	4.51	3.35	3.31	0.64	0.73	2.30	7.15	4.85	No	0.0009
Fibroblast 24h	13	2.47	2.04	1.79	0.50	0.72	1.67	2.36	0.70	No	0.0001

Table 7.3: Summary table of the mean, median, standard error of the mean, standard deviation, range and CV values for the corresponding distributions of individual territories volumes and individual ratios presented in Figure 7.2 for chromosome 2 in fibroblasts at the different time points considered. Volumes are expressed in μm^3.

7.3.1.2.2. Total chromosome volumes

Similarly to individual volumes, the different data sets (Figure 7.2, Column C and D) do not appear to be consistent with a normal distribution (Table 7.4) except for 1 hour ($p < 0.01$). The median values of the total territory volumes for the controls, 30 minutes and 2 hours appear to be similar (between 80 and 88 μm^3) whereas a clear increase can be seen for the median values at 1 hour (97 μm^3), 4 hours (116 μm^3) and 24 hours (134 μm^3).

The total volume ratios appear to be show similar results for the controls, 30 minutes and 2 hours with medians being similar. However, now 1 hour and 4 hours medians seem to present similar values and 24 hours median appears to be smaller than the other time points (Table 7.4).

Chr2 total volume	N	Mean	Median	SD	SE	CV	25% percentile	75% percentile	75%-25%	Normal?	P
Fibroblast Control	41	96.71	88.76	42.70	6.67	0.44	68.6	114.8	46.20	No	0.0174
Fibroblast 30 min	26	89.26	82.89	54.06	10.60	0.61	57.81	97.52	39.71	No	P<0.0001
Fibroblast 1h	23	102.44	96.91	55.88	11.65	0.55	58.39	130.9	72.51	Yes	P > 0.10
Fibroblast 2h	6	94.32	79.65	46.37	18.93	0.49	67.43	114.1	46.67	No	0.0107
Fibroblast 4h	17	122.50	116.01	45.36	11.00	0.37	107.3	137.7	30.40	No	0.0352
Fibroblast 24h	7	131.50	134.36	21.39	8.09	0.16	107.4	153.5	46.10	Yes	P > 0.10
Chr2 total percentage	N	Mean	Median	SD	SE	CV	25% percentile	75% percentile	75%-25%	Normal?	P
Fibroblast Control	41	5.23	4.63	2.13	0.33	0.41	3.587	6.934	3.35	No	0.0309
Fibroblast 30 min	26	5.66	5.21	2.47	0.48	0.44	4.542	6.109	1.57	No	0.0024
Fibroblast 1h	23	6.20	6.86	3.14	0.65	0.51	3.431	8.485	5.05	Yes	P > 0.10
Fibroblast 2h	6	5.39	4.77	1.68	0.69	0.31	4.234	7.075	2.84	Yes	P > 0.10
Fibroblast 4h	17	7.17	6.33	3.52	0.85	0.49	5.231	7.554	2.32	No	P<0.0001
Fibroblast 24h	7	4.59	4.14	1.80	0.68	0.39	3.343	5.384	2.04	Yes	P > 0.10

Table 7.4: Summary table of the mean, median, standard error of the mean, standard deviation, range and CV values for the corresponding distributions of total territory volumes and total volume ratios presented in Figure 7.2 for chromosome 2 in fibroblasts at the different time points considered. Volumes are expressed in μm^3.

The values for the different time points were compared with the control values using a Mann-Whitney test. There was a significant difference in terms of total volumes at 4 hours and 24 hours compared to the controls ($p = 0.02$ and $p = 0.0079$ respectively) but no significant difference was found between the controls and 30 minutes, 1 hour and, 2 hours ($p = 0.20$, $p = 0.70$, $p = 0.63$ and respectively). The results were confirmed using a false discovery rate (FDR) method (Benjamini & Hochberg, 1995) with a maximum FDR of 10%.

When subjecting the ratio values to the same analysis, the comparison between controls 4 hours showed a significant difference ($p = 0.03$) whereas no significant difference between the control and 30 minutes, 1 hour, 2 hours and, 24 hours was found ($p = 0.38$, $p = 0.23$, $p = 0.67$ and $p = 0.50$ respectively). The results were confirmed using a false discovery rate (FDR) method (Benjamini & Hochberg, 1995) with a maximum FDR of 10%.

7.3.1.3. Descriptive statistics of chromosome 1 and 2 territories following irradiation

Referring to Figure 7.3, the territory occurrence for chromosome 1 appears to be quite variable across the different time points. Most data sets present a majority of 1 or 2 territories except for 24 hours where the majority of the nuclei present 3 territories. All the time points considered presented occurrences of 3 or more territories with 30 minutes presenting up to 6 territories, controls, 1 hour, 2 hours and 4 hours presenting up to 4 territories and finally 24 hours presenting up to 3 territories.

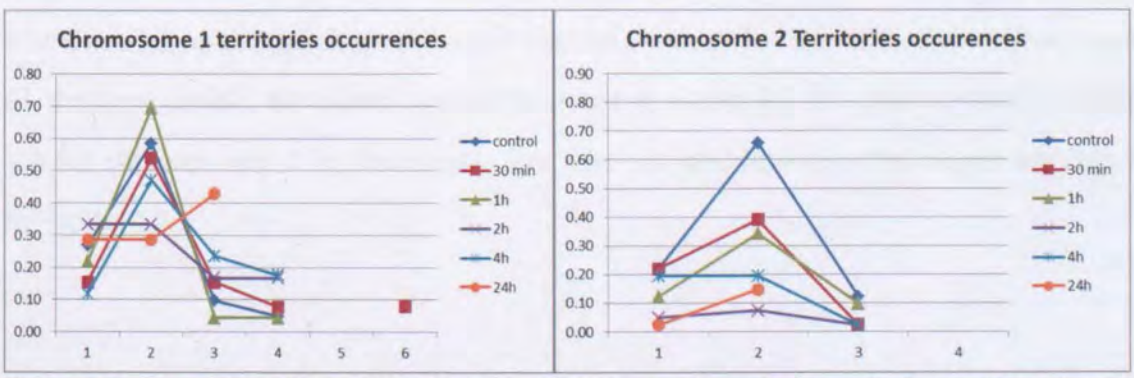

Figure 7.3: Proportion of the different territory occurrence (1 to 6) for each time point and controls for chromosome 1 and 2

Chromosome 2 appeared more homogenous with only up to 3 territories observed across the different time points and the majority of the cells presenting 2 territories.

Chr 1	Territory number	1 territory	2 territories	3 territories	4 territories	6 territories
Control	occurrence	11	24	4	2	
	Median	72.27	39.73	26.66	58.18	
	25% Percentile	46.67	29.51	5.914	53.38	
	75% Percentile	110.7	55.36	61.37	61.34	
	75%-25% Percentile	64.03	25.85	55.456	7.96	
30min	occurrence	4	14	4	2	2
	Median	66.95	30.32	15.94	5.5	5.412
	25% Percentile	42.54	22.91	4.15	1.649	2.388
	75% Percentile	116.4	43.64	38.6	28.71	20.11
	75%-25% Percentile	73.86	20.73	34.45	27.061	17.722
1h	occurrence	5	16	1	1	
	Median	83.94	38.54	20.55	50.1	
	25% Percentile	48.31	30.2	10.22	45.71	
	75% Percentile	87.54	80.97	53.9	64.64	
	75%-25% Percentile	39.23	50.77	43.68	18.93	
2h	occurrence	2	2	1	1	
	Median	38.35	43.98	16.61	72.77	
	25% Percentile	18.3	32.91	1.391	66.15	
	75% Percentile	58.4	50.87	24.41	90.59	
	75%-25% Percentile	40.1	17.96	23.019	24.44	
4h	occurrence	2	8	4	3	
	Median	115.7	43.26	39.67	46.63	
	25% Percentile	93.87	26.58	18.37	17.35	
	75% Percentile	137.6	97.9	57.7	71.7	
	75%-25% Percentile	43.73	71.32	39.33	54.35	
24h	occurrence	2	2	3		
	Median	164.8	81.7	36.21		
	25% Percentile	120	48.46	10.36		
	75% Percentile	209.6	123	59.33		
	75%-25% Percentile	89.6	74.54	48.97		

Table 7.5: Median values for the territory volumes for chromosome 1 sorted according to the number found in the cell nucleus considered and occurrences for each scenario. The 25% percentile, 75% percentile and the difference between the two are also given. Volumes are expressed in μm^3.

The descriptive statistics of individual volumes values for the different territory numbers at the time points measured are summarised in Table 7.5 for chromosome 1 and Table 7.6 for chromosome 2 in fibroblasts. The medians and interquartile ranges are illustrated in Figure 7.4.

Chr2	Territory number	1 territory	2 territories	3 territories
control	occurrence	9	27	5
	Median	82.52	42.84	34.7
	25% Percentile	76.11	33.48	10.34
	75% Percentile	119.1	54.04	47.73
	75%-25% Percentile	42.99	20.56	37.39
30min	occurrence	9	16	1
	Median	69.04	43.48	2.867
	25% Percentile	55.08	27.87	2.111
	75% Percentile	86.55	50.39	99.63
	75%-25% Percentile	31.47	22.52	97.519
1h	occurrence	5	14	4
	Median	90.42	48.9	29.5
	25% Percentile	43.76	28.82	19.73
	75% Percentile	113.8	66.95	65.96
	75%-25% Percentile	70.04		
2h	occurrence	2	3	1
	Median	69.99	41.28	52.68
	25% Percentile	69.65	30.58	42.73
	75% Percentile	70.32	48.21	90.54
	75%-25% Percentile	0.67	17.63	47.81
4h	occurrence	8	8	1
	Median	126.7	52.93	48.44
	25% Percentile	110.9	42.27	22.49
	75% Percentile	168.6	60.51	59.85
	75%-25% Percentile	57.7	18.24	37.36
24h	occurrence	1	6	
	Median	153.5	62.11	
	25% Percentile	153.5	55.19	
	75% Percentile	153.5	72.07	
	75%-25% Percentile	0	16.88	

Table 7.6: Median values for the territory volumes for chromosome 2 sorted according to the number found in the cell nucleus considered and occurrences for each scenario. The 25% percentile, 75% percentile and the difference between the two are also given. Volumes are expressed in μm^3.

There seems to be some variation as time increases in the volume medians when considering chromosome 1. For example, when 1G occurs the medians are similar for 0 hours, 30 minutes and 1 hour (72 μm^3, 67 μm^3 and 84 μm^3 respectively). At 2 hours the median for 1G decreases quite drastically to 38 μm^3 before increasing at 4 hours to 115 μm^3 and to 164 μm^3 at 24 hours.

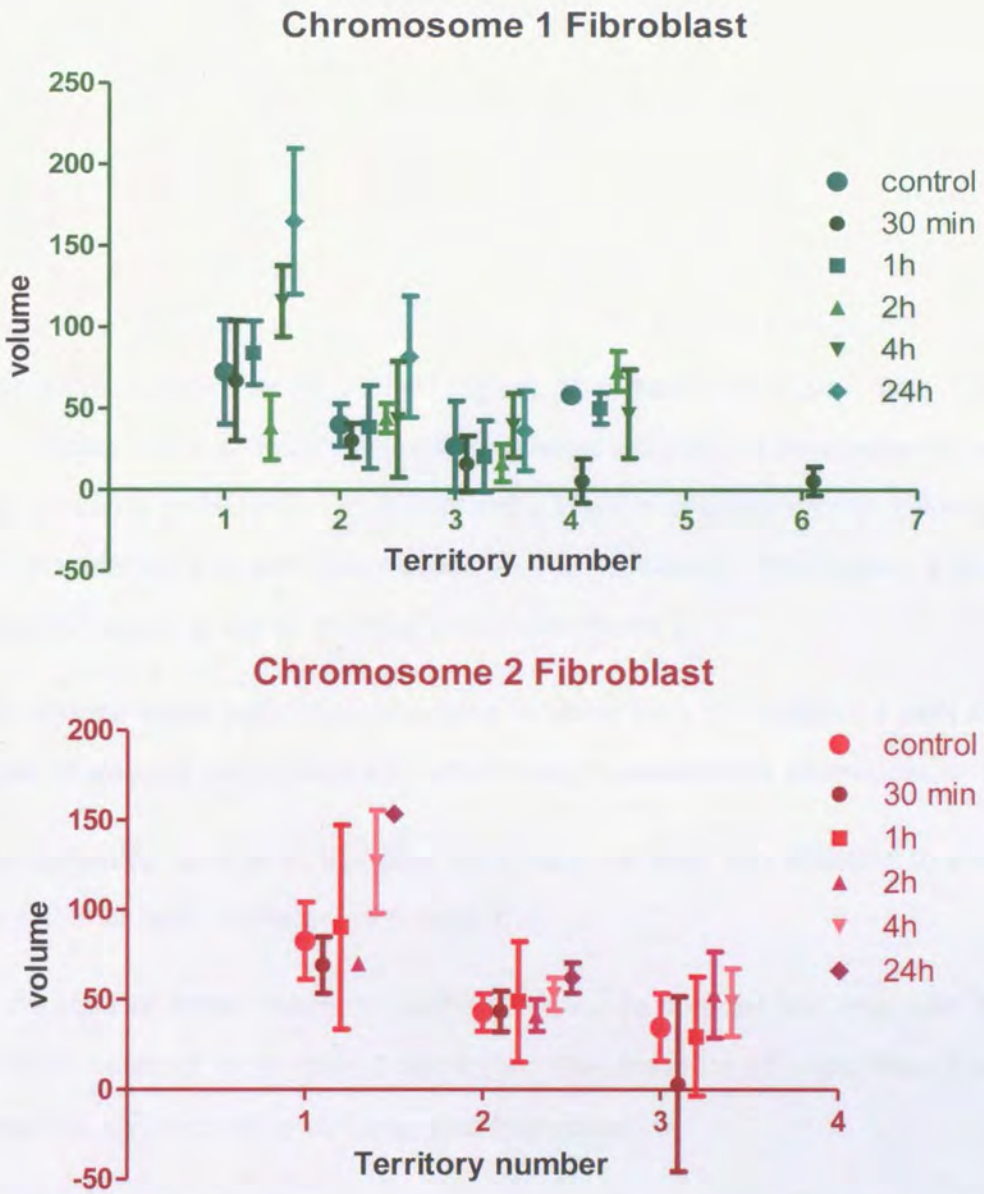

Figure 7.4: Graphic representation of the median and interquartile ranges for the different territory occurrences for the time points considered for chromosome 1 (top) and chromosome 2 (bottom) in fibroblasts. Volumes are expressed in μm^3.

When 2 G occurs the medians are between 40 and 44 μm^3 for 0 hour until 4 hours and doubles at 24 hours at 81 μm^3. When 3G is observed, the median values are much smaller than 0 hours (27 μm^3) at 30 minutes (16 μm^3), 1 hour (21 μm^3) and 2 hours (17 μm^3). An increase is seen at 4 hours (40 μm^3) and 24 hours (36 μm^3). When 4G is observed, the median values are similar at 0 hours (58 μm^3), 1 hour (50 μm^3) and 4 hours (47 μm^3) with a decrease at 30 minutes (5 μm^3) and an increase at 2 hours (72.77 μm^3).

When considering chromosome 2, a lesser number of territories are observed. Only 1, 2 or 3 territories are seen in the nuclei considered.

When 1R occurs the medians are similar for 0 hours and 1 hour (83 $\mu m^3$and 90 μm^3 respectively) and for 30 minutes and 2 hours (69 $\mu m^3$and 70 μm^3 respectively). A similar increase to the one seen in chromosome 1 is observable at 4 hours and at 24 hours with medians of 127 μm^3 and 153 μm^3.

When 2R occurs the medians are between 41 and 44 μm^3 for 0 hour, 30 minutes and 2 hours. The medians are slightly higher at 1 hours and 4 hours (49 $\mu m^3$and 53 μm^3 respectively) before being at their highest at 24 hours at 62 μm^3. When 3R is observed, the median value is much smaller than 0 hours (35 μm^3) at 30 minutes (3 μm^3). At 1 hour the median is quite similar at 21 μm^3 and a slight increase is seen at 2 hours (53 μm^3) and 4 hours (49 μm^3) as with chromosome 1. The increase in chromosome 2 territory volume when 4R occurs is not as sharp as with chromosome 1.

The volume splits were then examined as done with non-irradiated cells in chapter 6 in order to attempt at visualise the formation of fragments and aberrations.

The scenarios to note at this time points are the ones very different to a 50%/50% split for either or both chromosome (Figure 7.5).

In the case of either chromosome the scenarios to note are the ones with 2 territories of unequal splits or more than 2 territories. The presence of more than 3 territories can show the presence of newly generated fragments.

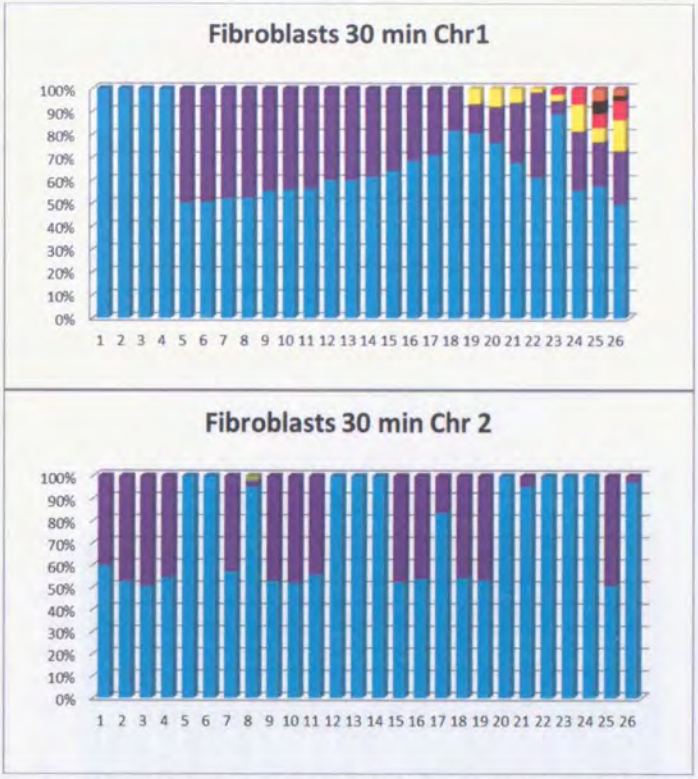

Figure 7.5: Graphic representation of the proportion of each individual territory volume compared to the corresponding total chromosome volume (100%) for both chromosome 1 (top) and 2 (bottom). Each bar corresponds to the territories observed in on cell nucleus for the chromosome considered. Each colour in the bar represents a fragment (territory) observed for the given chromosome. The data has been sorted using the number of territory observed for chromosome 1 with the corresponding chromosome 2 data aligned accordingly in the bottom graph. Territory 1, blue; territory 2, purple; territory 3, yellow; territory 4, pink; territory 5, black; territory6, light brown.

In the case of the fibroblasts at 30 minutes, the 3G scenarios do not appear to be 50%/25%/25% splits which exclude the possibility that these cells could be in G2. Similarly the 4G scenarios and 6G scenarios observed could be the result of the presence of extra fragments that have not been repaired yet.

When considering chromosome 2, only one occurrence of 3R was observed with a 95%/3%/2% split and a 50%/50% split for the corresponding chromosome 1. Only 3 occurrences of 2R were not a 50%/50% split or close. Like with chromosome 1, it is possible that fragments have been generated and not repaired yet.

After 1 hour post-irradiation, only 2 nuclei presented more than 2 territories for chromosome 1 with one of those nuclei presenting 4 territories with a 25%/25%/25%/25% split indicating the possible presence of two copies of each member of the chromosome 1 pair (Figure 7.6). This possibility was confirmed by the total chromosome volume for this occurrence being much higher than the volumes observed in the other fibroblasts at this time point at 213 μm^3. The nucleus volume of this particular

cell at 2159 μm^3 was higher than the median (1574 μm^3). The corresponding chromosome 2 split was similar to 50%/25%/25% which means it is possible that also 2 copies of each chromosome in the pair was present in the nucleus (with 2 territories being visualised together in the 50% part) and therefore confirming the high likelihood for the cell to be in G_2. The second nucleus presented 3G and 3R with splits slightly different to the 50%/25%/25%.

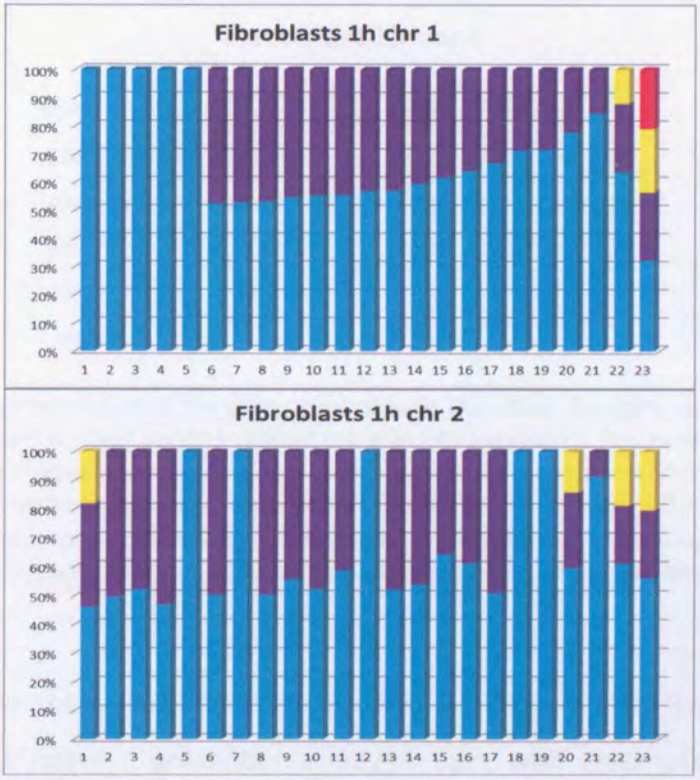

Figure 7.6: Graphic representation of the proportion of each individual territory volume compared to the corresponding total chromosome volume (100%) for both chromosome 1 (top) and 2 (bottom). Each bar corresponds to the territories observed in on cell nucleus for the chromosome considered. Each colour in the bar represents a fragment (territory) observed for the given chromosome. The data has been sorted using the number of territory observed for chromosome 1 with the corresponding chromosome 2 data aligned accordingly in the bottom graph. Territory 1, blue; territory 2, purple; territory 3, yellow; territory 4, pink.

When considering chromosome 2, two additional occurrences presented 3 territories with the corresponding chromosome 1 splits being 100% and 75%/25% with the corresponding nuclei volumes being 669 and 3174 μm^3 respectively. Only the latter, after considering the higher nuclear volume could be in G_2. Finally, the last interesting occurrence involved a cell with a 2G/2R split where both chromosome 1 and 2 did not have a 50%/50% split. The corresponding nucleus volume is 2304 μm^3 which was higher than the median.

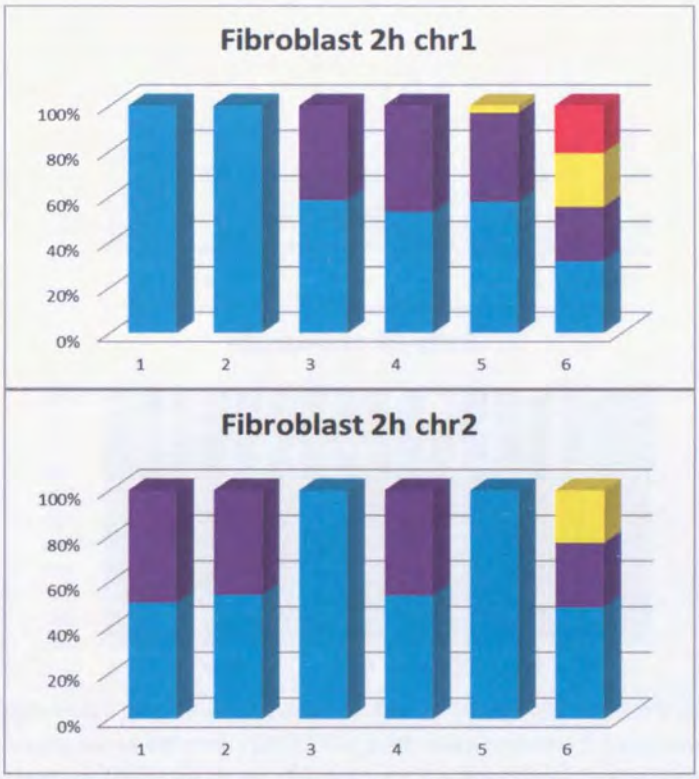

Figure 7.7: Graphic representation of the proportion of each individual territory volume compared to the corresponding total chromosome volume (100%) for both chromosome 1 (top) and 2 (bottom). Each bar corresponds to the territories observed in on cell nucleus for the chromosome considered. Each colour in the bar represents a fragment (territory) observed for the given chromosome. The data has been sorted using the number of territory observed for chromosome 1 with the corresponding chromosome 2 data aligned accordingly in the bottom graph. Territory 1, blue; territory 2, purple; territory 3, yellow; territory 4, pink.

At 2 hours, the data set is much smaller with only 6 cells examined (Figure 7.7). The only occurrence of real interest presented a 3G/1R split with chromosome 1 being split 57%/40%/3% and could indicate the presence of fragments generated following irradiation and not correctly repaired. The occurrences with 2, 3 or 4 territory followed the 50%/50%, 50%/25%/25% and 25%/25%/25%/25% scenarios indicating that the cells were likely to be in G_2. The 4G/3R occurrence corresponding nucleus had a much higher volumes than the rest of the sample at 2310 μm^3.

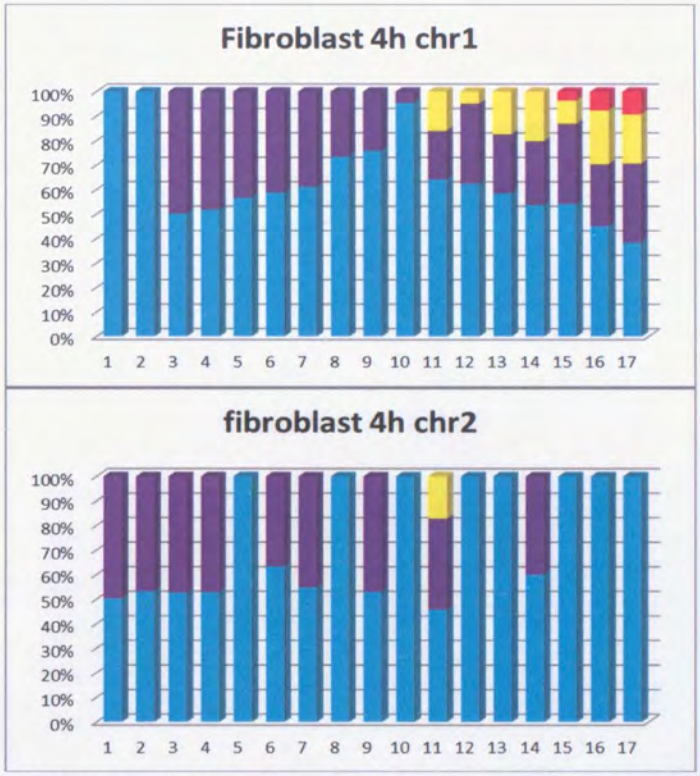

Figure 7.8: Graphic representation of the proportion of each individual territory volume compared to the corresponding total chromosome volume (100%) for both chromosome 1 (top) and 2 (bottom). Each bar corresponds to the territories observed in on cell nucleus for the chromosome considered. Each colour in the bar represents a fragment (territory) observed for the given chromosome. The data has been sorted using the number of territory observed for chromosome 1 with the corresponding chromosome 2 data aligned accordingly in the bottom graph. Territory 1, blue; territory 2, purple; territory 3, yellow; territory 4, pink.

At 4 hours, more than half of the cells considered presented 2 territories with a split much different from 50%/50% or more for chromosome 1 (Figure 7.8). When 4G was observed on 2 occurrences, the splits were not similar to 25%/25%/25%/25% and the corresponding chromosome 2 presented 1 territory. When 3G was observed, the splits were not similar to 50%/25%/25% for chromosome 1. The corresponding chromosome 2 splits were either 1R, 2R with a split close to 50%/50% and finally 3R with a 40%/40%/20% split.

When 2G was observed, 1 nucleus presented a split close to 90%/10% which could indicate the presence of a newly generated fragment.

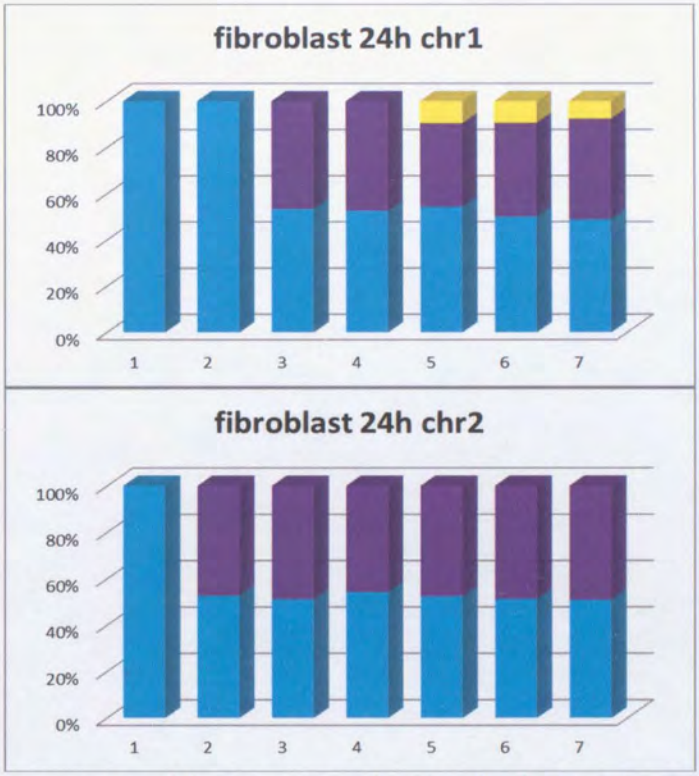

Figure 7.9: Graphic representation of the proportion of each individual territory volume compared to the corresponding total chromosome volume (100%) for both chromosome 1 (top) and 2 (bottom). Each bar corresponds to the territories observed in on cell nucleus for the chromosome considered. Each colour in the bar represents a fragment (territory) observed for the given chromosome. The data has been sorted using the number of territory observed for chromosome 1 with the corresponding chromosome 2 data aligned accordingly in the bottom graph. Territory 1, blue; territory 2, purple; territory 3, yellow.

At 24 hours chromosome 2 only presented 1R or 2R (Figure 7.9). No extra fragments were observed. In the case of chromosome 1, the presence of 2 occurrences of 3G with splits being similar to 40%/40%/10% could indicate the presence of unrepaired DSBs that were translated into the presence of an extra fragment.

7.3.1.4. Distances and ratio of relative radii

Distances were measured from the centre of gravity of the nucleus to the centre of gravity of the territory considered using the in-built 3D tool in Amira (Figure 7.10). The radii from the centre of gravity of the nucleus and passing through the centre of gravity of the territory were also measured. The ratios of the radii were then calculated for analysis.

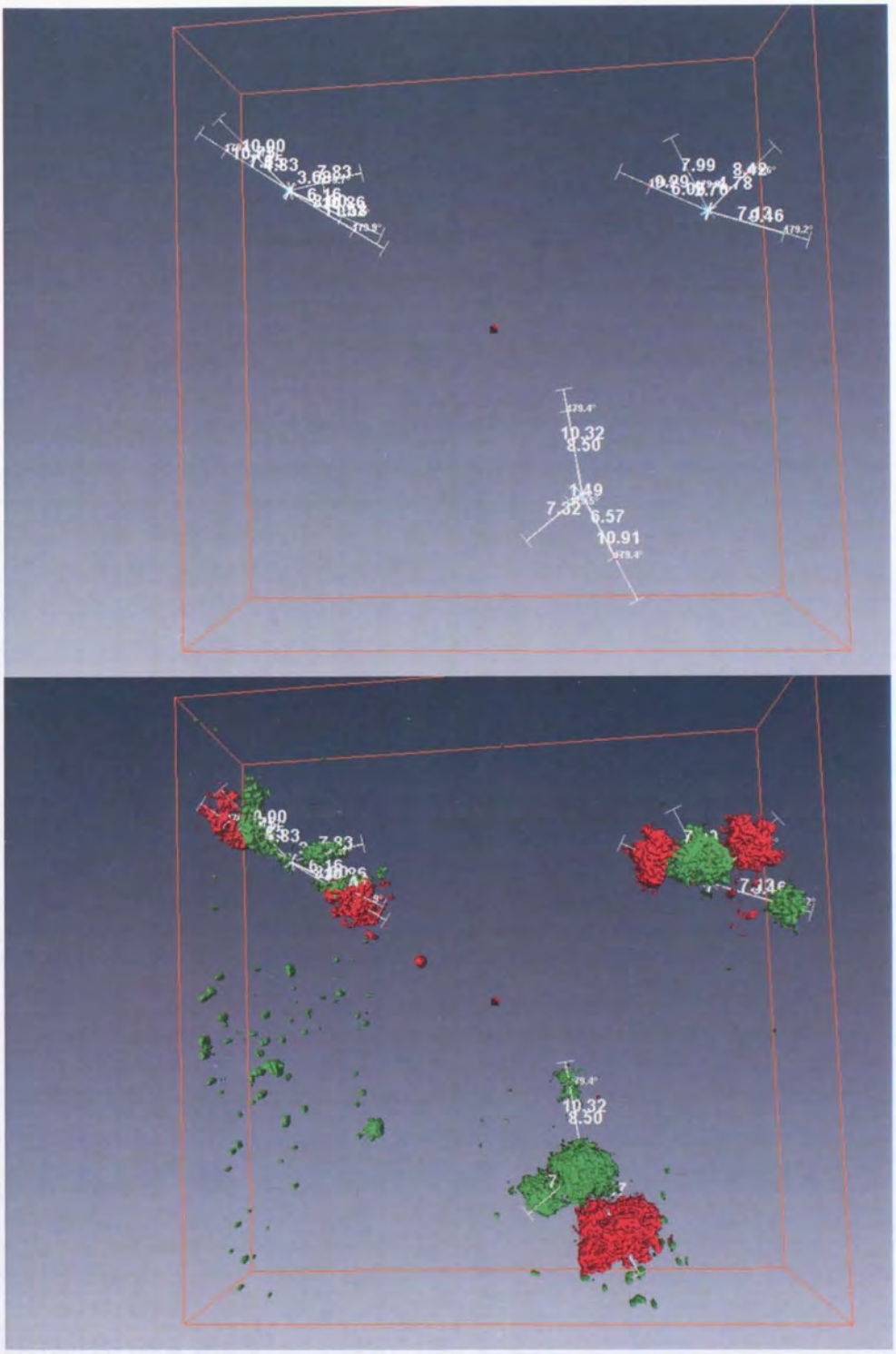

Figure 7.10: 3D visualisation example of chromosome territories for chromosome 1 (green) and chromosome 2 (red) within fibroblast nuclei 1 hour post-irradiation. The upper figure shows measurements of distances between the nucleus centre of gravity and the territories' centres of gravity. The lower figure shows the same measurements with the visualisation of the whole territories. Measurements are expressed in µm.

Chr1 distances	N	Mean	SD	SE	CV	Normal?	P	Chr1 Ratio of radius	N	Median	25% percentile	75% percentile	75%-25%	Normal?	P
Control	79	6.889	2.325	0.2616	0.34	Yes	P > 0.10	Control	79	65.96	54.15	74.3	20.15	No	0.0214
30 min	64	5.34	1.771	0.2214	0.33	Yes	P > 0.10	30 min	64	64.21	51.3	73.74	22.44	Yes	0.2
1h	44	6.15	1.977	0.2981	0.32	Yes	P > 0.10	1h	44	65.91	56.97	71.1	14.13	Yes	0.0791
2h	13	6.595	1.709	0.474	0.26	Yes	P > 0.10	2h	13	71.86	65.68	81.85	16.17	Yes	0.2
4h	42	6.023	2.333	0.3601	0.39	Yes	P > 0.10	4h	42	62.98	47.97	74.12	26.15	Yes	0.2
24h	15	8.682	1.697	0.4381	0.20	Yes	0.0608	24h	15	75.86	68.3	79.62	11.32	Yes	0.0522
Chr2 distances	N	Mean	SD	SE	CV	Normal?	P	Chr2 Ratio of radius	N	Median	25% percentile	75% percentile	75%-25%	Normal?	P
Control	78	6.448	1.979	0.2241	0.31	Yes	P> 0.10	Control	78	64.58	55.23	74.81	19.58	No	0.0136
30 min	44	5.473	1.87	0.2819	0.34	Yes	P> 0.10	30 min	44	69.95	50.52	82.23	31.71	Yes	0.2
1h	45	5.938	2.235	0.3332	0.38	Yes	P> 0.10	1h	45	62.65	50.84	73.71	22.87	Yes	0.2
2h	11	6.443	1.158	0.3493	0.18	Yes	P> 0.10	2h	11	70.47	61.56	81.21	19.65	Yes	0.2
4h	27	6.325	1.874	0.3606	0.30	Yes	P> 0.10	4h	27	62.97	56.72	74.58	17.86	Yes	0.2
24h	13	8.014	2.467	0.6844	0.31	Yes	P> 0.10	24h	13	73.13	59.29	80.21	20.92	No	0.0241

Table 7.7: Table of descriptive statistics for the distances between the nucleus centre of gravity and the territory centre of gravity measured using Amira software for chromosome 1 and chromosome 2 in fibroblast at the different time points considered. Distances are expressed in µm. Ratios of Radii are expressed in percentages.

The distances from the CoG of the nucleus appear to be fluctuating similarly to the nucleus size. For example the mean values for the distances at 30 minutes appear slightly smaller than the rest of the data sets considered. At 30 minutes, the median value for the nucleus size was also smaller than the rest of the time points considered. At 24 hours the median value for the nucleus size was much higher than the values for the other time points which translated into longer distances from the CoG of the nuclei for both chromosomes.

The values for the different time points were compared with the control values using an unpaired t-test. There was no significant difference in terms of distances for chromosome 1 at 1 hour, 2 hours and 4 hours compared to the controls ($p = 0.08$ and $p = 0.66$ and $p = 0.05$ respectively) but a significant difference was found between the controls and 30 minutes and, 24 hours ($p < 0.0001$ and $p = 0.01$ respectively). The results were confirmed using a false discovery rate (FDR) method (Benjamini & Hochberg, 1995) with a maximum FDR of 10%.

For chromosome 2, there was no significant difference in terms of distances at 1 hour, 2 hours and 4 hours compared to the controls ($p = 0.19$ and $p = 0.99$ and $p = 0.78$ respectively) but a significant difference was found between the controls and 30 minutes and, 24 hours ($p = 0.01$ and $p = 0.01$ respectively). The results were confirmed using a false discovery rate (FDR) method (Benjamini & Hochberg, 1995) with a maximum FDR of 10%.

Ratios of relative radii did not appear to follow a similar trend. The median value at 24 hours was higher than at other time points. The values for the different time points were compared with the control values using a Mann-Whitney test. There was no significant difference in terms of ratio of radius for chromosome 1 at 30 min, 1 hour and, 4 hours compared to the controls ($p = 0.90$ and $p = 0.89$ and $p = 0.48$ respectively) but a significant difference was found between the controls and 2 hours and, 24 hours ($p = 0.040$ and $p = 0.013$ respectively). The results were confirmed using a false discovery rate (FDR) method (Benjamini & Hochberg, 1995) with a maximum FDR of 10%.

For chromosome 2, there was no significant difference in terms of ratio of radius for all the timepoints compared to the controls ($p = 0.15$, $p = 0.77$, $p = 0.86$, $p = 0.86$ and $p =$

0.08 respectively). The results were confirmed using a false discovery rate (FDR) method (Benjamini & Hochberg, 1995) with a maximum FDR of 10%.

However, the increase in the ratio of relative radii was not as significant as the increase seen in distances. This could suggest a change in nucleus shape rather than territories positioning shifting towards the interior since the cells at 24 hours could potentially be in G_2. At 4 hours, the ratio of relative radius appears to decrease for both chromosome despite the distances being similar to the earlier time points and the nuclear sizes increasing. This could be due to the cells being in early G_2 before the drastic change in nuclear volume seen at 24 hours.

The distances and ratio of relative radii were plotted against their corresponding territory volumes and also against their corresponding nuclear volumes. The data for both chromosomes were plotted against one another in order to visually assess possible differences in positioning between chromosome 1 and 2 following irradiation. The plots are presented in Figure 7.11 and 7.12.

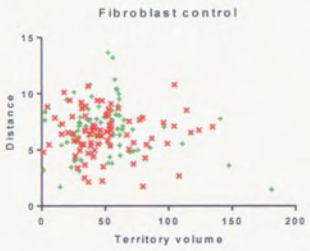
Fibroblast control
Distance
Territory volume

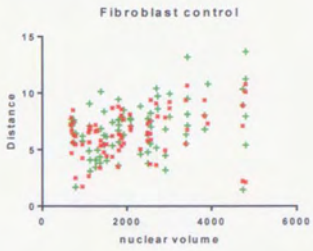
Fibroblast control
Distance
nuclear volume

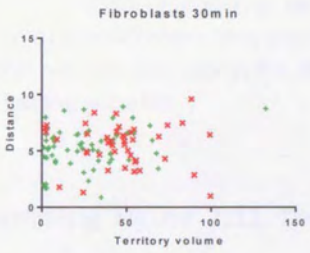
Fibroblasts 30min
Distance
Territory volume

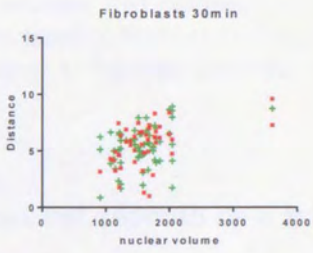
Fibroblasts 30min
Distance
nuclear volume

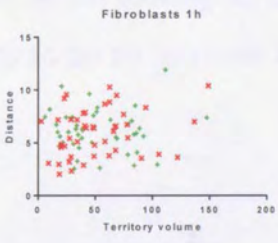
Fibroblasts 1h
Distance
Territory volume

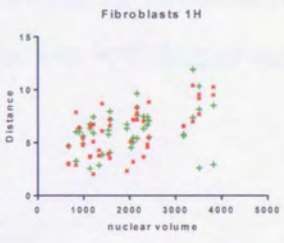
Fibroblasts 1H
Distance
nuclear volume

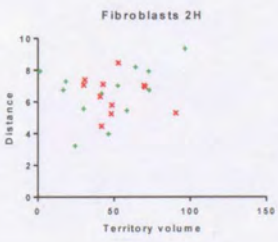
Fibroblasts 2H
Distance
Territory volume

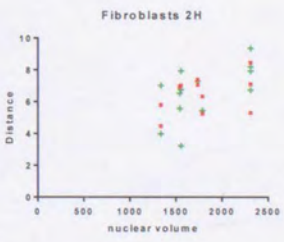
Fibroblasts 2H
Distance
nuclear volume

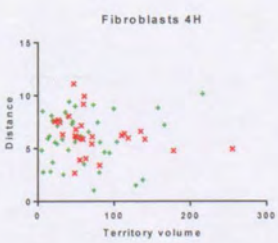
Fibroblasts 4H
Distance
Territory volume

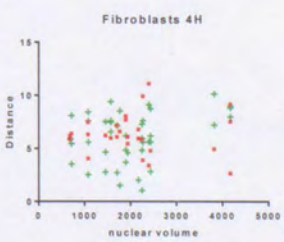
Fibroblasts 4H
Distance
nuclear volume

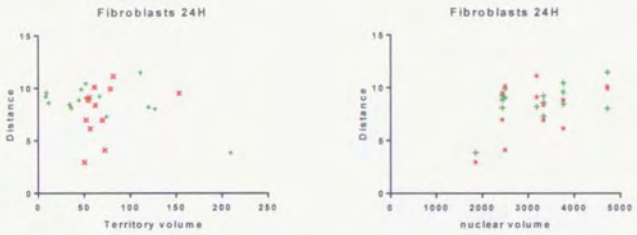

Figure 7.11: The distance from the centre of gravity of the nucleus to the centre of gravity of the territory are plotted against both the corresponding territory volumes (left column) and corresponding nuclei volumes (right column) at the different time points considered in fibroblasts. The green crosses represent chromosome 1 and the red crosses represent chromosome 2. The measurements are given in μm for the distances and in μm^3 for the volumes.

When visually examining Figure 7.11, there does not seem to be a relationship between territory size and distance from the CoG of the nucleus at any of the time points considered. However, when looking at the relationship between distances and nuclear volumes, there seems to be an increase in distances with bigger nuclei except at 4 hours and 30 minutes.

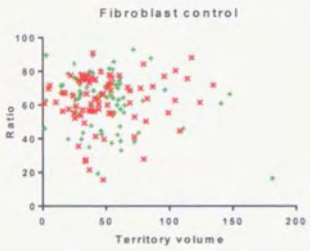
Fibroblast control
Ratio
Territory volume

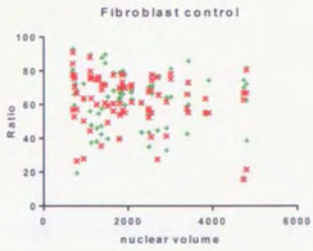
Fibroblast control
Ratio
nuclear volume

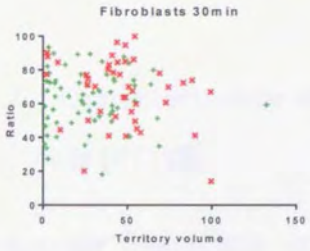
Fibroblasts 30min
Ratio
Territory volume

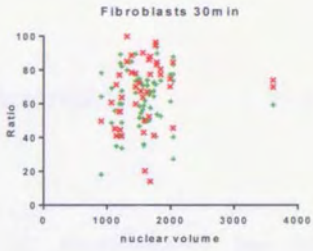
Fibroblasts 30min
Ratio
nuclear volume

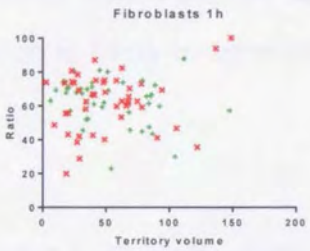
Fibroblasts 1h
Ratio
Territory volume

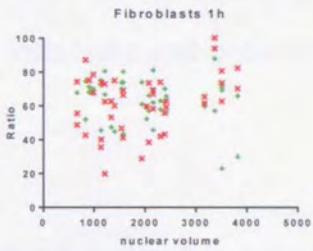
Fibroblasts 1h
Ratio
nuclear volume

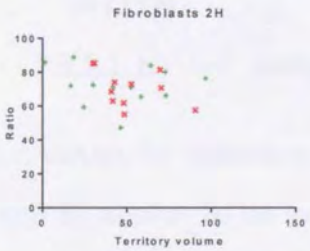
Fibroblasts 2H
Ratio
Territory volume

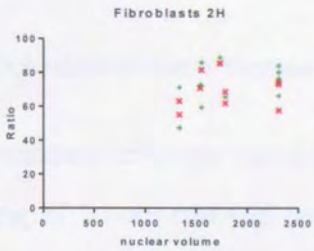
Fibroblasts 2H
Ratio
nuclear volume

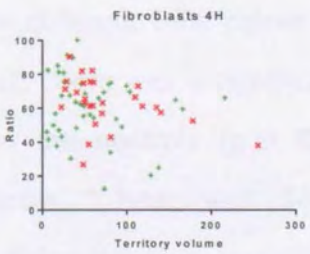
Fibroblasts 4H
Ratio
Territory volume

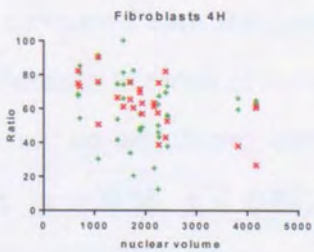
Fibroblasts 4H
Ratio
nuclear volume

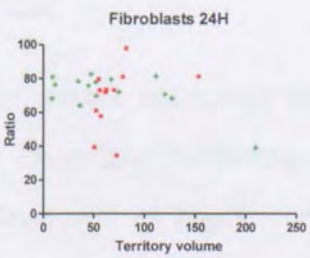
Fibroblasts 24H
Ratio
Territory volume

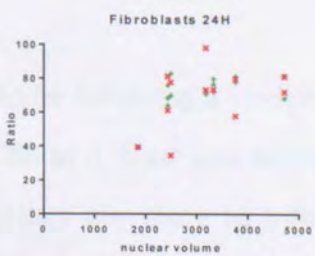
Fibroblasts 24H
Ratio
nuclear volume

Figure 7.12: The ratios of radii are plotted against both the corresponding territory volumes (left column) and corresponding nuclei volumes (right column) at the different time points considered in fibroblasts. The green crosses represent chromosome 1 and the red crosses represent chromosome 2. The measurements are given in μm for the distances and in μm^3 for the volumes.

The relation seen between distances and nucleus volume seems to disappear when examining ratios of relative radii. There does not seem to be a clear relation between ratios and both territory volumes and nuclear volumes.

7.3.2. Characterisation of chromosome 1 and 2 in bladder carcinoma cells (RT112)

The chromosome instability in RT112 manifested by higher numbers of chromosome territories within the cell nuclei studied for the control group. Subjecting the cell line to radiation is likely to increase this instability and possibly lead to increased variability in CTs.

7.3.2.1. Characterisation of chromosome 1 in bladder carcinoma cells (RT112)

7.3.2.1.1. Individual chromosome volumes

The medians values for individual chromosome volumes (data presented in Figure 7.13, Columns A and B) appear to be increasing at 1 hour from 23 μm^3 in controls to 33 μm^3 before decreasing to 27 μm^3 at 2 hours and to 22 μm^3 at 24 hours.

The values for the different time points were compared with the control values using a Mann-Whitney test. There was a significant difference in terms of individual volumes at 1 hour compared to the controls ($p = 0.001$) but no significant difference was found between the controls, 2 hours and, 24 hours ($p = 0.15$, $p = 0.86$). The results were confirmed using a false discovery rate (FDR) method (Benjamini & Hochberg, 1995) with a maximum FDR of 10%.

The percentages of volume occupancy appear to be following a similar trend with median values starting at 1% before increasing to 1.57% at 1 hour and decrease back to 1.39% and 0.84% at 2 hours and 24 hours. The CV values are close to 1 for most of the time points considered which indicates variability in the sample data.

When subjecting the ratio values to the same statistical analysis as the volumes, the comparison between controls and 1 hour and, controls and 2 hours showed a significant difference ($p = 0.02$ and $p = 0.03$) whereas no significant difference between the control and 24 hours was found ($p = 0.10$). The results were confirmed using a false discovery rate (FDR) method (Benjamini & Hochberg, 1995) with a maximum FDR of 10%.

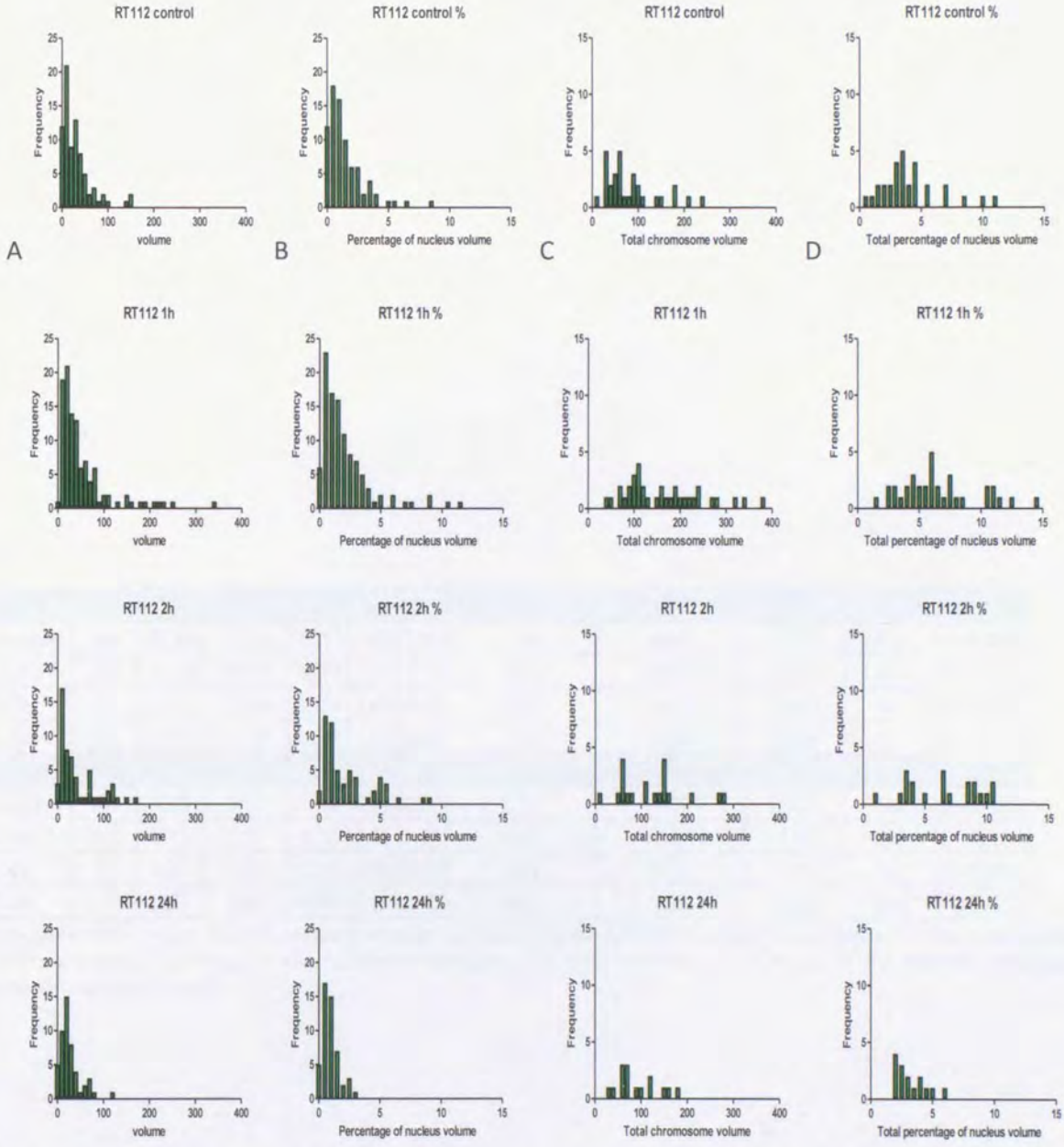

Figure 7.13: The volume measurements for Chromosome 1 at various times after irradiation at 8 gray are presented as frequency histograms. The descriptive statistics for those distributions are presented in Table 7.8. Horizontally, the four graphs show A: actual individual chromosome volumes, B: volumes expressed as a percentage of the nuclear volume, C: total actual chromosome volume calculated as the sum of the volume of all fragments in each nucleus and D: the sum of all fragments expressed as a percentage of the nuclear volume. Vertically the graphs show the respective distributions at various times after irradiation from 0 (from Figure 6.9) to 24h. Volumes are expressed in μm^3.

Chr1 volume	N	Mean	Median	SD	SE	CV	25% percentile	75% percentile	75%-25%	Normal?	P
RT112 Controls	80	31.56	23.55	32.73	3.66	1.04	8.39	40.16	31.77	No	P<0.0001
RT112 1h	107	53.48	33.39	59.23	5.73	1.11	19.51	64.80	45.29	No	P<0.0001
RT112 2h	57	43.23	27.04	42.68	5.65	0.99	11.97	71.64	59.67	No	P<0.0001
RT112 24h	50	27.30	21.89	23.25	3.29	0.85	11.52	34.58	23.06	No	P<0.0001
Chr1 percentage	N	Mean	Median	SD	SE	CV	25% percentile	75% percentile	75%-25%	Normal?	P
RT112 Controls	80	1.53	1.00	1.54	0.17	1.00	0.51	2.19	1.67	No	P<0.0001
RT112 1h	107	2.15	1.57	2.14	0.21	1.00	0.72	2.69	1.98	No	P<0.0001
RT112 2h	57	2.27	1.39	2.12	0.28	0.93	0.74	3.16	2.43	No	P<0.0001
RT112 24h	50	0.97	0.84	0.70	0.10	0.72	0.41	1.30	0.89	Yes	0.0755

Table 7.8: Summary table of the mean, median, standard error of the mean, standard deviation, range and CV values for the corresponding distributions of territory volumes and volume ratios presented in Figure 7.13 for chromosome 1 in RT112 at the different time points considered. Volumes are expressed in μm^3.

7.3.2.1.2. Total chromosome volumes

The total chromosome volumes (data presented in Figure 7.13, Column C and D) seem to increase until 2 hours (from 63 μm^3 to 121 μm^3) before decreasing back to values similar to the controls after 24 hours (74 μm^3). The increase is quite sharp and the values at 1 hour and 2 hours appear to be in the order of double and 1.5 the values obtained for the control group respectively (Table 7.9). The CV values have decreased to approximately 0.5 which is much smaller than the CV values observed for individual values. This could be explained by the presence of smaller individual fragments decreasing the homogeneity of the group of values when considering individual volumes. A phenomenon that tends to disappear when looking at total chromosome volume within the nucleus since, unless an considerable deletion has occurred, the chromosome copies present in the nucleus will occupy volumes within the range of the normal variability. This was also observed for percentage of the nucleus occupied by the total chromosome volume.

The values for the different time points were compared with the control values using a Mann-Whitney test. There was a significant difference in terms of total volumes at 1 hour and 2 hours compared to the controls ($p < 0.0001$ and $p = 0.03$) but no significant difference was found between the controls and 24 hours ($p = 0.32$). The results were confirmed using a false discovery rate (FDR) method (Benjamini & Hochberg, 1995) with a maximum FDR of 10%.

When subjecting the ratio values to the same analysis, the comparison between controls 1 hour and 2 hours showed a significant difference ($p = 0.0006$ and $p = 0.004$) whereas no significant difference between the control and 24 hours was found ($p = 0.33$). The results were confirmed using a false discovery rate (FDR) method (Benjamini & Hochberg, 1995) with a maximum FDR of 10%.

Chr1 total volume	N	Mean	Median	SD	SE	CV	25% percentile	75% percentile	75%-25%	Normal?	P
RT112 Controls	30	84.16	63.22	58.87	10.75	0.70	42.10	104.20	62.10	No	0.0054
RT112 1h	35	163.49	148.10	84.96	14.36	0.52	96.74	215.10	118.36	Yes	0.0635
RT112 2h	20	123.19	121.18	71.09	15.90	0.58	60.33	150.50	90.17	Yes	P > 0.10
RT112 24h	15	91.00	74.00	44.66	11.53	0.49	57.05	116.70	59.65	Yes	P > 0.10
Chr1 total percentage	N	Mean	Median	SD	SE	CV	25% percentile	75% percentile	75%-25%	Normal?	P
RT112 Controls	30	4.09	3.50	2.45	0.45	0.60	2.54	4.85	2.31	No	0.0188
RT112 1h	35	6.56	5.95	3.11	0.53	0.47	4.44	7.79	3.35	Yes	P > 0.10
RT112 2h	20	6.48	6.64	2.89	0.65	0.45	3.77	9.00	5.23	Yes	P > 0.10
RT112 24h	15	3.23	2.77	1.21	0.31	0.37	2.20	4.04	1.84	Yes	P > 0.10

Table 7.9: Summary table of the mean, median, standard error of the mean, standard deviation, range and CV values for the corresponding distributions of total territory volumes and total volume ratios presented in Figure 7.13 for chromosome 1 in RT112 at the different time points considered. Volumes are expressed in μm^3.

7.3.2.2. Characterisation of chromosome 2 in bladder carcinoma cells (RT112)

7.3.2.2.1. Individual chromosome volumes

The variability observed with chromosome 1 is not observed with chromosome 2 (Figure 7.14, Column A and B). The individual values medians appear to be increasing until 24h from 28 μm^3 to 61 μm^3. Despite still being relatively high, the CV values have decreased more compared to chromosome 1 (Table 7.10).

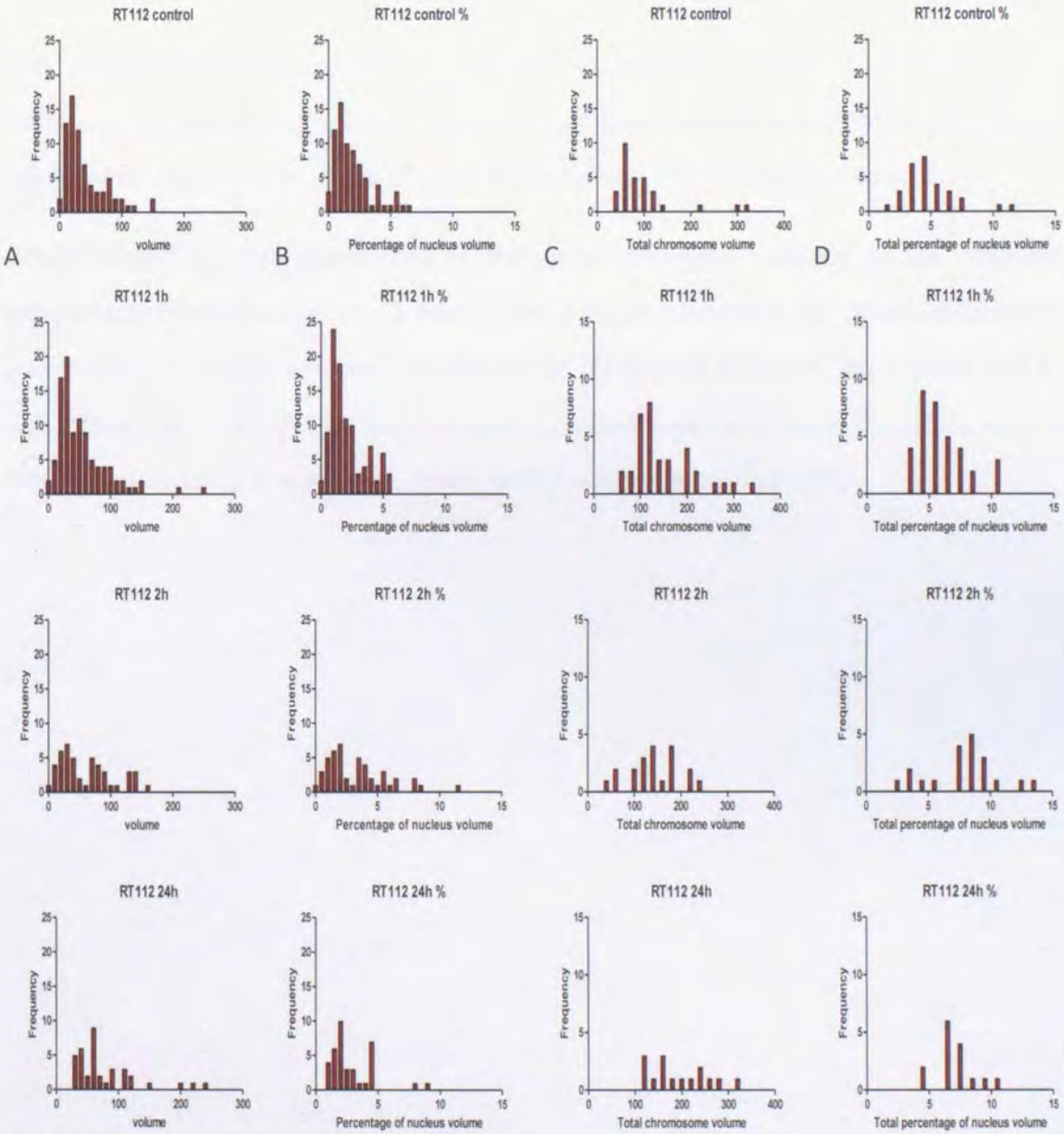

Figure 7.14: The volume measurements for Chromosome 2 at various times after irradiation at 8 gray are presented as frequency histograms. The descriptive statistics for those distributions are presented in Table 7.10. Horizontally, the four graphs show A: actual individual chromosome volumes, B: volumes expressed as a percentage of the nuclear volume, C: total actual chromosome volume calculated as the sum of the volume of all fragments in each nucleus and D: the sum of all fragments expressed as a percentage of the nuclear volume. Vertically the graphs show the respective distributions at various times after irradiation from 0 (from Figure 6.9) to 24h. Volumes are expressed in μm^3.

The distribution observed seem to contain the majority of the values close to 20 μm^3 for the controls, 1 hour and 2 hours whereas it appears the values shift more towards 70 μm^3 at 24 hours (Table 7.10). The values for the different time points were compared with the control values using a Mann-Whitney test. There was a significant difference in terms of individual volumes at 1 hours, 2 hours and 24 hours compared to the controls ($p = 0.01$, $p = 0.01$ and $p < 0.0001$ respectively). The results were confirmed using a false discovery rate (FDR) method (Benjamini & Hochberg, 1995) with a maximum FDR of 10%.

The values for the percentage of nucleus occupied by a territory do not seem to be following this trend. The median values for the percentages of nuclear occupancy appear to increase until 2 hours (from 1.5% to 2.5%) before slightly decreasing to 2.1%.

When subjecting the ratio values to the same statistical analysis as the volumes, the comparison between controls, 2 hours and 24 hours showed a significant difference ($p = 0.001$ and $p = 0.002$) whereas no significant difference between the control and 1 hour was found ($p = 0.30$). The results were confirmed using a false discovery rate (FDR) method (Benjamini & Hochberg, 1995) with a maximum FDR of 10%.

Chr2 volume	N	Mean	Median	SD	SE	CV	25% percentile	75% percentile	75%-25%	Normal?	P
RT112 Controls	74	40.65	28.19	33.05	3.84	0.81	16.14	56.22	40.08	No	P<0.0001
RT112 1h	100	53.74	43.29	42.22	4.22	0.79	25.94	68.44	42.50	No	P<0.0001
RT112 2h	47	60.52	48.71	42.52	6.20	0.70	27.89	89.13	61.24	No	0.0009
RT112 24h	37	78.22	61.27	52.68	8.66	0.67	40.53	99.01	58.48	No	0.0009
Chr2 percentage	N	Mean	Median	SD	SE	CV	25% percentile	75% percentile	75%-25%	Normal?	P
RT112 Controls	74	1.97	1.50	1.53	0.18	0.77	0.83	2.65	1.81	No	0.0002
RT112 1h	100	2.12	1.63	1.43	0.14	0.67	1.07	2.93	1.86	No	P<0.0001
RT112 2h	47	3.35	2.54	2.47	0.36	0.74	1.48	4.46	2.97	No	0.0046
RT112 24h	37	2.86	2.14	1.83	0.30	0.64	1.64	4.19	2.55	No	0.0016

Table 7.10: Summary table of the mean, median, standard error of the mean, standard deviation, range and CV values for the corresponding distributions of territory volumes and volume ratios presented in figure 7.14 for chromosome 2 in RT112 at the different time points considered. Volumes are expressed in μm^3.

7.3.2.2.2. Total chromosome volumes

The total chromosome volumes (data presented in Figure 7.14, Column C and D) seem to be increasing with time with median values starting at 81 μm^3 for the controls and going up to 181 μm^3 at 24 hours (Table 7.11).

The values for the different time points were compared with the control values using a Mann-Whitney test. There was a significant difference in terms of total chromosome volumes at 1 hours, 2 hours and 24 hours compared to the controls ($p < 0.0001$, $p = 0.002$ and $p < 0.0001$ respectively). The results were confirmed using a false discovery rate (FDR) method (Benjamini & Hochberg, 1995) with a maximum FDR of 10%.

The percentages of nucleus occupied by the total chromosome volumes in the other hand appear to increase until 2 hours from 4.5% to 8% before showing a decrease to 7% at 24 hours (Table 7.11).

When subjecting the total percentage of nucleus values to the same statistical analysis as the volumes, the comparison between controls, 1 hour, 2 hours and 24 hours showed a significant difference ($p = 0.02$, $p = 0.0003$ and $p = 0.0003$). The results were confirmed using a false discovery rate (FDR) method (Benjamini & Hochberg, 1995) with a maximum FDR of 10%.

Chr2 total volume	N	Mean	Median	SD	SE	CV	25% percentile	75% percentile	75%-25%	Normal?	P
RT112 Controls	30	100.26	81.11	68.84	12.57	0.69	55.49	108.9	53.41	Yes	P<0.0001
RT112 1h	35	150.58	128.76	68.23	11.53	0.45	102	197.7	95.70	Yes	0.0003
RT112 2h	20	142.22	138.64	52.34	11.70	0.37	106.6	176.8	70.20	Yes	P > 0.10
RT112 24h	15	192.93	180.59	61.84	15.97	0.32	136.7	242.2	105.50	Yes	P > 0.10
Chr2 total percentage	N	Mean	Median	SD	SE	CV	25% percentile	75% percentile	75%-25%	Normal?	P
RT112 Controls	30	4.87	4.50	2.22	0.40	0.46	3.305	5.997	2.69	No	P > 0.10
RT112 1h	35	5.94	5.47	2.04	0.34	0.34	4.378	7.212	2.83	Yes	P > 0.10
RT112 2h	20	7.87	8.02	2.86	0.64	0.36	5.667	9.483	3.82	Yes	0.0558
RT112 24h	15	7.05	6.98	1.48	0.38	0.21	6.215	7.56	1.35	Yes	P > 0.10

Table 7.11: Summary table of the mean, median, standard error of the mean, standard deviation, range and CV values for the corresponding distributions of total territory volumes and total volume ratios presented in Figure 7.14 for chromosome 2 in RT112 at the different time points considered. Volumes are expressed in μm^3.

7.3.2.3. Chromosome 1 and 2 territories analysis following irradiation

It appears that for chromosome 1, a higher number of territories are observed at 1 hour and 24 hours. This could be the illustration of aberrations already present within the nuclei and worsened following irradiation (1 hour) and stable fragments resulting from the irradiation treatment (24 hours).

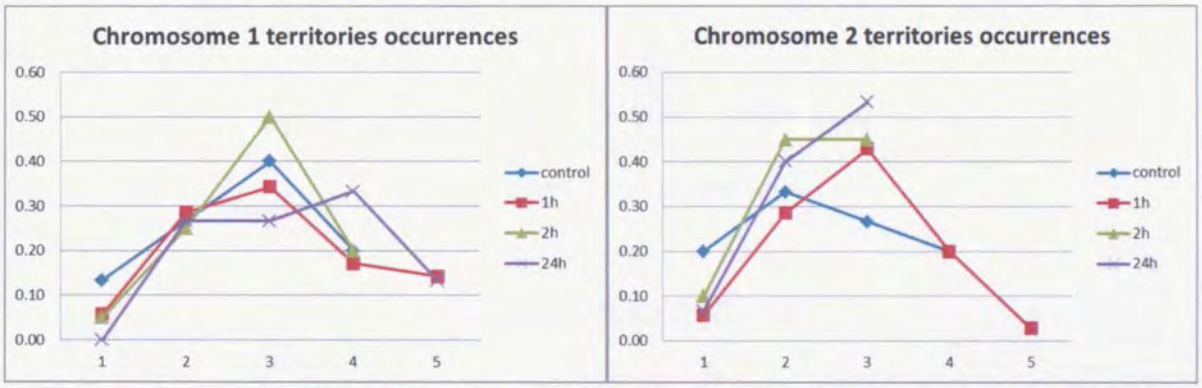

Figure 7.15: Proportion of the different territory occurrence (1 to 5) for each time point and controls in RT112 for chromosome 1 and 2.

A similar trend can be observed with chromosome 2. At 1 hour and 24 hours a majority of cell present 3 or more territory. It is difficult to say the reason why unless the proportion of each territory with regards to the total chromosome volume is examined which will be done later in this section.

The majority of the occurrences involve 3 territories which could explain the high variability in the volumes distribution observed in 7.3.4.2.1 and 7.3.4.2.2. At all the time points there are approximately a third of the cells with 2 territories.

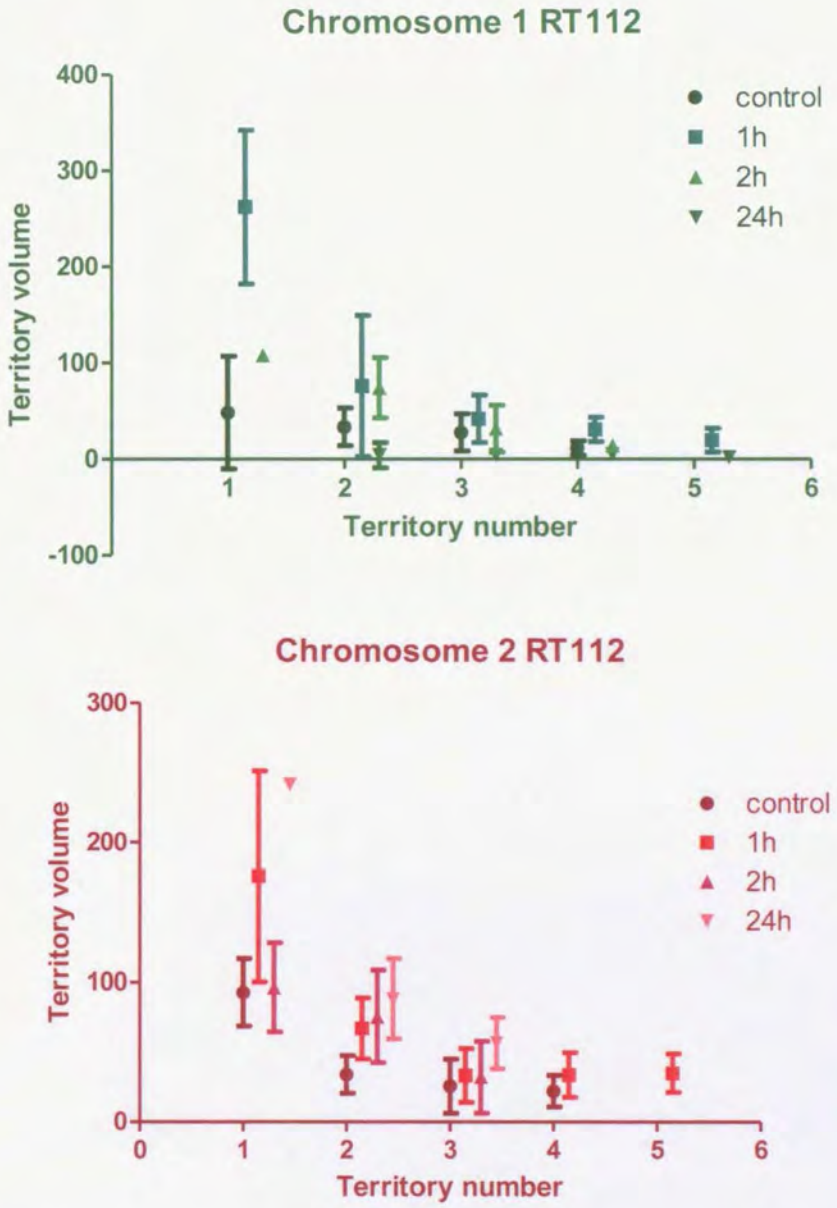

Figure 7.16: Graphic representation of the median and interquartile ranges for the different territory occurrences for the time points considered for chromosome 1 (top) and chromosome 2 (bottom) in RT112. Volumes are expressed in μm^3.

For both chromosomes up to 5 territories were observed (summary of descriptive statistics given in Tables 7.12 and 7.13 and graphic representation given in Figure 7.16).

When considering chromosome 1, there seem to be an increase in median values at one hour when 1 to 4 territories occur within the cell nucleus before a decrease up until 24 hours.

When 2G occurs, the medians appear to increase from 33 μm^3 to stay at similar values at 1 hour and 2 hours (75 μm^3 and 74 μm^3 respectively) before decreasing to 54 μm^3 at 24 hours.

When 3G occurs, a similar pattern can be seen with an increase from 28 μm^3 at 0 hour to 42 μm^3 at 1 hour before decreasing again at 2 hours (32 μm^3) and 24 hours (24 μm^3).

When 4G occurs, the median values are similar at 0 hours and 2 hours (12 μm^3 and 14 μm^3 respectively). A noticeable increase is also seen at 1 hour going from 12 μm^3 to 31 μm^3. The volume median at 24 hours is similar to 3G at 24 hours at 22 μm^3.

Chr1	Territory number	1 territory	2 territories	3 territories	4 territories	5 territories
control	occurrence	4	8	12	6	
	Median	48.21	33.49	27.64	11.48	
	25% Percentile	13.36	11.82	13.81	3.414	
	75% Percentile	130.6	50.68	52.15	18.5	
	75%-25% Percentile	117.24	38.86	38.34	15.086	
1h	occurrence	2	10	12	6	5
	Median	262	75.87	41.72	30.62	19.52
	25% Percentile	181.9	38.71	20.55	13.82	8.265
	75% Percentile	342.1	185.2	69.52	39.24	33.23
	75%-25% Percentile	160.2	146.49	48.97	25.42	24.965
2h	occurrence	1	5	10	4	
	Median	107.7	74.06	31.55	13.97	
	25% Percentile	107.7	62.28	13.87	6.032	
	75% Percentile	107.7	124.8	62.78	15.35	
	75%-25% Percentile	0	62.52	48.91	9.318	
24h	occurrence		4	4	5	2
	Median		53.91	23.72	22.01	8.823
	25% Percentile		27.44	15.51	12.81	2.221
	75% Percentile		79.58	50.91	32.33	18.34
	75%-25% Percentile		26.47	8.21	9.2	6.602

Table 7.12: Median values for the territory volumes for chromosome 1 sorted according to the number found in the cell nucleus considered and occurrences for each scenario in RT112. The 25% percentile, 75% percentile and the difference between the two are also given. Volumes are expressed in μm^3.

When considering chromosome 2 (Table 7.13), the increase seen at 1 hour in chromosome 1 does not seem to be as sharp except when 1 territory is observed. However, there seem to be a continuous increase of territory median volumes with time when 2R, 3R and 4R occur.

Chr2	Territory number	1 territory	2 territories	3 territories	4 territories	5 territories
control	occurrence	6	10	8	6	
	Median	92.64	33.98	25.69	22.15	
	25% Percentile	76.76	18.83	15.37	12.9	
	75% Percentile	124.8	45.82	54.4	35.57	
	75%-25% Percentile	48.04	26.99	39.03	22.67	
1h	occurrence	2	10	15	7	1
	Median	175.6	66.99	33.18	33.62	35
	25% Percentile	100.1	47.12	25.11	20.77	17.5
	75% Percentile	251.1	90.71	63.71	52.7	44.95
	75%-25% Percentile	151	43.59	38.6	31.93	27.45
2h	occurrence	2	9	9		
	Median	96	75.28	32.07		
	25% Percentile	64.28	37.02	18.35		
	75% Percentile	127.7	102.8	69.89		
	75%-25% Percentile	63.42	65.78	51.54		
24h	occurrence	1	6	8		
	Median	241.4	87.98	56.47		
	25% Percentile	241.4	57.48	36.48		
	75% Percentile	241.4	114.7	73.42		
	75%-25% Percentile	0	57.22	36.94		

Table 7.13: Median values for the territory volumes for chromosome 2 sorted according to the number found in the cell nucleus considered and occurrences for each scenario in RT112. The 25% percentile, 75% percentile and the difference between the two are also given. Volumes are expressed in μm^3.

At 1 hour, hardly any 2G occurrences were a 50%/50% split if any. In the case of 3G occurrences, the majority of the splits were 50%/25%/25% with the remainder being mostly with the presence of fragments smaller than 15% of the total volumes (Figure 7.17). The corresponding splits for chromosome 2 were mainly 50%/25%/25% or 25%/25%/25%/25% except for one occasion where the split was 80%/20%, one occasion where it was 70%/30% and one occasion where it was 60%/35%/5%.

When 4G occurs (Figure 7.17), hardly any of the occurrences look like a 25%/25%/25%/25% for chromosome 1 where most corresponding occurrences for chromosome 2 appear to be 50%/25%/25% except for 3 were the chromosome 2 splits are 2R (70%/30% and 50%/50%) and 4R (53%/22%/20%/5%).

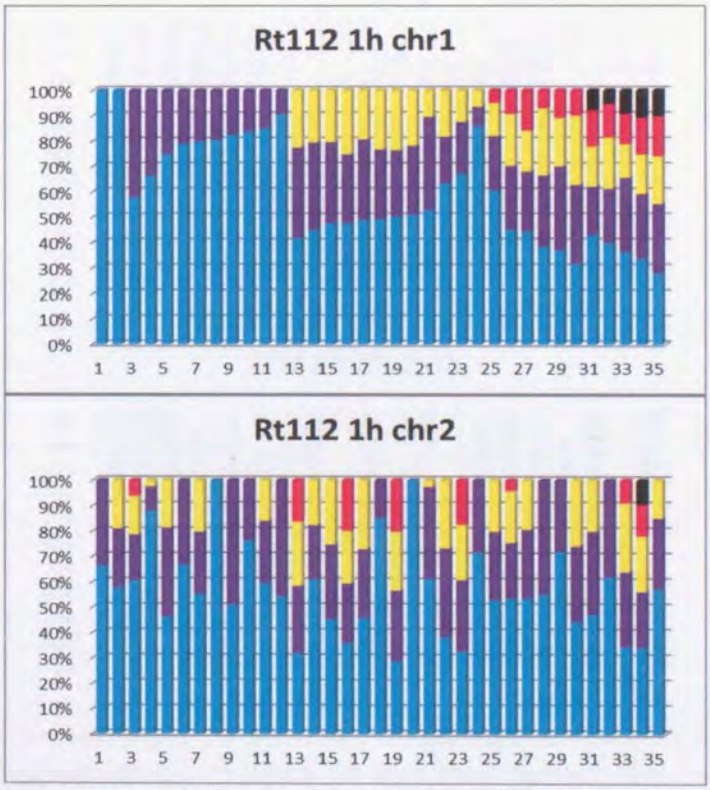

Figure 7.17: Graphic representation of the proportion of each individual territory volume compared to the corresponding total chromosome volume (100%) for both chromosome 1 (top) and 2 (bottom). Each bar corresponds to the territories observed in on cell nucleus for the chromosome considered. Each colour in the bar represents a fragment (territory) observed for the given chromosome. The data has been sorted using the number of territory observed for chromosome 1 with the corresponding chromosome 2 data aligned accordingly in the bottom graph. Territory 1, blue; territory 2, purple; territory 3, yellow; territory 4, pink; territory 5, black.

The presence of 5G in the data set indicates fractionation of chromosome 1, 1 hour after irradiation. Two corresponding occurrences for chromosome 2 are 50%/25%/25%, one is 60%/40%, and in the case of the corresponding 4R the split is 30%/30%/30%/10%. Chromosome 2 does not appear to present as many fragments as chromosome 1 does but on one occurrence 5R is seen.

At 2 hours, when considering chromosome 1 and 2G occurs, only 2 occurrences appears to be the result of a fragmentation of the chromosome with a split of 70%/30% and 95.9%/4.1%. Unlike 1 hour, the corresponding chromosome 2 splits appear to show a high number of smaller fragments.

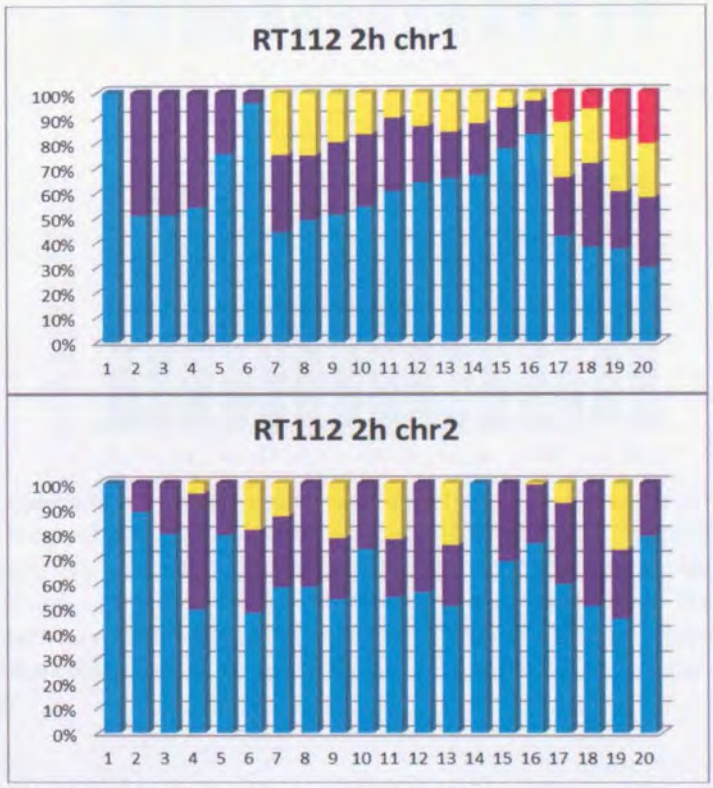

Figure 7.18: Graphic representation of the proportion of each individual territory volume compared to the corresponding total chromosome volume (100%) for both chromosome 1 (top) and 2 (bottom). Each bar corresponds to the territories observed in on cell nucleus for the chromosome considered. Each colour in the bar represents a fragment (territory) observed for the given chromosome. The data has been sorted using the number of territory observed for chromosome 1 with the corresponding chromosome 2 data aligned accordingly in the bottom graph. Territory 1, blue; territory 2, purple; territory 3, yellow; territory 4, pink.

When 3G occurs almost half of the splits are 50%/25%/25% indicating that the cells could possess 2 copies of each chromosome. However, 3 of the corresponding chromosome 2

split present a 50%/25%/25%, 2 present a 50%/50% split and the rest present a 70%/30% split or a 3R split with a very small fragment.

When 4G occurs, the splits appear to be 25%/25%/25%/25% most with the corresponding chromosome 2 splits being 50%/50%, 50%/25%/25%, 70%/30% and 60%/30%/10%.

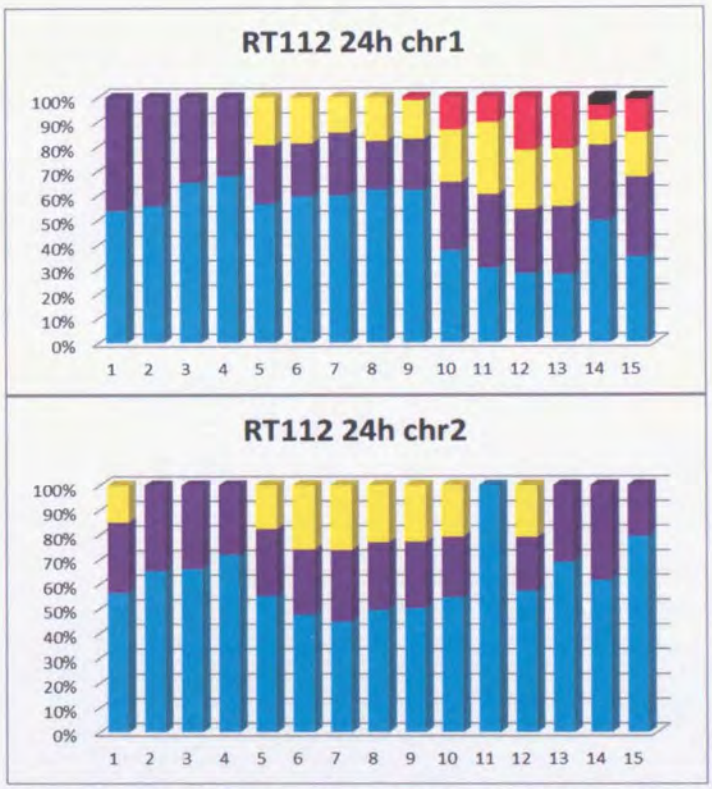

Figure 7.19: Graphic representation of the proportion of each individual territory volume compared to the corresponding total chromosome volume (100%) for both chromosome 1 (top) and 2 (bottom). Each bar corresponds to the territories observed in on cell nucleus for the chromosome considered. Each colour in the bar represents a fragment (territory) observed for the given chromosome. The data has been sorted using the number of territory observed for chromosome 1 with the corresponding chromosome 2 data aligned accordingly in the bottom graph. Territory 1, blue; territory 2, purple; territory 3, yellow; territory 4, pink; territory 5, black.

Finally at 24 hours, most of the chromosome 1 occurrences are 2G with a 50%/50% split, 3G with a 50%/25%/25% split and 4G with a 25%/25%/25%/25% split with a couple of exceptions with chromosome 2 following a similar pattern indicating that most of these cells are in fact in G_2 except for a few. Only the occurrences with 5G happen to highlight the presence of fragments and or aberrations.

7.3.2.4. Distances and ratio of relative radii

The descriptive statistics of the distances measured (Example of the measurements given in figure 7.20) between the nuclei CoG and the territory CoG for RT112 at the time points considered are summarised in Table 7.14.

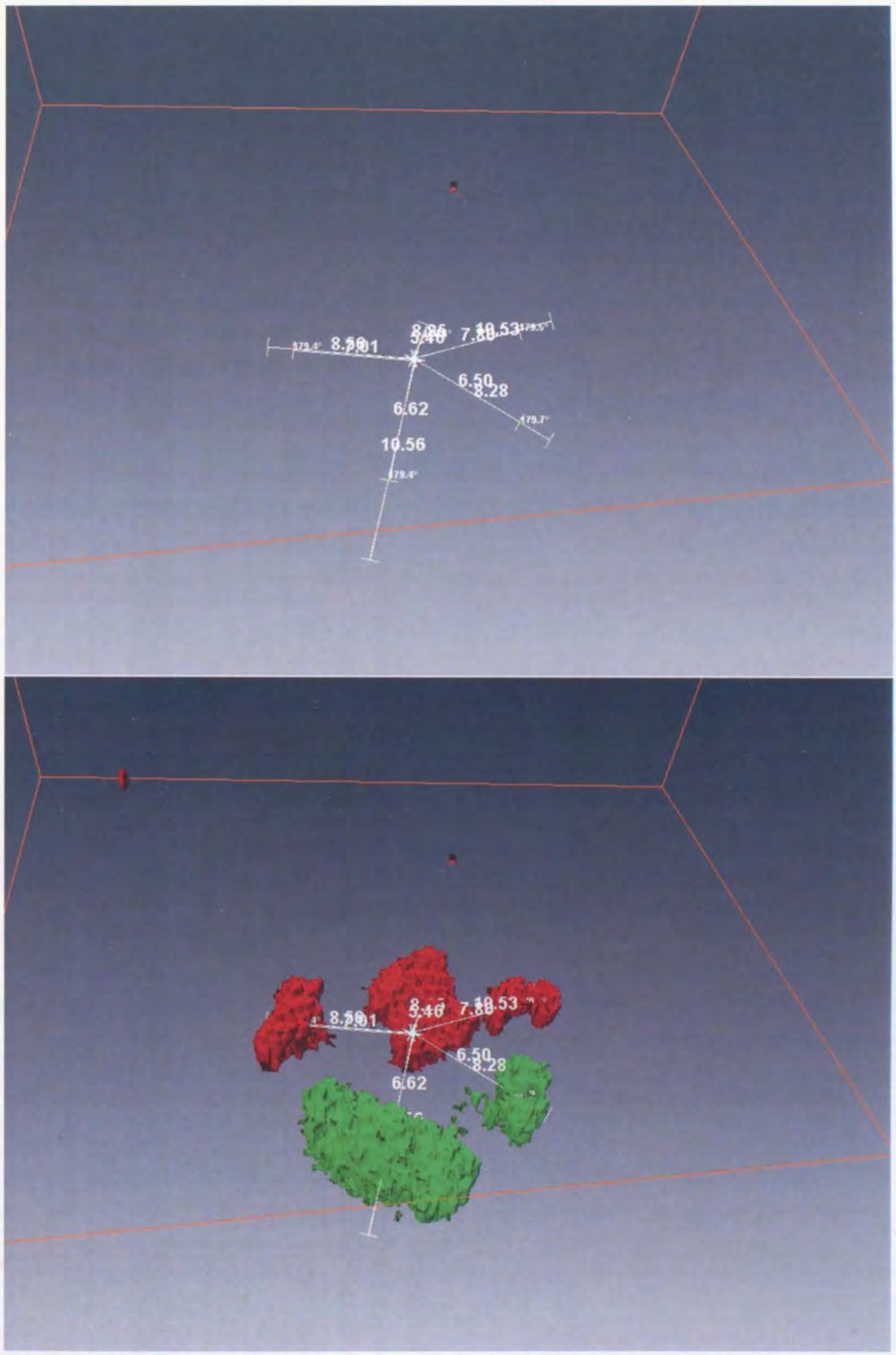

Figure 7.20: 3D visualisation example of chromosome territories for chromome 1 (green) and chromosome 2 (red) within a RT112 nucleus 1 hour post-irradiation. The upper figure shows measurements of distances between the nucleus centre of gravity and the territories' centres of gravity. The lower figure shows the same measurements with the visualisation of the whole territories. Measurements are expressed in µm.

Chr1 distance	N	Mean	SD	SE	CV	Normal?	P	Chr1 Ratio of radius	N	Median	25% percentile	75% percentile	75%-25%	Normal?	P
RT112 Controls	80	5.812	1.895	0.2119	0.33	yes	0.2	RT112 Controls	80	67.95	50.59	75.19	24.6	No	0.0007
RT112 1h	107	6.229	1.734	0.1676	0.28	yes	0.2	RT112 1h	107	66.44	54.78	74.95	20.17	Yes	0.1412
RT112 2h	57	5.352	1.539	0.2038	0.29	yes	0.2	RT112 2h	57	63.19	53.64	70.64	17	No	0.0283
RT112 24h	50	7.941	2.928	0.414	0.37	yes	0.2	RT112 24h	50	67.8	54.02	75.24	21.22	No	0.0229
Chr2 distance	N	Mean	SD	SE	CV	Normal?	P	Chr2 Ratio of radius	N	Median	25% percentile	75% percentile	75%-25%	Normal?	P
RT112 Controls	74	5.795	2.23	0.2592	0.38	yes	0.2	RT112 Controls	74	66.07	51.33	76.04	24.71	No	0.0019
RT112 1h	100	6.456	2.267	0.2267	0.35	yes	0.2	RT112 1h	100	70.6	59.02	78.31	19.29	No	0.0042
RT112 2h	47	5.78	1.722	0.2511	0.30	yes	0.2	RT112 2h	47	64.84	54.87	76.04	21.17	Yes	0.2
RT112 24h	37	8.678	2.078	0.3417	0.24	yes	0.2	RT112 24h	37	70.89	61.14	75.74	14.6	No	0.0094

Table 7.14: Table of descriptive statistics for the distances between the nucleus centre of gravity and the territory centre of gravity measured using Amira software for chromosome 1 and chromosome 2 in fibroblast at the different time points considered. Distances are expressed in µm. Ratios of radii are expressed in percentages.

As previously seen in fibroblasts, the distances from the centre of the nucleus and the CoG of the territory appear to follow the changes in size of the nuclei as well. The mean values for the distances increase at 1 hour and 24 hours for both chromosome 1 and 2.

The values for the distances for the different time points were compared with the control values using an unpaired t-test. There was no significant difference in terms of distances for chromosome 1 at 1 hour and 2 hours compared to the controls ($p = 0.06$ and $p = 0.24$) but a significant difference was found between the controls and 24 hours ($p < 0.0001$). The results were confirmed using a false discovery rate (FDR) method (Benjamini & Hochberg, 1995) with a maximum FDR of 10%.

For chromosome 2, there was no significant difference in terms of distances at 2 hours compared to the controls ($p = 0.22$) but a significant difference was found between the controls and 1 hour and, 24 hours ($p = 0.001$ and $p < 0.0001$ respectively). The results were confirmed using a false discovery rate (FDR) method (Benjamini & Hochberg, 1995) with a maximum FDR of 10%.

The relative ratio of the radii for chromosome 1, however appear to decrease up to 2 hours for chromosome 1 before increasing again at 24 hours. In the case of chromosome 2, the ratios do follow the trend seen for the distances and for the nuclear size.

The median value for the ratios of relative radii at 24 hours was higher than at other time points. The values for the different time points were compared with the control values using a Mann-Whitney test. There was no significant difference in terms of ratio of radius for chromosome 1 at 1 hour, 2 hours and, 24 hours compared to the controls ($p = 0.59$ and $p = 0.40$ and $p = 0.78$ respectively). The results were confirmed using a false discovery rate (FDR) method (Benjamini & Hochberg, 1995) with a maximum FDR of 10%.

For chromosome 2, there was no significant difference in terms of ratios of radius at 2 hours and, 24 hours compared to the controls ($p = 0.44$ and $p = 0.06$) but a significant difference was found between the controls and 1 hour ($p = 0.03$). The results were confirmed using a false discovery rate (FDR) method (Benjamini & Hochberg, 1995) with a maximum FDR of 10%.

The change in nuclear shape does not appear to be as evident as with fibroblasts. This could be due to the RT112 nuclei being more spherical to begin with and the changes associated in distances and ratios being the result of passage into G2.

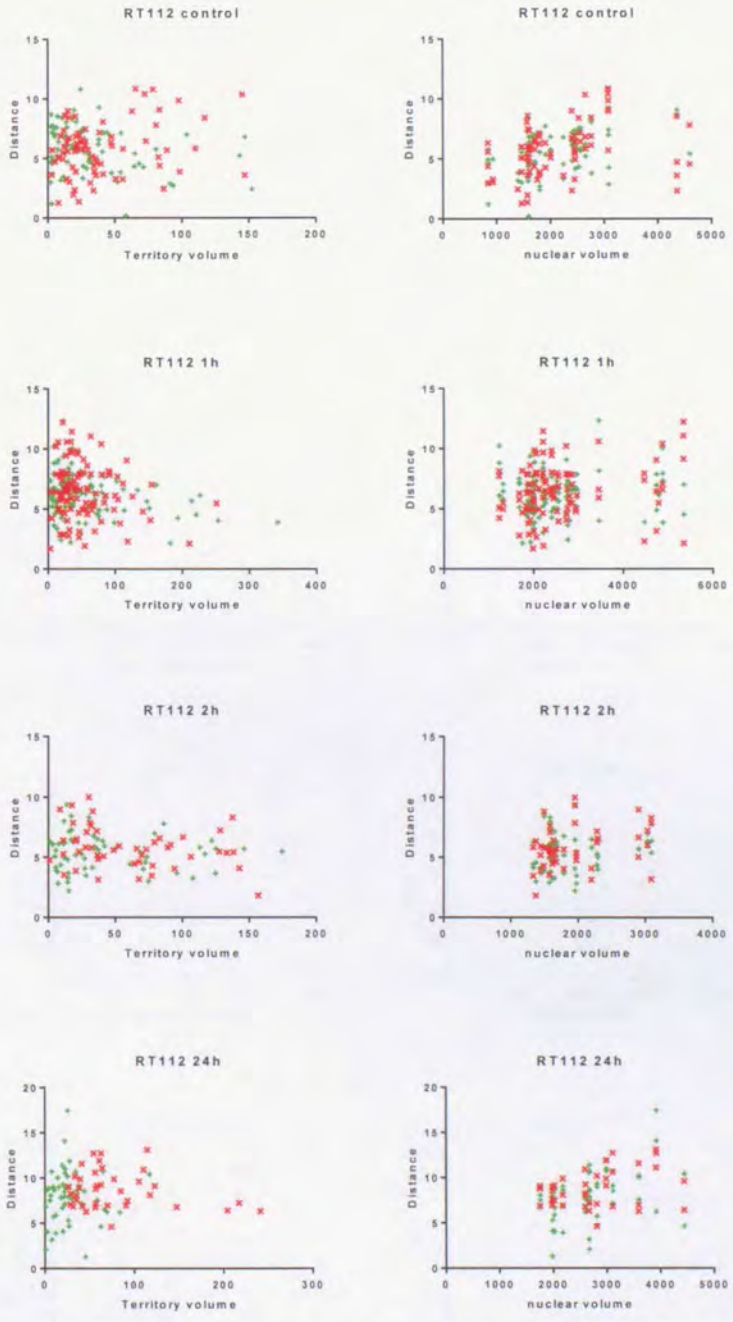

Figure 7.21: The distance from the centre of gravity of the nucleus to the centre of gravity of the territory are plotted against both the corresponding territory volumes (left column) and corresponding nuclei volumes (right column) at the different time points considered in RT112. The green crosses represent chromosome 1 and the red crosses represent chromosome 2. The measurements are given in μm for the distances and in μm^3 for the volumes.

As seen with the fibroblasts, when visually examining Figure 7.21 and Figure 7.22, there does not seem to be an obvious relationship between territory size and distance from the

CoG of the nucleus at any of the time points considered. However, there seem to be a relation between distances and nuclear volumes. This relationship does not seem to be as visually obvious as with fibroblasts especially at 1 hour. This could be due to the pool of nuclei examined consisting of nuclei with very similar volumes.

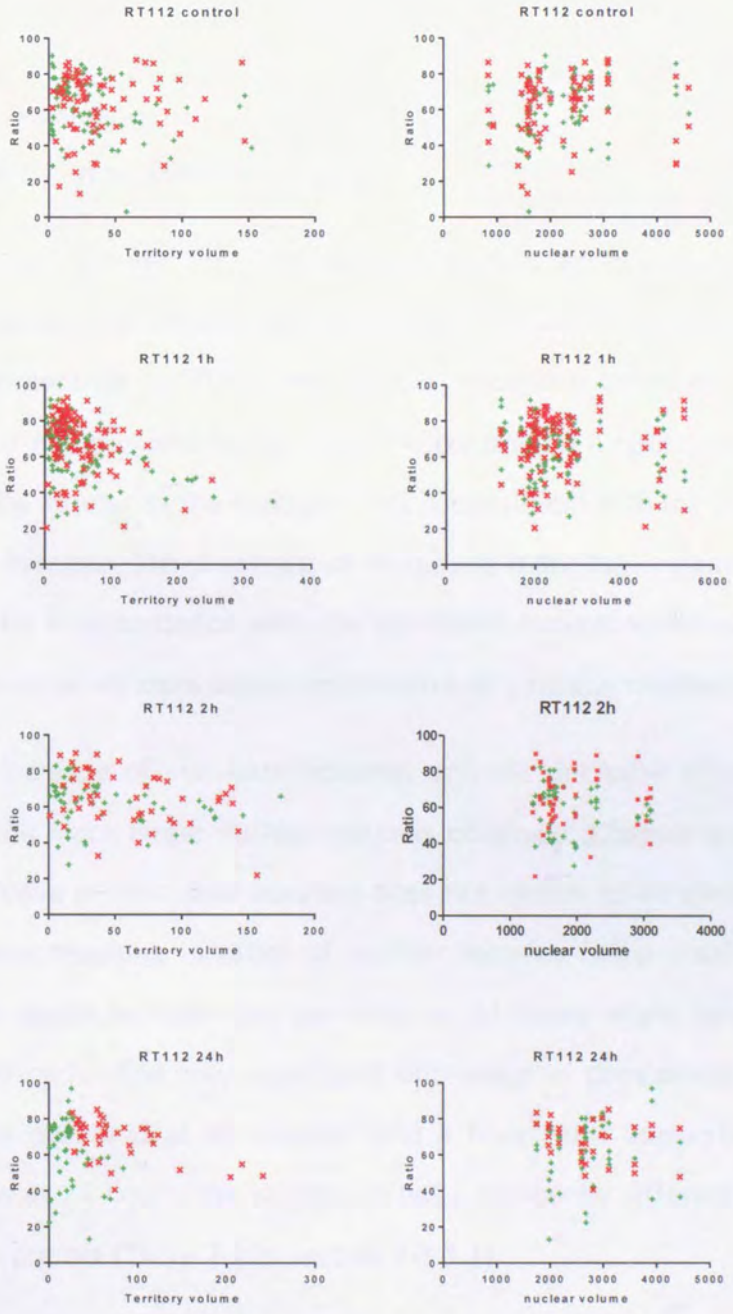

Figure 7.22: The ratios of radii are plotted against both the corresponding territory volumes (left column) and corresponding nuclei volumes (right column) at the different time points considered in RT112. The green crosses represent chromosome 1 and the red crosses represent chromosome 2.

The relation seen between distances and nucleus volume seems to disappear when examining ratios of relative radii. There does not seem to be a clear relation between ratios and both territory volumes and nuclear volumes.

There does not seem to be a clear difference in positioning between chromosome 1 and 2.

7.4. Discussion

7.4.1. Irradiated fibroblasts

The individual volumes for chromosome 1 show an increase at 4 hours and 24 hours and a decrease at 30 minutes with only the 30 minutes decrease being significantly different from the controls. Similarly, the ratios of nuclear volumes are also smaller than the controls at 30 minutes and higher than the controls at 4 hours whereas at 24 hours ratios appear to be similar to the controls. This is consistent with the presence of smaller fragments at 30 minutes. The presence of increased individual volumes and ratios at 4 hours appear to be in accordance with the increased nuclear volumes compared to the controls. The individual volumes appear to increase in a similar manner to the nuclei.

At 24 hours the increase of individual volumes and the decrease of ratios could be the consequence of the much larger nuclear volumes observed (Chapter 6 section 6.3.1). The considerable increase in individual volumes does not appear to be similar to the increase in nuclear volumes resulting in ratios of nuclear volumes being smaller than the other time points. This could indicate that the cells at 24 hours might have reached the G_2 phase of the cell cycle. The only significant difference in comparison with controls for ratio values were observed at 30 minutes and 4 hours; this suggests that despite the decrease in ratios at 24 hours, the values are not significantly different from the volumes measured in the controls (Table 7.7 in section 7.3.1.1).

The total chromosome volumes for chromosome 1 were smaller in size at 30 minutes and 2 hours but larger at 4 hours and 24 hours compared with controls. The smaller total chromosome volumes seen at 30 minutes could be the consequence of smaller nuclear volumes and this can be confirmed by the ratio of nuclear volumes occupied for total chromosomes at 30 minutes being similar to the controls. This can also apply to the 2

hours data as nuclei sizes at this time point are also smaller than the controls. As seen with individual volumes, the total chromosome volumes are higher at 4 hours and 24 hours with the ratios only being much higher than the controls at 4 hours. The increase in volume seen at 4 hours with the ratios being also much higher could be due to the initiation of the passage into the next step of the cell cycle where DNA is being replicated before the other nuclear components.

When considering chromosome 2 the data obtained are quite similar to chromosome 1 with the exception of smaller volumes at 30 minutes for chromosome 1. The increase in individual volumes at 4 hours and 24 hours is also seen for chromosome 2 which indicates the timings for chromosome dynamics are likely to be similar for the two chromosomes. The ratios of nuclear volumes for both individual and total chromosome volumes behave in a similar manner compared to chromosome 1; the ratio at 24 hours is smaller than that at the early time points and similar to the control values.

The increase in volumes and percentage of nuclear occupancy for both individual territories and overall sums at 4 hours could be the manifestation of a global chromatin decondensation for chromosome 2 since the nucleus sizes do not appear to show increase from the control sample.

Although the number of CTs detected by FISH can give a good indication of the effect of radiation on the cells studied, it is not sufficient to allow a complete overview. Since the method used has limitations in differentiating two very close CTs, as discussed in 6.4.2, the proportion of the total chromosome volumes and the cell nuclei sizes have also to be taken into consideration.

Studies have shown that the majority of the DNA DSBs are repaired within 60 minutes of irradiation (Cornforth & Bedford, 1983; Lobrich *et al.*, 1995; Nevaldine *et al.*, 1993) in normal cells with repair proteins co-localising at DSBs sites within 30 minutes (Nelms, 1998) but in repair-deficient fibroblasts, partially irradiated using a mask (Nelms, 1998), traces of DSBs have been observed after 300 minutes. So the decrease in the number of territories observed within a cell nucleus could be the result of successful repair of the DSBs.

The presence of one territory observed at every time point tested is potentially the result of the close proximity of both members of the chromosome pair considered which did not allow differentiation between them using the technique developed in this project. Similarly, the occurrence of three territories within a cell nucleus could be the outcome of two scenarios. Firstly, a fragment has been generated following irradiation. One of the fragments observed should be of a much smaller volume than the two other present in the same nucleus. Secondly, the cell initially possessed 4 territories and two of them were too close to be distinguished when the data were acquired which should result in two of the values being of similar order and the third value approximately twice the size of the others.

In the instance when one territory occurs, only at 4 hours and 24 hours does the total territory volume appear to be greater than the controls. As discussed above, when looking at the corresponding nuclear volumes, only at 24 hours are they greater than the control values. So the difference in volumes seen at 4 hours could be due to a change in condensation levels as mentioned above which is illustrated by the increased ratios of nuclear occupancy at 4 hours. It is also possible that the resolution of the method used could be a limiting factor by preventing two separate entities from being discerned; this could result in a miscount of the territories present but also an artefactual increase in the volume measured caused by incorporating elements of the nucleus into the structure being measured. However, the techniques are sufficiently sensitive to detect increases in chromosome volumes and corresponding similar change in ratios in contrast to a smaller increase in nuclei size.

It appears that for chromosome 1 the increase in the number of fragments is seen at 30 minutes and at 4 hours and is still present after 24 hours. This could be the manifestation of an incomplete or failure of repair and the creation of fragments for chromosome 1.

In the case of chromosome 2, the presence of smaller fragments is not as obvious. It could be due to chromosome 2 being more readily repaired or that all the copies of the chromosome lie close in the interphase nucleus resulting in their distinction not being possible.

Chromosome 1 and 2 appear to be positioned at similar distances from the centre of the nucleus with also similar ratios of relative radius. The distances between CoG of the nucleus and CoG of the territories appears to increase with increasing nucleus volume which is strongly highlighted by the longer distances at 24 hours. The distances do not seem to increase with territory size.

The corresponding ratios of relative radii do not seem to follow this trend and the ratio values appear to be similar for the nuclei considered for both chromosomes 1 and 2 except at 4 hours. At 4 hours the distances are similar to the earlier time points and control but the ratio of relative radii appear smaller. This could be the result of the nuclei moving into the next step of the cell cycle meaning the nuclear sizes are increasing but the shift along the radius to preserve the same ratio of radii in the cell has yet to happen. At 24 hours, it is possible that the increase in distance but the conservation of the ratios of radii is the illustration of a further advancement into G_2. So it can be concluded that despite the distances increasing, it appears that the relative positioning is preserved over the 24 hour time period.

7.4.2. Irradiated RT112

When considering chromosome 1, the volumes show an increase after 1 hour. This could be due to a change in DNA compaction levels in the nucleus. However, after examining the data set, it appears that one of the values is considerably higher and a cluster of values are approximately double the size of the rest of the data. This could explain the shift in median values for chromosome 1 territories at 1 hour.

The percentage of nuclear occupancy follows a similar trend and when looking at the nuclear volume medians it appears there is an increase at 1 hour. The increase in individual volumes and percentages of nucleus seem to follow the nuclear sizes trend and do not seem to be the result of a change in DNA compaction levels.

When looking at the total chromosome values and the corresponding percentage of nucleus there is a considerable increase until 2 hours before a return to control-like values at 24 hours. When examining the corresponding nuclear sizes, the values increase

until 1 hour, before slightly decreasing at 2 hours and increasing again at 24 hours. The return of the percentage of nuclear occupancy at 24 hours suggests being due to larger nuclear sizes. The increase at 2 hours in territories volumes could be as seen in fibroblasts at 4 hours, the result of cells being in transition to the next cell cycle phase.

When considering chromosome 2, it appears the data are not as variable as chromosome 1. No reference to aberrations has been recorded in the literature which could explain the greater homogeneity in the chromosome 2 data. The trend in individual volumes for chromosome 2 shows an increase until 24 hours where the percentages of nuclear occupancy appear to increase until 2 hours before slightly decreasing at 24 hours. Once again, the nuclear volumes trend could be the explanation as seen with the total chromosome volumes for chromosome 1.

The total chromosome volumes for chromosome 2 also show a considerable increase until 24 hours whereas the percentages of nuclear occupancy seem to increase only until 2 hours before decreasing at 24 hours. Once again, this could be explained by a change in nuclear volume between 2 hours and 24 hours. The nuclei being much larger at 24 hours mean that a 30% increase of 50 μm^3 in total chromosome volumes translates in a decrease of 1% in nuclear occupancy.

On approach to understanding whether the changes in volumes are linked to passage into another phase of the cell cycle is to look at the chromosome territories number and also their splits with regards to the total chromosome volume. However, in cancerous cell lines several parameters can be perturbed and these include the ability for the cell to arrest progression through the cell cycle, the number and sizes of chromosomes as a result of the absences of cell cycle regulation. Therefore aberrations are likely to be carried through the cell divisions with sometimes an cumulative effect. Exposure to IR is likely to enhance this by creating more numerous breaks and increasing the probability of these to be misrepaired.

When examining the territory numbers and chromosomes splits, it appears that despite the presence of a high number of 25%/25%/25%/25% or 50%/25%/25% splits for either chromosome indicating the presence of tetraploid cells, extra fragments appear to also be generated. The presence of higher number of territories at 2 hours and 24 hours for both

chromosomes indicates that repair has not taken place and the high number of cells apparently in G_2 configuration could indicate that the aberrations resulting from the fragmentation might be likely to have been carried through as stable aberrations.

The chromosome positioning in RT112 with regards to distances and ratios of relative radii seems to follow the trend of nuclear size. The mean values for the distances increase at 1 hour and 24 hours for both chromosomes 1 and 2. For chromosome 1 the ratios appear to decrease until 2 hours before increasing at 24 hours again whereas chromosome 2 ratios seem to follow the trend seen in nuclear sizes (i.e. an increase at 1 hour and 24 hours). The change in nuclear shape does not appear to be as evident as with fibroblasts. This could be due to the RT112 nuclei being more spherical to begin with and the changes associated in distances and ratios being the result of passage into G2.

There does not seem to be an obvious relationship between territory size and distances at the time points measured for both chromosomes. However, similarly to fibroblasts, there seems to be a relation between distances and nuclear volumes but this relationship is not as obvious. This relationship disappears when considering the ratios which means the territories seem to assume similar positions in the nuclei regardless of size or even radiation treatment.

REFERENCES

Benjamini, Y., & Hochberg, Y. (1995). Controlling the False Discovery Rate: A Practical and Powerful Approach to Multiple Testing. *Journal of the Royal Statistical Society. Series B (Methodological)*, ***57***(1), 289 – 300.

Cornforth, M. N. & Bedford, J. S. (1983). X-ray--induced breakage and rejoining of human interphase chromosomes. *Science,* **222**(4628), 1141–3.

Löbrich, M., Rydberg, B. & Cooper, P. K. (1995). Repair of x-ray-induced DNA double-strand breaks in specific Not I restriction fragments in human fibroblasts : Joining of correct and incorrect ends. *Biochemistry*, **92**, 12050–12054.

Nelms, B. E. (1998). *In Situ* Visualization of DNA Double-Strand Break Repair in Human Fibroblasts. *Science*, **280**(5363), 590–592.

Nevaldine, B., Longo, J. A., King, G. A., Vilenchik, M., Sagerman, R. H. & Hahn, P. J. (1993). Induction and repair of DNA double-strand breaks. *Radiation Research*, **133**(3), 370–4.

Chapter 8 Discussion, conclusions and future work

8.1. Discussion

8.1.1. Protocol optimisation

A key aim of this study was to characterise chromosome 1 and 2 and their positioning within the interphase nucleus in normal human fibroblasts and bladder carcinoma RT112 using 3D imaging. This project also aimed at characterising possible changes in chromosome characteristics following irradiation in order to investigate the chromosome positioning, nuclear architectures and CA formations.

The investigation involved developing a method to study chromosome positioning using fluorescence *in situ* hybridisation, 3D imaging and confocal microscopy. Furthermore methods for analysis of chromosome 1 and 2 territory features in both non-irradiated and irradiated cells were developed and applied.

The method development was initially aimed at obtaining the best possible quality for the images and also potentially at being able to include an automated component in the protocol that would allow the generation of significant quantities of data in a time efficient manner. This would then at later stages help with implementing the method routinely in order to study chromosome positioning.

The methods developed involved integrated optimisation of several parameters in the different steps involved in the protocol such as slide preparation, FISH, confocal microscopy, image processing and image analysis. It was important to adopt an integrated approach as each stage in the methodology can have an impact on other stages. For example a key objective of this optimisation was to reduce background staining which was successfully achieved. Hence as some steps are dependent on preceding methodology stages, optimisation of the overall protocol is very important. To achieve such optimisation, detailed study of each stage was performed individually where possible. For example the steps involved the slide preparation such as fixation times aging, and FISH pre-treatments were tested first without making significant changes to the FISH protocol.

Once the pre-treatment steps were optimised the parameters involved in FISH such as the probes, the quantity of the probe and the post-hybridisation washes investigated.

Optimisation during the generation and acquisition of raw data was performed based on the results obtained using confocal microscopy. For example appropriate settings in confocal microscopy contribute to minimising fading and minimising the effects of background by appropriate adjustment of laser power, lasers setting, number of z-slices and photomultiplier gain.

A main challenge that had to be addressed was signal intensity fading. Fading occurs following the exhaustion of the fluorochrome present in the whole chromosome paint. Reduction in the effect of fading can be achieved using anti-fade agents when mounting the slides. However, the protective effect of anti-fades is limited and in the case of samples subjected to repetitive scanning, some fading would be expected. Hence a balance had to be achieved involving for example microscope laser and number of z-stack slices in order to obtain good 3D visualisation of the image datasets.

Image processing of the confocal microscope z-stacks was also key in the achieving high quality 3D visualisations. After examining different options in the image processing, it appeared that despite the FISH protocol optimisation, the raw data sets obtained still presented some variability in terms of consistence and quality. As a result, full automation of the image processing could not be implemented without risking a loss in quality of 3D visualisation. Instead of subjecting the whole stack to the same brightness and contrast parameters, each picture was reviewed individually.

The techniques could be further developed to measure the effect of targeted irradiation and therefore measure more localised and controlled damage. This could help with further confirming the presence of "hot-spots" for CA and to assess if targeting a specific area of the cell increases the formation of aberrations.

The use of M-FISH with a whole chromosome paint in combination with paints targeting a highly transcribed region and a low transcribed region could allow studying whether exposure to irradiation leads to increase CA aberrations in the regions of interest.

8.1.2. Characterisation of chromosome 1 and 2 in fibroblasts and RT112

Following protocol optimisation the initial analysis involved characterisation of chromosome 1 and 2 in fibroblasts and RT112. It was observed that nuclear sizes appeared to be similar for both cells lines.

The results also showed that chromosome 1 territory volumes are bigger in fibroblasts than in RT112 whereas chromosome 2 was smaller in RT112 which has not been documented in the literature. The results also showed little difference in volume between chromosome 1 and 2. The results described in chapter 6 are in accordance with those found by Morton (1991) with regards to their similarity in physical length of 8.2% for chromosome 1 and 8.0% for chromosome 2. The physical length does not account for variations in levels of compaction. The limitation induced by the resolution of the FISH does not allow the differentiation in degree of compaction, local or global, within the chromosome. So it is possible that the slight variations seen in the volume data could also be related to differences in DNA compaction which are not detected by the method. The percentage of the nucleus occupied by chromosome territories in this study is in accordance with the data presented by Heslop-Harrison *et al.* (1989) using micrographs of serial sections.

The results also showed that there seems to be a relationship between total chromosome volumes and nuclear sizes for both chromosomes and in both cell lines. This relationship is not seen with individual territory volumes.

The analysis of the territory numbers highlighted the presence of up to 4 territories in a cell in fibroblast controls. This showed that the cells presenting 3 or 4 territories were likely to be cells in G_2 phase of the cell cycle. This was confirmed during the examination of the chromosome splits, showing that 3 or 4 territories with 50%/25%/25% and 25%/25% /25%/25% were likely to be cells in G_2.

The method also allowed the measurement of distances between the centre of gravity (CoG) of the nucleus and the CoG of the territory and the corresponding relative radii. This allowed the calculation of the ratio of relative radii in order to assess possible differences in positioning in the presence of nuclei of different shapes and sizes. The

distances appeared slightly smaller in RT112 for both chromosome 1 and chromosome 2 (5.8 μm for both chromosomes in RT112 and 6.9 μm and 6.4 μm for chromosome 1 and 2 respectively in fibroblasts). Despite the difference in distances, the ratios of relative radii were similar which suggested that both chromosomes are positioned in a similar outer "layer" of the nucleus. The values obtained were in agreement with the data presented by Sun *et al.* (2000) Boyle *et al.* (2001) and Bolzer *et al.* (2005). The characterisation of chromosome positioning in RT112 has however not been described before.

8.1.3. Characterisation of chromosome 1 and 2 following irradiation in fibroblasts and RT112

This part of the project aimed at investigating and characterising chromosome 1 and 2 in fibroblasts and RT112. The study was performed by comparing irradiated cells with non-irradiated cells using FISH and confocal microscopy. Examination of chromosome territory volumes showed that individual territory volumes appear to stay the same following irradiation in the absence of fragmentation except at 30 minutes for chromosome 1 and 4 hours for chromosome 2 in fibroblasts. The total chromosome volumes on the other hand appeared to increase with time following irradiation for both chromosome 1 and 2 in fibroblasts. In RT112, only chromosome 2 appeared to show a similar trend to fibroblasts for total chromosome volumes.

The number of territories appeared to be higher for chromosome 1 following radiation in fibroblasts. A similar trend was observed in RT112. This could be due to chromosome 2 being more readily repaired in fibroblasts. In RT112, the presence of more numerous fragments for chromosome 1 could be the reflection of the instability inferred by the deletion in 1p (Walker *et al.*, 1990; Williams *et al.*, 2005) .

The distances from the nucleus CoG for both chromosomes in both cell lines do not appear to be different in the early stages following irradiation. The only noticeable increase happens at 24 hours and can be explained by an increase in nuclear volume seen in both cells lines. The clear increase in nuclear volume could be a sign of the passage of the cell from G_1 through S and into G_2. This is in agreement with the conclusions drawn by the examination of territories numbers and splits. This also could also reflect the change

in shape undergone by the nuclei when transitioning between G_1 and G_2. Despite the increase in distances from the nuclei CoG, the ratio of relative radii appears to stay the same except at 4 hours for fibroblasts. This, in addition to the nuclear volumes data, could illustrate start of the passage of the cell from G_1 to G_2. In the case of the measurement at 4 hours, the distance was similar to the other time points and the ratios are slightly lower. This suggests that the measurement could have taken place before the territory finished the shift along the radius into the outer shell since the nuclear size had increased the radii would have increased too resulting in a lower ratio of relative radii.

8.2. Conclusions

In these studies methods were developed and applied to enable chromosome 1 and chromosome 2 territories to be successfully imaged in fibroblasts and RT112 nuclei using FISH and confocal microscopy. Cells were irradiated and changes in chromosomes territory characteristics were identified.

3D visualisations of the image data sets enabled identification of complete and fragmented chromosomes territories. This visualisation allowed the quantification of chromosome volume and nuclear volume as well as chromosome territories positioning.

The techniques involved the successful combination of 3 different fluorochromes.

The calculation of the relative radii from the distances was a successful adaptation of a technique used in 2D (Sun *et al.*, 2000) to a 3D setup.

The methods developed may thus help to elucidate the mechanisms of radiation induced chromosome aberrations and hence have application in cancer cell biology.

8.3. Future work

Future work would involve the use of M-FISH with a whole chromosome paint in combination with paints targeting a highly transcribed region and a lowly transcribed region of chromosome 1 and/or 2. This would allow studying the difference in localisation

of the region of interest following irradiation with regards to the rest of the chromosome territory positioning.

Future work would include the use of the method to visualise the effect of targeted irradiation and therefore study more localised and controlled damage. This could be done using particle irradiation in conjunction with confocal microscopy allowing tracking individual cells following irradiation.

REFERENCES

Bolzer, A., Kreth, G., Solovei, I., Koehler, D., Saracoglu, K., Fauth, C., Müller, S., Eils, R., Cremer, C., Speicher, M. R. & Cremer, T. (2005). Three-dimensional maps of all chromosomes in human male fibroblast nuclei and prometaphase rosettes. *PLoS Biology*, **3**(5), e157.

Boyle, S., Gilchrist, S., Bridger, J. M., Mahy, N. L., Ellis, J. A. & Bickmore, W. A. (2001). The spatial organization of human chromosomes within the nuclei of normal and emerin-mutant cells. *Human Molecular Genetics*, **10**(3), 211–9.

Heslop-Harrison, J. S., Leitch, A. R., Schwarzacher, T., Smith, J. B., Atkinson, M.D. & Bennett, M.D. (1989). The volumes and morphology of human chromosomes in mitotic reconstructions. *Human Genetics*, **84** (1), 27–34.

Morton, N. E. (1991). Parameters of the human genome. *Proc. Nat. Acad. Sci. USA*, **88** (17), 7474–6.

Sun, H. B., Shen, J. & Yokota, H. (2000). Size-Dependent Positioning of Human Chromosomes in Interphase Nuclei. *Biophysical Journa*, **79**(1), 184–190.

Walker, M. C., Povey, S., Parrington, J. M., Riddle, P. N., Knuechel, R. & Masters, J. R. (1990). Development and characterization of cisplatin-resistant human testicular and bladder tumour cell lines. *European Journal of Cancer*, **26**(6), 742–7.

Williams, S. V, Adams, J., Coulter, J., Summersgill, B. M., Shipley, J. & Knowles, M. A. (2005). Assessment by M-FISH of karyotypic complexity and cytogenetic evolution in bladder cancer in vitro. *Genes, Chromosomes & Cancer*, **43**(4), 315–28.